FINAL REPORT

U.F. Project No. 00054863
RPWO#: 60
Contract No: BD545

DEVELOPMENT OF DESIGN PARAMETERS FOR MASS CONCRETE USING FINITE ELEMENT ANALYSIS

Mang Tia
Christopher Ferraro
Adrian Lawrence
Samuel Smith
Eiji Ochiai

February 2010

Department of Civil & Coastal Engineering
College of Engineering
University of Florida
Gainesville, Florida 32611

DISCLAIMER

"The opinions, findings, and conclusions expressed in this publication are those of the authors and not necessarily those of the State of Florida Department of Transportation or the U.S. Department of Transportation.

Prepared in cooperation with the State of Florida Department of Transportation and the U.S. Department of Transportation."

SI (MODERN METRIC) CONVERSION FACTORS (from FHWA)

APPROXIMATE CONVERSIONS TO SI UNITS

SYMBOL	WHEN YOU KNOW	MULTIPLY BY	TO FIND	SYMBOL
		LENGTH		
in	inches	25.4	millimeters	mm
ft	feet	0.305	meters	m
yd	yards	0.914	meters	m
mi	miles	1.61	kilometers	km

SYMBOL	WHEN YOU KNOW	MULTIPLY BY	TO FIND	SYMBOL
		AREA		
in^2	squareinches	645.2	square millimeters	mm^2
ft^2	squarefeet	0.093	square meters	m^2
yd^2	square yard	0.836	square meters	m^2
ac	acres	0.405	hectares	ha
mi^2	square miles	2.59	square kilometers	km^2

SYMBOL	WHEN YOU KNOW	MULTIPLY BY	TO FIND	SYMBOL
		VOLUME		
fl oz	fluid ounces	29.57	milliliters	mL
gal	gallons	3.785	liters	L
ft^3	cubic feet	0.028	cubic meters	m^3
yd^3	cubic yards	0.765	cubic meters	m^3
NOTE: volumes greater than 1000 L shall be shown in m^3				

SYMBOL	WHEN YOU KNOW	MULTIPLY BY	TO FIND	SYMBOL
		MASS		
oz	ounces	28.35	grams	g
lb	pounds	0.454	kilograms	kg
T	short tons (2000 lb)	0.907	megagrams (or "metric ton")	Mg (or "t")

SYMBOL	WHEN YOU KNOW	MULTIPLY BY	TO FIND	SYMBOL
		TEMPERATURE (exact degrees)		
°F	Fahrenheit	5 (F-32)/9 or (F-32)/1.8	Celsius	°C

SYMBOL	WHEN YOU KNOW	MULTIPLY BY	TO FIND	SYMBOL
		ILLUMINATION		
fc	foot-candles	10.76	lux	lx
fl	foot-Lamberts	3.426	candela/m^2	cd/m^2

SYMBOL	WHEN YOU KNOW	MULTIPLY BY	TO FIND	SYMBOL
		FORCE and PRESSURE or STRESS		
lbf	poundforce	4.45	newtons	N
lbf/in^2	poundforce per square inch	6.89	kilopascals	kPa

APPROXIMATE CONVERSIONS TO SI UNITS

SYMBOL	WHEN YOU KNOW	MULTIPLY BY	TO FIND	SYMBOL
		LENGTH		
mm	millimeters	0.039	inches	in
m	meters	3.28	feet	ft
m	meters	1.09	yards	yd
km	kilometers	0.621	miles	mi

SYMBOL	WHEN YOU KNOW	MULTIPLY BY	TO FIND	SYMBOL
		AREA		
mm^2	square millimeters	0.0016	square inches	in^2
m^2	square meters	10.764	square feet	ft^2
m^2	square meters	1.195	square yards	yd^2
ha	hectares	2.47	acres	ac
km^2	square kilometers	0.386	square miles	mi^2

SYMBOL	WHEN YOU KNOW	MULTIPLY BY	TO FIND	SYMBOL
		VOLUME		
mL	milliliters	0.034	fluid ounces	fl oz
L	liters	0.264	gallons	gal
m^3	cubic meters	35.314	cubic feet	ft^3
m^3	cubic meters	1.307	cubic yards	yd^3

SYMBOL	WHEN YOU KNOW	MULTIPLY BY	TO FIND	SYMBOL
		MASS		
g	grams	0.035	ounces	oz
kg	kilograms	2.202	pounds	lb
Mg (or "t")	megagrams (or "metric ton")	1.103	short tons (2000 lb)	T

SYMBOL	WHEN YOU KNOW	MULTIPLY BY	TO FIND	SYMBOL
		TEMPERATURE (exact degrees)		
°C	Celsius	1.8C+32	Fahrenheit	°F

SYMBOL	WHEN YOU KNOW	MULTIPLY BY	TO FIND	SYMBOL
		ILLUMINATION		
lx	lux	0.0929	foot-candles	fc
cd/m^2	candela/m^2	0.2919	foot-Lamberts	fl

SYMBOL	WHEN YOU KNOW	MULTIPLY BY	TO FIND	SYMBOL
		FORCE and PRESSURE or STRESS		
N	newtons	0.225	poundforce	lbf
kPa	kilopascals	0.145	poundforce per square inch	lbf/in^2

*SI is the symbol for International System of Units. Appropriate rounding should be made to comply with Section 4 of ASTM E380.
(Revised March 2003)

TECHNICAL REPORT DOCUMENTATION PAGE

1. Report No. 000548 63	2. Government Accession No.	3. Recipient's Catalog No.
4. Title and Subtitle Development of Design Parameters for Mass Concrete Using Finite Element Analysis		5. Report Date February 2010 6. Performing Organization Code
7. Author(s) Mang Tia, Christopher Ferraro, Adrian Lawrence, Samuel Smith, and Fiji Ochiai		8. Performing Organization Report No. 000548 63
9. Performing Organization Name and Address Department of Civil and Coastal Engineering 365 Weil Hall – P.O. Box 116580 University of Florida Gainesville, FL 32611-6580		10. Work Unit No. (TRAIS) 11. Contract or Grant No. BD-545 #60
12. Sponsoring Agency Name and Address Florida Department of Transportation 605 Suwannee Street, MS 30 Tallahassee, FL 32399		13. Type of Report and Period Covered Final Report 11/10/05 - 12/15/09 14. Sponsoring Agency Code
15. Supplementary Notes Prepared in cooperation with the U.S. Department of Transportation and the Federal Highway Administration		

16. Abstract

A finite element model for analysis of mass concrete was developed in this study. To validate the developed model, large concrete blocks made with four different mixes of concrete, typical of use in mass concrete applications in Florida, were made and monitored for their temperature and strain developments, and compared with the computed temperature and stress distributions from the finite element model. A parametric analysis was also conducted to determine the effects of various factors on the temperature distribution, induced stresses and the cracking risk. Investigation was also made on testing methods to measure the thermal and mechanical properties of mass concrete needed as input parameters for the finite element model.

The findings from this study are as follows: (1) Results from the isothermal calorimetry test should be used for input for the heat generation function in the finite element modeling of concrete hydration; (2) Reliance on a limiting maximum temperature differential to control cracking in massive concrete applications should be supplemented with a suitable analysis to show that expected stresses will not exceed the strength of the concrete; (3) Adequate insulation should be used in conjunction with the usual formwork material to reduce the temperature differentials during the early age hydration of massive concrete; (4) A safety factor should be applied to the tensile strength values for concrete to guard against the initiation of micro-cracks; and (5) The current restrictions on maximum temperature imposed by state regulating bodies should take into consideration the type of cementitious materials that will be used in the concrete mix.

17. Key Words Mass Concrete, Finite Element Model, Isothermal Calorimetry, Heat of Hydration, Insulation, Temperature Differential, Cracking Risk, Micro-cracks, Parametric Study, Tensile Strength.		18. Distribution Statement No restrictions.	
19. Security Classif. (of this report) Unclassified	20. Security Classif. (of this page) Unclassified	21. No. of Pages 194	22. Price

Form DOT F 1700.7 (8-72) Reproduction of completed page authorized

ACKNOWLEDGMENTS

The Florida Department of Transportation (FDOT) is gratefully acknowledged for providing the financial support for this study. The FDOT Materials Office provided the additional testing equipment, materials, and personnel needed for this investigation. Sincere thanks go to the project manager, Mr. Michael Bergin, for providing his technical coordination and advice throughout the project. Sincere gratitude is extended to the FDOT Materials Office personnel, particularly to Messrs. Charles Ishee, Mario Paredes, Richard DeLorenzo, Craig Roberts, Joseph Fitzgerald, Toby Dillow, Luke Goolsby, Steven Sauls, Fred Yon, Alfred Camps, Duane Robertson, Rahman Henderson, Dr. H. Deford, Ms. Susan Blazo, and Ms.Teresa Risher for their invaluable help in this study. Sincere thanks also go to the support of the staff and students at the Department of Civil and Coastal Engineering at the University of Florida, particularly to Messrs. Chuck Broward, Tony Murphy, Hubert Martin, Boris Haranki, Patrick Bekoe, Christopher Egan, James Falls, Gustavo Morris, and Ms. Carrie Ulm for their technical support in the lab. Special thanks are due to Ms. Candace Leggett for her expert editing of this report.

EXECUTIVE SUMMARY

Background and Research Needs

Mass concrete is defined by the American Concrete Institute (ACI) as "any volume of concrete with dimensions large enough to require that measures be taken to cope with generation of heat from hydration of the cement and attendant volume change, to minimize cracking." The requirements for the control of heat generation and temperature distribution in mass concrete vary on a state-by-state basis. Currently, there is no uniformity on the specifications on mass concrete among the different state department of transportations in the United States. There is a need to have an effective tool which can be used to accurately determine the temperature and stress development in mass concrete elements and the conditions at which cracking may develop, so that mass concrete can be properly specified, controlled, and produced with minimum problems in service.

Research Objectives

The goal of this study is to develop a finite element model of mass concrete, which can predict the temperature distribution during hydration and the thermal stresses that result from the thermal gradients within the structure. Previous attempts at predicting the temperature distribution in mass concrete by way of finite element models has mainly focused on using generic heat generation functions for the calculation of adiabatic temperature rise. The heat generated by hydrating mass concrete has also been widely modeled as being uniform throughout the concrete mass, whereas in reality the heat generation is a function of the temperature and time history of individual locations in the concrete mass. The developed finite element model will use accurately measured thermal and mechanical properties as input parameters, and will take into considera-

tion the time-temperature conditions of individual locations within a hydrating mass concrete structure. A stress analysis utilizing changing strength properties of the concrete will also be conducted and the results compared with the experimental observation as a means of validation.

Another main objective of this study is to develop a test regimen and analysis methodology to provide these necessary input parameters for the finite element model.

Research Approach

The modeling of a mass concrete element is done with the aid of the commercially available TNO DIANA software. The analysis is done in two parts, firstly, a thermal analysis in which the thermal properties are modeled, the hydration process simulated, and the resulting temperature distribution obtained. The second part of the analysis is a stress analysis in which the physical properties such as elastic modulus and coefficient of thermal expansion are used along with the temperature histories obtained in the thermal analysis to calculate the stresses and strains produced by the thermal gradients. The cracking potential is then assessed.

As a means of validation, four different mixes of concrete, typical of use in mass concrete applications in Florida, were produced and each mix used to make two 3.5-ft. × 3.5-ft. × 3.5-ft. concrete blocks. For each mix, one block was insulated on all six sides to simulate a fully adiabatic process, while the other block was insulated on five of the faces with the top face left open and exposed to environmental conditions. Measurements of the temperature and strain at predetermined locations within the blocks were recorded until the equilibrium temperature was achieved.

At the time of casting the blocks, concrete was taken from the same mix and evaluated for mechanical properties at different ages, as well as thermal properties, heat of hydration, specific heat capacity, and thermal diffusivity, which were then used as input to the finite element model.

Finally, a parametric analysis was conducted to determine what effects the size of the concrete structure, amount of insulation used, specific heat capacity, and diffusivity would have on the temperature distribution, induced stresses, and the cracking risk.

Separate physical and thermal testing programs were also conducted to investigate state-of-the-art testing methods and to determine those methods which are suitable as input parameters for analysis of the behavior of mass concrete.

Findings

The two types of tests done on the concrete mixtures to determine the energy released during hydration were semi-adiabatic calorimetry and isothermal calorimetry. The calculated adiabatic energy rise obtained from each test was used in the model to determine which procedure would give the best results when compared with the temperatures measured in the experimental block.

Based on the results of the thermal analysis of the concrete block model, the following findings were made:

- The semi-adiabatic calorimetry test consistently gave lower heat of hydration and lower predicted temperature of concrete as compared with the isothermal calorimetry test.
- The input of adiabatic energy captured in the isothermal calorimetry test provided temperature distributions that were very similar to those measured in the experimental blocks. At some locations, the predicted temperatures were higher than the measured temperatures, and so the isothermal test can be said to provide conservative predictions of the temperature distribution.

The induced stresses caused by the varying temperatures within the concrete element of each mixture were analyzed using the results from the model that utilized the energy from the

isothermal calorimetry test. The results of this structural analysis for the concrete block study led to the following observations:

- The highest tensile stresses were located at the top edge of the surface exposed to ambient conditions.
- Concrete containing 100% Portland cement experienced tensile stresses high enough to cause cracking on all surfaces, even those insulated, when the temperature difference was 17.3° C (31.1° F).
- In the case where 50% of the Portland cement was replaced with ground granulated blast-furnace slag, the rate of hydration reaction, and hence, rate of temperature increase was significantly slower. The associated reduction in early age tensile strength resulted in the cracking risk not being reduced.
- In the case where 35% of the Portland cement was substituted with fly ash, there was little effect on the early age rate of hydration, and thus, the time in which the maximum temperature was achieved was not affected significantly. However, the maximum temperature achieved was itself significantly less. Again, the early age tensile strength was less than the 100% Portland cement case, resulting in similar cracking on all surfaces as before, even though the tensile stresses experienced were less.
- Concrete that had a blend of 50% Portland cement, 30% slag, and 20% fly ash performed the best in terms of reducing the induced thermal stresses relative to the tensile strength, and hence, the cracking potential.
- The temperature differential that induced cracking in the concretes used in this project varied from mixture to mixture. This was due to the corresponding changes in the tensile strength.

The parametric study on factors affecting the temperature distribution in concrete produced the following results:

- The thermal stresses in large mass concrete elements were effectively reduced with the use of thick layers of insulating polystyrene foam. This method is advantageous because the polystyrene foam, if removed carefully, can be reused, often making it

relatively inexpensive when compared to other single-use methods such as cooling pipes and liquid nitrogen.

- Although the tensile stresses that resulted from the removal of formwork and insulation 12 hours, 1 day, 2 days, and 3 days after the pouring concrete were less than the tensile strength of the concrete as measured in the laboratory, the stresses could be large enough to initiate micro-cracking. These micro-cracks can serve as an entry point for deleterious materials that can undermine the durability of the concrete. For insulation removed after 4 days, the tensile stresses were significantly less than the tensile strength, reducing the risk of micro-cracking.

Conclusions

Based on the results obtained in this study, the following conclusions are made:

- The heat of hydration energy data obtained from the isothermal calorimetry test should be used as the input for the heat generation function in the finite element modeling of concrete hydration.
- Reliance on a limiting maximum temperature differential to control cracking in massive concrete applications should be supplemented with a requirement for the presentation of a finite element analysis showing the calculated stress response to the predicted temperature distribution within the concrete, to ensure that the induced tensile stresses will not exceed the tensile strength of the concrete.
- Adequate insulation should be used in conjunction with the usual formwork material to reduce the temperature differentials during the early age hydration of massive concrete. However, caution should be taken, as the occurrence of delayed ettringite formation (DEF) and drying shrinkage due to high concrete temperatures was not studied.
- A safety factor should be applied to the tensile strength values for concrete obtained from the splitting tension and third-point flexural strength tests to guard against the initiation of micro-cracks which, although by themselves, will not cause structural failure, can act as an entry point for deleterious materials which can undermine the durability of the concrete.

- The current restrictions on maximum temperature imposed by state regulating bodies should take into consideration the type of cementitious materials that will be used in the concrete mix.

Recommendations for Future Research

It is recommended that additional blends of cementitious materials and additional large blocks of mass concrete be tested in order to assess the universal applicability of the hypotheses deduced and concluded from this study.

TABLE OF CONTENTS

page

ACKNOWLEDGMENTS vi

EXECUTIVE SUMMARY vii

LIST OF TABLES xvi

LIST OF FIGURES xvii

CHAPTER

1 INTRODUCTION 1
- 1.1 Background 1
- 1.2 Present Specifications on Mass Concrete 3
- 1.3 Research Needs 4
- 1.4 Objective of Study 5
- 1.5 Research Approach 6
- 1.6 Outline of Report 8

2 LITERATURE REVIEW 9
- 2.1 Introduction 9
- 2.2 Tensile Stresses in Mass Concrete 13
  - 2.2.1 Tensile Stresses Due to Thermal Gradients 13
  - 2.2.2 Tensile Stresses Due to Delayed Ettringite Formation 17
- 2.3 Supplementary Cementitious Materials 22
- 2.4 Long Spruce Dam Rehabilitation Project 23
- 2.5 Reinforced Concrete Wall on Basemat Concrete Slab Project 27
- 2.6 The James Bay Concrete Monolith Project 30

3 FINITE ELEMENT THERMAL MODEL 34
- 3.1 Introduction 34
- 3.2 Element Selection 35
- 3.3 Input Parameters 37
  - 3.3.1 Heat of Hydration 37
  - 3.3.2 Conductivity and Heat Capacity 42
  - 3.3.3 Convection 44
- 3.4 Model Geometry 46
- 3.5 Boundary Conditions 46

4 FINITE ELEMENT STRUCTURAL MODEL 49
- 4.1 Introduction 49
- 4.2 Element Selection 49
- 4.3 Material Model 50

4.4 Input Parameters 50
4.4.1 Modulus of Elasticity 50
4.4.2 Poisson's Ratio 51
4.4.3 Coefficient of Thermal Expansion 51
4.4.4 Tensile Strength 52
4.5 Symmetry and Boundary Conditions 52

5 BLOCK EXPERIMENT 53
5.1 Introduction 53
5.2 Concrete Mix Design 53
5.3 Block Geometry 53
5.4 Instrumentation for Data Collection 55
5.5 Temperature Profiles 55

6 MATERIAL TESTS AND PROPERTIES 62
6.1 Introduction 62
6.2 Heat of Hydration 62
6.2.1 Semi-Adiabatic Calorimetry 62
6.2.2 Isothermal Conduction Calorimetry 63
6.3 Specific Heat Capacity 66
6.4 Thermal Diffusivity 67
6.5 Flexural Strength 69
6.6 Splitting Tensile Strength 71
6.7 Modulus of Elasticity and Poisson's Ratio Testing 73
6.8 Coefficient of Thermal Expansion Testing 74
6.9 Summary of Material Properties 75

7 THERMAL ANALYSIS RESULTS 78
7.1 Introduction 78
7.2 Semi-Adiabatic Calorimetry Finite Element Results 81
7.3 Isothermal Calorimetry Finite Element Results 88
7.4 Summary of Findings 96

8 STRUCTURAL ANALYSIS RESULTS 99
8.1 Stress Results 99
8.2 Cracking Potential 105
8.3 Temperature Difference and Cracking 109
8.4 Summary of Findings 114

9 PARAMETRIC STUDY 115
9.1 Introduction 115
9.2 Effect of Specimen Size 115
9.3 Effect of Insulation Thickness 120
9.4 Time of Formwork Removal Effect 128
9.5 Heat Generation Rate Effect 134
9.6 Summary of Findings 135

10 RECOMMENDED TESTING REGIMEN FOR MASS CONCRETE 136
10.1 Recommended Testing Method for Measurement of Heat Generation 136
10.2 Recommended Testing Method for Measuring Maturity/Equivalent Age 137
10.3 Recommended Testing Methods for Strength and Modulus of Elasticity 138
10.3.1 Compressive Strength 138
10.3.2 Compressive Modulus of Elasticity 138
10.3.3 Tensile Strength 139
10.4 Recommended Testing Method for Measurement of Coefficient of Thermal Expansion 139
10.5 Recommended Physical Parameter for the Concrete Diffusivity 140
10.6 Recommended Physical Parameter for the Specific Heat Capacity 140
10.7 Summary of Testing Program 141

11 CONCLUSIONS AND RECOMMENDATIONS 142
11.1 Findings 142
11.2 Conclusions 144
11.3 Recommendations for Future Research 145

LIST OF REFERENCES 146

APPENDIX
A GRAPHICAL USER INTERFACE INPUT COMMANDS A-1
B BATCH FILE INPUT COMMANDS B-1
C STAGGERED ANALYSIS COMMANDS C-1
D PHASED ANALYSIS COMMANDS D-1
E METHOD OF TESTING FOR MEASURING THE HEAT OF HYDRATION OF HYDRAULIC CEMENT USING ISOTHERMAL CONDUCTIVE CALORIMETRY E-1

LIST OF TABLES

Table		page
2-1	Cementitious Material Content for Concrete Materials	10
2-2	FDOT Bridge Environmental Database Results	10
2-3	Mass Concrete Requirements per State Agency	12
2-4	Typical Cementitious Content used for Mass Concrete	14
3-1	Example of Direct Input of Concrete Internal Heat Production	36
3-2	Example of Adiabatic Temperature Rise Input	36
3-3	Cementitious Content of Each Mixture	40
5-1	Mix Designs of Concrete Used in the Large-Scale Blocks	54
6-1	Thermal Properties of Concrete	75
6-2	Thermal Properties of Plywood and Polystyrene	75
6-3	Modulus of Elasticity and Tensile Strength of Concrete	76
6-4	Poisson's Ratio and Coefficient of Thermal Expansion of Concrete	77

LIST OF FIGURES

Figure page

1-1 Typical temperature characteristics of a mass concrete element 2

1-2 Stress and strength versus time plots showing time of crack initiation..... 3

2-1 Effect on the heat of hydration of Portland cement when substituting with an Italian natural pozzolan (Massazza and Costa 1979) 23

2-2 K and α values of adiabatic temperature rise (Radovanic 1998) 25

2-3 Locations for temperature and stress measurements in a reinforced concrete wall (Machida and Uehara 1987) 27

2-4 Thermocouple and strain gage locations in the James Bay concrete monolith (Ayotte et al. 1997)..... 31

3-1 Elements used to model early age concrete behavior: A) Twenty-node isoparametric solid brick element CHX60; B) Eight-node isoparametric brick element HX8HT 35

3-2 Four-node isoparametric boundary element BQ4HT 37

3-3 Adiabatic temperature rise of each concrete mixture obtained from semi-adiabatic calorimetry testing 39

3-4 Hydration power of each cementitious mixture obtained from isothermal calorimetry testing..... 40

3-5 Adiabatic temperature rise of each concrete mixture calculated from the hydration power obtained in the isothermal calorimetry testing of cementitious mixtures..... 41

3-6 One-dimensional conduction heat transfer..... 42

3-7 Differential volume for a rectangular solid 43

3-8 Convection heat transfer..... 45

3-9 Finite element model of concrete block with insulation 46

3-10 Ambient temperatures during experimental block monitoring 47

3-11 External temperatures imposed on finite element model representing the ambient conditions of the laboratory..... 48

4-1 Twenty-node isoparametric solid brick element CHX60..... 50

4-2 Symmetry conditions and supports of model 52

5-1 Experimental block geometry 54

5-2 Uninsulated (left) and insulated (right) mass concrete block specimens 55

5-3 Thermocouple location (plan) 56

5-4 Thermocouple location (section)..... 56

5-5 Instrumentation layout for experimental block 57
5-6 Temperatures along the center line of the uncovered concrete block Mix 1 58
5-7 Temperatures 2 in. from the side of the uncovered block in Mix 1 58
5-8 Temperatures along the center line of the uncovered block in Mix 2 59
5-9 Temperatures along the center line of the uncovered block in Mix 3 60
5-10 Temperatures along the center line of the uncovered block in Mix 4 61
6-1 Resultant semi-adiabatic calorimetric energy curve for Mix 1 63
6-2 Resultant isothermal calorimetric curves with regard to energy versus time for Mix 1 64
6-3 Resultant isothermal calorimetric curves with regard to energy versus equivalent Age for Mix 1 64
6-4 Resultant isothermal calorimetric curves with regard to energy versus equivalent Age for Mix 2 65
6-5 Resultant isothermal calorimetric curves with regard to energy versus equivalent Age for Mix 3 65
6-6 Resultant isothermal calorimetric curves with regard to energy versus equivalent Age for Mix 4 66
6-7 Schematic of the specific heat capacity calorimeter 67
6-8 Thermal diffusivity vs. age of the experimental blocks 68
6-9 Beam specimens for flexural strength testing 69
6-10 Beam specimen undergoing flexural strength testing 70
6-11 Theoretical stress and strain distribution through beam cross section 70
6-12 The modulus of rupture of the beam specimens taken from Mixes 1, 2, 3 and 4 71
6-13 Diagrammatic arrangement of splitting tension test ASTM C496 72
6-14 Splitting tensile strength of concrete used in Mixes 1, 2, 3 and 4 72
6-15 Compressive modulus of elasticity versus time 73
6-16 Tensile modulus of elasticity versus time 74
6-17 Coefficient of thermal expansion versus time for each mixture 74
7-1 Thermocouple location (plan) 79
7-2 Thermocouple location (section) 79
7-3 Degree of hydration at the center and top of the block in Mixture 1 80
7-4 Equivalent age at the center and top of the block in Mixture 1 80
7-5 Concrete quarter block with insulation at time step 1 81

7-6 Semi-adiabatic and experimentally measured temperature-time histories at the center of the block, 2 in. below the exposed top surface of Mixture 1 82

7-7 Semi-adiabatic and experimentally measured temperature-time histories at the center of the block, 4 in. below the exposed top surface of Mixture 1 83

7-8 Semi-adiabatic and experimentally measured temperature-time histories at the center of the block, 21 in. below the exposed top surface of Mixture 1 84

7-9 Semi-adiabatic and experimentally measured temperature-time histories at the center of the block, 2 in. below the exposed top surface of Mixture 2 85

7-10 Semi-adiabatic and experimentally measured temperature-time histories at the center of the block, 4 in. below the exposed top surface of Mixture 2 85

7-11 Semi-adiabatic and experimentally measured temperature-time histories at the center of the block, 21 in. below the exposed top surface of Mixture 2 86

7-12 Semi-adiabatic and experimentally measured temperature-time histories at the center of the block, 2 in. below the exposed top surface of Mixture 3 87

7-13 Semi-adiabatic and experimentally measured temperature-time histories at the center of the block, 4 in. below the exposed top surface of Mixture 3 87

7-14 Semi-adiabatic and experimentally measured temperature-time histories at the center of the block, 21 in. below the exposed top surface of Mixture 3 88

7-15 Semi-adiabatic and experimentally measured temperature-time histories at the center of the block, 2 in. below the exposed top surface of Mixture 4 89

7-16 Semi-adiabatic and experimentally measured temperature-time histories at the center of the block, 4 in. below the exposed top surface of Mixture 4 89

7-17 Semi-adiabatic and experimentally measured temperature-time histories at the center of the block, 21 in. below the exposed top surface of Mixture 4 90

7-18 Isothermal and experimentally measured temperature-time histories..... 91

7-19 Isothermal and experimentally measured temperature-time histories at the center of the block, 4 in. below the exposed top surface of Mixture 1 91

7-20 Isothermal and experimentally measured temperature-time histories at the center of the block, 21 in. below the exposed top surface of Mixture 1 92

7-21 Isothermal and experimentally measured temperature-time histories at the center of the block, 2 in. below the exposed top surface of Mixture 2 93

7-22 Isothermal and experimentally measured temperature-time histories at the center of the block, 4 in. below the exposed top surface of Mixture 2 93

7-23 Isothermal and experimentally measured temperature-time histories at the center of the block, 21 in. below the exposed top surface of Mixture 2 94

7-24 Isothermal and experimentally measured temperature-time histories..... 95

7-25 Isothermal and experimentally measured temperature-time histories at the center of the block, 4 in. below the exposed top surface of Mixture 3 95

7-26 Isothermal and experimentally measured temperature-time histories at the center of the block, 21 in. below the exposed top surface of Mixture 3 96

7-27 Isothermal and experimentally measured temperature-time histories at the center of the block, 2 in. below the exposed top surface of Mixture 4 97

7-28 Isothermal and experimentally measured temperature-time histories at the center of the block, 4 in. below the exposed top surface of Mixture 4 97

7-29 Isothermal and experimentally measured temperature-time histories at the center of the block, 21 in. below the exposed top surface of Mixture 4 98

8-1 Location of elements analyzed for stress 100

8-2 Stress state at the top center and center of the finite element concrete block with Mixture 1 100

8-3 Stress state at the top edge and center edge of the finite element concrete block with Mixture 1 101

8-4 Stress state at the top center and center of the finite element concrete block with Mixture 2 102

8-5 Stress state at the top edge and center edge of the finite element concrete block with Mixture 2 102

8-6 Stress state at the top center and center of the finite element concrete block with Mixture 3 103

8-7 Stress state at the top edge and center edge of the finite element concrete block with Mixture 3 104

8-8 Stress state at the top center and center of the finite element concrete block with Mixture 4 104

8-9 Stress state at the top edge and center edge of the finite element concrete block with Mixture 4 105

8-10 Crack index for elements along the center line of block with Mixture 1 106

8-11 Crack index for elements along the edge of block with Mixture 1 107

8-12 Top surface of experimental block containing mixture 1 showing numerous cracks along the edges 107

8-13 Crack index for elements along the center line of block with Mixture 2 108

8-14 Crack index for elements along the edge of block with Mixture 2 108

8-15 Crack index for elements along the center line of block with Mixture 3 109

8-16 Crack index for elements along the edge of block with Mixture 3 110

8-17 Crack index for elements along the center line of block with Mixture 4 110

8-18 Crack index for elements along the edge of block with Mixture 4 111

8-19 Induced stress with respect to temperature differential for Mixture 1 112

8-20 Induced stress with respect to temperature differential for Mixture 2 112
8-21 Induced stress with Respect to temperature differential for Mixture 3 113
8-22 Induced stress with respect to temperature differential for Mixture 4 114
9-1 Comparison of temperature profiles calculated at the center of each block..... 116
9-2 Calculated peak temperature values with respect to block size 116
9-3 Effect of concrete block size on the maximum internal temperature difference..... 117
9-4 Comparison of stresses at the center of the top surface of each block 117
9-5 Comparison of stresses at the top surface edge of each block 118
9-6 Maximum induced stress with respect to maximum temperature differential as a result of increasing block size 119
9-7 Plot of maximum stress versus maximum temperature difference with respect to block size and type of concrete used 119
9-8 Plot of maximum stress versus maximum temperature gradient with respect to block size and type of concrete used 120
9-9 Temperature profiles with respect to time 2 in., 4 in., and 21 in. below the top surface of the block insulated with a 1.5-in. thick layer of polystyrene foam 121
9-10 Temperature profiles with respect to time 2 in., 4 in., and 21 in. below the top surface of the block insulated with a 6.0-in. thick layer of polystyrene foam 121
9-11 Comparison of temperature profiles with respect to time 2 in. below the top surface of the blocks with varying thicknesses of polystyrene foam insulation 123
9-12 Comparison of temperature profiles with respect to time 4 in. below the top surface of the blocks with varying thicknesses of polystyrene foam insulation 123
9-13 Comparison of temperature profiles with respect to time 21 in. below the top surface of the blocks with varying thicknesses of polystyrene foam insulation 124
9-14 Temperatures calculated at the side and center of a concrete block with 1.5-in. thick insulation 124
9-15 Temperatures calculated at the side and center of a concrete block with 3.0-in. thick insulation 126
9-16 Temperatures calculated at the side and center of a concrete block with 6.0-in. thick insulation 126
9-17 Comparison of experimentally measured and calculated temperature profiles 2 in. below the top surface at the centerline of concrete block with 3.0-in. thick insulation 127
9-18 Comparison of experimentally measured and calculated temperature profiles 4 in. below the top surface at the centerline of concrete block with 3.0-in. thick insulation 127

9-19 Variation in maximum temperature differential within the concrete with respect to insulation thickness for each block size 128

9-20 Effect of reduction of temperature differential caused by increasing insulation thickness on the maximum induced stress 129

9-21 Effect of insulation thickness on the maximum induced stress in each block size 129

9-22 Plot of stress versus time at a point on the center of the surface of the concrete block when formwork is removed 12 hours after casting 131

9-23 Plot of stress versus time at a point on the center of the surface of the concrete block when formwork is removed 1 day after casting 131

9-24 Plot of stress versus time at a point on the center of the surface of the concrete block when formwork is removed 2 days after casting 132

9-25 Plot of stress versus time at a point on the center of the surface of the concrete block when formwork is removed 3 days after casting 132

9-26 Plot of stress versus time at a point on the center of the surface of the concrete block when formwork is removed 4 days after casting 133

9-27 Plot of stress versus time at a point on the center of the surface of the concrete block when formwork is removed 6 days after casting 133

9-28 Temperature profiles with respect to time at the center of a concrete block with varying heat generation rates 134

CHAPTER 1
INTRODUCTION

1.1 Background

Whenever fresh concrete is used in the construction of large structures such as foundations and dams, consideration is always given to the amount of heat that will be generated and the resulting volume change. Volume changes occur due to temperature changes in the structure, which initially increase as the concrete hydrates and decrease as the reaction is exhausted. Temperature difference per unit distance between one point and another in a structure is called a thermal gradient. Temperature gradients are produced when the heat being generated in the concrete is dissipated to the surrounding environment, causing the temperature at the surface of the concrete to be lower than the temperature at the interior of the concrete. This temperature drop at the surface results in the contraction of the concrete. With the interior of the concrete being more mature than the surface, it acts as a restraint against the contraction, creating tensile stresses in the surface. Since the concrete is still in its early age, its full tensile strength is not developed, and if the tensile stresses are larger than the early age tensile strength, cracking will occur.

The behavior of concrete in its early age is influenced by the heat generated, which, by extension, dictates the temperature distribution during hydration. The temperature profile of a concrete element is further affected by the specific heat capacity, thermal diffusivity, and emissivity of the concrete, and by external factors such as the environmental temperature, wind speed and precipitation. At the same time, the rate of development of mechanical strength of concretes in early age increases with increasing temperature, and hence, can be expressed as a function of temperature and time.

As depicted in Figure 1-1, the central region of the mass concrete in early age experiences high but uniform temperatures while the temperature in the outer region decreases as we move closer to the surface. Since the maturity of concrete and strength are functions of temperature, the central region of the mass concrete structure will be more mature and stronger than the outer region.

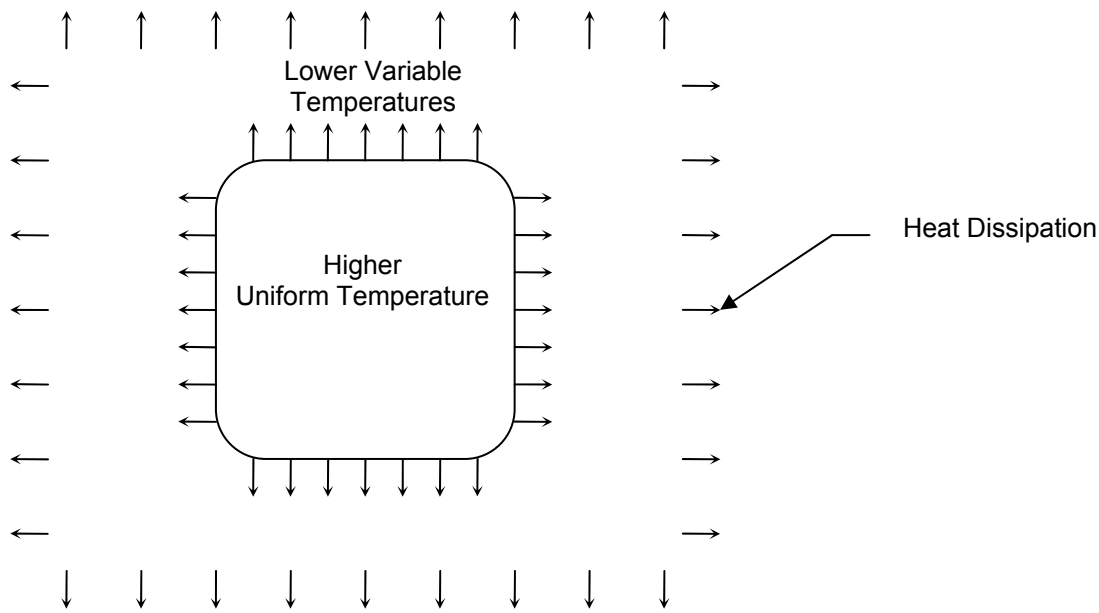

Figure 1-1. Typical temperature characteristics of a mass concrete element.

As the concrete hydrates faster in the middle, large thermal gradients are produced, and strength and maturity decreases as the distance to the surface decreases. Since the concrete in the outer region of mass concrete is being cooled by the atmospheric environment, contraction will occur. Restraint against this contraction will cause tensile stresses and strains to develop, creating the possibility that cracks will occur at or close to the surface of the concrete. These cracks will initiate when the tensile stresses exceed the low tensile strength at the surface as depicted in Figure 1-2. The magnitude of the tensile stresses are dependent on the thermal differential in the mass concrete, the coefficient of thermal expansion, modulus of elasticity,

creep or relaxation of the concrete, and the degree of restraint in the concrete. If cracking does occur, it will ultimately affect the ability of the concrete to withstand its design load and allow the infiltration of deleterious materials, which undermine durability.

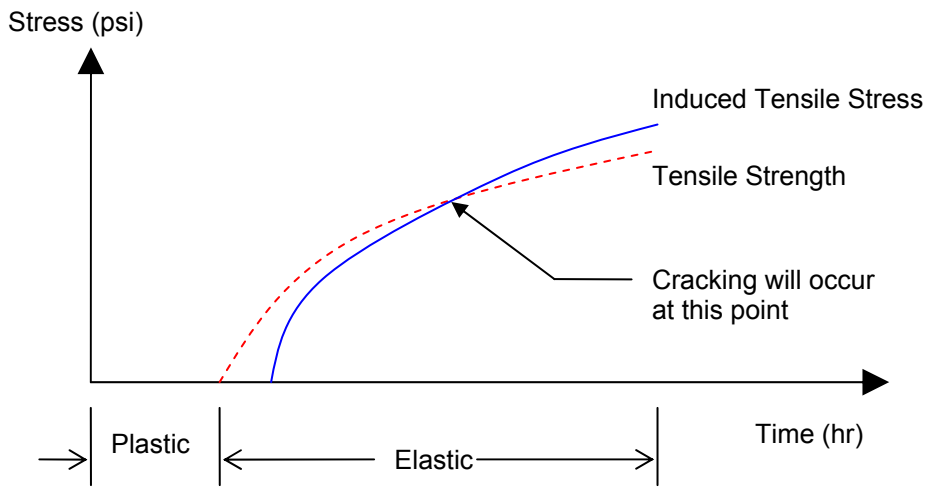

Figure 1-2. Stress and strength versus time plots showing time of crack initiation.

1.2 Present Specifications on Mass Concrete

The requirements for the control of heat generation and temperature distribution in mass concrete vary on a state-by-state basis. Currently, there is no agreement on the specifications of mass concrete.

The specifications of the Florida, Iowa, Virginia, and West Virginia Departments of Transportation currently include a requirement that the temperature differential in elements designated as mass concrete be controlled to a maximum of 35 degrees Fahrenheit (35° F) or 20 degrees Celsius (20° C).

Colorado's specification states that the temperature differential between the midpoint and a point 2 inches (in.) inside the exposed face of all mass concrete elements shall not exceed 45° F

(25° C) as measured between temperature sensors. It further states that the maximum peak curing temperature of all mass concrete elements shall not exceed 165° F (74° C).

The state of Delaware's specification calls for a range of maximum differential temperatures based on the number of hours after casting of the concrete as follows:

First 48 hours	40° F (22.2° C)
Next 2 to 7 days	50° F (27.8° C)
Next 8 to 14 days	60° F (33.3° C)

North Dakota's Department of Transportation specifies that measures and procedures should be taken to maintain, monitor, and control the temperature differential of 50° F (27.8° C) or less between the interior and exterior of the mass concrete element.

1.3 Research Needs

There are apparent disparities in the maximum allowable temperature differential in mass concrete structures among the different state departments of transportation (DOT's). It is not clear how the various states have arrived at their respective specification values. There is a need to have an effective tool which can be used to accurately determine the temperature and stress development in mass concrete elements and the conditions at which cracking may develop, so that mass concrete can be properly specified, controlled, and produced with minimum problems in service.

Past research leading to the creation of numerical models for the prediction of temperature distribution in mass concrete has mainly focused on using generic heat generation functions for the calculation of adiabatic temperature rise. The use of actual measured heat of hydration results from calorimetry testing of the concrete paste has been mostly neglected. At the same time, attempts at modeling hydrating mass concrete (Radovanic 1998) have treated the heat

generated by the reacting cement as being uniform throughout the concrete mass, whereas in reality, the heat generation is a function of the temperature and time history of the concrete at individual locations in the concrete mass. Different locations in a mass concrete element have different time-temperature conditions and will have different effects on heat generation of the concrete.

This research is aimed at formulating a finite element model, using the actual measured heat of hydration and, taking into consideration the non-homogeneity of heat generation within concrete, to accurately predict the distribution of temperature in a hydrating concrete mass and the associated thermal stresses and strains. Knowledge of these phenomena will allow for a reasonably accurate prediction of the location and potential for cracking of concrete, as well as the use of proper measures to reduce possible problems in mass concrete.

1.4 Objective of Study

The goal of the research is to develop a finite element model of mass concrete, which is based on the input of measured thermal and mechanical characteristics that can predict the temperature distribution during hydration and the thermal stresses resulting from the thermal gradients within the structure. Previous attempts at predicting the temperature distribution in mass concrete by way of finite element models has mainly focused on using generic heat generation functions for the calculation of adiabatic temperature rise. The heat generated by hydrating mass concrete has also been widely modeled as being uniform throughout the concrete mass, whereas in reality, the heat generation is a function of the temperature and time history of individual locations in the concrete mass. The developed finite element model will take into consideration the time-temperature conditions of individual locations within a hydrating mass concrete structure. A stress analysis utilizing changing strength properties of the concrete will

also be conducted and the results compared with the experimentally measured strain data as a means of validation.

Another main objective of this study is to develop a test regimen and analysis methodology to provide the necessary input parameters for the finite element model. The specific properties of concrete needed as input parameters include the following:

1) Heat generation rate
2) Specific heat capacity
3) Thermal diffusivity
4) Coefficient of thermal expansion
5) Compressive strength
6) Tensile and flexural strength
7) Compressive modulus of elasticity
8) Tensile modulus of elasticity

1.5 Research Approach

The modeling of a mass concrete element is done with the aid of the commercially available TNO DIANA software. The analysis is done in two parts, first a thermal analysis, in which the thermal properties are modeled, the hydration process simulated, and the resulting temperature distribution obtained. The second part of the analysis is a stress analysis in which the physical properties, such as elastic modulus and coefficient of thermal expansion, are used along with the temperature histories obtained in the thermal analysis to calculate the stresses and strains produced by the thermal gradients. The cracking potential is then assessed.

As a means of validation, four different mixes of concrete, typical of use in mass concrete applications in Florida, were produced and each mix used to make two 3.5-ft. × 3.5-ft. × 3.5-ft. (1.07-m × 1.07-m × 1.07-m) concrete blocks. For each mix, one block was insulated on all six

sides to simulate a fully adiabatic process, while the other block was insulated on five of the faces with the top face left open and exposed to environmental conditions. Measurements of the temperature and strain at predetermined locations within the blocks were recorded until the equilibrium temperature was achieved.

At the time of casting the blocks, concrete taken from the same mix was used to perform the evaluation of small-scale samples which were then stored at 73° F ± 2° F (23° C ±1° C) and 100% relative humidity until the time of testing for the mechanical properties at ages of 1 day, 2 days, 3 days, 7 days, 14 days, and 28 days. Tests for the thermal properties, heat of hydration, specific heat capacity, and thermal diffusivity were also done at these ages.

Finally, a parametric analysis was conducted to determine what effects the size of the concrete structure, amount of insulation used, specific heat capacity, and diffusivity would have on the temperature distribution, induced stresses, and the cracking risk.

Separate physical and thermal testing programs were developed to investigate state-of-the-art testing methods and to determine which of those methods are suitable as input parameters for analysis of the behavior of mass concrete.

The thermal testing regimen consisted of the following:

1) Isothermal conduction calorimetry;
2) Semi-adiabatic calorimetry;
3) Sure-Cure/adiabatic calorimetry;
4) Heat of solution calorimetry (ASTM C186);
5) Thermal diffusivity (CRD C 36-73); and
6) Specific heat capacity.

The physical testing regimen involved the following tests:

1) Compressive strength (ASTM C39/109);
2) Compressive modulus of elasticity (ASTM C469);

3) Splitting tensile strength (ASTM C496);
4) Flexural Strength (ASTM C-78);
5) Tensile Modulus of elasticity; and
6) Coefficient of thermal expansion (AASHTO TP60).

1.6 Outline of Report

Chapter 2 is a review of the literature citing specifications currently in use and other attempts at modeling the behavior of mass concrete. Chapters 3 and 4 discuss the finite element model input parameters, material model, element type, and boundary conditions used in the thermal and stress analyses, respectively.

Chapter 5 discusses the mix proportions of the concrete used in the experimental blocks, as well as, the types and location of the monitoring instruments used.

Chapter 6 describes the test procedures carried out on concrete specimens sampled directly from the concrete used in the construction of the experimental blocks.

Chapters 7 and 8 present and discuss the results obtained from the finite element analyses, with comparisons of the analytical results of the temperature distribution and stress state with those measured in the experimental blocks.

Chapter 9 presents a parametric study of mass concrete elements of varying sizes and levels of insulation in order to determine the limiting temperature gradient to prevent thermal cracking.

Chapter 10 presents the recommendations for a testing regimen for characterizing the thermal and mechanical properties of mass concrete, which are needed as input parameters to the finite element model.

Chapter 11 presents the findings and conclusions from this study, and recommendations for future research efforts.

CHAPTER 2
LITERATURE REVIEW

2.1 Introduction

More recently, *American Concrete Institute (ACI) Specifications for Structural Concrete* (ACI 301-05) has made provisions pertaining to mass concrete within the Optional Requirements Checklist, which identifies actions required by the architect/engineer to include the following: "Designate portions of the structure to be treated as either plain mass concrete or reinforced mass concrete. Whether or not concrete should be designated as mass concrete depends on many factors, including weather conditions, the volume-surface ratio, rate of hydration, degree of restraint to volume change, temperature and mass of surrounding materials, and functional and aesthetic effect of cracking. In general, heat generation should be considered when the minimum cross-sectional dimension approaches or exceeds 2.5 ft.(760 mm) or when cement contents above 600 lb/yd^3 (356 kg/m^3) are used. The requirements for each project however, should be evaluated on their own merits" (ACI 301-R05).

The ACI 301 document defines mass concrete by both a minimum dimension and a minimum cementitious content. However, to consider any concrete with a total cementitious content above 600 lb/yd^3 (356 kg/m^3) to be mass concrete is not a practical requirement for concrete construction in the state of Florida. Table 2-1 lists the structural classifications of concrete as per Section 346 of "Florida Department of Transportation (FDOT) Road and Bridge Construction." Per Table 2-1, any structural concrete with requirements above a Class II bridge deck is required to have a total cementitious content above 608 lb/yd^3 (361 kg/m^3). The *FDOT Structures Manual* states all structural elements exposed to a moderately or severely aggressive environment must be made of Class IV, V, or VI concrete.

Table 2-1. Cementitious Material Content for Concrete Materials

Class of Concrete	Minimum Total Cementitious Materials Content (lb/yd^3)	Maximum Water Cementitious Materials Ratio (lb/lb)
I (Pavement)	508	0.50
I (Special)	508	0.50
II	564	0.49
II Bridge Deck	611	0.44
III	611	0.44
III (Seal)	611	0.52
IV	658	0.41
IV (Drilled Shaft)	658	0.41
V (Special)	752	0.37
V	752	0.37
VI	752	0.37

A general survey of the FDOT's bridge environmental database was used to determine the approximate percentage of bridge structures which are located in moderately or severely aggressive environments in the state of Florida. Table 2-2 provides the number of bridges in Florida and the classification of each.

Table 2-2. FDOT Bridge Environmental Database Results

Total number of bridges in Florida*	11,734
Number of bridges in the FDOT Bridge Environmental Database	6,800
Number of bridges in severely or moderately aggressive environments	3,262
Percentage of bridges in severely or moderately aggressive environments	48%

*Per National Bridge Inventory Records

Therefore, if the construction industry within the state of Florida adopted the Optional Requirements Checklist from ACI 301-R05, then a large percentage of the structural concrete produced in the state would be considered mass concrete.

Many state departments of transportation (DOTs) define mass concrete with a minimum dimension or in a volumetric manner similar to ACI 207. The *FDOT Structures Manual* defines mass concrete to be the following:

1) "All Bridge components Except Drilled Shafts: When the minimum dimension of the concrete exceeds 36-inches and the ratio of volume of concrete to the surface area is greater than 12-inches, provide for mass concrete. (The surface area for this ratio includes the summation of all the surface areas of the concrete component being considered, including the full underside (bottom) surface of footings, caps, construction joints, etc.) Note volume and surface area calculations in units of feet.

2) Drilled Shafts: All drilled shafts with diameters greater than 72-inches shall be designated as mass concrete and a Technical Special Provision may be required" (FDOT 2009).

Seventeen out of the fifty state DOTs have requirements incorporated into the definition and the conditions of mass concrete structural elements. Table 2-3 provides a summary of the requirements for mass concrete regarding minimum dimension for the classification of mass concrete elements, specifications for maximum placing temperature, maximum allowable curing temperature, and maximum allowable temperature differential (Chini et al. 2003).

As per Table 2-3, the FDOT does not have requirements on the maximum placement temperature nor the maximum allowable temperature in mass concrete. The FDOT requires that a temperature control plan be submitted to and accepted by the State Materials Office (SMO) prior to the placement of mass concrete on a given project. Therefore, the FDOT may decide not to accept a given concrete mixture design as provided by the contractor.

A survey of mixes within the FDOT SMO database was performed to determine the typical cementitious material type and content mass concrete mix design. The database contains mass concrete mix design information for mixes used in the state of Florida between 1980 and the present.

Table 2-3. Mass Concrete Requirements per State Agency

State	Minimum Dimension (ft)	Maximum Placement Temperature (° F)	Maximum Curing Temperature (° F)	Maximum Temperature Differential (° F)
Arkansas	-	75	-	36
California	6.5	-	160	Specified by thermal control plan provided by contractor
Colorado	5	-	165	45
Delaware	Determined on project basis	-	160	First 48 hrs = 40° F 2-7 days = 50° F 8-14 days = 60° F
Florida	3 (structural) / 6 (drill shaft)	-	185	35
Georgia	-	-	-	50
Illinois	-	-	160	35
Indiana	-	-	-	35
Iowa	3.9	65	160	35
Kentucky	-	-	160	35
Minnesota	-	-	160	35
Nebraska	-	-	176	27
North Carolina	-	75	-	36
North Dakota	-	-	160	50
South Carolina	-	80	-	35
Texas	-	75	-	35
Virginia	5	-	170 (slag) 160 (fly ash)	35
West Virginia	4	-	160	35

Table 2-4 provides a brief summary of 32 typical mix designs used for mass concrete. The mix designs include the use of Type II cement, replacement of Portland cement with Grade 100, granulated blast furnace slag, or Type F fly ash. A search of the FDOT database revealed that, since 1980, the FDOT has not accepted a mass concrete mix design that does not incorporate supplementary cementitious materials. Type II Portland cement produces less heat during the process of hydration than Type I cement (ASTM C 150). Supplementary cementitious materials (as a replacement for Portland cement) generate less heat than concrete mixes which utilize Portland cement alone (Malhotra and Mehta 1996). The physical and chemical attributes of supplementary cementitious materials are discussed in further detail in subsequent chapters.

2.2 Tensile Stresses in Mass Concrete

As stated earlier, tensile stresses are the primary cause of failure of mass concrete structures. Tensile stresses in mass concrete typically evolve from two primary sources: thermal gradients throughout the concrete structure; and delayed ettringite formation.

2.2.1 Tensile Stresses Due to Thermal Gradients

Thermal gradients are primarily induced by heat loss from the outer surface of the mass concrete structure. As cement hydrates, it produces heat increasing the temperature of the concrete. Should the outer surface of the concrete be exposed to external temperatures lower than those developed inside the structure by hydration, a temperature gradient will be created. Large differences in temperature will lead to thermal stresses that can result in cracking. This phenomenon is intensified by the use of cements high in tri-calcium silicate (C_3S) and/or tri-calcium aluminate (C_3A), as these compounds are responsible for the majority of early heat development. It can also be intensified by cements with higher fineness, resulting in faster

Table 2-4. Typical Cementitious Content used for Mass Concrete

Name	FDOT Class	Cement Type	Cement (lbs)	Fly Ash (lbs)	Blast Furnace Slag (lbs)	Fly Ash (%)	Blast Furnace Slag (%)
Mix #1	IV	II	610	134	0	18.01	0
Mix #2	IV	II	600	132	0	18.03	0
Mix #3	IV	II	359	83	0	18.78	0
Mix #4	IV	I	625	150	0	19.35	0
Mix #5	IV	II	314	77	0	19.69	0
Mix #6	IV	II	584	146	0	20	0
Mix #7	IV	II	576	144	0	20	0
Mix #8	II	II	457	115	0	20.1	0
Mix #9	II	II	344	83	0	19.44	0
Mix #10	II	II	329	0	115	0	25.9
Mix #11	IV	II	500	200	0	28.57	0
Mix #12	IV Drilled Shaft	II	523	257	0	32.95	0
Mix #13	IV	II	500	260	0	34.21	0
Mix #14	IV	II	428	230	0	34.95	0
Mix #15	IV Drilled Shaft	II	478	257	0	34.97	0
Mix #16	II	II	500	270	0	35.06	0
Mix #17	IV	II	438	243	0	35.68	0
Mix #18	IV	II	438	292	0	40	0
Mix #19	IV	II	450	383	0	45.98	0
Mix #20	IV Drilled Shaft	II	440	390	0	46.99	0
Mix #21	IV	II	346	320	0	48.05	0
Mix #22	II	II	296	274	0	48.07	0
Mix #23	II	II	296	274	0	48.07	0
Mix #24	IV	II	336	329	0	49.47	0
Mix #25	II	II	196	0	196	0	50
Mix #26	IV	II	450	450	0	50	0
Mix #27	IV	II	330	0	330	0	50
Mix #30	V	II	370	0	520	0	58.43
Mix #31	IV Drilled Shaft	I/II	290	0	436	0	60.06
Mix #32	IV	II	200	0	460	0	69.7

reaction due to increased surface area (Price 1974; Poole 2004; Neville 1995; Woods et al. 1933; Larsen 1991; Higginson 1970).

As shown in Table 2-3, those DOTs which have requirements for mass concrete also specify limitations on the maximum allowable temperature gradients for early-age mass concrete. Most of these DOTs require a maximum temperature differential of 35° F (19.4° C), which has become the most commonly used temperature differential for mass concrete applications today. This approach was based on the data collected from a project involving the construction of small concrete dams in England more than 50 years ago (Gajda 2007). Although no readily available laboratory data confirms the suitability of a maximum temperature differential of 35° F (19.4° C), it is nonetheless still required in many mass concrete specification documents today.

The exact magnitude of the temperature gradient depends on a number of factors, including the initial concrete temperature, the ambient temperature around the structure, and the thermal properties of the concrete itself. A number of early-age concrete properties affect the thermal attributes of concrete, including heat development, tensile strength development, coefficient of thermal expansion, thermal diffusivity, resultant strain gradients, temperature gradients, and the chemistry of the cement paste. Supplementary cementitious materials can dramatically reduce the amount of heat generated.

One of the principal difficulties in predicting cracking of concrete during hydration is that the tensile stresses develop before the concrete has reached its ultimate strength. Under certain conditions, such stresses can develop while portions of the concrete placement are still in the plastic state, resulting in plastic shrinkage cracking. To model mass concrete performance

throughout the early hydration stage (wherein heat generation is maximized), it is first necessary to characterize the development of stress-strain behavior of the concrete.

Stresses due to thermal gradients within a mass structure change over time, as does the stress-strain behavior of the concrete. The relative magnitude of these two variables is important when considering the potential for cracking. In at least one instance, published research has claimed that thermal gradients can be mitigated by using faster hydrating cements, asserting that tensile strength develops faster than the thermally induced tensile stresses (Lindstrom and Westerberg 2003). Though intriguing as a possibility, this research did not consider the rate of development of tensile elastic modulus. While strength could very well develop more rapidly than the thermal stresses, stiffness may possibly increase at an even faster pace. This would result in a lack of strain capacity that would lead to cracking due to thermal expansion. To account for the effect of these interrelated factors, the stress-strain behavior of concretes at different ages and temperatures must be investigated.

Additionally, past research has focused on the compressive strength of the concrete when determining its resistance to applied stresses. Though compressive strength is the primary design parameter in mass concrete, thermal cracking is inherently a tensile phenomenon. Thus, the tensile strength properties are critically important in the modeling of mass concrete behavior. Unfortunately, tensile strength of concrete can be very difficult to measure with traditional techniques that are either extremely difficult to perform (direct tension) or insensitive to early micro-cracking (splitting tension) (Bremner et al. 1998; Boyd and Mindess 2002; Boyd and Mindess 2004). An alternative method for determining tensile properties is to test the tensile modulus of elasticity using flexural beam testing.

2.2.2 Tensile Stresses Due to Delayed Ettringite Formation

Delayed ettringite formation (DEF) is a form of internal sulfate attack on concrete that can lead to severe cracking and damage and eventual material failure. During the hydration of Portland cement under normal conditions, ettringite forms as a result of the chemical reaction between C_3A and gypsum. The ettringite then further reacts with the remaining C_3A to produce monosulfoaluminate, a relatively inert compound. Gypsum is added to cement in order to force this ettringite formation and prevent flash set of the C_3A. As long as the ettringite forms while the concrete is still plastic, it is essentially harmless.

Under high temperatures, however, the ettringite is destroyed and its components sulfate and aluminate are absorbed by the calcium-silicate-hydrate (C-S-H) in the hydrated cement paste. After cooling, the sulfate is released and again becomes available to form ettringite. Ettringite is an especially crystalline compound with a high aspect ratio that can form long needle-like crystals. Once nucleation has occurred, ettringite crystals tend to grow lengthwise. Even when the tips of the crystals encounter solid material, the growth continues, resulting in very high localized stresses that lead to expansion and cracking of the hydrated cement paste matrix.

The exact temperature required for the formation of DEF has been extensively debated. The majority of available research reports 158° F (70° C) as the minimum temperature necessary for the formation of DEF (Lawrence 1998; Taylor 1997; Gajda 2007; Drimalas 2004). Most of the DOT specifications listed in Table 2-2 require a maximum curing temperature of 160° F (71° C) for mass concrete structures in an effort to avoid the onset of DEF. However, there are specific conditions necessary for the initiation of DEF. Even in the presence of high temperatures, it only occurs within cements with large amounts of sulfur trioxide (SO_3)(4%),

alkalis, or magnesium oxide (MgO), and in the presence of moisture. However, the exact effect of cement chemistries is not fully understood (Taylor 1997).

The combination of high curing temperatures and moist environments is most common in two situations: pre-cast concrete exposed to steam curing; and massive concrete members in a damp environment (drilled shaft piles, foundations, abutments, etc.). To avoid DEF in mass concrete, it is necessary to prevent the temperature rise in the concrete from exceeding the threshold value at which ettringite nucleation occurs. The exact threshold temperature is affected by several factors though little information is currently available concerning these parameters for Florida concretes.

DEF can be difficult to diagnose, especially at the early ages necessary for this research. The minute scale of the crystals makes them impossible to find using optical microscopy, and their formation does not change the chemical composition of the bulk hydrated cement paste, thereby making traditional chemical analysis inadequate. The ettringite crystals themselves do exhibit a unique chemical makeup from the rest of the paste, but they form due to chemical realignment in the paste, and thus any reasonable sample size will exhibit the same chemical makeup as it did before DEF formation.

Identification of ettringite alone is not sufficient to indicate DEF, since ettringite does form during normal hydration and can be left over if the C_3A/gypsum balance of the cement is not perfect. Small amounts of late-forming DEF are also harmless and could actually be beneficial since they will initially fill in any voids in the hydrated cement paste, thus densifying the microstructure and improving strength and permeability. This is commonly called *secondary ettringite* formation (Skalny et al. 2002). Only when sufficient ettringite forms to expand beyond

the allowable void space does it become a problem. Such incidents are evidenced by cracks in the microstructure initiating from the ettringite crystals.

A rigorous literature search was performed in an effort to properly address the relevant issues concerning DEF and mass concrete structures in Florida. As previously stated, DEF is a form of internal sulfate attack which is a result of the high heat of hydration coupled with sulfates in the cement paste and a relatively high C_3A content of the cement (Ghorab 2002).

The FDOT permits the use of supplementary cementitious materials to replace Portland cement in the construction of massive elements in which the core temperature of the concrete is expected to exceed 165° F (74° C). FDOT specification allows use of 18% to 50% Portland cement replacement of fly ash and 50% to 70% replacement of ground blast furnace slag to ensure lower heats of hydration (FDOT 2007). Currently, all mass concrete construction in the state of Florida utilizes Class F fly ash or slag as a major constituent of the cementitious material in the concrete mix design. A significant portion of the literature review was dedicated to the effect of fly ash and slag on DEF and sulfate attack of concrete materials and structures. It has been shown that using 25% fly ash or 25% slag replacement in concrete mitigates the physical mechanisms of DEF (Ramlochan et al. 2003). Similar findings have been reported by other researchers (Lane and Ozyildrum 1999; Miller and Conway 2003; Thomas et al. 2008).

Despite the fact that the separate physiochemical mechanisms that cause internal sulfate attack (DEF) and external sulfate attack are different, the expansive nature of the resultant product (ettringite) is the same for both. Consequently, the literature review included the study of external sulfate attack on ordinary and mass concrete and the effect of fly ash and slag on the mitigation of sulfate attack. "The use of fly ash and blast furnace slag in making sulfate-resisting concrete has frequently been reported" (Bhatty and Taylor 2006). Other researchers have

reported similar findings (Skalny et al. 2002; Malhotra and Mehta 1996; Schlorholtz and Bergeson 1993).

Research has also been performed to evaluate massive concrete structures which have shown deterioration due to sulfate attack. Several bridge structures in Europe were investigated to determine the nature of sulfate attack and the possible mechanisms of the deterioration. The study determined that the most likely cause of initial cracking was thermal expansion. The sulfate attack which took place after the initial cracking was more likely to be due to an external sulfate source rather than from within (Divet and Pavione 2002). The initial cracking of the structure was attributed to a severe temperature differential between the outer concrete strata and the internal core. Upon the initiation of the initial cracking, it was determined that the presence of moisture and sulfate from the environment, rather than internal sulfate attack or DEF contributed to years of deterioration (Divet and Pavione 2002).

More recently, DEF has been found in a mass concrete bridge structure that is currently in service. The bridge structure was diagnosed with alkali silica reaction (ASR) in some portions, DEF in others, and some of the structure was considered to be free of significant damage. This is the first well-documented case of DEF occurring in a concrete structure in which the temperature rise of the concrete was due solely to internal hydration (i.e., the structure was not steam cured). Interestingly, the structure that sustained damage due to ASR and DEF was concrete which did not contain supplementary cementitious materials. The portion of the structure that was free of significant damage contained fly-ash (Thomas et al. 2008).

Research has been performed investigating the use of granulated blast furnace slag as a partial replacement of Portland cement in mortars exposed to high temperatures. The results of this research indicate that mortars which use 30% and 50% granulated blast furnace slag

experience damage due to expansion or DEF when exposed to curing temperatures of 208° F (98° C) (Kelham 2002). Thus, it is likely that mass concrete containing large replacements of supplementary cementitious materials approved per the FDOT standard specification for road and bridge construction will not be subject to DEF due to the following reasons:

- Temperatures necessary to cause the dissolution DEF at early ages are less likely within concrete structures containing supplementary materials;
- Addition of supplementary materials mitigates the damage produced by DEF; and
- DEF in massive structures containing supplementary cementitious materials is less likely as the near surface temperature is less than the core temperature. However, the core temperature is less likely to be exposed to moisture due to the relatively large amount of concrete cover.

As a result of the literature review, as well as interviews conducted with FDOT personnel and several onsite visits, it was determined that the factors most relevant to cracking in massive structures are thermal stresses induced by a thermal gradients. Therefore, the DEF study was altered to include a rigorous study of the components which are most likely to contribute to large thermal gradients in massive concrete structures. The major components are as follows:

- High internal heats of hydration caused by the concrete mix design;
- Poor insulation of mass concrete at early ages;
- Mix designs which utilize too much cementitious material; and
- The use of cements with high heats of hydration.

Along with FDOT personnel interviews, a review of the current practice of the development of thermal control plans for mass concrete construction was conducted to determine which issues contribute to thermal gradients in mass concrete. The majority of FDOT construction using mass concrete involves bridge components in severely aggressive environments. Per the FDOT standard specification, Type II Portland cement must be used on projects constructed in aggressive environments. Consequently, this research will investigate the chemical and physical

properties of concrete mixes using primarily Type II cement enhanced with Type F fly ash and/or ground blast furnace slag. Concrete with Type I Portland cement will also be studied for comparison purposes.

2.3 Supplementary Cementitious Materials

The temperature rise in the centers of large concrete sections is approximately proportional to the cement content used in the mix design of the concrete. This temperature rise is affected by the rate at which heat is developed due to the hydration of the cement. The rate and quantity of heat generated is further affected by the fineness and chemical composition of the Portland cement. Cements with high C_3A content tend to hydrate rapidly producing high adiabatic temperature rises.

The most direct way of reducing the temperature rise in concrete is by lowering the cement content in the concrete mix design. However, this cannot always be done due to strength and durability restrictions, hence the use of supplementary cementitious materials such as fly ash (FA) and ground granulated blast-furnace slag (GGBF) as an effective way of reducing the temperature in the concrete without compromising the strength and durability. This reduction in the temperature rise is due to the slower rate of hydration reaction that occurs in concretes with these materials. Figure 2-1 shows the effect of increasing the percent content of these supplementary cementitious materials on the heat of hydration.

There is, however, a negative to replacing a percentage of Portland cement with fly ash and or blast-furnace slag in concrete. It has been observed that for a given strength, blended cement concretes tend to be less ductile, resulting in a higher elastic modulus, lower creep, and a reduced strain capacity (Bamforth 1984). It is important therefore to ensure that the percentage of replacement will result in temperatures low enough to compensate for the loss of ductility.

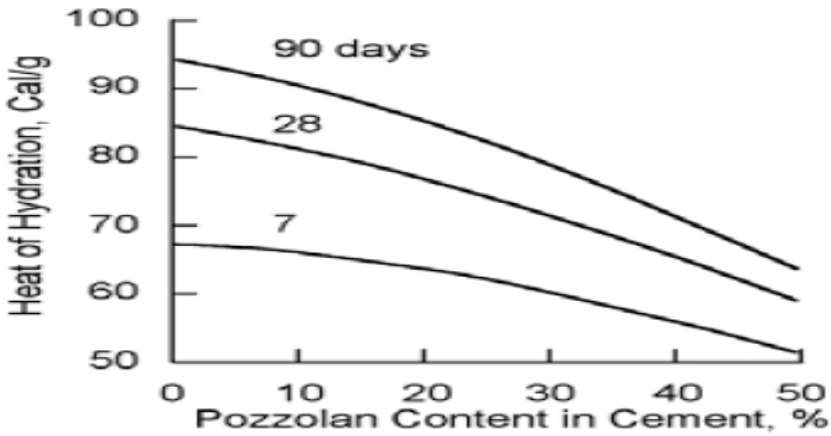

Figure 2-1. Effect on the heat of hydration of Portland cement when substituting with an Italian natural pozzolan (Massazza and Costa 1979).

2.4 Long Spruce Dam Rehabilitation Project

The Long Spruce Dam in northern Manitoba, Canada, was found to have a crack that runs from the downstream side to the upstream side of the structure. In order to perform an effective rehabilitation procedure, an in-depth analysis to understand the stresses involved in the failure of the crack was undertaken. A two-dimensional finite element analysis with the aid of the commercial software, ANSYS, was conducted to achieve this goal.

Two theoretical models, namely a transient thermal model and a transient stress model, were developed to predict the early stage behavior of the concrete used in the construction of the dam. The finite element analysis sought to investigate whether the residual thermal stresses caused by the heat of hydration of the massive concrete pour were responsible for the apparent loss of strength in the construction joints. The early thermal behavior of a 0.6-m × 0.6-m laboratory concrete specimen and a dam structure model consisting of an upper and lower block cast 102 hours apart were modeled and observed. The thermal qualities of interest were the temperature field, thermal flux, and thermal gradient.

The thermal properties of the concrete in the laboratory specimen model were assumed to be independent of time and temperature during hydration. The thermal conductivity was assigned a constant value of 4.1 KJ/m-hr-°C, and the specific heat 1971 KJ/m^3-°C, obtained from literature. The ambient temperature in the laboratory analysis was also kept constant at 73° F (23° C) to represent a controlled environment.

For the dam structure model, the thermal properties were slightly different to reflect the use of larger aggregate. The initial temperature of the concrete was set at 50° F (10° C) because of the use of ice water to pre-cool the large blocks. The boundary condition of convection is imposed on all sides, except the bottom where a prescribed temperature is described. For the stress analysis, the bottom surface is constrained in all directions, representing the contact friction of the block resting on the floor.

The analysis for the laboratory specimen model was conducted in six-hour load steps. The beginning of thermal process in the dam structure model was analyzed every six hours, then increased to every 12 hours, and then finally every 24 hours.

The adiabatic temperature rise resulting from the heat of hydration was calculated using the expression developed and presented by Tanabe et al. (1986) in Seminar Proceedings for Finite Element Analysis of Reinforced Structure, Tokyo, Japan, in 1985, and published by the American Society of Civil Engineers (ASCE) the following year:

$$T(t) = K(1 - e^{-\alpha t}) \tag{2-1}$$

where T = temperature (° C);
t = time (days);
K = constant based on casting temperature (° C); and
α = constant based on casting temperature.

The values for K and α are obtained from the plots in Figure 2-2.

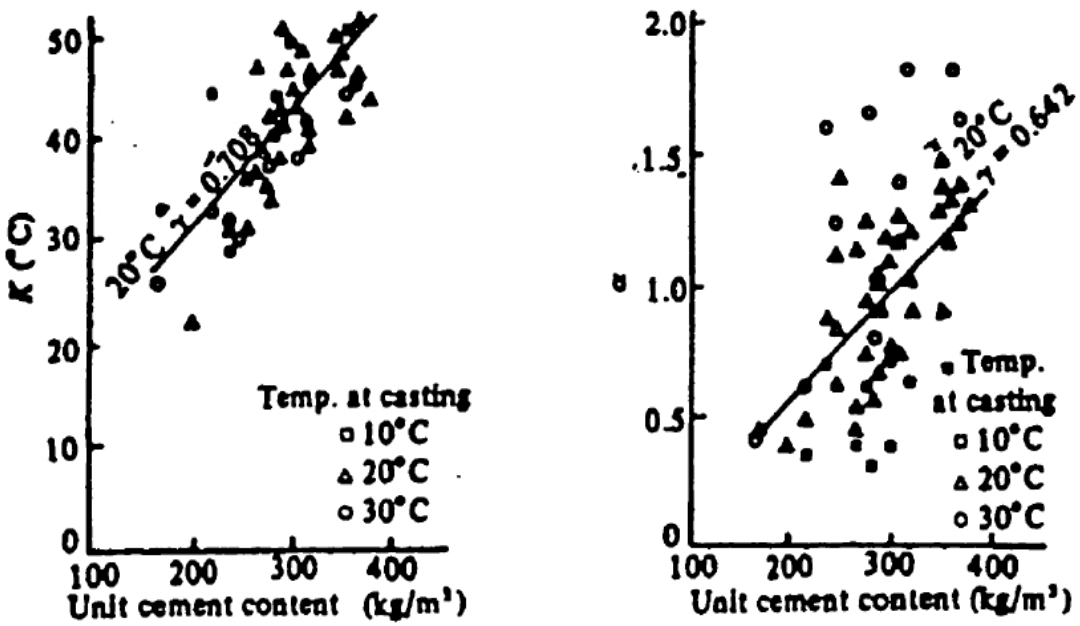

Figure 2-2. K and α values of adiabatic temperature rise (Radovanic 1998).

The total amount of heat generated was then calculated by the following equation:

$$Q(t) = C_p r_T(t) = KC_p r\,(1 - e^{-\alpha t}) \qquad (2\text{-}2)$$

where C_p = specific heat capacity of the concrete (J/g-°C);
r_T = density of the concrete (g/m^3);
t = time (days);
K = constant based on casting temperature (° C); and
α = constant based on casting temperature;

and the rate of heat generation calculated as:

$$R(t) = KC_p r\alpha e^{-\alpha t} \qquad (2\text{-}3)$$

where C_p = specific heat capacity of the concrete (J/g-°C);
r_T = density of the concrete (g/m^3);
t = time (days);
K = constant based on casting temperature (° C); and
α = constant based on casting temperature.

The highest temperature was found to occur in the middle section of the specimen and decreased as it got closer to the sides of the model. This confirms the theory that the outer section of the concrete loses heat more quickly than the middle because of its greater exposure to the atmospheric conditions.

Radovanic (1998) found that the 0.6-m × 0.6-m laboratory specimen was too small to realistically predict the behavior of massive concrete structures. This led to the enlargement of the FE model by the two, five and ten orders of magnitude. The size that came closest to a realistic characterization of the behavior of the Long Spruce Dam was the 6-m × 6-m model. However, the maximum temperature for this size model was much higher than the dam specimen. The reason given by Radovanic (1998) was that the dam specimen was cast in September, when the outside temperature was much lower than the initial temperature used for the laboratory specimen. Radovanic (1998) concluded that assumptions made in the calculation of the heat generation rates, material properties, and boundary conditions were reasonable and that the finite element algorithm was accurate enough to predict the early age thermal behavior of the laboratory concrete specimen and dam.

A finite element stress analysis of the laboratory specimen and the dam were conducted. As a worse case scenario, the maximum stress occurring in the models was considered as the residual stress. The process of hardening was implemented by calculating the development of the modulus of elasticity of the concrete with time based on the ACI charts. Radovanic (1998) concluded that the results of the analysis showed that the stresses produced by the thermal gradients were significant enough to cause cracking in the early age concrete.

2.5 Reinforced Concrete Wall on Basemat Concrete Slab Project

As part of a field study (Machida and Uehara 1987), a wall structure consisting of reinforced concrete measuring 1.0-m thick, varying height of between 3.9 m and 4.73 m, and 15.0-m long, was cast on a 1.5-m thick basemat concrete slab. The wall was instrumented with thermocouples, effective stress meters, mold type strain gages, and non-stress strain gages, to capture the temperatures, strain, and stress responses at different locations within the wall, as shown in Figure 2-3. The measurement time interval used for this instrumentation setup was 1 hour in the first three days, 3 hours until the seventh day, and 6 hours until the thirtieth day, the last day of the experiment.

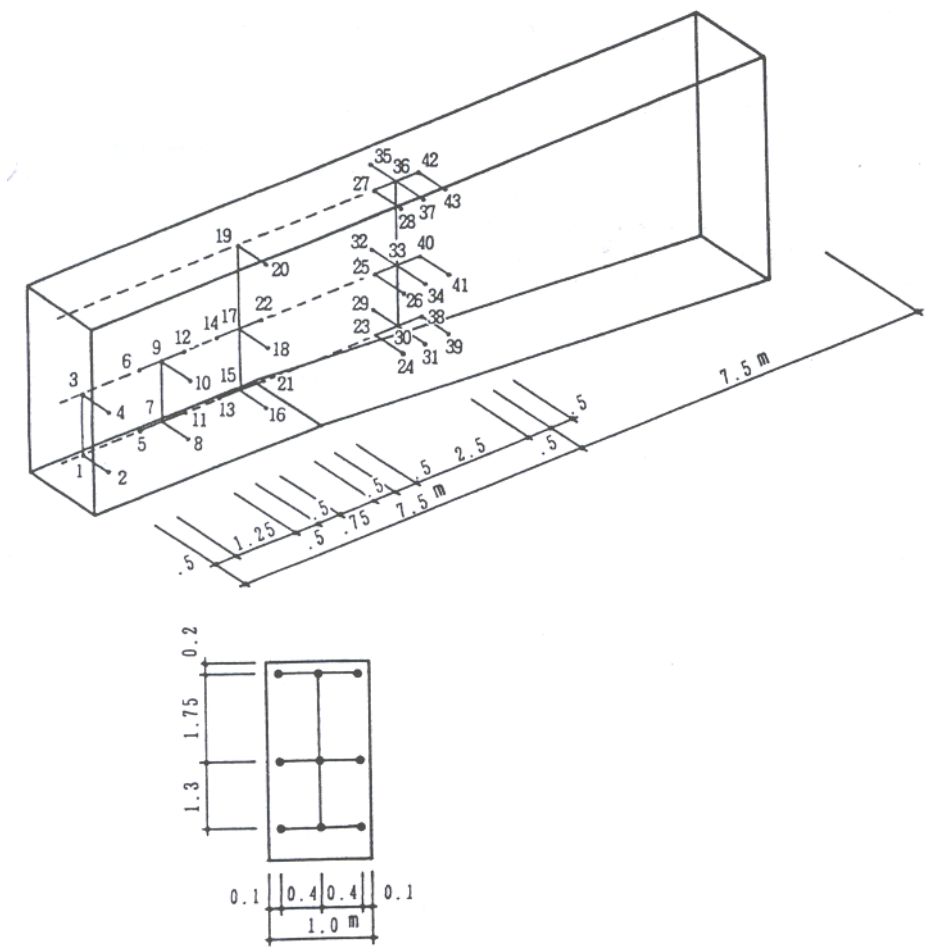

Figure 2-3. Locations for temperature and stress measurements in a reinforced concrete wall (Machida and Uehara 1987).

The concrete stress and strain condition immediately after placing was unstable, with recordings becoming stable after 6 hours. The tensile strength was measured using the cleavage test, and the elastic modulus taken as the secant modulus of one-third the collapse strength. The stress-strain relation of one of the non-stress gages was used to calculate the coefficient of thermal expansion which was then assumed to be a constant value throughout the experiment.

A finite element model of half of the concrete wall, basemat slab, and the soil beneath was created to evaluate and forecast cracking in the concrete wall. This was achieved by conducting a heat transfer analysis of the heat of hydration of the cement, and the phenomena of heat conduction and convection, followed by a thermal stress analysis for the mechanical characteristics.

Although the atmospheric temperature of the actual structure varied day by day, a fixed temperature of 72° F (22° C) was assumed for this analysis. The heat generation rate for the concrete used in the wall was calculated by differentiating with respect to time the equation for adiabatic temperature rise developed by Tanabe et al. (1986),

$$q = 1/24\ KC_p r\alpha e^{-\alpha t/24}\ \ (\text{kcal/m}^3\text{h}) \tag{2-4}$$

where C_p = specific heat capacity of the concrete (cal/g-°C);
r_T = density of the concrete (g/m^3);
t = time (hours);
K = constant based on casting temperature (° C); and
α = constant based on casting temperature.

A comparison of the thermal analysis results with the experimental results revealed that the maximum measured temperature occurred along the mid-length of the wall and was 3.8° F (2.1° C) higher than the maximum analytical temperature which also occurred along the mid-length of the wall model. After the peak temperature was obtained, the analytical temperature

decrease was larger than the experimental, but after 12 days the temperature of the structure equaled the ambient temperature. The difference in the estimation of temperature decrease was attributed to the difference in the assumed heat convectivity in the model and the actual convection, and the variance in atmospheric temperature of the experimental wall instead of the assumed constant temperature in the model.

The stress analysis model was similar to the one used in the thermal analysis. It was assumed that no sliding took place between the basemat and the subsoil. The degrees of freedom were constrained in the direction perpendicular to the structural symmetry plane and perpendicular to the outside surface plane of the subsoil. The compressive and tensile strengths and elastic modulus of the wall were calculated using empirical formulas that related their development with the temperature of the hydrating concrete. Constant values for the Poisson's ratio and coefficient of thermal expansion were also assumed.

The results showed that the maximum expansion in the structure was recorded after 24 hours. The maximum compressive stress occurred in the mid-length one day after concrete placement in both the experiment and finite element analysis. The compressive stress became a tension stress in the middle and bottom of the wall as the concrete aged.

The experiment showed that the upper mid-length of the structure experienced a small compression peak at 18 hours which then became a tensile stress, peaking after about 2 days becoming a compressive stress again peaking at 8 days after placement. On the other hand, the finite element analysis results showed no clear compressive stress peak, but a tensile peak at 60 hours, after which it began to decrease but remained in the tensile stress region. Again, the difference in the measured and analytical results for the mid-length point close to the surface was

attributed to the real atmospheric conditions of the structure being different than the assumed constant values assigned in the finite element model.

2.6 The James Bay Concrete Monolith Project

The James Bay concrete monolith project (Ayotte et al. 1997), a joint effort between the Société d'énergie de la Baie James (SEBJ) and the École Polytechnique de Montréal, focused on developing a methodology, based on finite elements, that could be used to predict the heat generated and resulting thermal stresses in mass concrete. The project included both an experimental component and a modeling component.

Three concrete monoliths were built directly on bedrock in the St. James Bay Territory in Northern Quebec, Canada, on the site of a major hydroelectric project. The dimensions of the monoliths were 2-m wide, 10-m long, and 2- to 3-m high, with the height depending on the bedrock profile. Each monolith was instrumented with 26 T-type (Copper-Constantan alloy) thermocouples to monitor temperature distribution with time, and 8 pairs of mechanical strain targets on the skin reinforcement to measure the induced strain (see Figure 2-4). To observe the performance of the concrete when subjected to severe freeze-thaw cycles, the monoliths were cast in February inside large individual heated shelters in which the temperature was maintained at 86° to 90° F (30° to 32° C) during the construction phase.

Two- and three-dimensional modeling of the concrete thermal behavior was conducted using the finite element software, ADINA-T, while the mechanical response, stresses, and strains were obtained using ADINA. To accommodate simultaneous changes of temperature and mechanical property, a modeling technique which employed a step-by-step incremental approach of calculating the thermally induced strains was developed to bypass the link between ADINA-T and ADINA.

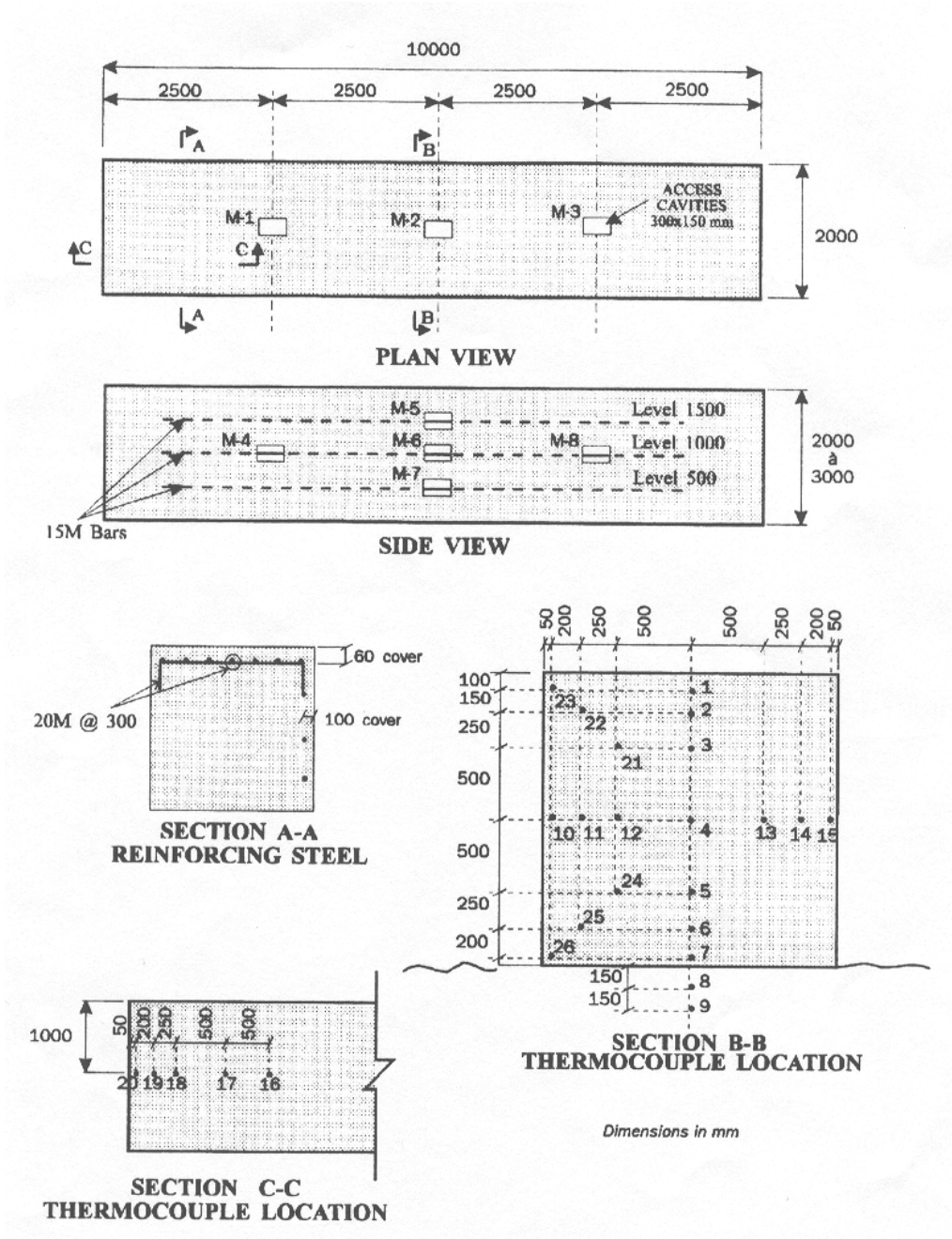

Figure 2-4. Thermocouple and strain gage locations in the James Bay concrete monolith (Ayotte et al. 1997).

The cement type used was Portland cement Type 20M, which was specially made for Hydro-Quebec, so a generic function for the heat of hydration as a function of time was obtained by interpolating between the known functions of Type 20 and Type 50 cements, which was then calibrated by comparing the calculated temperatures with the temperatures measured by the

thermocouples. The values for other concrete thermal properties, which included specific heat, the thermal conductivity, and convection coefficient, were obtained from various literature sources. Radiation was not considered because the monoliths were built inside shelters which blocked the heat radiation. Convection boundary conditions were used to model the heat loss to the ambient air, while rock elements were added below the concrete elements for heat dissipation through the rock foundation.

The structural model for the monolith was identical to the three-dimensional model used in the thermal analysis. Displacements were restricted in the directions of the planes of symmetry and in all directions at the bottom of the rock elements. The mechanical properties, which included elastic modulus, and compressive and tensile strengths, were modeled as varying with time, while the coefficient of thermal expansion was given a constant value of 10 $\mu\varepsilon/°C$. To include creep and relaxation, an effective reduced elastic modulus that accounts for the reduction in stresses was adopted. The computation of the incremental stresses was done by modifying the ADINA file containing the temperatures from the thermal analysis by calculating the incremental temperature,

$$\Delta T_i = T_i - T_{i-1} \tag{2-5}$$

then computing the incremental stresses in which the current Young's Modulus E_i at each step is used,

$$\Delta\sigma = E_i \, \Delta\varepsilon = E_i \, \alpha(\Delta T_i - 0) \tag{2-6}$$

Then finally, the total stresses were obtained using the previous time step (σ_{i-1})

$$\sigma_i = \sigma_{i-1} + \Delta\sigma_i \tag{2-7}$$

Ayotte et al. (1997) found that the calculated temperature at the center of the monolith model followed almost perfectly the temperatures measured experimentally. However, there was a gap between the temperatures calculated at a point near the top of the monolith and those experimentally measured. In the structural analysis, they found that the largest strains were located at the top of the monolith where there was the least restraint, while the strains at the base were very small due to the restraint of the foundation. It was also observed that the stress variation on the top surface of the monolith was in tension while compressive stresses were computed on the vertical faces due to the insulating effect of the formwork which limited the temperature difference between this surface and the core.

CHAPTER 3
FINITE ELEMENT THERMAL MODEL

3.1 Introduction

The modeling of the early age thermal behavior of concrete was conducted with the aid of the commercially available TNO DIANA software package. This software package was chosen because it offers a wide range of material models for the analysis of non-linear concrete material behavior, including the behavior of young hardening concrete. It can make the assessment of the temperature development due to the cement hydration and the computation of the associated stress development within the concrete mass. Main modeling features utilized are:

- Equivalent age calculation;
- Temperature and time dependent material properties; and
- Crack index calculation to assess risk of cracking.

The finite element analysis utilized DIANA's 'staggered flow-stress analysis' feature, in which the thermal analysis is combined with a subsequent structural analysis. The model comprises two domains: one for the thermal flow analysis; and one for the structural analysis. These domains overlap for a considerable part of the analysis and so reside in a domain called the 'flow-stress domain'.

Formwork used in the construction of massive concrete structures, including plywood and polystyrene foam, was explicitly modeled. Since researchers were interested only in their effects on the transfer of the thermal energy generated by the concrete, these materials were modeled with flow elements, and thus, are only active in the thermal analysis. The concrete, however, is active in both the thermal analysis and structural analysis, and therefore, lies in the flow-stress domain. For this reason, the concrete is modeled with a quadratically interpolated structural element that is converted during the thermal analysis to a linearly interpolated flow element.

3.2 Element Selection

As stated above, the concrete in this analysis is active in the flow-stress domain, and therefore, is modeled with a structural element. For this, researchers selected the structural element CHX60, a three-dimensional twenty-node brick element that is converted to the three-dimensional eight-node HX8HT isoparametric brick element for the thermal analysis. Both types of elements shown in Figure 3-1 have coinciding corner nodes. However, because the structural CHX60 element is quadratically interpolated, and element HX8HT is a linearly interpolated element, the mid-nodes of the CHX60 are disregarded in the thermal analysis. The basic theory and required material properties needed for the structural analysis with element CHX60 will be discussed in further detail in Chapter 4.

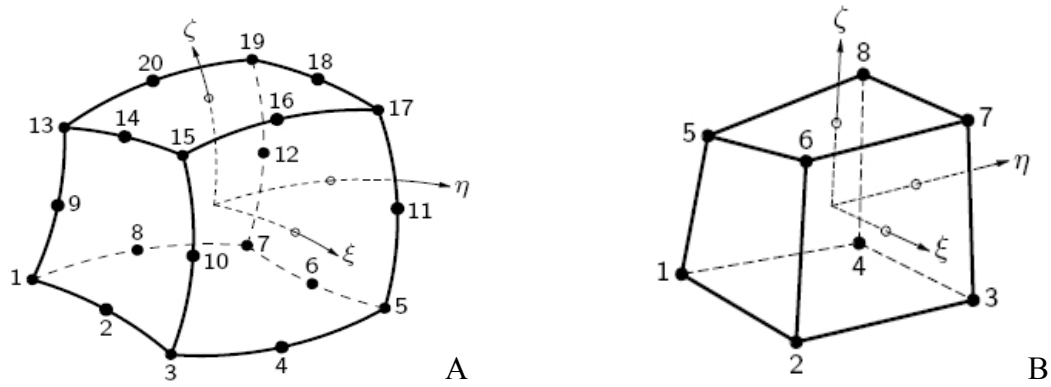

Figure 3-1. Elements used to model early age concrete behavior:
A) Twenty-node isoparametric solid brick element CHX60;
B) Eight-node isoparametric brick element HX8HT.

Element HX8HT is effective in simulating the phenomenon of convection-diffusion and is especially useful for the analysis of heat transfer problems. It utilizes linear interpolation and Gauss integration with a $2 \times 2 \times 2$ integration scheme. Heat transfer is modeled by assigning the thermal conductivity and heat capacity of the concrete, where the conductivity can be modeled as isotropic, orthotropic, or anisotropic, while the heat capacity is always isotropic. Both the

conductivity and capacitance may be constant or depend on temperature, or time or both. For the model described in this paper, both the conductivity and heat capacity were modeled as constant.

Additional properties used to model the internal heat generation of the concrete are the Arrhenius constant (activation energy divided by the universal gas constant) and the heat generation function, which can either be a table that provides a direct description of the heat production rate with respect to the degree of hydration as shown in Table 3-1, or a table that describes the adiabatic temperature rise in degrees Celsius (° C) with respect to time as shown in Table 3-2.

Table 3-1. Example of Direct Input of Concrete Internal Heat Production

Degree of Hydration	0.10	0.20	0.25	0.40	0.5	0.60	0.75	0.90	1.0
Heat Production Rate (J/m^3-hr)	0.320	0.850	0.960	1.00	0.890	0.400	0.230	0.060	0.00
Total Heat Produced (J/m^3)	3.23e4								
Maximum Value of Heat Production Rate (J/m^3-hr)	7.5e9								
ARRHEN	5000								

Table 3-2. Example of Adiabatic Temperature Rise Input

ADIAB	0.0	23.0
	0.1	25.5
	0.2	31.8
	0.3	34.3
	0.4	38.7
	0.5	44.1
	1.0	50.9
	2.0	54.6
	3.0	57.4
	4.0	61.6
	5.0	66.7
	6.0	69.5
	8.0	73.3
	10.0	75.3
	70.0	75.3
ARRHEN	5000	

The plywood and polystyrene were directly modeled with element HX8HT (using the conductivity and heat capacity of each as input parameters) to describe the way the heat would be transferred among the concrete, plywood, and polystyrene.

The boundary convection was modeled using the BQ4HT element, shown in Figure 3-2, which is a four-node isoparametric quadrilateral element specially used to describe boundaries in three-dimensional thermal analyses. It uses linear interpolation and Gauss integration in its computational scheme. The four nodes in this element were modeled to coincide with the corner nodes of the surface of the brick elements they lay on.

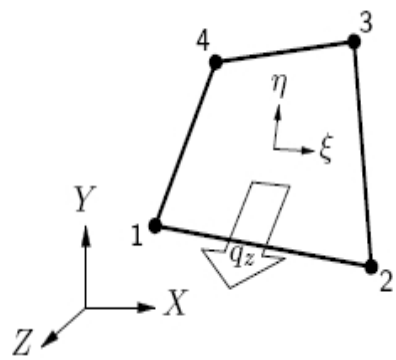

Figure 3-2. Four-node isoparametric boundary element BQ4HT.

3.3 Input Parameters

3.3.1 Heat of Hydration

To properly model the behavior of hydrating concrete, knowledge of the heat produced during the hydration reaction, as well as both the material properties of the concrete itself and the environmental conditions in which it is placed, are needed.

As previously stated, the heat produced during hydration is a function of the temperature history of the concrete. The momentary heat production rate is defined as

$$qv(r,T) = \alpha \cdot q_r(r) \cdot q_T(T) \tag{3-1}$$

where r = degree of reaction;
T = temperature (° C);
α = maximum value of the heat production rate (J/m^3-hr);
q_r = degree of reaction dependent heat production (J/m^3-hr); and
q_T = temperature dependent heat production (J/m^3-hr); and

$$q_T(T) = e^{\frac{E_a / R(r,T)}{T+273}} \tag{3-2}$$

in which E_a = activation energy of the concrete J/mol; and
R = universal gas constant, 8.3144 J/mol-°C.

The heat production rate, which is dependent on degree of reaction (q_r,), can also be determined by DIANA using preprocessing. The temperature history produced under adiabatic hydration conditions is used as the input in this case. DIANA derives the heat production q(t) from

$$q(t) = c(T,r)\frac{\partial T}{\partial t} \tag{3-3}$$

where $c(T,r)$ = capacitance dependent on temperature and degree of reaction.

DIANA then approximates the degree of reaction and the temperature dependent heat production,

$$r_m = \frac{Q_m}{Q_n} \tag{3-4}$$

$$Q_m \approx \sum_{i=1}^{m} c(T_i^*, r_i^*)\Delta T_i \tag{3-5}$$

where n = specified time points; and
m = 1,…,n;

and

$$\Delta T = T_i - T_{i-1} \tag{3-6}$$

$$r_i^* = \frac{r_{i-1} + r_i}{2} \tag{3-7}$$

$$T_i^* = \frac{T_{i-1} + T_i}{2} \tag{3-8}$$

Finally, DIANA approximates $\partial T/\partial t$ numerically at m = 1,…,n points and uses Equations 3-1 and 3-2 to calculate the corresponding degree of reaction dependent on heat production rate ($q_{r,m}$)

$$q_m = c_m \frac{\partial T}{\partial t} \approx c \frac{T_{m+1} - T_{m-1}}{t_{m+1} - t_{m-1}} \tag{3-9}$$

$$\alpha q_{r,m} = \frac{q_m}{q_{T,m}} \tag{3-10}$$

The preprocessing method was utilized in this research. This method was chosen because the rise in adiabatic temperature with respect to time, which is the output obtained from the semi-adiabatic calorimetry test (shown in Figure 3-3), could be conveniently input into DIANA directly.

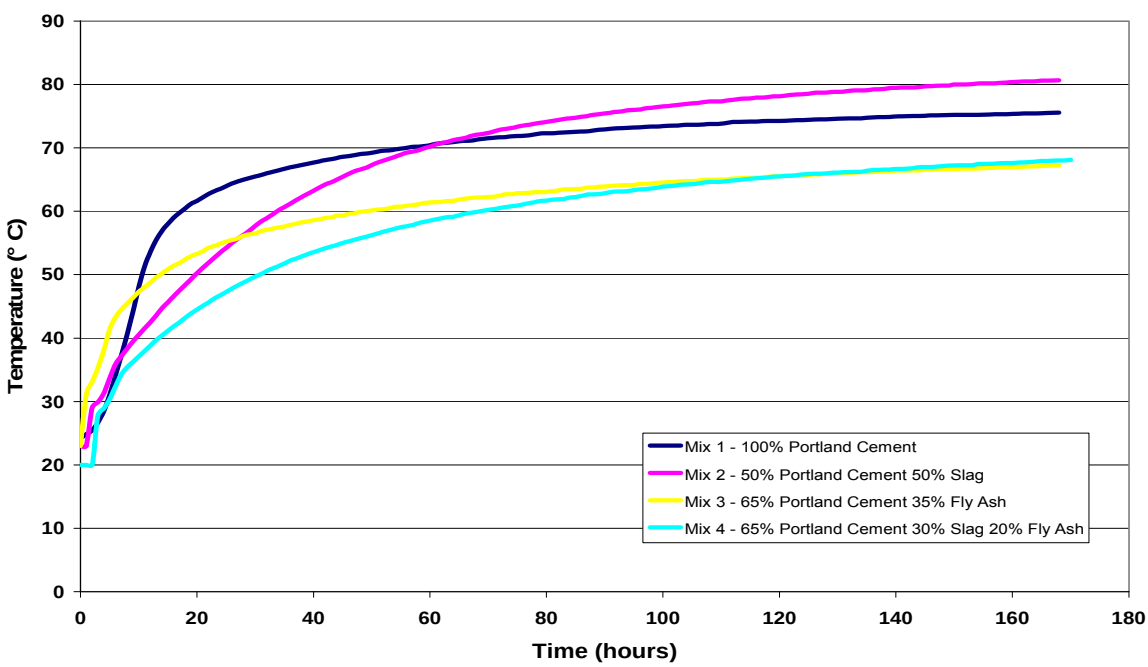

Figure 3-3. Adiabatic temperature rise of each concrete mixture obtained from semi-adiabatic calorimetry testing.

Power data obtained from isothermal calorimetry testing on cementitious mixtures, shown in Figure 3-4, can be integrated with respect to time to obtain the energy rise,

$$Q = \int_{t=0}^{t} P \, dt \tag{3-11}$$

which is then approximated to the energy rise of the hydrating concrete that is being represented by the mixture by multiplying by the percent cementitious content. The cementitious content of concrete mixtures that will be used to validate the model is presented in Table 3-3.

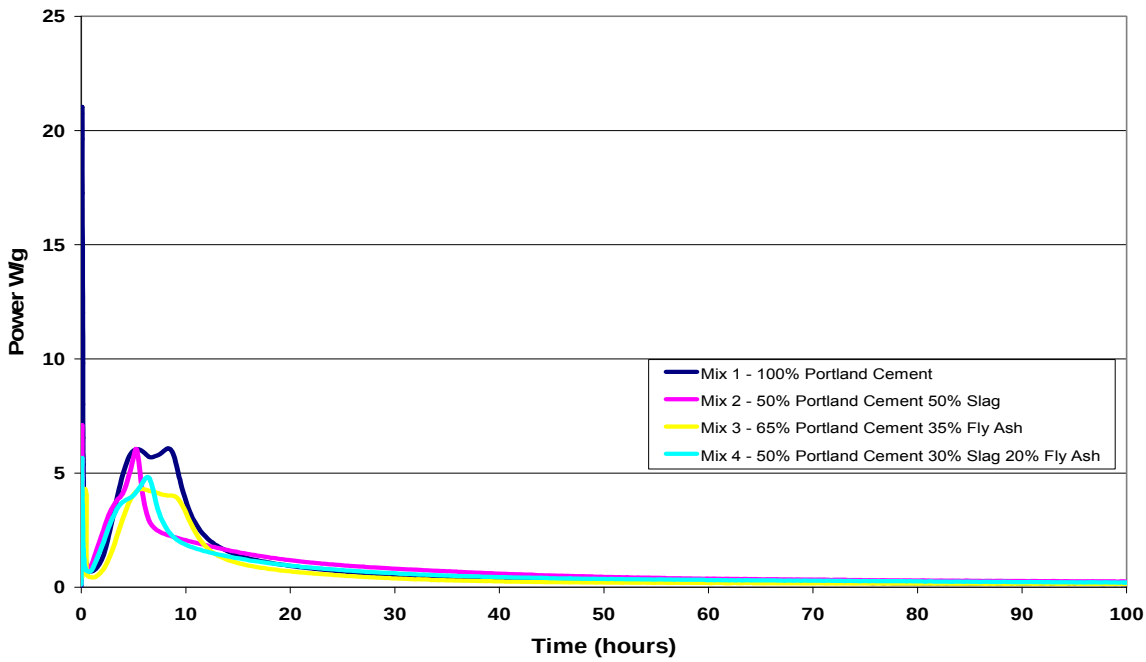

Figure 3-4. Hydration power of each cementitious mixture obtained from isothermal calorimetry testing.

Table 3-3. Cementitious Content of Each Mixture

Mixture #	1	2	3	4
Percentage of Mixture that is cementitious paste by weight	27.10%	27.10%	27.50%	27.50%

Finally, the adiabatic temperature rise, presented in Figure 3-5, is calculated from the energy using the relationship described by the first law of thermodynamics and expressed in Equation 3-12. This method was used to maintain consistency in the type of input used to describe the concrete hydration,

$$\Delta Q = m \cdot C_p \cdot \Delta T \qquad \text{or} \qquad \Delta T = \frac{\Delta Q}{m \cdot C_p} \tag{3-12}$$

where ΔQ = energy rise (J);
m = mass of concrete (g);
C_p = specific heat capacity (J/g-°C); and
ΔT = the change in temperature or temperature rise (° C).

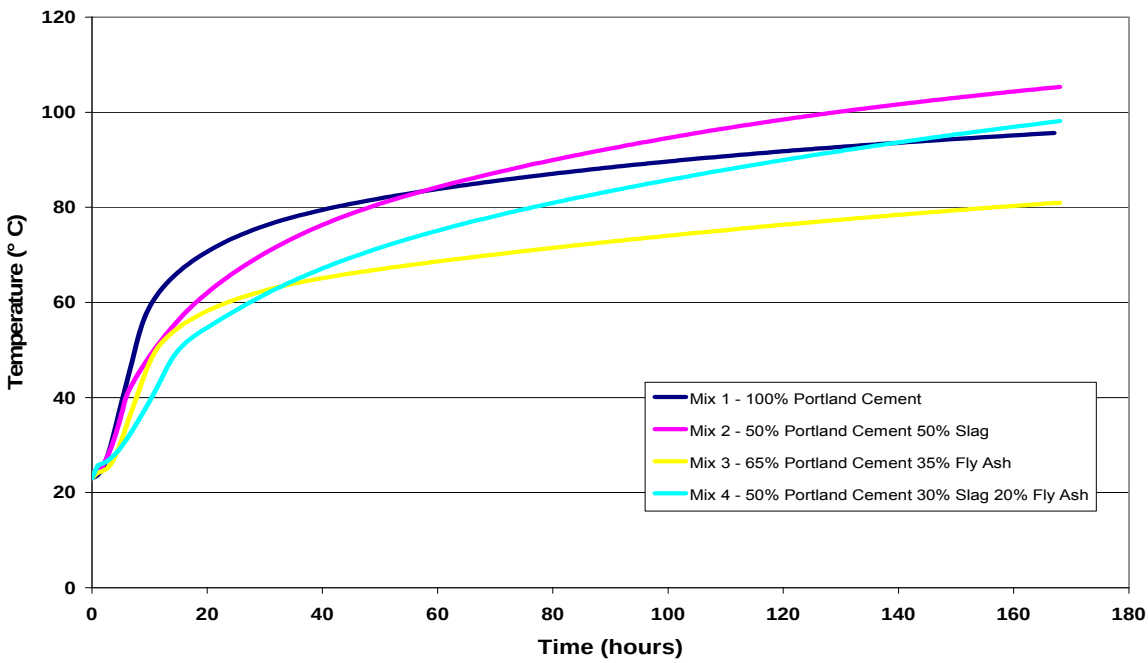

Figure 3-5. Adiabatic temperature rise of each concrete mixture calculated from the hydration power obtained in the isothermal calorimetry testing of cementitious mixtures.

3.3.2 Conductivity and Heat Capacity

Heat energy transferred by way of conduction is caused by the physical interaction between adjacent molecules that have different temperatures. Experimental observations have shown that in the one-dimensional plane, the rate of heat transfer through a finite area can be expressed by what is known as the Fourier law of conduction, expressed in Equation 3-13 and illustrated in Figure 3-6,

$$q_x = -kA_x \frac{\partial T}{\partial x} \tag{3-13}$$

where q_x = heat flow (J);
k = thermal conductivity (J/m-hr-°C);
A = surface area (m^2);
T = temperature, (° C); and
x = coordinate (m).

The thermal conductivity of a solid is its ability or the ease with which it transmits heat. The minus sign denotes a negative temperature gradient reflecting the fact that the heat flows in the direction of decreasing temperature.

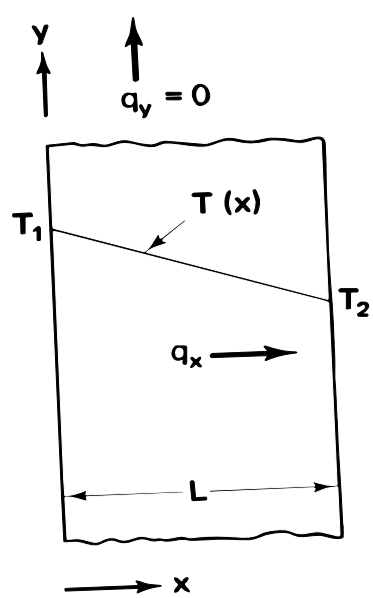

Figure 3-6. One-dimensional conduction heat transfer.

Expanded to the three-dimensional case, as shown in Figure 3-7, the Fourier equation for heat transfer becomes

$$q^n = -k\,\nabla T = -k\left(i\frac{\partial T}{\partial x} + j\frac{\partial T}{\partial y} + k\frac{\partial T}{\partial z}\right) \tag{3-14}$$

where x, y, z = axes of the coordinate system; and
i, j, k = vector directions in the coordinate system.

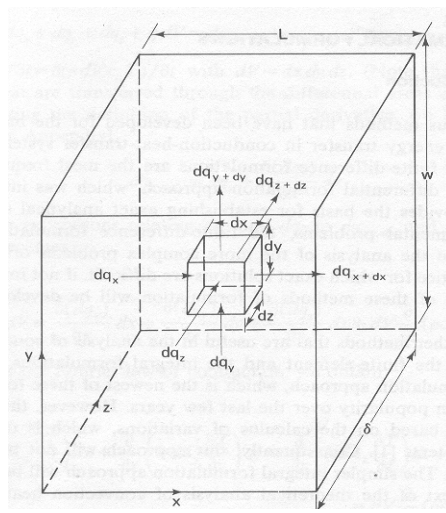

Figure 3-7. Differential volume for a rectangular solid.

Consider the case of a heat-conducting solid, such as mass concrete, which also has an internal source of heat generation. If q* is used to denote the rate at which heat is being internally generated per unit volume, then

$$\text{total heat generated} = q^*(dx\ dy\ dz) \tag{3-15}$$

The law of conservation of energy then states that energies in Equations 3-14 and 3-15 must be equal to the rate of energy storage reflected in the time rate of change of the average temperature (t_{avg}) given by

$$\rho c_p \frac{\partial t}{\partial \tau} = \frac{\partial t_{avg}}{\partial x}\,dx\ dy\ dz \tag{3-16}$$

If the equality is set and divided by the volume of the element (dx dy dz), while allowing dx, dy, and dz to go to zero, and t_{avg} to go to t,

$$\rho c_p \frac{\partial t}{\partial \tau} = \frac{\partial}{\partial x}\left(k\frac{\partial t}{\partial x}\right) + \frac{\partial}{\partial y}\left(k\frac{\partial t}{\partial y}\right) + \frac{\partial}{\partial z}\left(k\frac{\partial t}{\partial z}\right) + q^* \tag{3-17}$$

This equation represents a volumetric heat balance which must be satisfied at each point in the body, and describes the dependence of the temperature in a solid on the spatial coordinates and on time.

With the results of the thermal diffusivity and specific heat capacity experiments described in Chapter 6, the conductivity of concrete created based on the cementitious mixtures can be calculated by using the relationship

$$k = \alpha \cdot \rho \cdot C_p \tag{3-18}$$

where α = diffusivity (m^2/hr);
ρ = density (kg/m^3); and
C_p = heat capacity (J/gram-°C).

The conductivity and heat capacity values of the polystyrene foam were obtained from the manufacturer's specifications, while for the plywood, the typical conductivity and specific heat capacities for plywood used in North America were used.

3.3.3 Convection

Convection refers to the energy transported as a result of macroscopic motion, in other words, the transfer of heat from the surface of a material to a fluid that is moving over it. Figure 3-8 presents an approach to the analysis of convection heat transfer from a surface from which Equation 3-19 is derived,

$$q_c = \bar{h} A_s \left(T_s - T_F\right) \tag{3-19}$$

where q_c = rate of heat transfer (W/m^2-°C);
T_s = temperature at the surface (° C);
T_F = fluid temperature (° C);
A_s = surface area (m^2); and
$\bar{h}$ = mean coefficient of heat transfer.

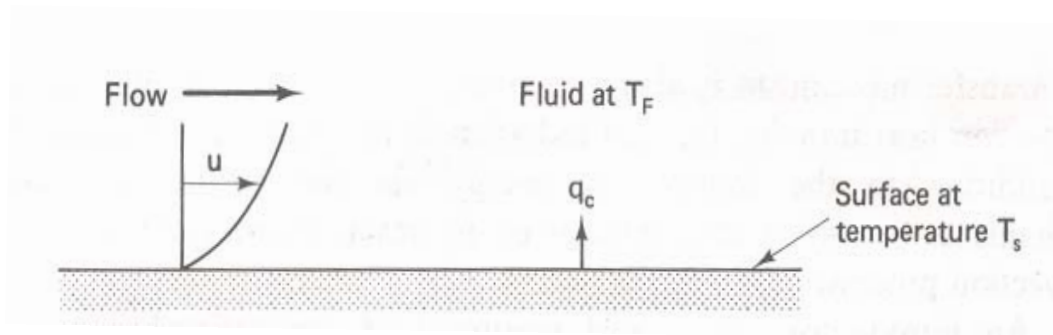

Figure 3-8. Convection heat transfer (Fundamentals of Heat Transfer, Lindon C. Thomas).

The heat lost and gained to the surrounding environment by the exposed surface of the hydrating concrete, and also the interaction of the foam with ambient conditions, is modeled by imposing boundary convection elements. This is conveniently done using the convection element found in DIANA to specify the convection and boundary conditions. The heat flow through the surface of the elements (q^S), due to convection, is modeled by the following equation:

$$q^S = h_c (\theta_e - \theta^S) \tag{3-20}$$

where h_c = convection coefficient (W/m^2-°C);
θ_e = external environment temperature (° C); and
θ^S = surface temperature of the concrete block (° C).

The convection coefficient can be constant, temperature-dependent, or time dependent.

The convection coefficient was calculated using the equation

$$h_c = \begin{cases} 5.6 + 3.95v, & v \le 5\ \mathrm{m/s} \\ 7.6v^{0.78}, & v \ge 5\ \mathrm{m/s} \end{cases} \tag{3-21}$$

where v = wind speed (m/s).

In this research, a constant convection coefficient value of 5.6 W/m^2-°C or 20106 J/m^2-hr-°C was used for all analyses, since all experimentation was conducted in a controlled environment that was maintained at a constant temperature with negligible forced air flow.

3.4 Model Geometry

Figure 3-9 shows the model depicting the concrete exposed to ambient conditions at the top surface and with the plywood and polystyrene insulation at the bottom and sides. To improve the efficiency of the analysis, advantage was taken of the double symmetry of the block, which allowed for the modeling of one-quarter of the block. The polystyrene insulation, plywood, and concrete were explicitly discretized and modeled according to their corresponding thermal properties.

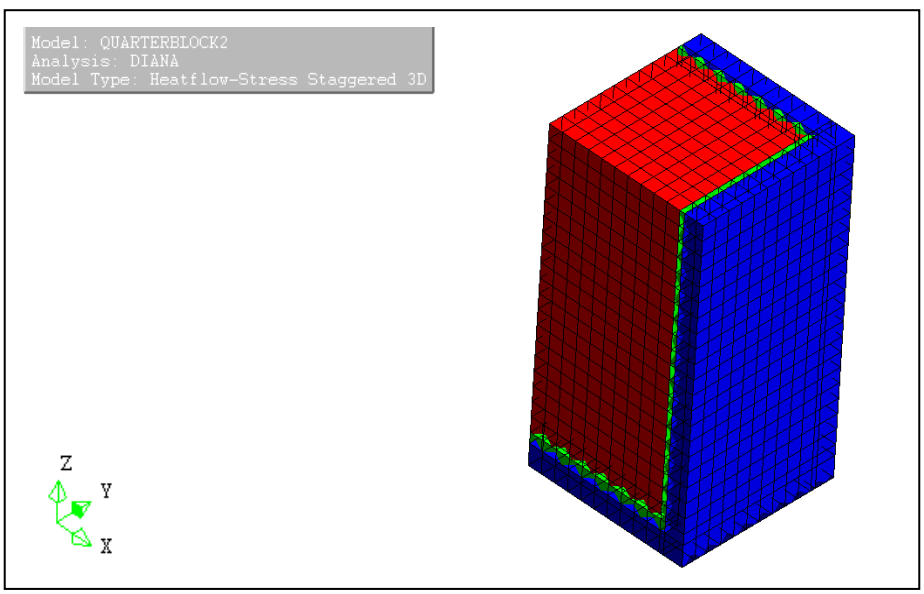

Figure 3-9. Finite element model of concrete block with insulation.

3.5 Boundary Conditions

The boundary conditions imposed for the thermal analysis consisted of an initial temperature of the model and the external temperature. Both temperatures were set at the temperatures

recorded inside the laboratory on the day each concrete mix was made. Figure 3-10 presents the temperature history of the laboratory during the monitoring of the experimental blocks. The description of the block experiment is presented in Chapter 5.

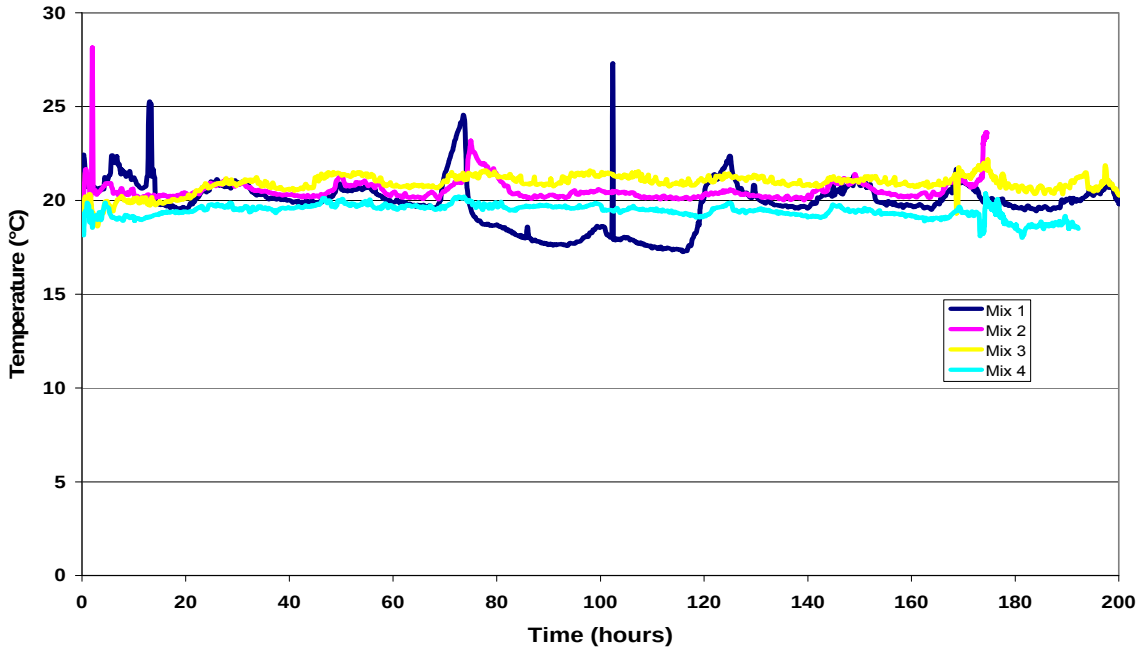

Figure 3-10. Ambient temperatures during experimental block monitoring.

The average temperature of the laboratory for Blocks 1, 2, and 3, which were cast during the summer months of July and August, was approximately 73° F (23° C), while for Block 4, which was cast in October was 35° F (20° C). Figure 3-11 shows the external temperature load of 73° F (23° C) that was imposed on the BQ4HT boundary convection elements in the model for Mixture 1.

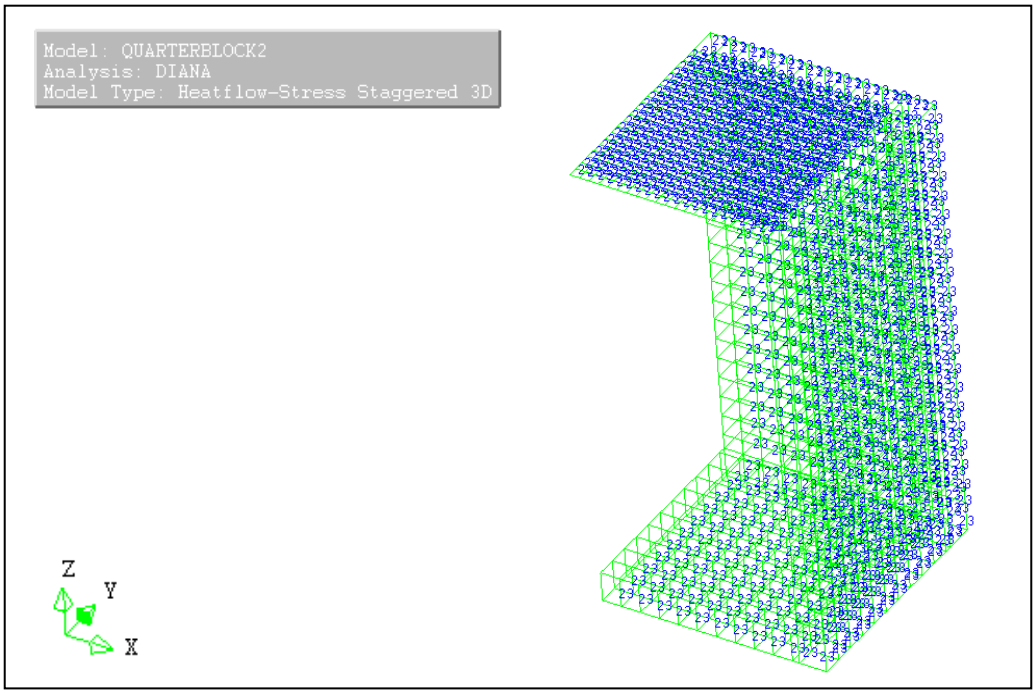

Figure 3-11. External temperatures imposed on finite element model representing the ambient conditions of the laboratory.

CHAPTER 4
FINITE ELEMENT STRUCTURAL MODEL

4.1 Introduction

Heat produced during the hydration of concrete causes an increase in its temperature. However, because there is the combined effect of the hydration process not being homogeneous and a loss of heat to the surrounding environment, temperature differences will occur throughout the concrete element. These temperature differences can induce thermal strains and stresses that could potentially initiate cracking, if they exceed the early age tensile strength of the concrete.

The temperature distribution solution obtained from the thermal analysis is imposed as a thermal load in the structural analysis of the concrete. The mechanical response to the stresses induced by the thermal gradient is greatly dependent on the physical characteristics of the concrete.

This chapter will describe the elements used in DIANA to model the concrete and the physical input parameters required to measure the mechanical behavior.

4.2 Element Selection

As stated in Chapter 3, the structural behavior of the concrete block was modeled using the three-dimensional twenty-node CHX60 isoparametric solid brick element reproduced here in Figure 4-1. By default, a $3 \times 3 \times 3$ integration scheme is applied, but a $2 \times 2 \times 2$ integration scheme can be used in a patch of more than one element to obtain optimal stress points. The stress and strain distribution is approximated over the volume of the element. Stress σ_{xx} and strain ε_{xx} vary linearly in the *x* direction, and quadratically in the *y* and *z* directions. Stress σ_{yy} and strain ε_{yy} vary linearly in the *y* direction, and quadratically in the *x* and *z* directions. Stress

σ_{zz} and strain ε_{zz} vary linearly in the *z* direction, and quadratically in the *x* and *y* directions. It utilizes linear interpolation and Gauss integration in its computational scheme.

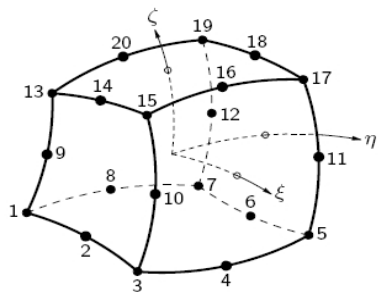

Figure 4-1. Twenty-node isoparametric solid brick element CHX60.

4.3 Material Model

The modeling of the structural behavior presented a few challenges as early age concrete exhibits both an elastic component and a viscous component.

To model the linear elasticity of the concrete, the Young's modulus E, Poisson's ratio *v*, and coefficient of thermal expansion *a*, were directly input into the model. The viscoelastic behavior was modeled based on a Maxwell chain, which is also in the form of the direct input of the progression of the Young's modulus with age.

The potential for cracking is tracked by specifying the tensile strength evolution by way of a discrete function that is dependent on time.

4.4 Input Parameters

4.4.1 Modulus of Elasticity

Cracking in mass concrete occurs when the tensile stresses induced by the thermal gradients are greater than the tensile strength. The modulus of elasticity (MOE) of concrete is the ratio between the stress and reversible strain and is important because it influences the

rigidity of the concrete structure. This linear relationship is known as Hooke's Law and is expressed in Equation 4-1,

$$\sigma = E\varepsilon \tag{4-1}$$

where σ = stress (MPa);
E = Young's Modulus (MPa); and
ε = linear strain.

The elastic limit represents the maximum allowable stress before the concrete will crack and undergo permanent deformation.

In heterogeneous multiphase materials like concrete, the modulus of elasticity increases as it hydrates, which is detrimental to the concrete because the probability of cracking increases as the modulus increases.

4.4.2 Poisson's Ratio

Poisson's ratio is the ratio of the lateral strain to the axial strain within the elastic range of the concrete. According to Mehta and Monteiro (2006), Poisson's ratio has no consistent relationship with the curing age of the concrete. Values obtained during the testing for compression modulus of elasticity was consistently 0.2, which is within the universally accepted range of 0.15 and 0.20 for concrete.

4.4.3 Coefficient of Thermal Expansion

The coefficient of thermal expansion is used to describe the sensitivity of concrete expansion or contraction to changes in temperature. It is defined as the change in unit length per degree of temperature change (Mehta and Monteiro, 2006). The value of the coefficient of thermal expansion is particularly important in mass concrete because the strain induced during the cooling period is dependent on both the magnitude of the change in temperature and the coefficient of thermal expansion.

4.4.4 Tensile Strength

In normal concrete applications, the low tensile strength of concrete is usually of little concern because reinforcing steel bars, which have high tensile strength values, are used to increase the overall strength of the structure. However, in mass concrete applications, the use of steel is either impractical, such as in the case of dams, or due to the size of the structure, the spaces between the steel are large creating elements that are weak in tension.

There are two tests commonly used to estimate the tensile strength of concrete. They are the ASTM C 78 third-point flexural loading test, and the ASTM C 496 splitting tension test, both of which are described in Chapter 6.

4.5 Symmetry and Boundary Conditions

The boundary conditions imposed for the structural analysis of the quarter block consisted of the restriction of displacements along the symmetry planes. The base of the block was modeled as being in a fixed support condition and so displacements along the Z direction were also restricted. Both conditions are presented in Figure 4-2.

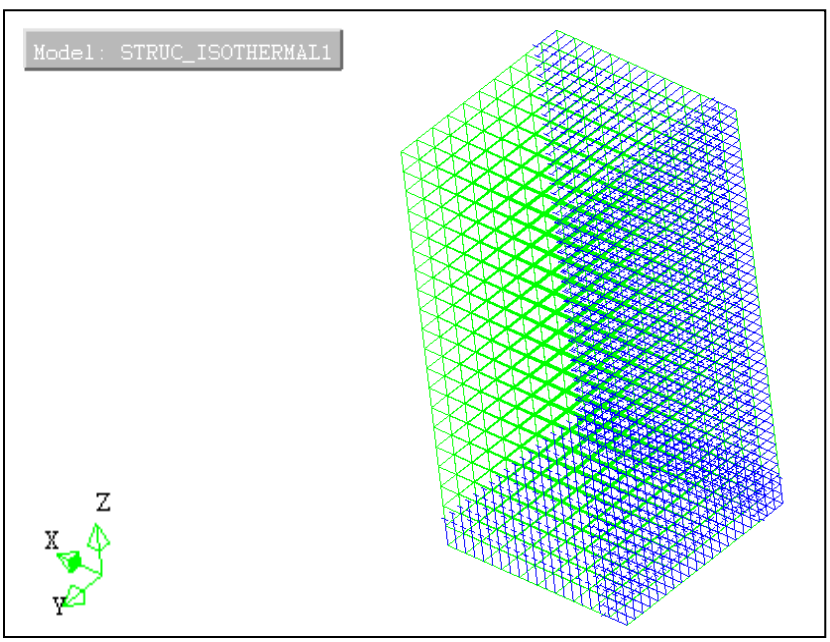

Figure 4-2. Symmetry conditions and supports of model.

CHAPTER 5
BLOCK EXPERIMENT

5.1 Introduction

To verify that the finite element model created is effective in modeling the early age behavior of hydrating mass concrete, four different mixes of concrete, typical of use in mass concrete applications in Florida, were produced. Each mixture was used to make large concrete blocks with dimensions that qualify them to be characterized as massive concrete elements. Measurements of the temperature and strain at predetermined locations within the blocks were recorded until the equilibrium temperature was achieved. These temperatures and strains will then be compared with the results obtained from the finite element model.

5.2 Concrete Mix Design

All of the four concrete mixes used in this study had a water-to-cementitious material ratio of 0.5 to allow for compatibility with isothermal calorimetry testing that will be used to determine the activation energies and heat of hydration of each concrete mix.

Mix 1 consisted of 100% Type I Portland cement concrete; Mix 2 had 50% of the Portland cement mass replaced by ground granulated blast-furnace slag; Mix 3 contained 65% Portland cement and 35% Class F fly ash; and Mix 4 was a blend of 50% Portland cement, 30% granulated blast furnace slag, 20% Class F fly ash. The mix designs for each block are shown in Table 5-1. The coarse and fine aggregates were adjusted according to the volumetric differences caused by the varying densities of each cementitious material.

5.3 Block Geometry

Two 42-in. × 42-in. × 42-in. (1.07-m × 1.07-m × 1.07-m) forms were created for pouring of the experimental concrete blocks. The geometry of the blocks is presented in Figure 5-1. The

Table 5-1. Mix Designs of Concrete Used in the Large-Scale Blocks

Material	Mix 1 100% Portland Cement (lb/yd^3)	Mix 2 50% Portland - 50% Slag (lb/yd^3)	Mix 3 65% Portland - 35% Fly Ash (lb/yd^3)	Mix 4 50% Portland - 30% Slag - 20% Fly Ash (lb/yd^3)
Cement	681	341	443	341
GGBF slag	0	341	0	204
Fly ash	0	0	238	136
Water	341	341	341	341
Fine aggregate	1095	1088	1036	1050
Course aggregate	1650	1668	1660	1650

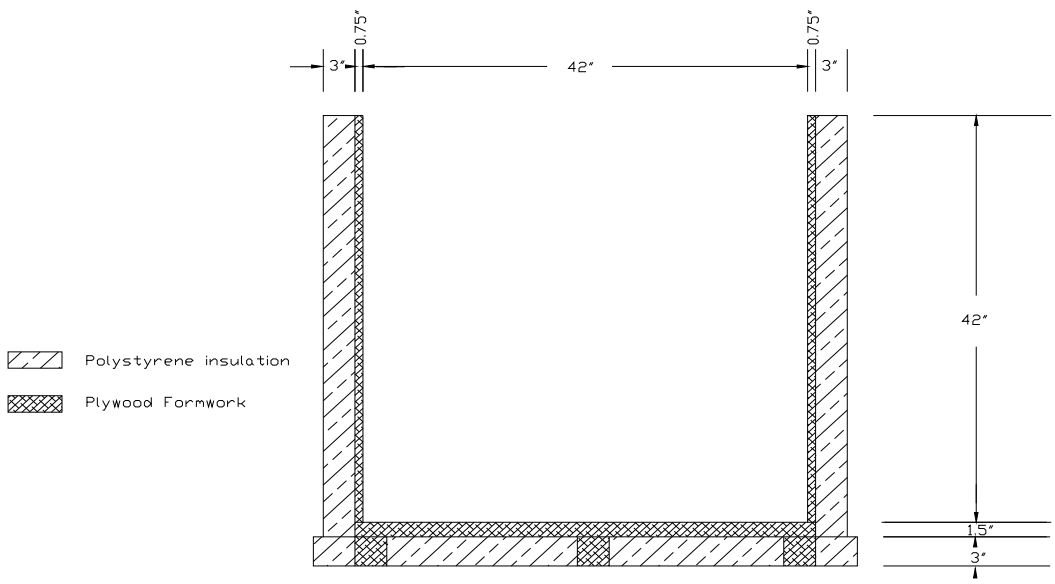

Figure 5-1. Experimental block geometry.

side faces and base of both blocks consisted of a 0.75-in. thick plywood formwork surrounded by a 3-in. thick layer of polystyrene plates. However, one of the blocks had a cover with the same make up as the sides placed on its top surface after pouring was completed in an effort to simulate a fully adiabatic process, while the top face of the other block was left open and exposed to environmental conditions. Figure 5-2 is a photograph of the two blocks after the concrete had been poured.

Figure 5-2. Uninsulated (left) and insulated (right) mass concrete block specimens.

5.4 Instrumentation for Data Collection

The two concrete blocks were instrumented for the monitoring of early age temperatures and strain at predetermined locations. The data acquisition equipment consisted of Type K thermocouples with an accuracy of ±2.2° C (±4° F) and embedded strain gages.

The layout of the thermocouples and strain gages are presented in Figure 5-3 through Figure 5-5. The thermocouple data and the strain data were recorded in order to validate the ability of the finite element model to accurately predict the early age behavior of the concrete block specimens.

5.5 Temperature Profiles

The location of the thermocouples in the blocks were chosen to capture the temperature difference between the center of the block and the exposed surface, as well as to monitor the near surface temperature gradient to determine if it would contribute to thermal cracking of the concrete. The thermocouples at the sides and bottom of the block were placed to validate the

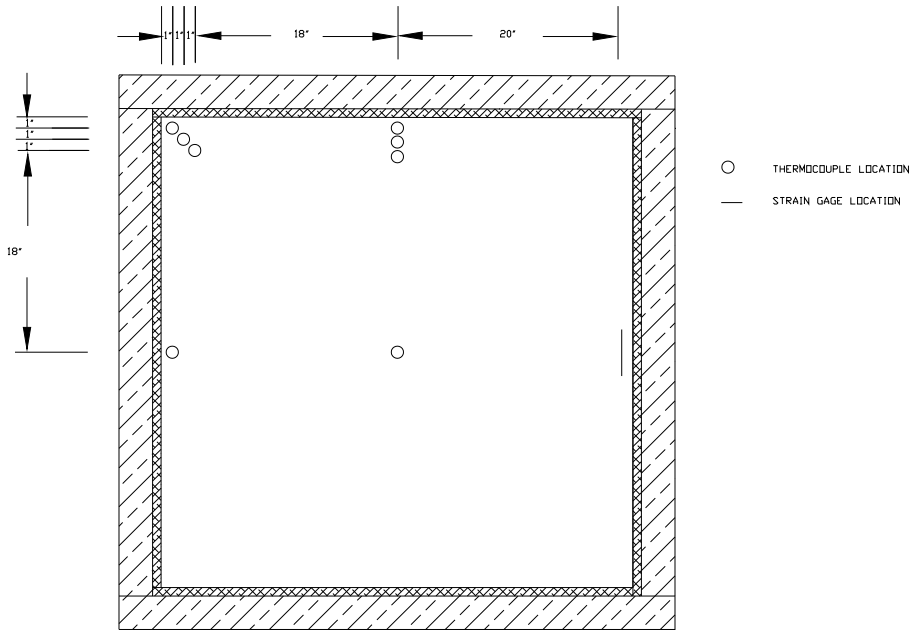

Figure 5-3. Thermocouple location (plan).

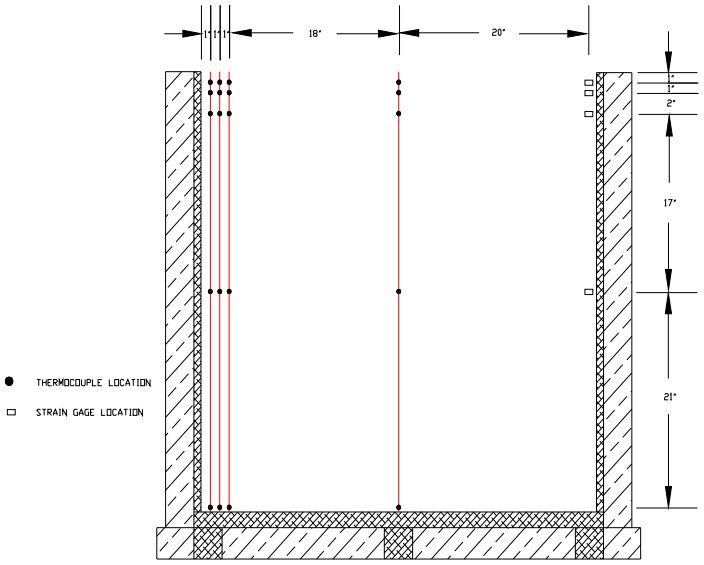

Figure 5-4. Thermocouple location (section).

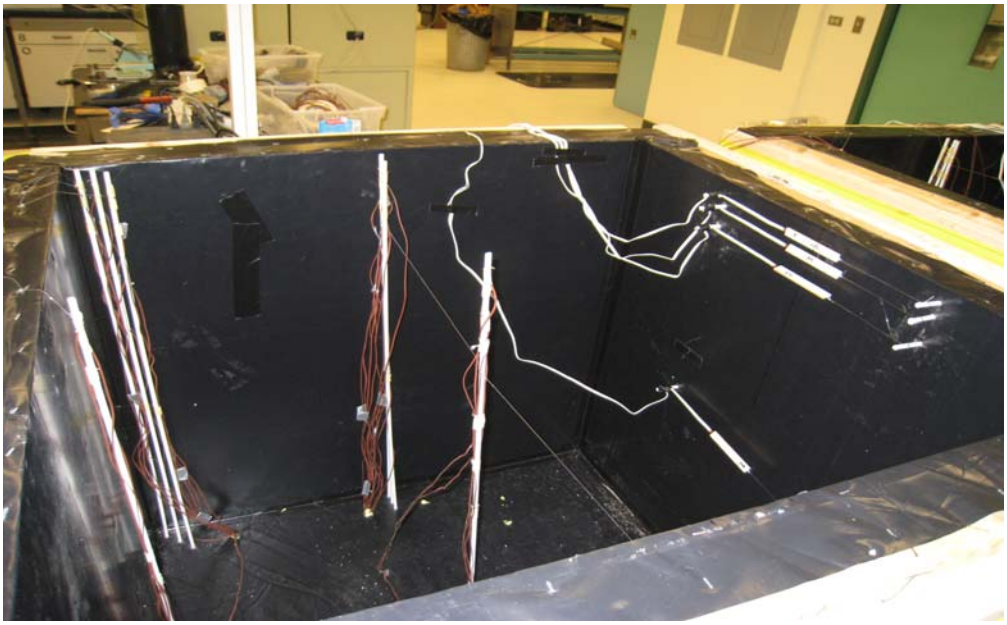

Figure 5-5. Instrumentation layout for experimental block.

effectiveness of the insulation and by extension the thermal boundary conditions that would be used in the finite element model.

The temperatures measured by the thermocouples placed along the center of the uncovered concrete block of Mix 1 are presented in Figure 5-6. It can be seen that, as expected, the highest temperature, 67° C (153° F) at 20 hours after pouring, was measured at the center of the block (21 in. below the top surface). The peak temperature measured at the bottom of the block (42 in. below the top surface), also 67° C (153° F), but occurring 33 hours after the concrete is poured, shows that the assumption that the bottom is insulated is valid. It is also shown, as expected, that the lowest temperatures were recorded in the thermocouples located nearest to the exposed top surface of the concrete block.

The temperature data shown in Figure 5-7 provide the temperature profiles measured by the thermocouples located 2 in. from the side surface of the uncovered block. The maximum temperature of 65° C (153° F) is again recorded at the thermocouple located 21 in. below the top

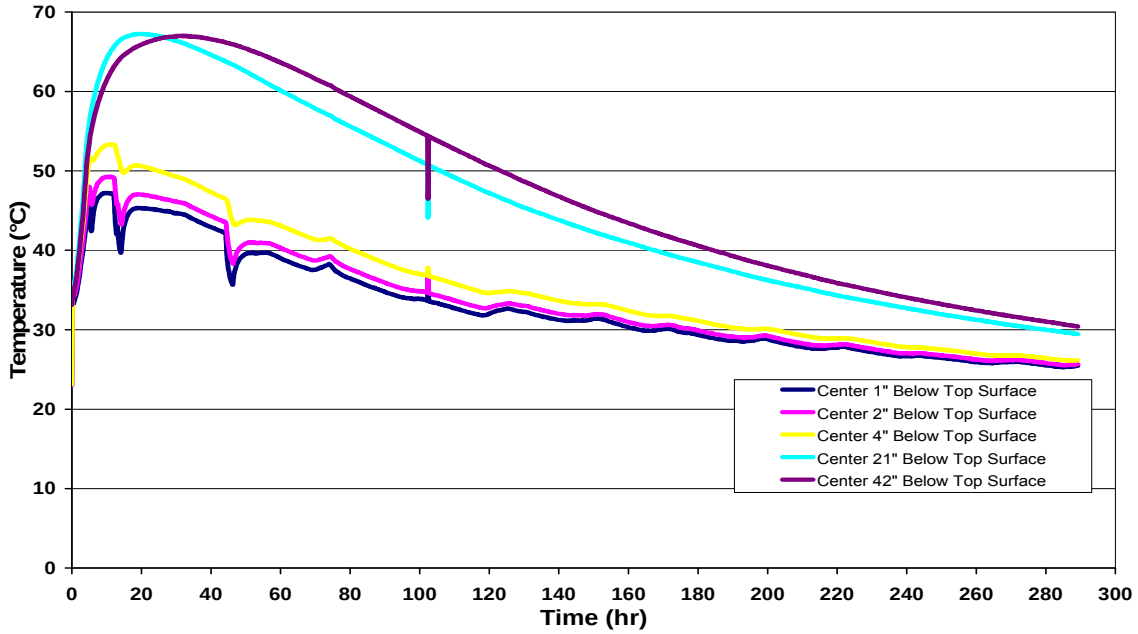

Figure 5-6. Temperatures along the center line of the uncovered concrete block Mix 1.

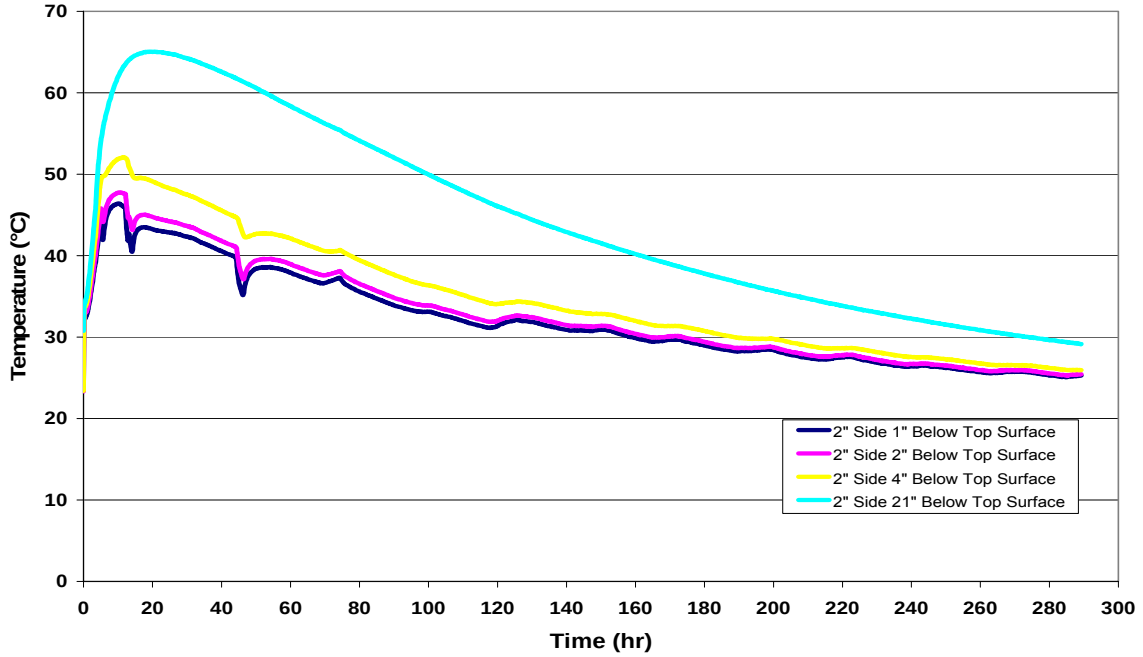

Figure 5-7. Temperatures 2 in. from the side of the uncovered block in Mix 1.

surface. This temperature is 2.0° C (3.6° F) less than the temperature recorded at the center of the block, which is within the thermal tolerance of ±2.2° C (±4.0° F) of the thermocouples. This again serves to validate the assumption of the sides of the block being well insulated.

The temperature profile for the uncovered concrete block with a cement replacement of 50% ground granulated blast-furnace slag is presented in Figure 5-8. As expected in concrete containing slag, the section of the profile representing the increasing temperatures has a slope that is less than that obtained in the concrete containing 100% Portland cement. This is due to ground granulated blast-furnace slag having a very slow rate of hydration reaction. It is interesting to note that while the peak temperature for this concrete was approximately the same as the concrete containing 100% Portland cement in Mix 1, it occurred 40 hours after being poured, approximately twice as long.

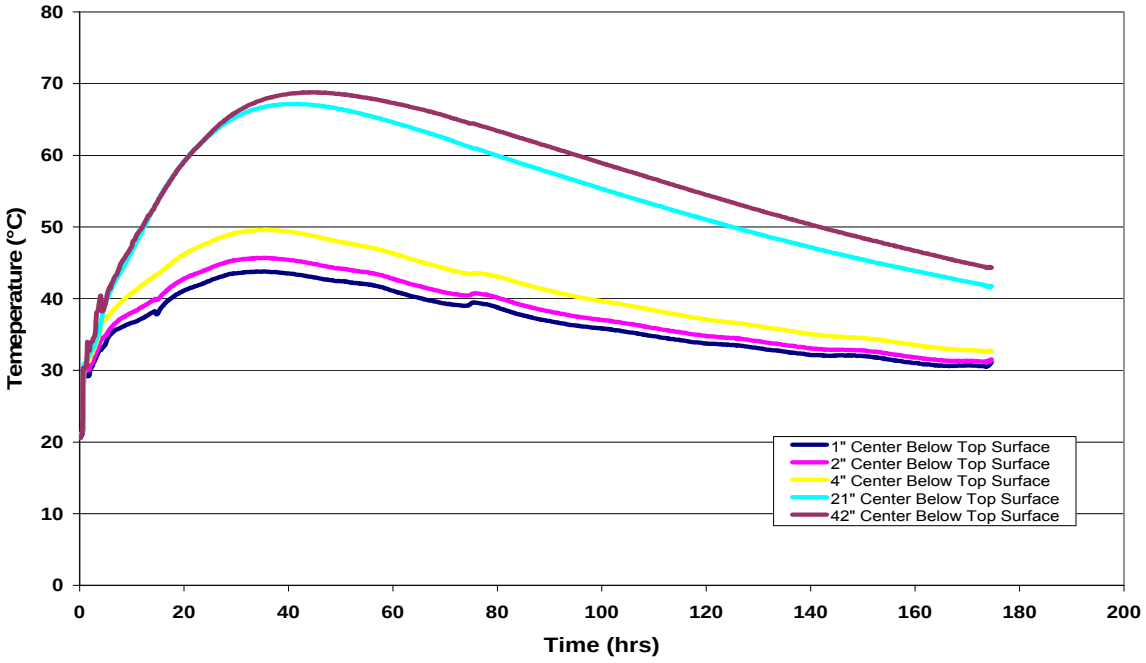

Figure 5-8. Temperatures along the center line of the uncovered block in Mix 2.

Figure 5-9 shows the temperatures measured in the concrete of Mix 3 in which 35% of the Portland cement was replaced by fly ash. The temperature increase trend in this block shows a lower heat of hydration rate as compared with what was obtained in Mix 1 containing 100% Portland cement. The peak temperatures at each location were lower in Mix 3.

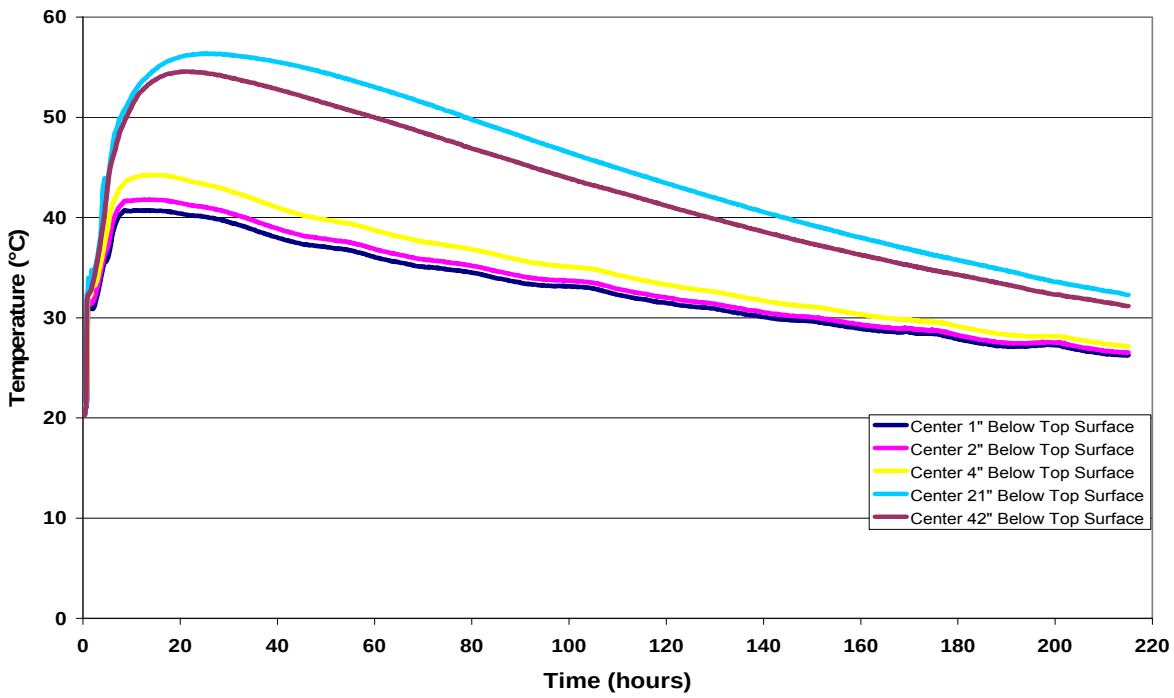

Figure 5-9. Temperatures along the center line of the uncovered block in Mix 3.

The combined effects of the ground granulated blast-furnace slag and the fly ash on the hydration rate and peak temperatures of the concrete, respectively, is seen in the temperature-time plots of Mix 4 presented in Figure 5-10. The slope of the profile during the temperature increase period is very similar to the trend observed in Mix 2, showing a slower rate of temperature rise as compared with Mix 1 and Mix 3. The peak temperature in Mix 4 was much lower than those of Mixes 1 and 2, similar to that of Mix 3.

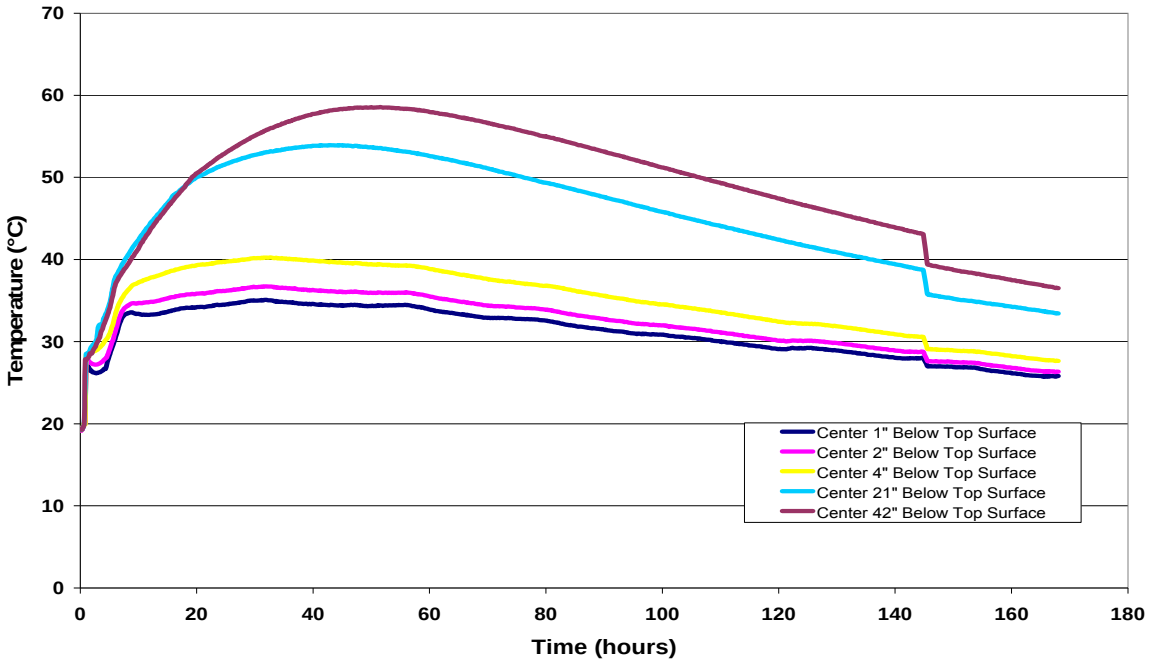

Figure 5-10. Temperatures along the center line of the uncovered block in Mix 4.

CHAPTER 6
MATERIAL TESTS AND PROPERTIES

6.1 Introduction

The laboratory testing of the concrete mixtures used to create each of the experimental blocks focused on characterizing and relating the heat production, maturity, physical, and strength properties of concrete at early ages. The results obtained were used as input parameters for the finite element model of the blocks.

6.2 Heat of Hydration

The determination of the heat generated during the hydration of the concrete is essential for the characterization of its thermal behavior at early ages. Two of the experimental methods in use today, semi-adiabatic calorimetry and isothermal calorimetry testing, were utilized in this research.

6.2.1 Semi-Adiabatic Calorimetry

A semi-adiabatic calorimeter is defined as "a calorimeter where the maximum heat losses are less than 100J/(K·h)" (RILEM 1997, p. 451). Semi-adiabatic calorimetry is used in this research instead of adiabatic testing, because producing a true adiabatic testing system is extremely difficult and technically advanced, since it requires a controlled supply of heat to the system over time. The semi-adiabatic calorimetry system is a purely passive one which only requires the monitoring of time, temperature, and the heat flux for the acquisition of temperature data. The system consists of an insulated cylinder which contains two thermocouples and a heat-flux sensor. One of the thermocouples is embedded into the concrete specimen in the center of the calorimeter, while the other thermocouple is located on the exterior. The heat flux sensor is embedded within the insulation of the semi adiabatic calorimeter. Figure 6-1 presents the energy history recorded from the concrete produced from Mix 1.

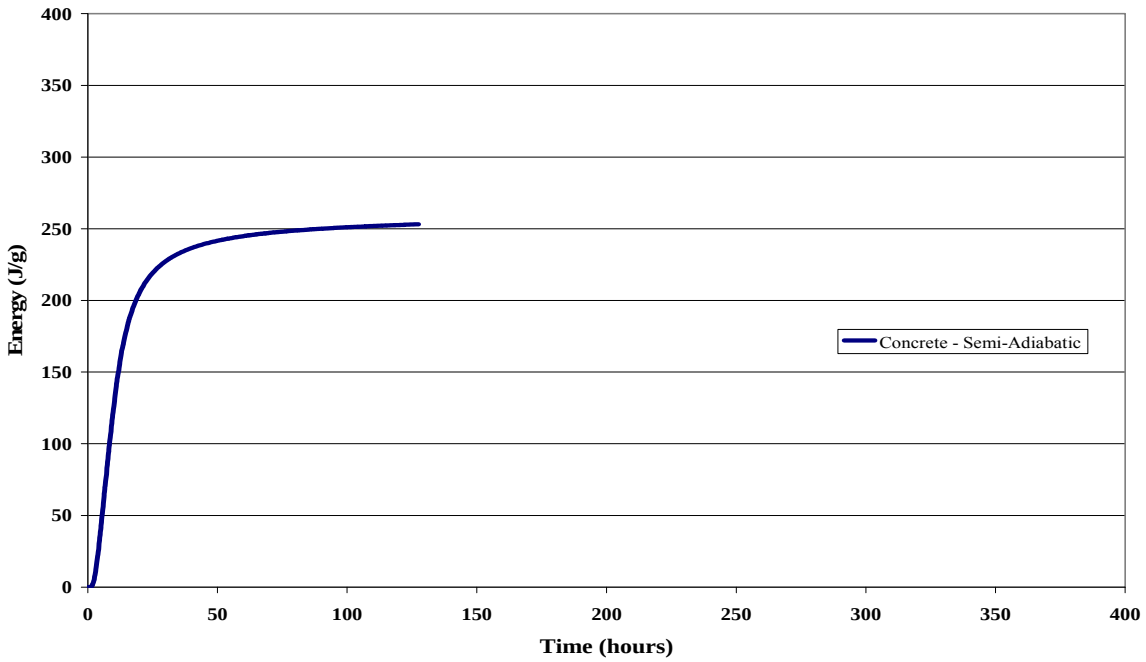

Figure 6-1. Resultant semi-adiabatic calorimetric energy curve for Mix 1.

6.2.2 Isothermal Conduction Calorimetry

Isothermal conduction calorimetry is a very useful testing method for the determination of the heat energy that is evolved from the hydration of a cementitious material over time. It provides a direct measurement of the heat generated by a specimen, avoiding the errors associated with methods that utilize chemical analyses. The resulting data from the heat-flow sensor in the calorimeter is a voltage signal (in the order of milli-volts) that is proportional to the thermal power from the sample. The integral of the thermal power over the time of the test is the heat of hydration of the specimen. For this research, a relatively small sample (6 grams) of the cementitious material used in each mass concrete block was taken and tested in the isothermal calorimeter. The specimens were tested at temperatures of 15°, 23°, 38°, and 49° C (59°, 73°, 100°, and 120° F). The data curves produced by the test at each temperature were analyzed for the energy rise versus time, as presented in Figure 6-2. This plot shows a trend of the energy rise with respect to time being significantly larger as the test temperature is increased. However,

Figure 6-3 indicates that regardless of the test temperature, the values for the energy rise with respect to equivalent age are virtually equal. Therefore, from this observation, we can obtain the relationship between energy rise and temperature rise, which can then be used in the input for the finite element model.

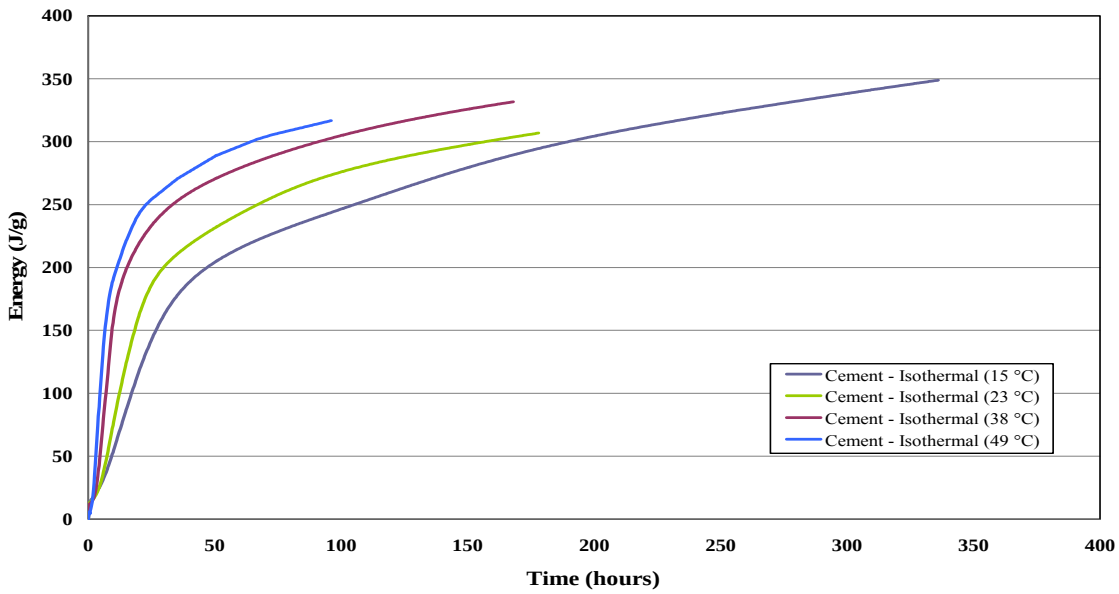

Figure 6-2. Resultant isothermal calorimetric curves with regard to energy versus time for Mix 1.

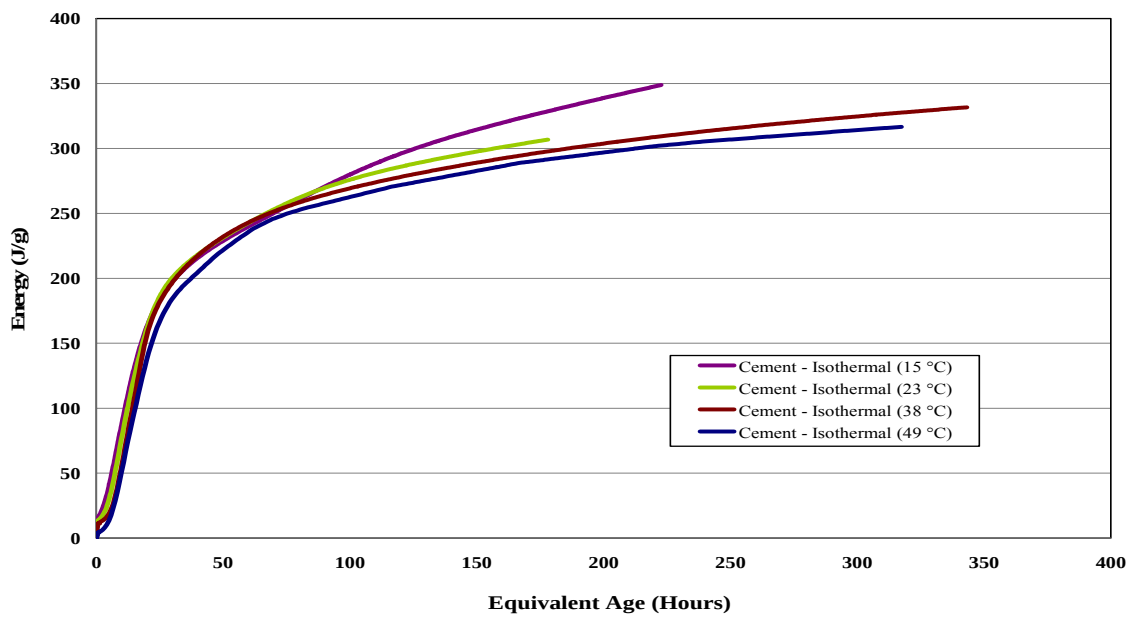

Figure 6-3. Resultant isothermal calorimetric curves with regard to energy versus equivalent Age for Mix 1.

Figures 6-4 to 6-6 show the energy rise with respect to equivalent age for Mixes 2, 3, and 4, respectively. All except the plot for Mix 2 indicate that the values of the energy rise with

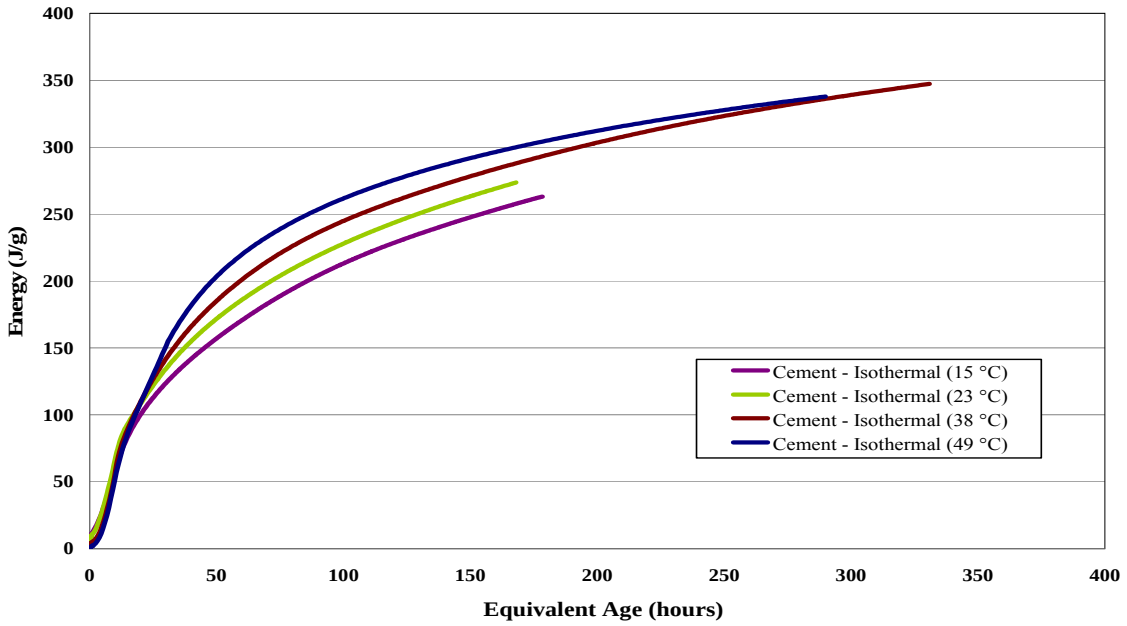

Figure 6-4. Resultant isothermal calorimetric curves with regard to energy versus equivalent Age for Mix 2.

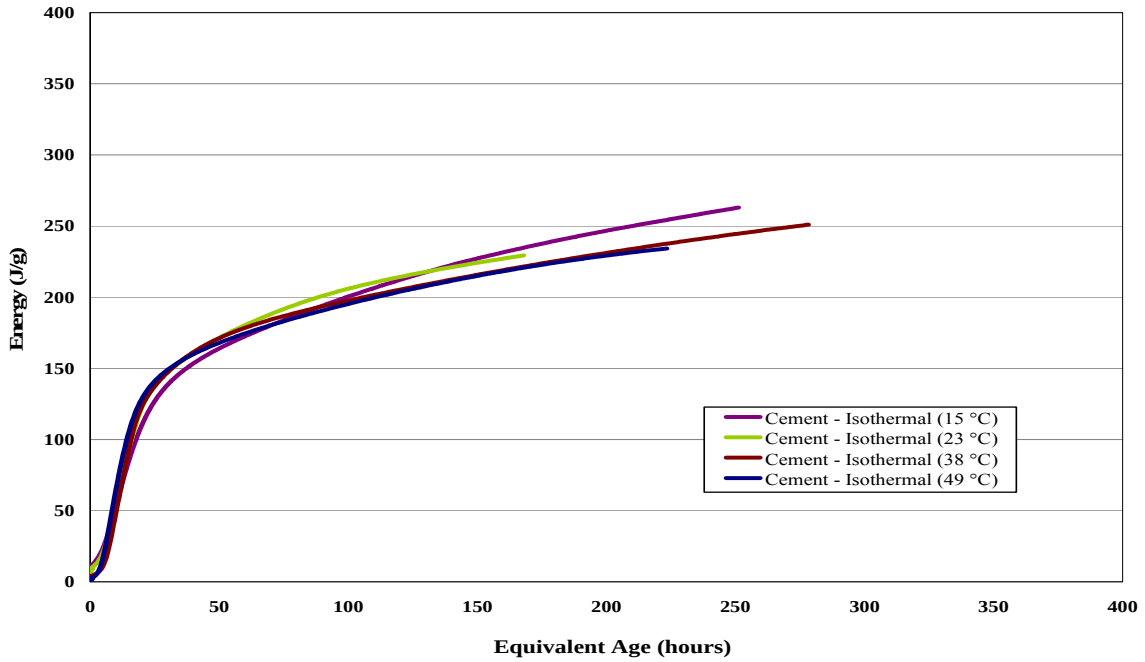

Figure 6-5. Resultant isothermal calorimetric curves with regard to energy versus equivalent Age for Mix 3.

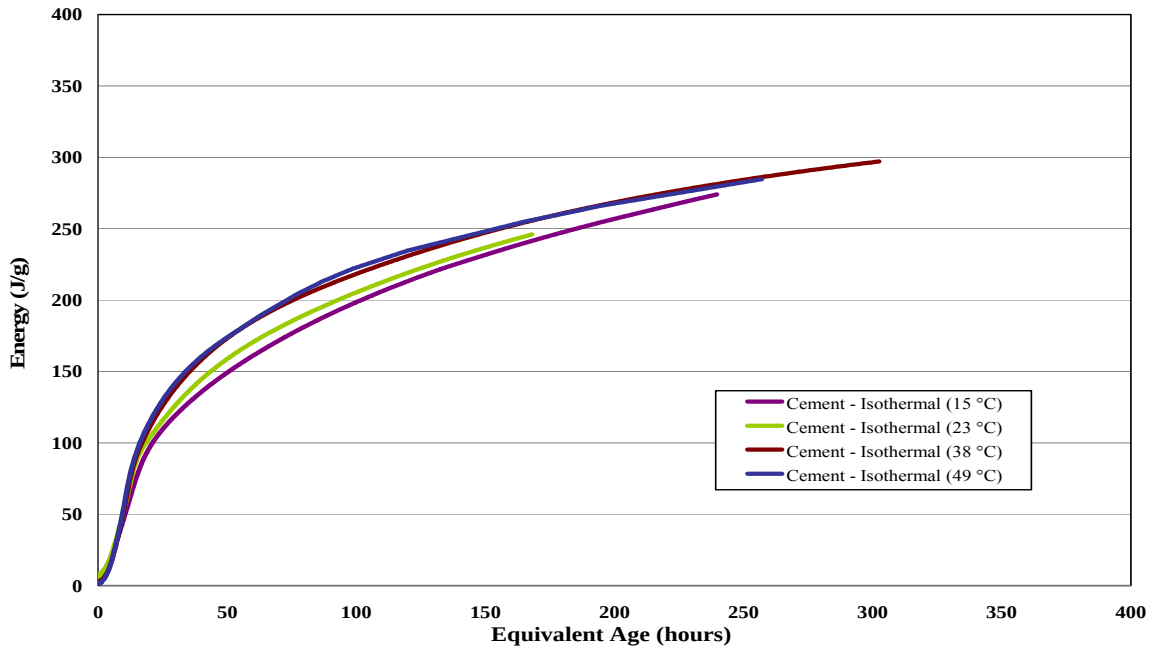

Figure 6-6. Resultant isothermal calorimetric curves with regard to energy versus equivalent Age for Mix 4.

respect to equivalent age are essentially same. The reason for the anomaly in Mix 2 is not fully understood, but is attributed to the high replacement of Portland cement (50%) with ground granulated blast-furnace slag.

6.3 Specific Heat Capacity

Specific heat is the amount of heat required per unit mass to cause a unit rise of temperature. The specific heat capacity testing in this research is being conducted with a calorimeter similar to the apparatus used by De Schutter and Taerwe (1995) shown in Figure 6-7. It contains an interior bath of oil and an exterior bath of polypropylene glycol. These liquids were chosen because of their ability to rapidly transfer heat.

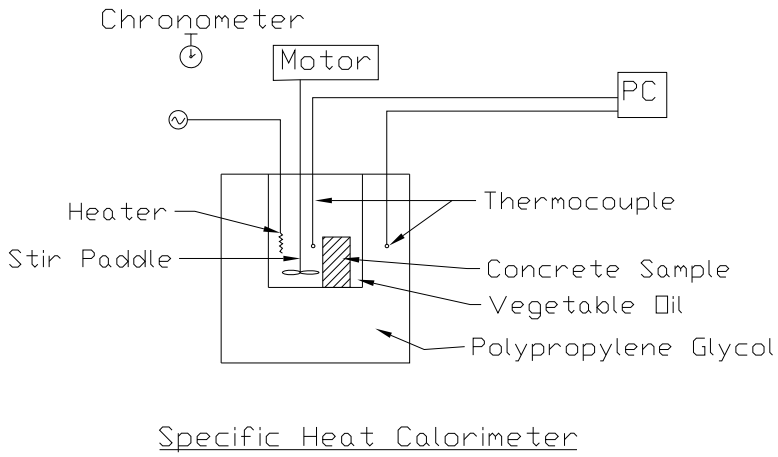

Figure 6-7. Schematic of the specific heat capacity calorimeter.

A known flux of heat energy (E1) is supplied to the interior bath containing oil and the resulting temperature increase ($\Delta\theta 1$) observed. The stir paddle is used to distribute the heat evenly throughout the interior bath. The cementitious material was then added to the oil bath and energy (E2) was again supplied to the bath. The resulting change in temperature of the cementitious material ($\Delta\theta 2$) is the final temperature minus the initial temperature of the cementitious material at introduction to the bath. The specific heat capacity of cementitious material was then calculated using the following formula.

$$C = \frac{1}{m_c}\left(\frac{E2}{\Delta\theta 2} - \frac{E1}{\Delta\theta 1}\right) \tag{6-1}$$

6.4 Thermal Diffusivity

Thermal diffusivity is a measure of the ease or difficulty with which concrete undergoes temperature change (ACI 207.2). Diffusivity is directly related to the type of aggregate used and the density of the concrete. The higher the diffusivity value, the easier it is for the concrete to gain or lose heat.

Three cylindrical 6-in. × 12-in. concrete specimens, instrumented with thermocouples at the center of their mass, are removed from the moist cure room where they were maintained at a temperature of 73° F ± 2° F (θ_0) (23° C ± 1° C) and 100% relative humidity and placed in a water bath at temperature $\theta_0 + \Delta\theta$. As the cylinders are heated by the hot water, the temperature $\theta(t)$ at the center axis of the specimens are measured with respect to time until they reach a steady temperature of 176° F (80° C). The results of the three cylinders are averaged, and inserted in the following equation:

$$\log [(\theta_0 + \Delta\theta - \theta(t))/\Delta\theta] \tag{6-2}$$

Plotted as a function of time, the curve becomes linear after some time, and the slope of this curve is directly related to the thermal diffusivity. The results of the test show that thermal diffusivity of the concrete used in the first three blocks varies as concrete ages, presented in Figure 6-8.

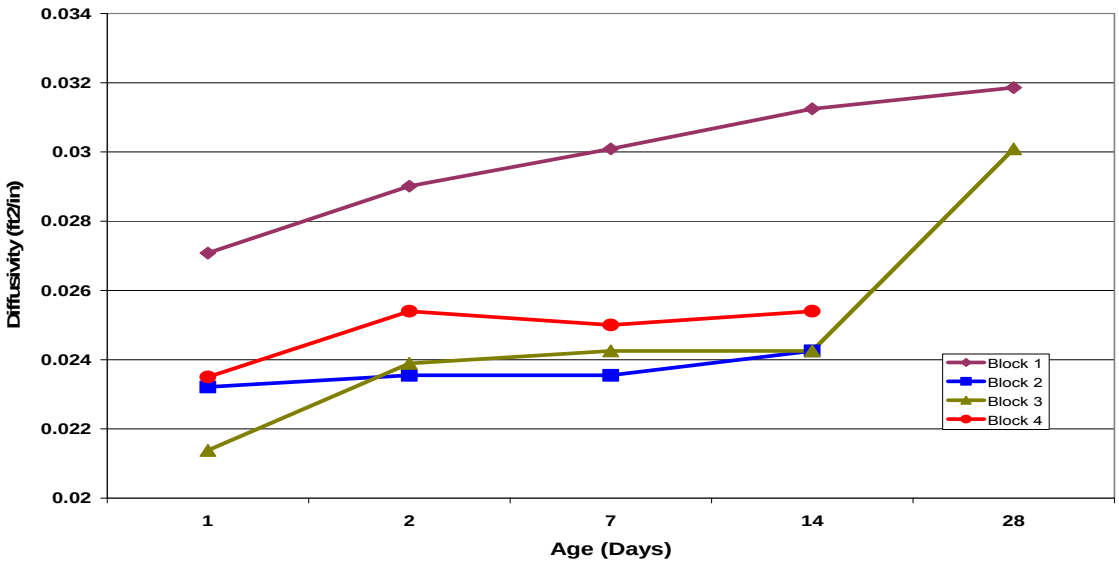

Figure 6-8. Thermal diffusivity vs. age of the experimental blocks.

6.5 Flexural Strength

The flexural strength of concrete is a measure of the tensile strength of the concrete. It is also often referred to as the modulus of rupture (MOR). Beam specimens, shown in Figure 6-9, with dimensions of 6 in. × 6 in. × 22 in. are cast from the concrete used in mass concrete blocks. The flexural strength of the concrete in this research was measured by applying two point loads to the unreinforced beam at 1/3 and 2/3 of the loaded span length of 18 in., as shown in Figure 6-10. A load rate of 30 lbs/sec, which is approximately 6% of the ultimate load as specified in ASTM C78, is applied to the beams so as to not induce significant creep, while restricting the occurrence of premature rupture.

Figure 6-11 shows the stress and strain distribution, according to Bernoulli's theorem. The modulus of rupture (MOR) of the beam cross-section shown is taken as the maximum stresses in the extreme fibers.

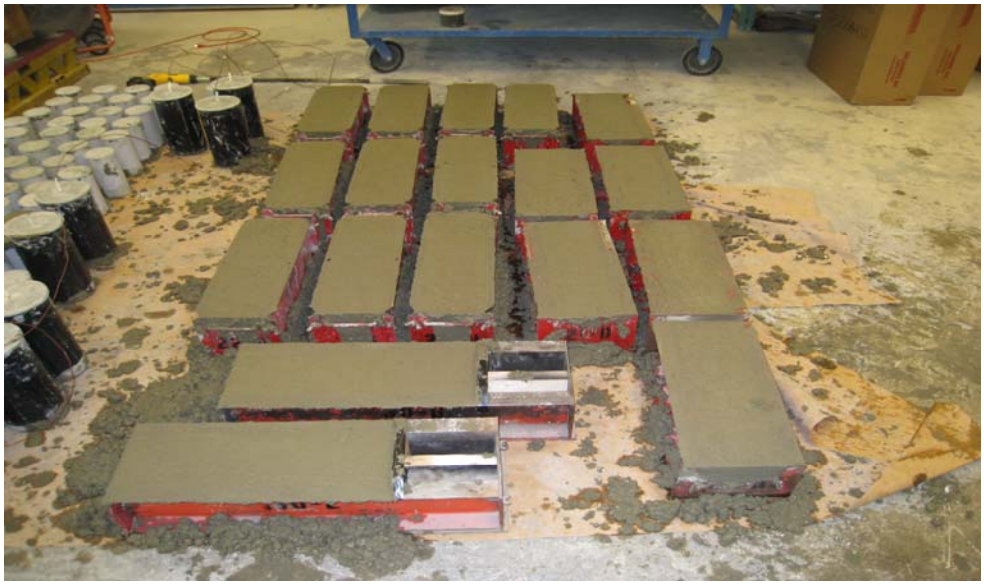

Figure 6-9. Beam specimens for flexural strength testing.

Figure 6-10. Beam specimen undergoing flexural strength testing.

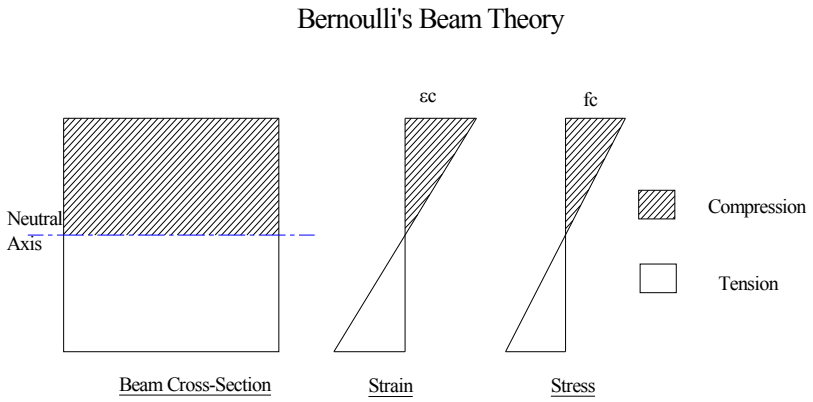

Figure 6-11. Theoretical stress and strain distribution through beam cross section.

Figure 6-12 is a graphical representation MOR versus time for the companion beam specimens cast from each mixture. The results are consistent with typical findings where the mixture containing 100% Portland cement gained flexural strength the fastest while the mixture in which 35% of the Portland cement is replaced by fly ash gains flexural strength the slowest. The mixture containing 50% slag and the mixture containing the ternary blend gained flexural strength at a rate between the mixtures with 100% Portland cement and 35% fly ash.

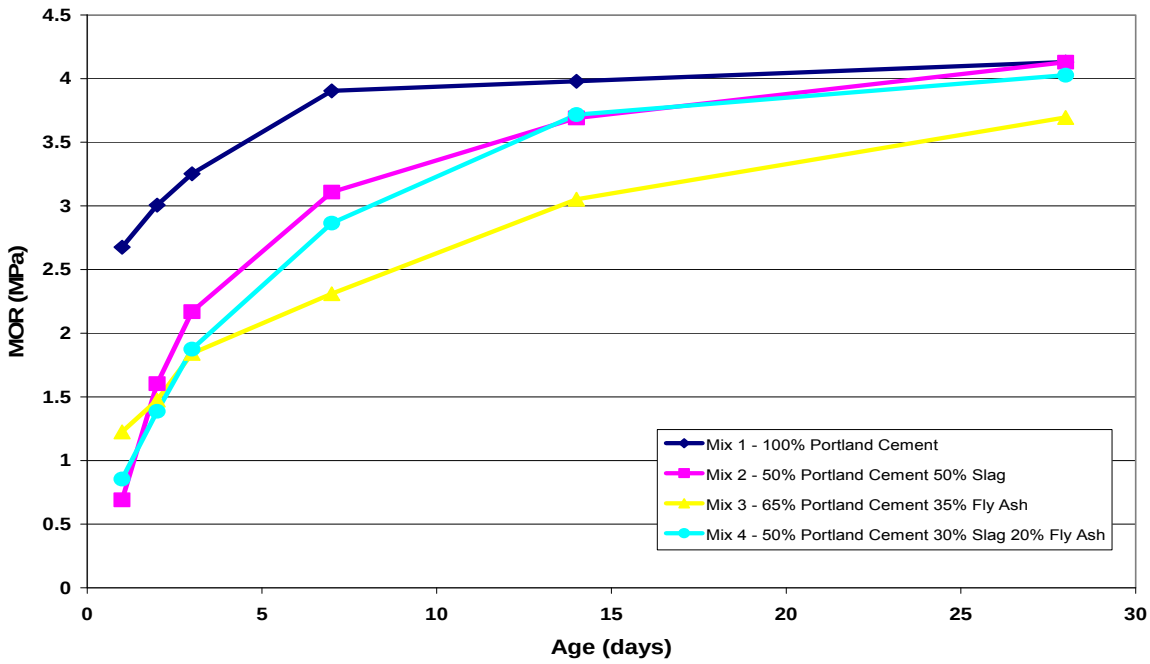

Figure 6-12. The modulus of rupture of the beam specimens taken from Mixes 1, 2, 3 and 4.

6.6 Splitting Tensile Strength

The splitting tensile strength test was performed on 4-in. × 8-in. cylinders specimens, sampled from each concrete mixture, in accordance with ASTM C496, the set up of which is shown in Figure 6-13. The tests were carried out at ages of 1, 2, 3, 7, 14, and 28 days and are presented in Figure 6-14, where the strength development of the concrete of each mix over time is observed. As was the case in the flexural beam test, the concrete containing 100% Portland cement gained strength the fastest, the concrete with 35% fly ash gained strength the slowest, while the concretes containing 50% slag and the ternary blend gained strength at a rate between them.

The results obtained from the splitting tension test were used as input for the finite element model of the experimental concrete blocks. These results were chosen because they are smaller than the results obtained from the flexural test and, therefore, are more conservative.

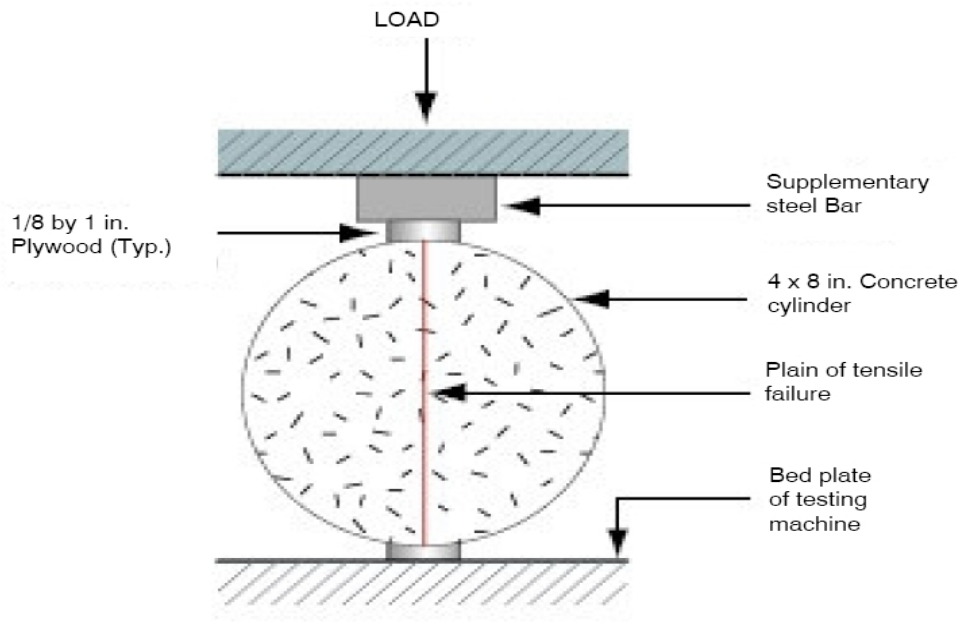

Figure 6-13. Diagrammatic arrangement of splitting tension test ASTM C496.

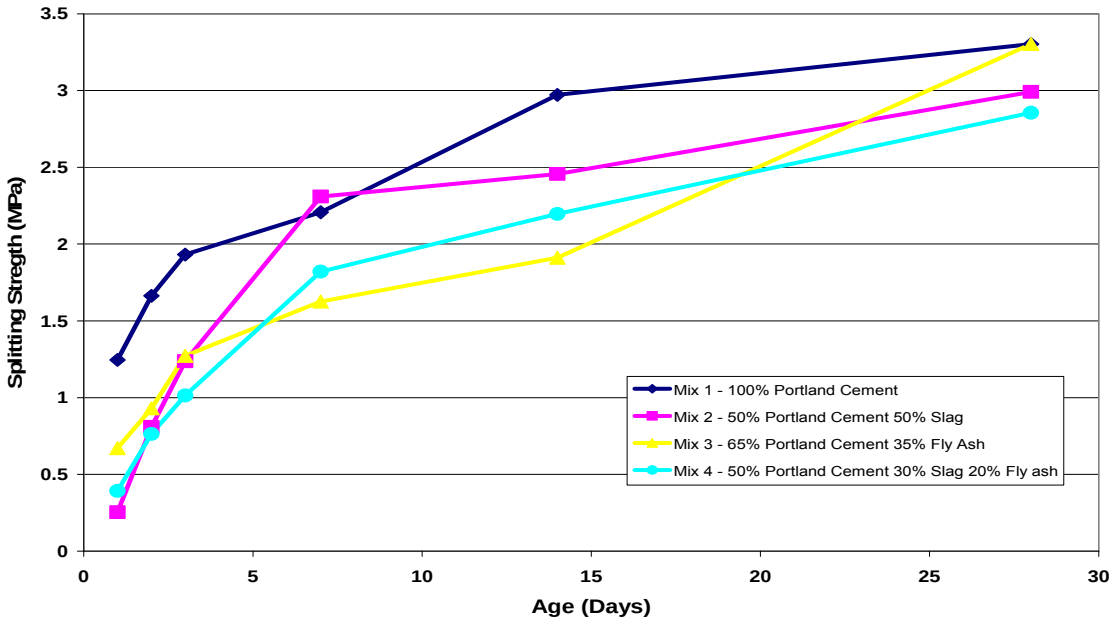

Figure 6-14. Splitting tensile strength of concrete used in Mixes 1, 2, 3 and 4.

6.7 Modulus of Elasticity and Poisson's Ratio Testing

The compressive modulus of elasticity and Poisson's ratio of concrete was determined using the ASTM C469 standard test method. The rate of development of the modulus of elasticity with age obtained from the compression testing of 4-in. × 8-in. cylinder samples taken from each concrete mix used in the experimental blocks is presented in Figure 6-15.

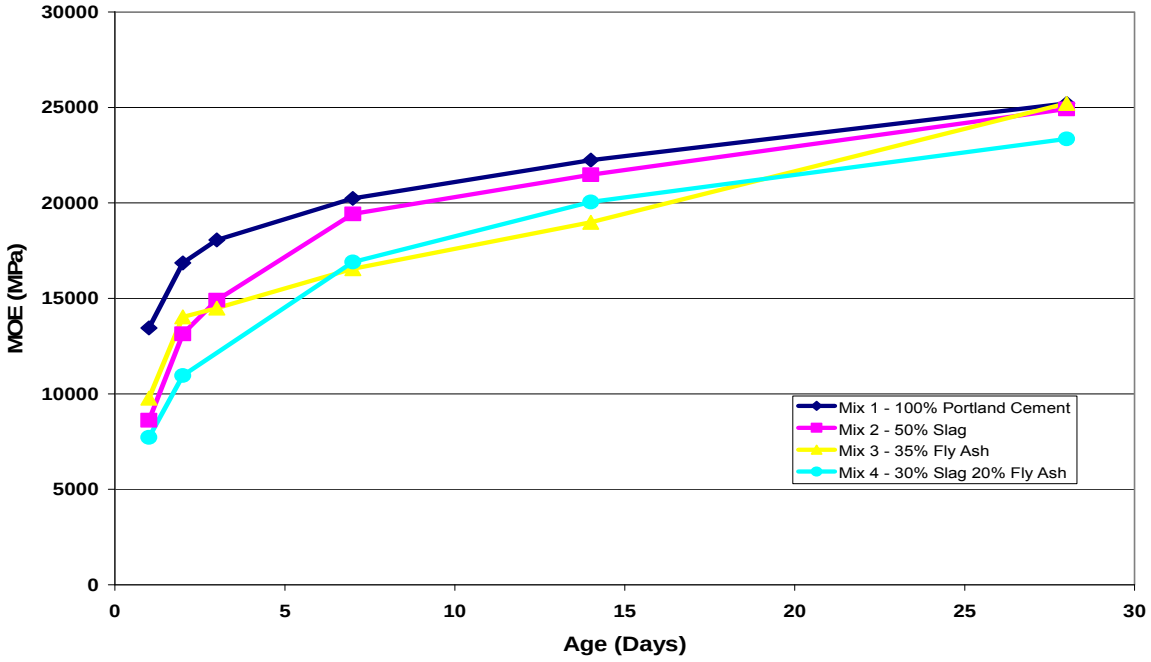

Figure 6-15. Compressive modulus of elasticity versus time.

The stress-strain relationship obtained from the middle third section of the beams during the flexural tests described previously was used to calculate the tensile modulus of elasticity of the respective concrete mixtures, shown in Figure 6-16. This was done because cracking in mass concrete is primarily a phenomenon of tensile action, which is also the failure mode of the flexural test beams.

The compressive modulus, which was the higher of two types of modulus of elasticity, was used in the finite element analysis as it is the more conservative description of the stress-strain relationship of the concrete.

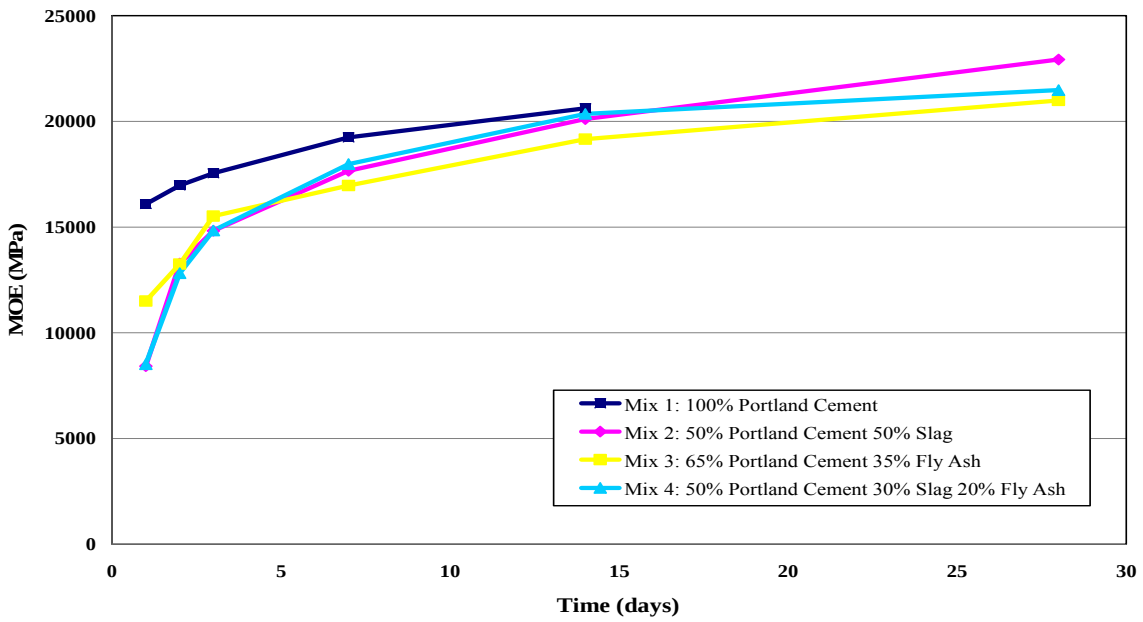

Figure 6-16. Tensile modulus of elasticity versus time.

6.8 Coefficient of Thermal Expansion Testing

The results of testing for the coefficient of thermal expansion of the concrete mixtures used in this research are shown in Figure 6-17. There was very little change in the values for each

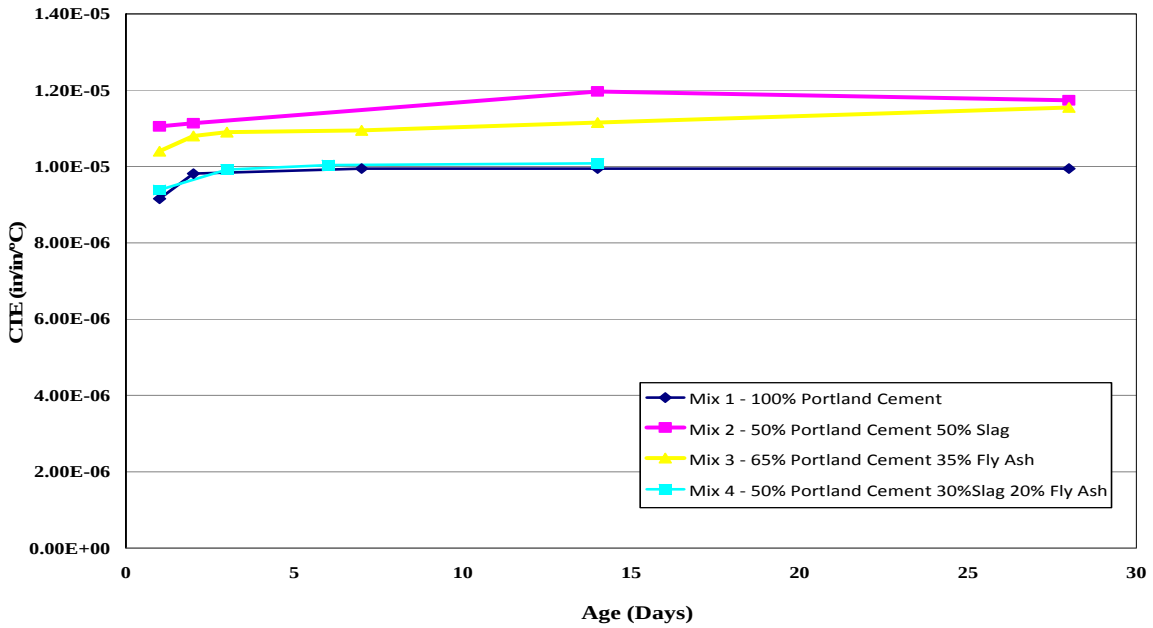

Figure 6-17. Coefficient of thermal expansion versus time for each mixture.

mix over the first seven days, which is the duration of the analysis of the finite element model. It was thus decided that a constant input value for the coefficient of thermal expansion of each model block was sufficient for the analysis.

6.9 Summary of Material Properties

The thermal properties of the concrete are listed in Table 6-1. The effect of the ground granulated blast-furnace slag on the thermal behavior of the concrete in Mix 2 and Mix 4 is evident. The slower adiabatic temperature increases observed in the experimental blocks with these mixes can be attributed to the high activation energies, which is the energy that must be overcome in order for the hydration reaction to occur. Table 6-2 presents the thermal conductivities and heat capacities of the plywood and polystyrene insulation used in the formwork of the block.

Table 6-1. Thermal Properties of Concrete

	Conductivity (J/m-hr-°C)	Heat Capacity (J/m^3-°C)	Activation Energy (J/mol)
Mixture 1	7920	2675596	34235
Mixture 2	4418	2017434	50400
Mixture 3	5883	2603101	32982
Mixture 4	4838	2024985	37330

Table 6-2. Thermal Properties of Plywood and Polystyrene

	Conductivity (J/m-hr-°C)	Heat Capacity (J/m^3-°C)
Plywood	540	85440
Polystyrene	224.85	20824

The mechanical properties used to describe the strength development of the concrete are listed in Table 6-3. The effect of the ground granulated blast-furnace slag and fly ash on the

early age strength of the concrete in Mixtures 2, 3, and 4 is evident. The tensile strength at day one in each mix is extremely low, confirming the theory that the benefit of lower rates of temperature rise produced by the use of supplementary cementitious materials occurs at the expense of lower ductility; a higher elastic modulus-to-strength ratio; and, a reduced strain capacity.

Table 6-3. Modulus of Elasticity and Tensile Strength of Concrete

	Time (Days)	Modulus of Elasticity (MPa)	Tensile Strength (MPa)
Block 1 (100% Portland cement)	1	13445	1.25
	2	16892	1.66
	3	18064	1.93
	7	20236	2.206
	14	22248	2.972
	28	25213	3.303
Block 2 (50% Portland, 50% slag)	1	8618	0.255
	2	13170	0.807
	3	14893	1.23
	7	19443	2.31
	14	21481	2.45
	28	24921	2.99
Block 3 (65% Portland, 35% fly ash)	1	9791	0.669
	2	13996	0.931
	3	14479	1.28
	7	16547	1.63
	14	18985	1.91
	28	25235	3.30
Block 4 (50% Portland, 30% slag, 20% fly ash)	1	7722	0.393
	2	10963	0.765
	3		1.01
	7	16905	1.82
	14	20053	2.20
	28	23352	2.85

The constant values of Poisson's ratio and the coefficient of thermal expansion are presented in Table 6-4.

Table 6-4. Poisson's Ratio and Coefficient of Thermal Expansion of Concrete

	Poisson's Ratio	Coefficient of Thermal Expansion (in/in -°C)
Block 1	0.19	9.16E-06
Block 2	0.20	1.11E-05
Block 3	0.20	1.11E-05
Block 4	0.20	1.00E-05

CHAPTER 7
THERMAL ANALYSIS RESULTS

7.1 Introduction

In this chapter, the temperatures calculated in the model block using the energy input from semi-adiabatic and isothermal calorimetry testing are presented and discussed. The results are compared with temperatures in the experimental block measured by embedded thermocouples. The locations of the thermocouples in the block were presented in Chapter 5. They are duplicated in Figures 7-1 and 7-2 for convenience.

The degree of hydration and the equivalent age, with respect to actual time at the top (Element 5069) and central (Element 4069) regions of the model block, were conducted and are presented in Figures 7-3 and 7-4, respectively. The equivalent age of each point in the concrete is calculated according to the Arrhenius-type equation

$$t_e = \int_0^t e^{\frac{E_a}{R}\left(\frac{1}{T_{ref}} - \frac{1}{T(t)}\right)} dt \qquad (7\text{-}1)$$

where t_e = equivalent age at the reference temperature (hours);
$T(t)$ = average temperature of concrete at time t (° C);
T = reference temperature (° C);
E_a = activation energy of concrete (J/mol); and
R = universal gas constant (8.3144 J/mol-° C).

It can be seen from these two plots that the rate of hydration, and hence, the maturity of the concrete, varies within the block due to the different time-temperature histories of the hydrating cement.

Figure 7-5 shows the quarter block of hydrating concrete with insulation on the bottom and sides at time step 1.

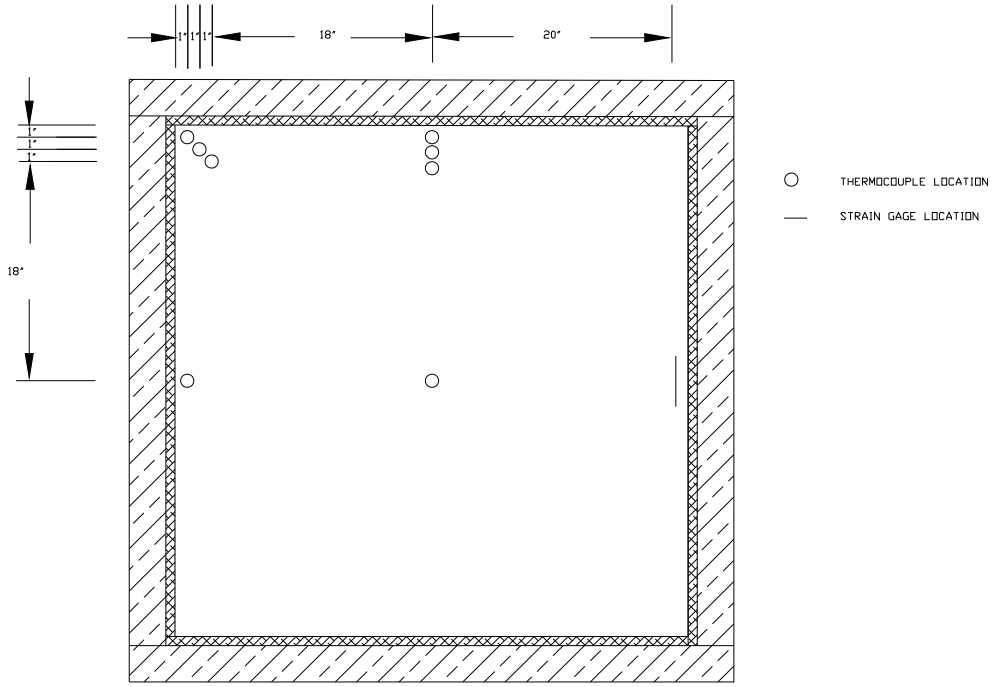

Figure 7-1. Thermocouple location (plan).

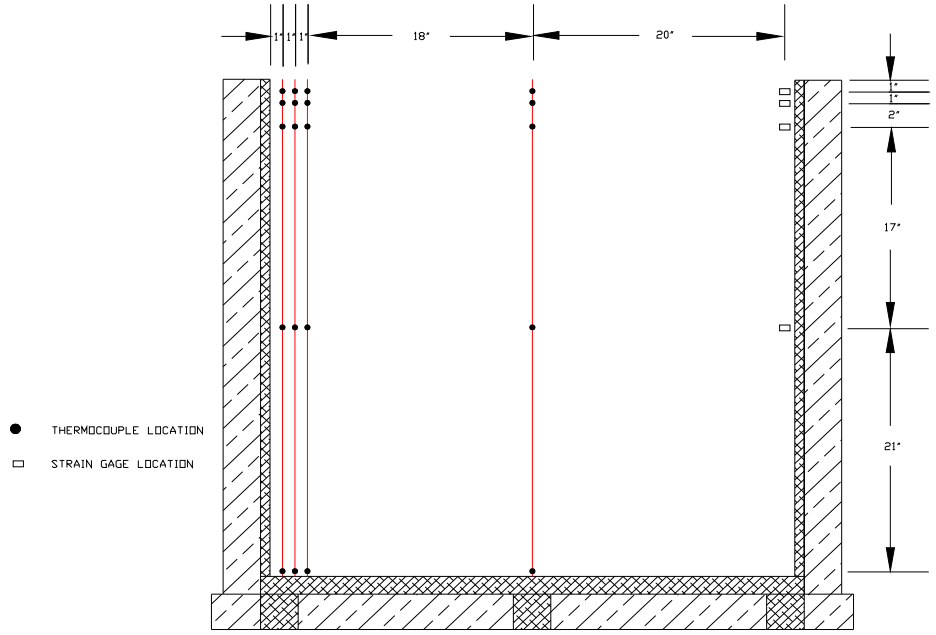

Figure 7-2. Thermocouple location (section).

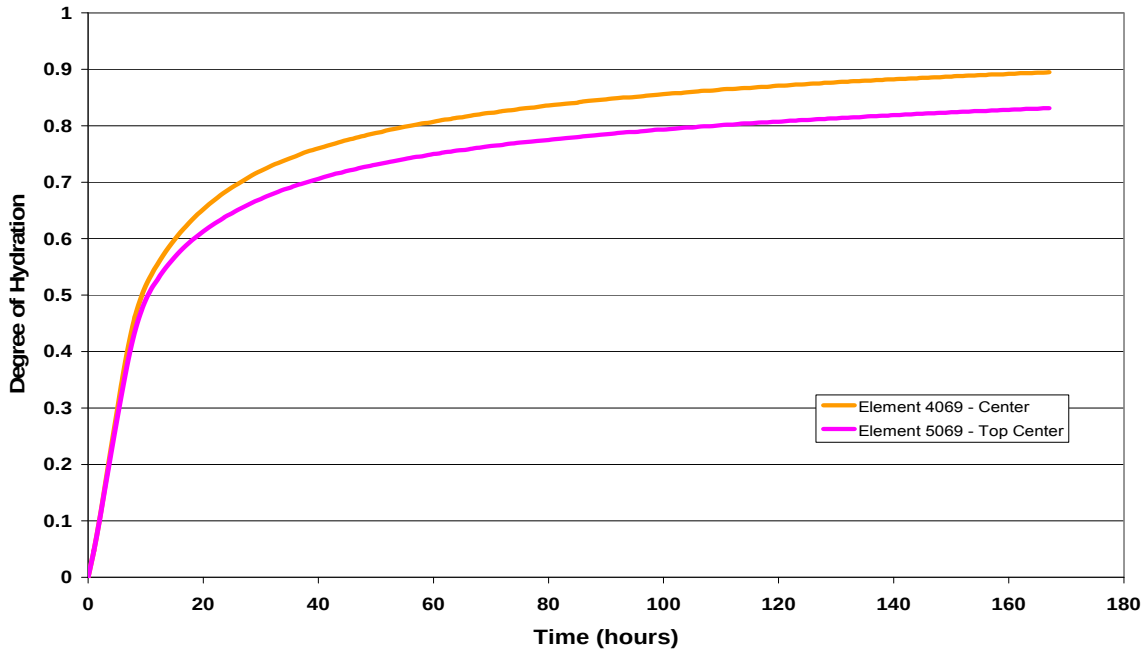

Figure 7-3. Degree of hydration at the center and top of the block in Mixture 1.

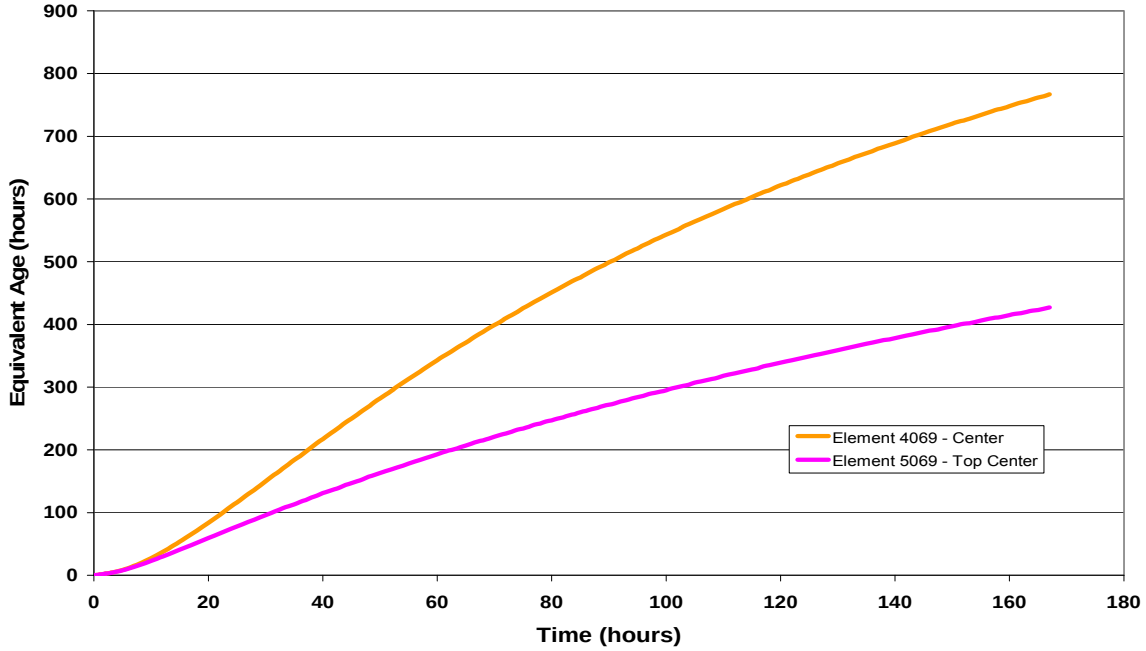

Figure 7-4. Equivalent age at the center and top of the block in Mixture 1.

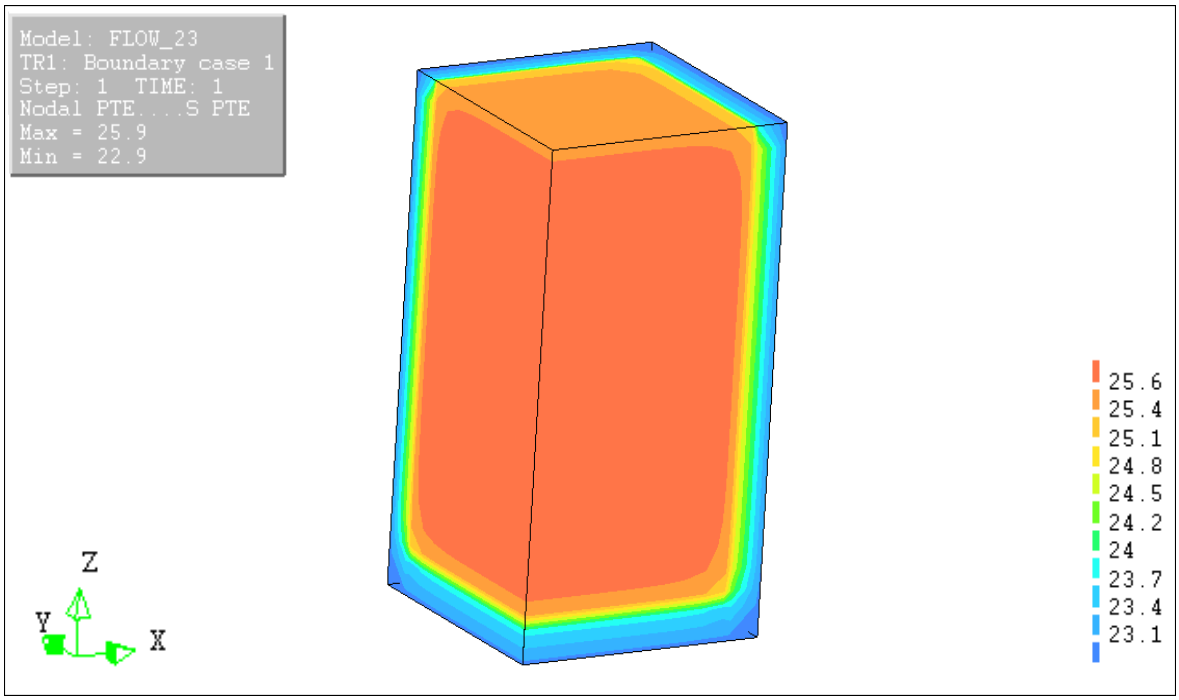

Figure 7-5. Concrete quarter block with insulation at time step 1.

7.2 Semi-Adiabatic Calorimetry Finite Element Results

Points at 2 in., 4 in., and 21 in. below the top surface, along the centerline of the block, were chosen for the analysis. These locations were chosen because various DOT specifications for mass concrete generally limit the temperature differential measured between temperature sensors to between the midpoint and a point 2 in. inside the exposed face.

Figures 7-6 through 7-17 show the comparison of temperatures measured in the experimental blocks of each mixture, with the temperature profiles (with respect to time) produced by the analysis with DIANA.

The trends for the increase and decrease in temperature produced by the finite element model for the block containing Mixture 1 were similar to the trend recorded experimentally at all three locations. The time lag in the finite element model with respect to the experimental temperatures can be attributed to the delivery of the concrete over an hour after the commencement

of mixing, whereas the beginning of the hydration reaction was captured by the semi-adiabatic calorimetry test. Usually, the semi-adiabatic test is conducted on a sample of concrete obtained directly from the batch used in the block, however, at the time of delivery for Mixture 1, the FDOT computer server experienced a communication failure delaying the initiation of the semi-adiabatic test per the IQ drum by approximately 7 hours. To correct this discrepancy, the mixture was recreated in the lab at a starting temperature of 23° C (73° F), and new specimens were created and used in the semi-adiabatic test.

Figure 7-6 presents the temperatures 2 in. below the exposed top surface of the block. The peak temperature of 49.5° C (121.1° F) calculated by the model is identical to the peak temperature of 49.3° C (120.7° F) measured in the experimental block. On the face of it, this is an impressively accurate simulation, however, the fact that the concrete in the experimental block spent over an hour in the delivery truck means that some energy, which cannot be measured, was

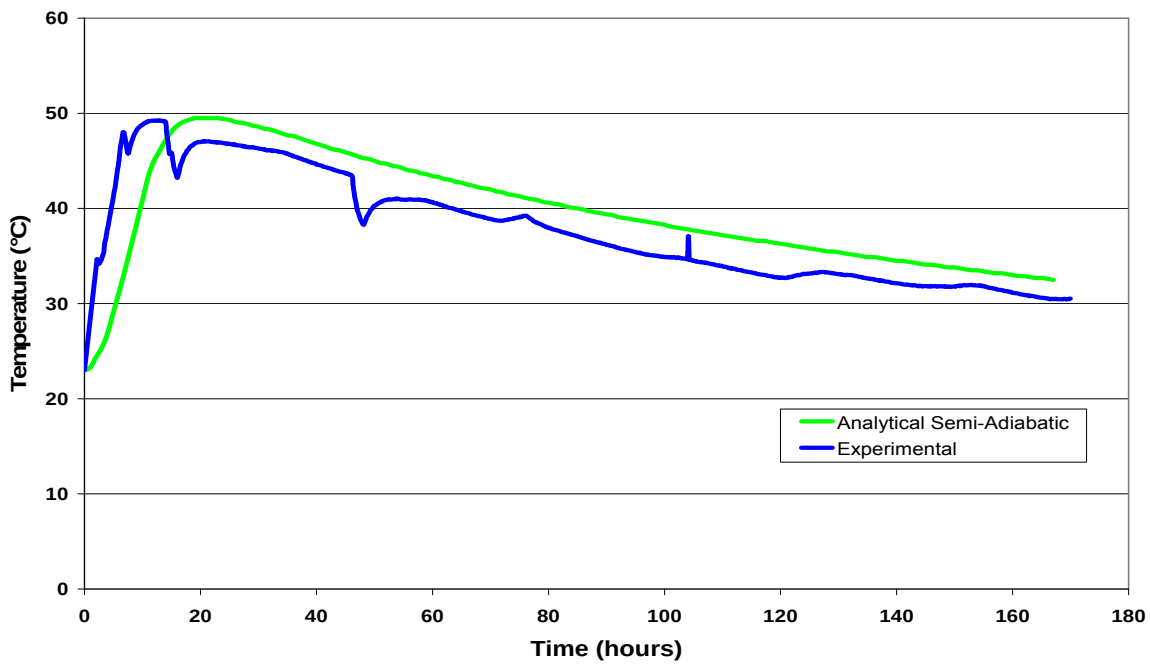

Figure 7-6. Semi-adiabatic and experimentally measured temperature-time histories at the center of the block, 2 in. below the exposed top surface of Mixture 1.

lost to the environment. Another factor that should be taken into consideration is that a companion test that monitored cracking with the aid of acoustic emissions apparatus was being conducted. The dips in the temperature of the experimental block represents each time the plastic cover was lifted off to place the sensors.

Figure 7-7 presents the temperatures 4 in. below the top surface. The peak temperatures of 52° C (125.6° F) in the model and the peak temperature of 53.34° C (128.0° F) measured in the experimental block lie within the ± 2.2° C (±4° F) accuracy of the thermocouples used. Again, the peak temperature in the experimental block is affected by the energy lost while the concrete was in the delivery truck and the lifting off of the cover when placing the acoustic emission sensors.

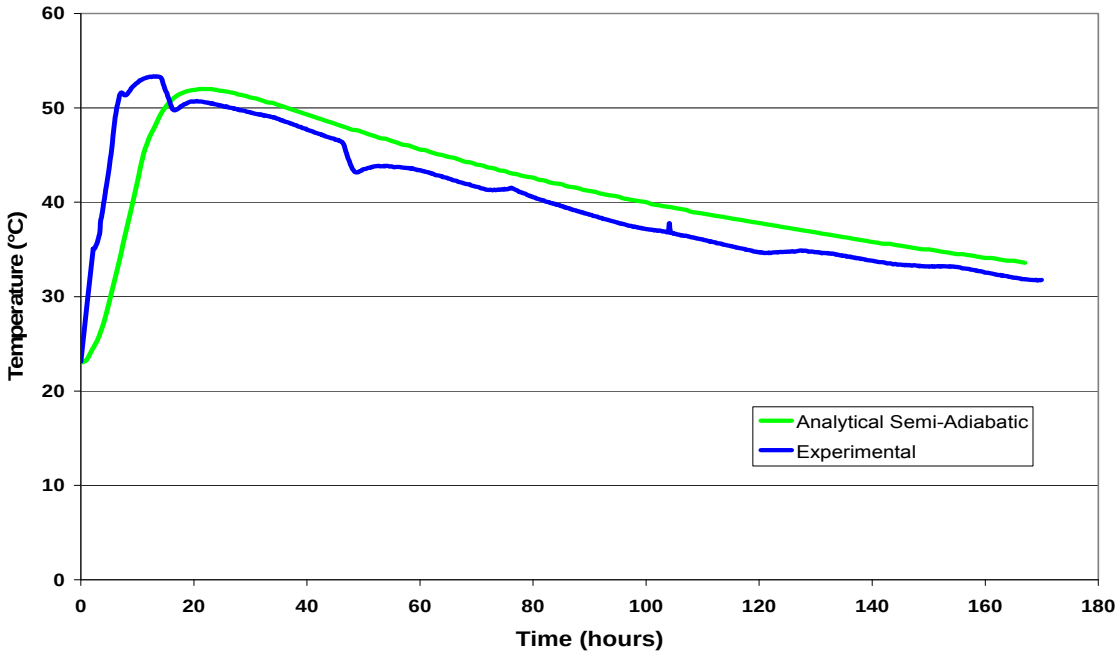

Figure 7-7. Semi-adiabatic and experimentally measured temperature-time histories at the center of the block, 4 in. below the exposed top surface of Mixture 1.

The block temperatures 21 in. below the top surface of the block are presented in Figure 7-8. At this distance from the surface, there seems to be little effect from the cover being lifted

off to place the acoustic emission sensors. The peak temperature of 67.2° C (153.0° F) measured in the experimental block is 6° C (10.8° F) higher than the temperature calculated by the finite element model. It is important to reiterate that the trends in temperature gain and loss are similar.

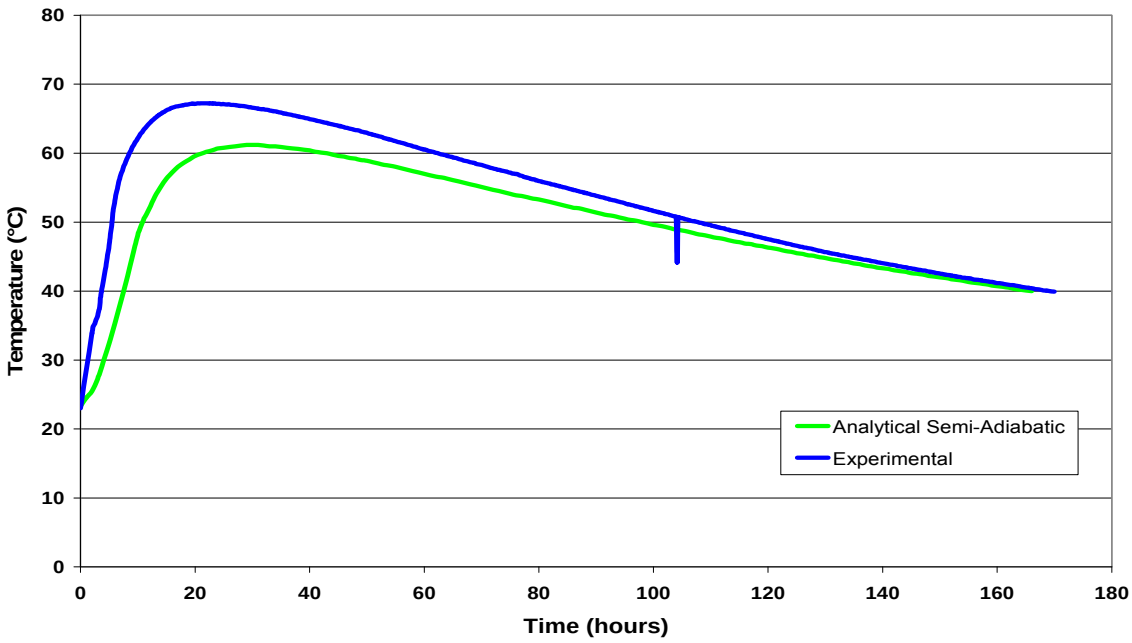

Figure 7-8. Semi-adiabatic and experimentally measured temperature-time histories at the center of the block, 21 in. below the exposed top surface of Mixture 1.

The results for Mixture 2 show that the finite element model again produced an increasing temperature trend similar to that measured in the experimental block. The calculated temperatures in the model, shown in Figure 7-9, peaked at 39.6° C (103.3° F), thirty-eight hours after the start of the analysis. This is a significant 6° C (10.8° F) lower than the peak temperature of 45.7° C (114.3° F) occurring at 35 hours, measured in the experimental block.

Figure 7-10 presents the temperatures 4 in. below the top surface where a similar difference between the model and experimental temperatures was observed. The temperature in the model peaked at 39 hours with a value of 42.4° C (108.3° F) while the experimental block

peaked at 49.6° C (121.3° F) in 33.6 hours. An even more significant difference between the analytical and experimental peak temperatures is observed 21 in. below the top surface of the block, 55° C and 67° C (131° F and152.6° F), respectively, as presented in Figure 7-11.

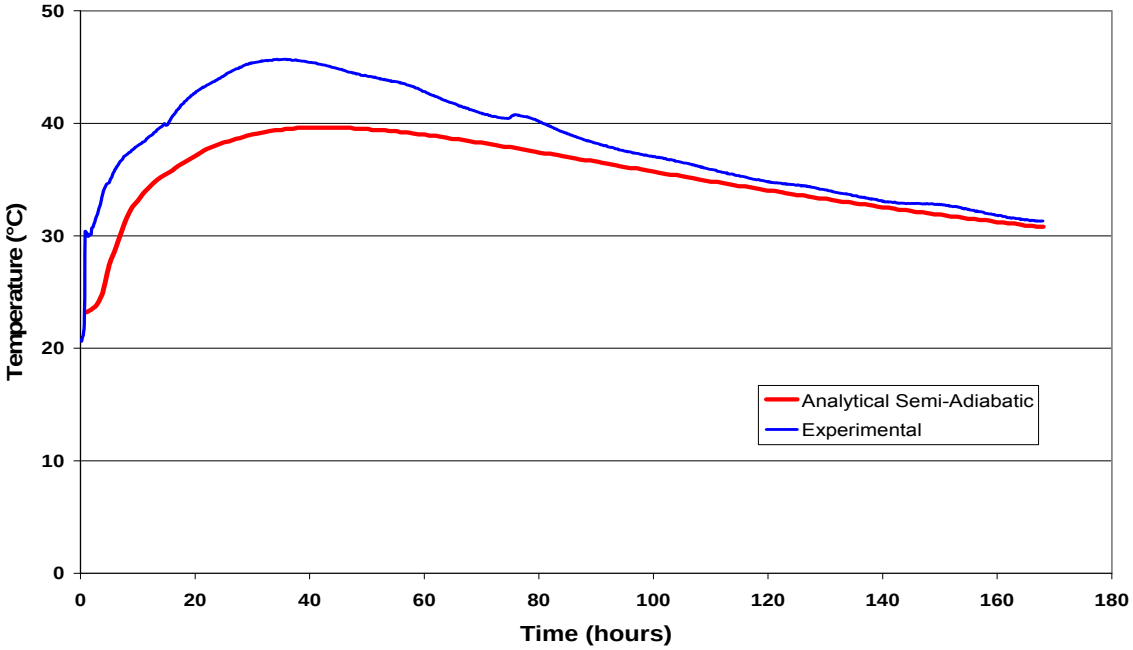

Figure 7-9. Semi-adiabatic and experimentally measured temperature-time histories at the center of the block, 2 in. below the exposed top surface of Mixture 2.

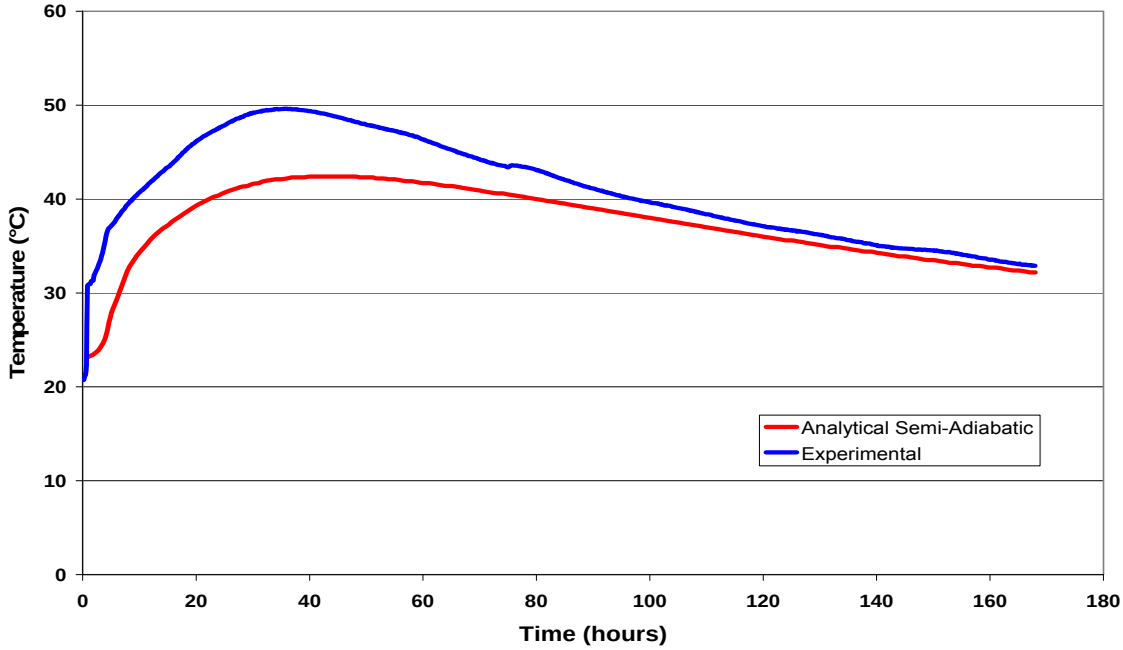

Figure 7-10. Semi-adiabatic and experimentally measured temperature-time histories at the center of the block, 4 in. below the exposed top surface of Mixture 2.

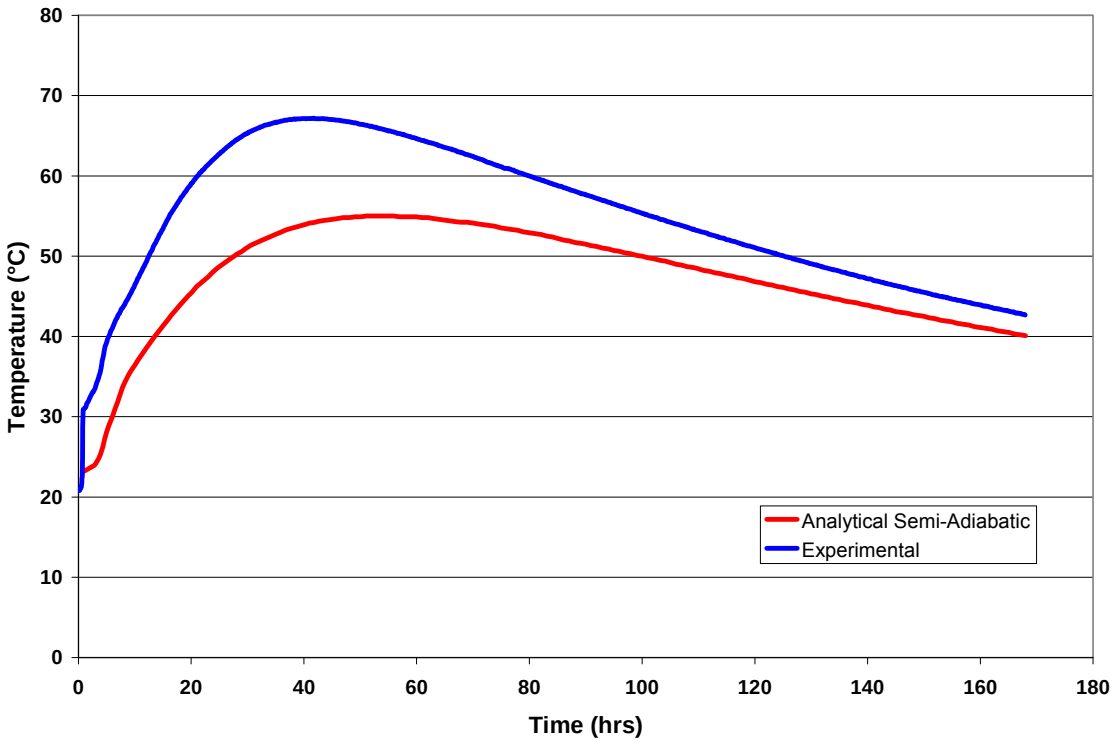

Figure 7-11. Semi-adiabatic and experimentally measured temperature-time histories at the center of the block, 21 in. below the exposed top surface of Mixture 2.

The results for Mixture 3 show better correspondence between the finite element model and the experimentally measured temperatures. Both the increase and decrease in temperature trends are similar. At a depth of 2 in. below the top surface, the calculated peak temperature shown in the model in Figure 7-12 was 40.2° C (104.4° F), while the peak temperature measured in the experimental block at the same depth was 41.8° C (107.2° F). Figure 7-13 shows that at 4 in. below the top surface, the peak temperatures were 42.5° C and 44.3° C (108.5° F and 111.7° F) in the model experimental block, respectively. The temperatures at 21 in. are presented in Figure 7-14. Although the temperature trends are similar, the peak temperature in the model is 51.6° C (124.9° F), while the experimentally measured temperature was 56.4° C (133.5° F), a difference of 4.8° C (8.6° F), which is greater than the accuracy range of the thermocouples.

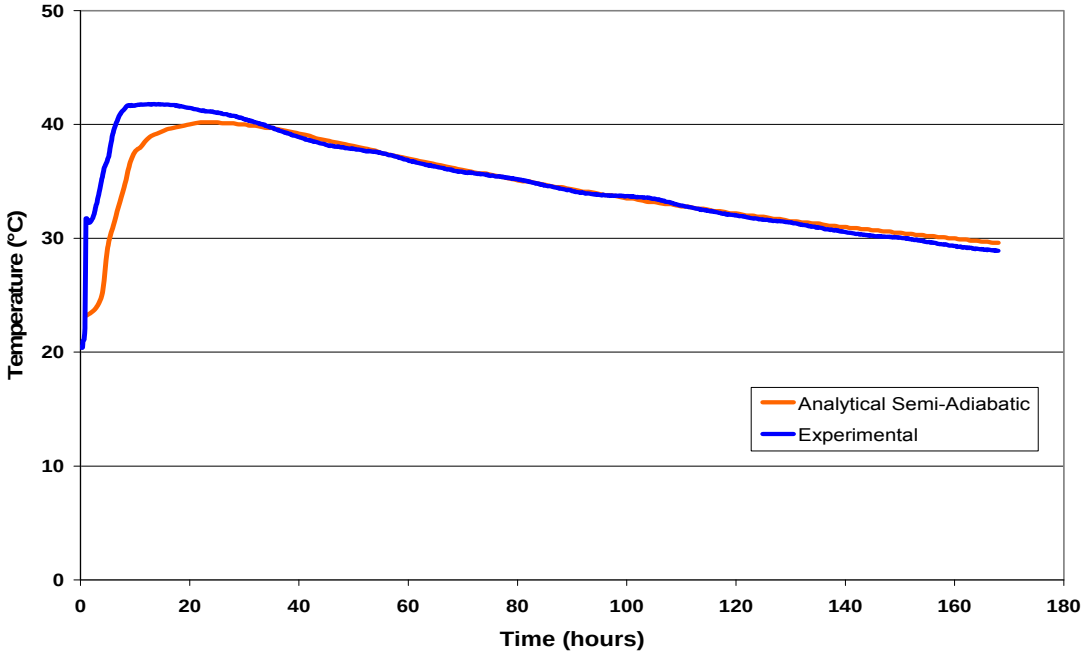

Figure 7-12. Semi-adiabatic and experimentally measured temperature-time histories at the center of the block, 2 in. below the exposed top surface of Mixture 3.

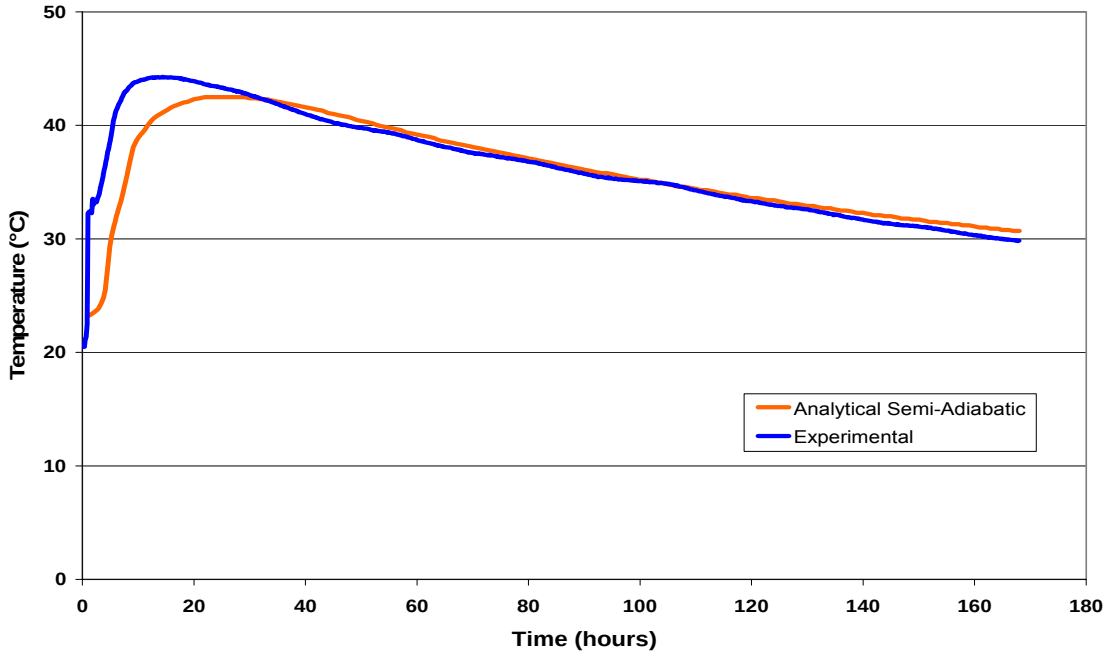

Figure 7-13. Semi-adiabatic and experimentally measured temperature-time histories at the center of the block, 4 in. below the exposed top surface of Mixture 3.

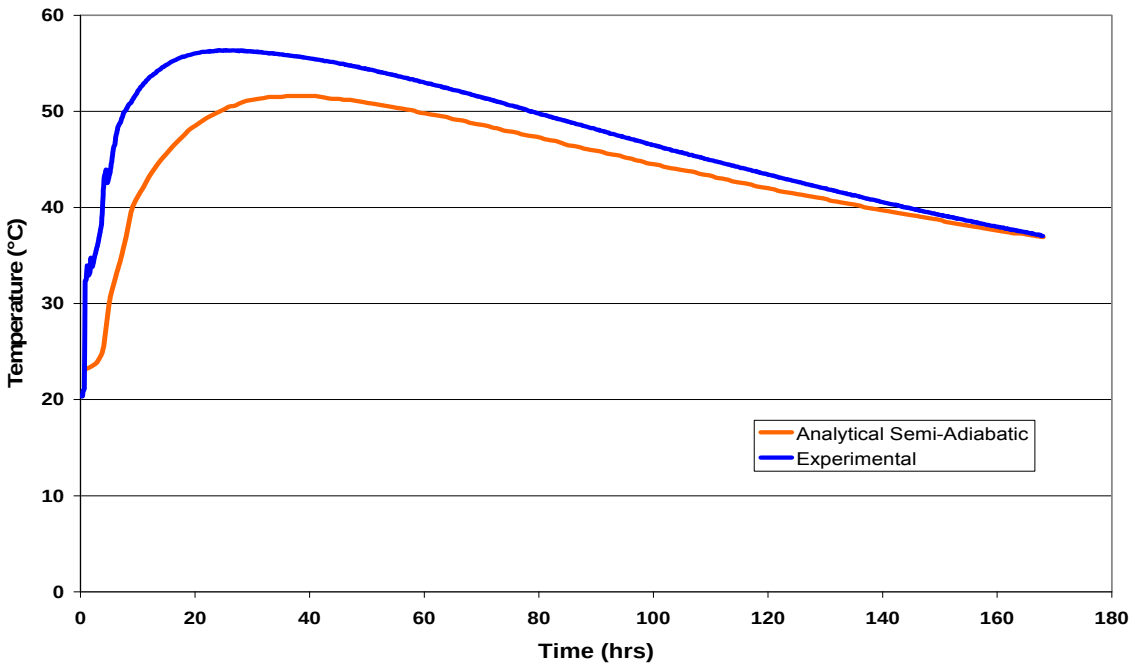

Figure 7-14. Semi-adiabatic and experimentally measured temperature-time histories at the center of the block, 21 in. below the exposed top surface of Mixture 3.

The results for Mixture 4 presented in Figure 7-15 through to Figure 7-17 show the same trends as was reported previously for Mixtures 1 and 3 where at depths of 2 in. and 4 in. below the top surface, the difference between the calculated peak temperatures in the model and the measured peak temperatures in the experimental blocks were within the accuracy of ±2.2° C (±4° F) of the thermocouples. However at 21 in., the difference increases to approximately 4° C (7.2° F).

7.3 Isothermal Calorimetry Finite Element Results

Figures 7-18 through to 7-29 show a comparison of the temperature profiles with respect to time measured in the experimental block, with those obtained from the analytical finite element model using the energy input from the isothermal calorimetry tests. Again, the locations within the block chosen for analysis are 2 in., 4 in., and 21 in. below the top surface along the centerline of the block.

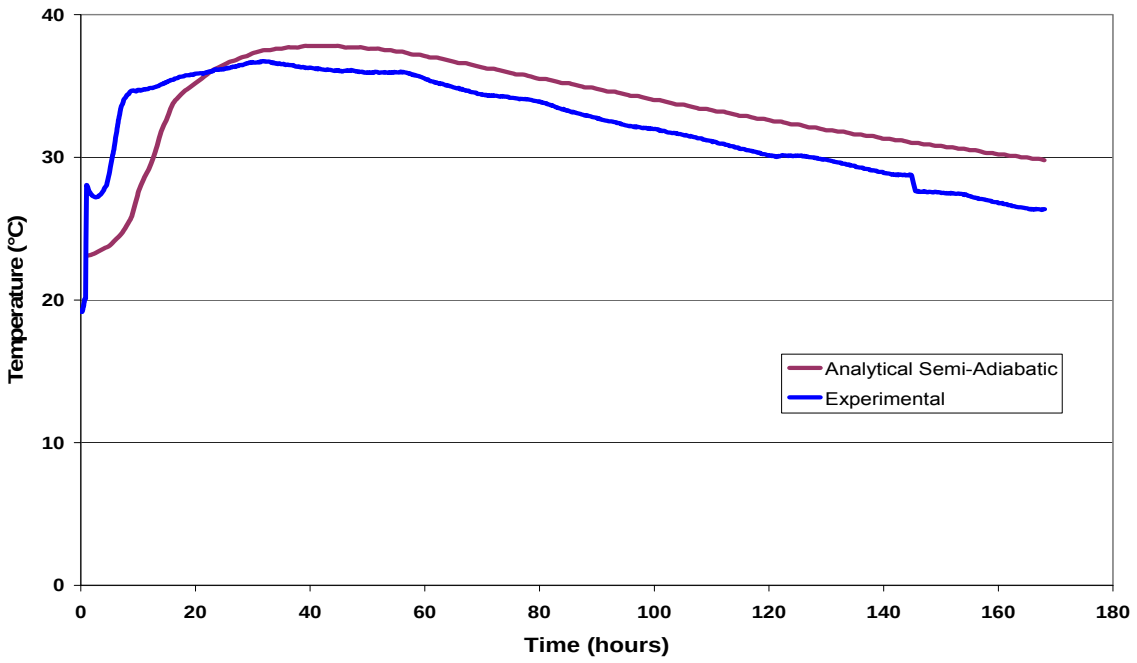

Figure 7-15. Semi-adiabatic and experimentally measured temperature-time histories at the center of the block, 2 in. below the exposed top surface of Mixture 4.

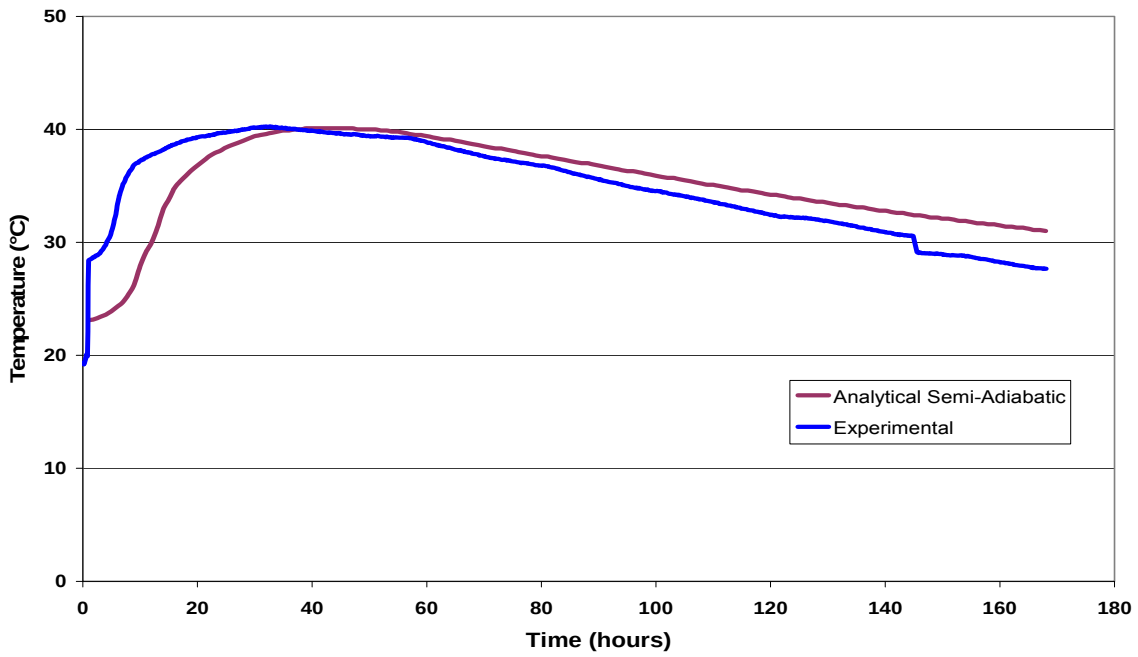

Figure 7-16. Semi-adiabatic and experimentally measured temperature-time histories at the center of the block, 4 in. below the exposed top surface of Mixture 4.

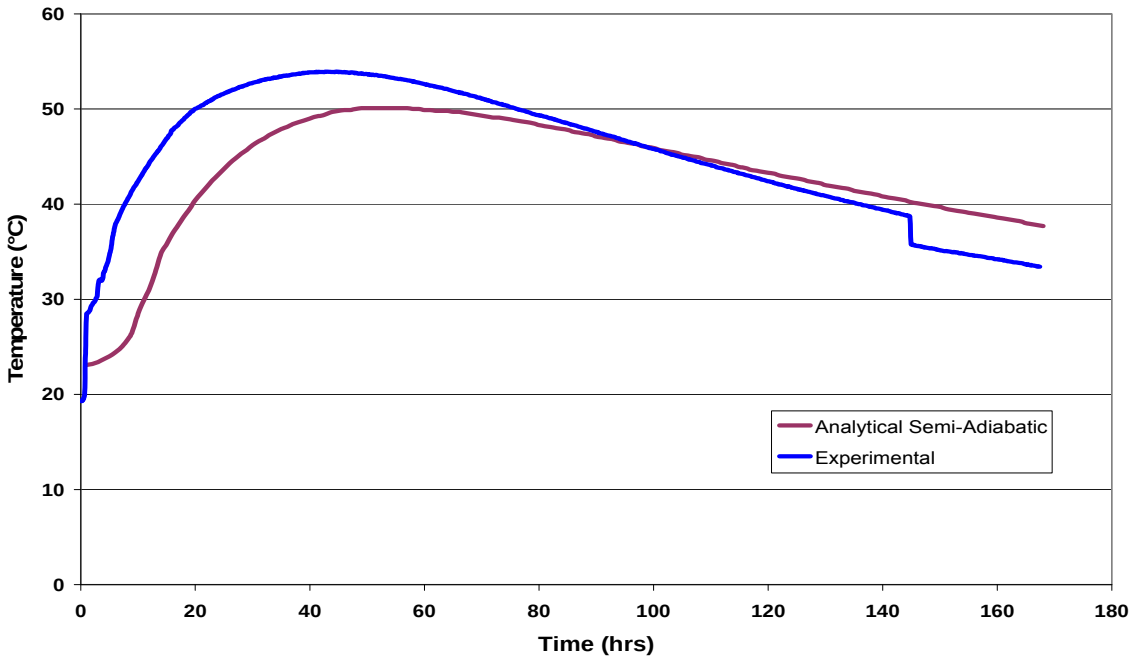

Figure 7-17. Semi-adiabatic and experimentally measured temperature-time histories at the center of the block, 21 in. below the exposed top surface of Mixture 4.

The temperature-time histories of Mixture 1 at 2 in. below the top surface, produced by the finite element model and measured in the experimental block, are presented in Figure 7-18. The increases in temperature for both are identical, however, the predicted peak temperature in the model is 54.6° C (130.3° F), while the experimentally measured peak temperature was 49.3° C (120.7° F). As reported earlier, the dips in the temperature of the experimental block represent each time the plastic cover placed over the block (to prevent evaporation of the surface water) was lifted off to place the sensors used by the crack monitoring acoustic emissions apparatus. This, no doubt, affected the peak temperature of points close to the top surface of the block.

Figure 7-19 shows the comparison of the temperature profiles 4 in. below the top surface. Again, the peak temperature measured experimentally is affected by the removal of the plastic cover. The increase and subsequent decrease in temperatures, however, are identical.

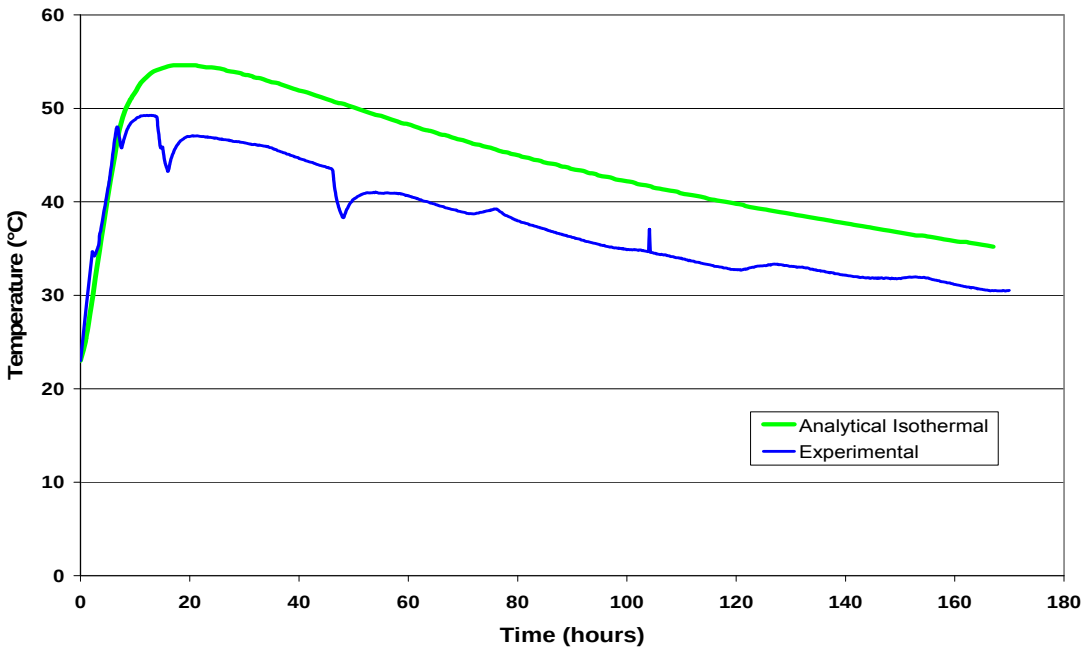

Figure 7-18. Isothermal and experimentally measured temperature-time histories at the center of the block, 2 in. below the exposed top surface of Mixture 1.

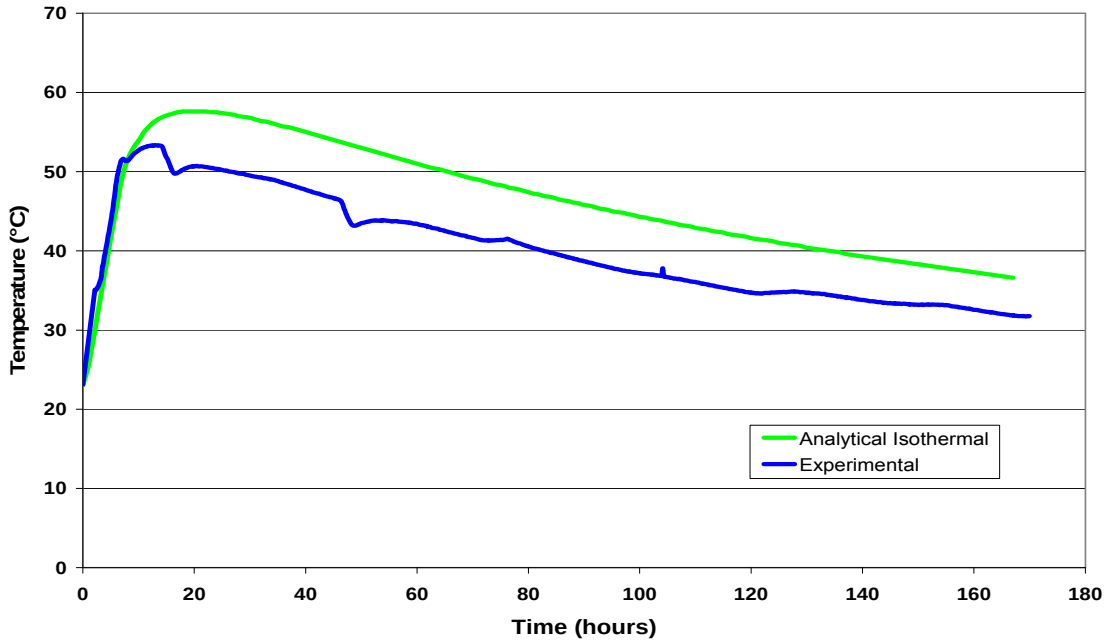

Figure 7-19. Isothermal and experimentally measured temperature-time histories at the center of the block, 4 in. below the exposed top surface of Mixture 1.

At 21 in. below the top surface, the effect of the removal of the plastic cover is negligible, and it can be seen in Figure 7-20 that the peak temperature of 69° C (156.2° F) calculated in the finite element model is only 2° C (3.6° F) greater than the 67.2° C (153.0° F) measured experimentally.

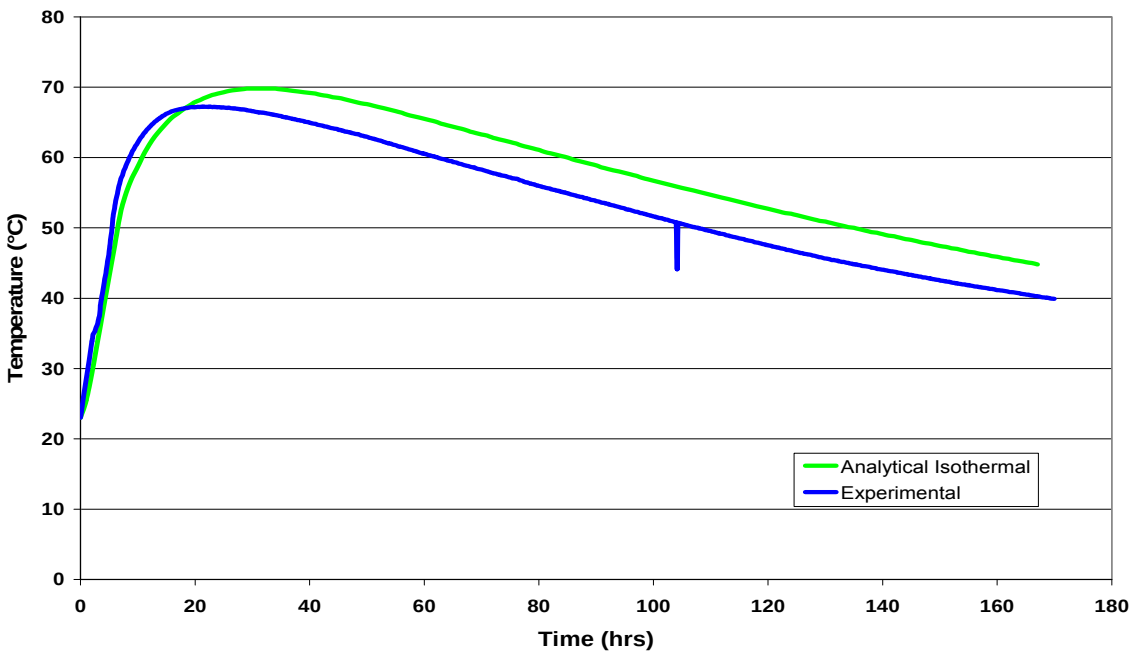

Figure 7-20. Isothermal and experimentally measured temperature-time histories at the center of the block, 21 in. below the exposed top surface of Mixture 1.

Figure 7-21 shows the comparison between temperatures calculated in the finite element model and those measured experimentally in the block containing Mixture 2. Figure 7-22 is the comparison at 4 in. and Figure 7-23 at 21 in.

The maximum temperatures obtained in the model at the three locations are all within 2° C (3.6° F) of the temperatures recorded experimentally. Considering that the accuracy of the thermocouples used to measure the temperatures in the experimental block ±2.2° C (±4° F), it can be concluded that the model has exactly modeled the behavior of the experimental block.

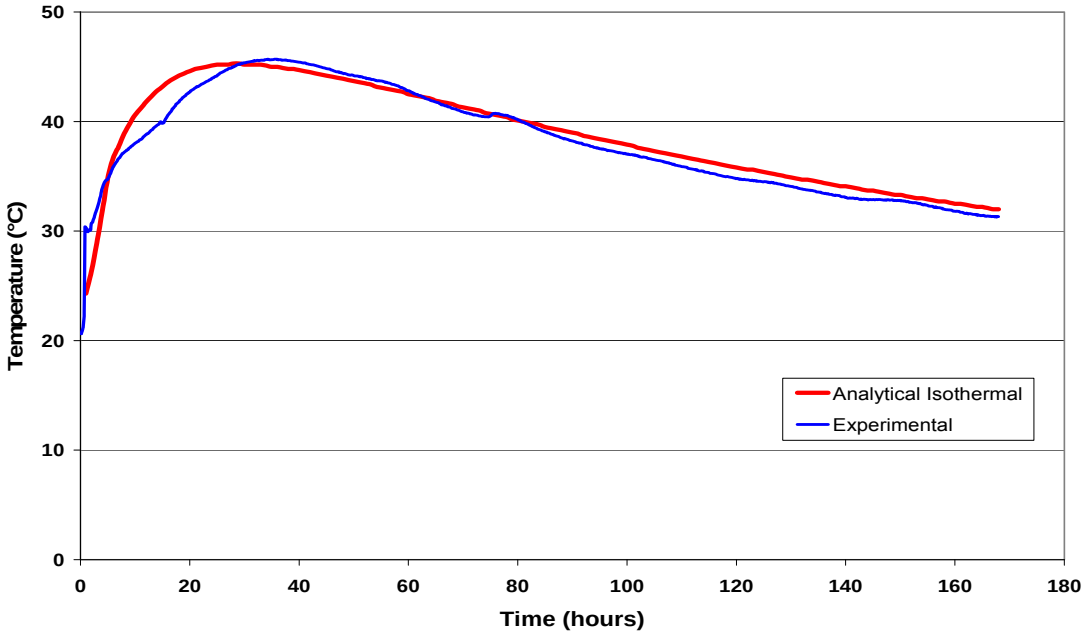

Figure 7-21. Isothermal and experimentally measured temperature-time histories at the center of the block, 2 in. below the exposed top surface of Mixture 2.

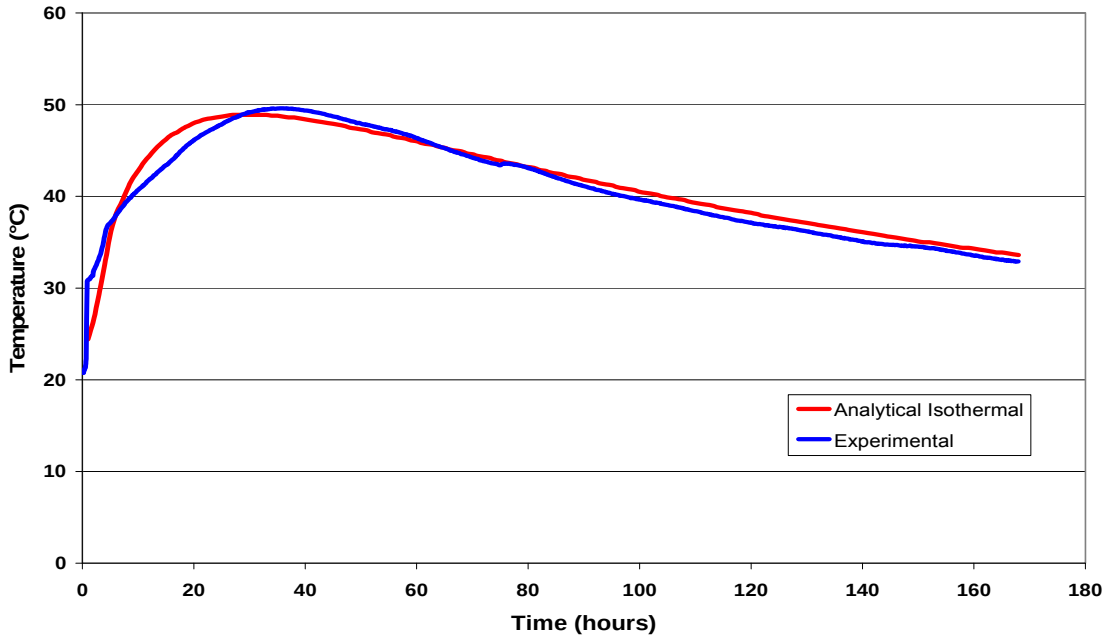

Figure 7-22. Isothermal and experimentally measured temperature-time histories at the center of the block, 4 in. below the exposed top surface of Mixture 2.

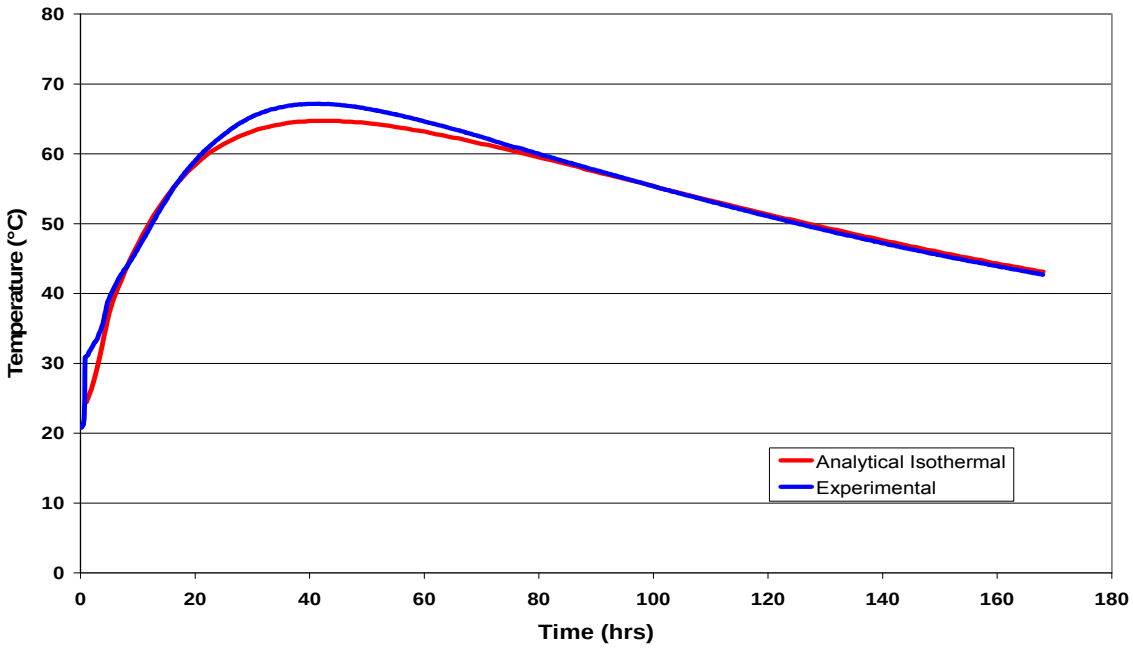

Figure 7-23. Isothermal and experimentally measured temperature-time histories at the center of the block, 21 in. below the exposed top surface of Mixture 2.

The results for Mixture 3 show good correspondence between the finite element model and the experimentally measured temperatures. Both the increase and decrease in temperature trends are similar. At a depth of 2 in. below the top surface, the calculated peak temperature in the model shown in Figure 7-24 was 43.6° C (110.5° F), while the peak temperature measured in the experimental block at the same depth was 41.8° C (107.2° F). Figure 7-25 shows that at 4 in. below the top surface, the peak temperatures were 46.4° C and 44.3° C (115.5° F and 111.7° F) in the model and experimental block, respectively. The temperatures at 21 in. are presented in Figure 7-26. Although the temperature trends are similar, the peak temperature in the model is 56.7° C (134.1° F), while the experimentally measured temperature was 56.4° C (133.5° F), an insignificant difference of 0.3° C (0.5° F).

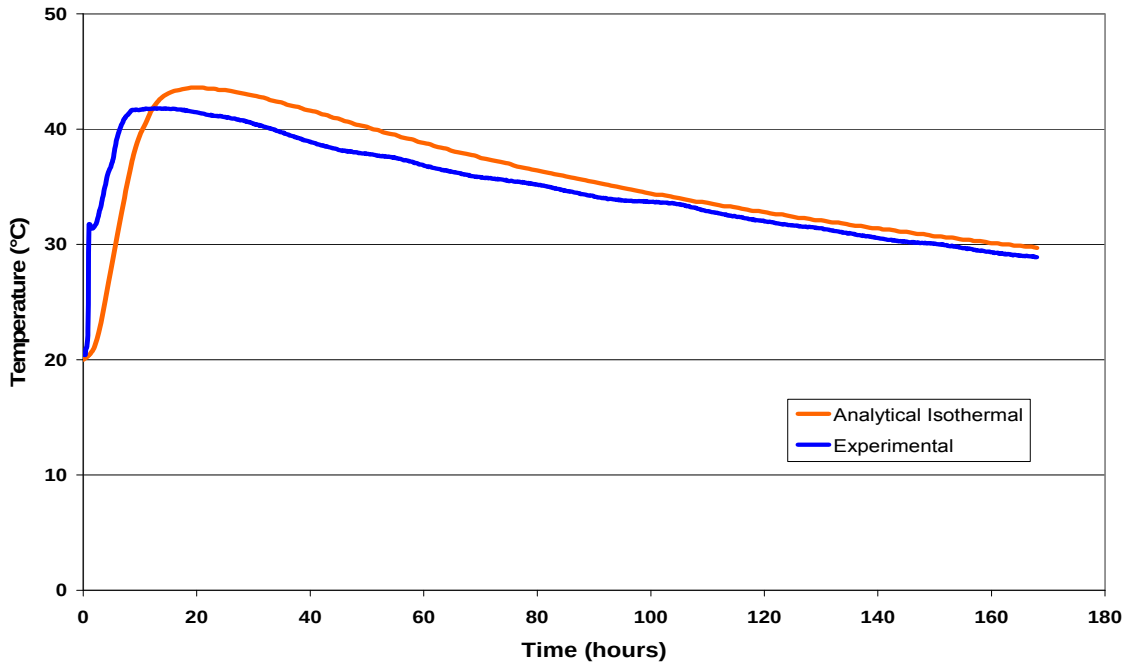

Figure 7-24. Isothermal and experimentally measured temperature-time histories at the center of the block, 2 in. below the exposed top surface of Mixture 3.

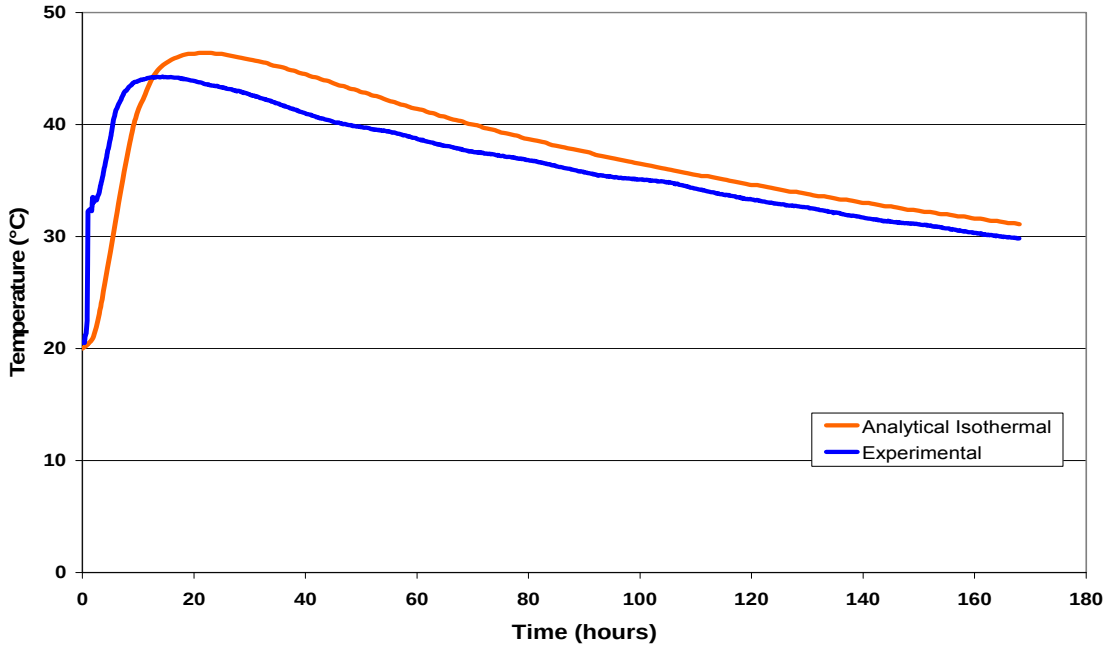

Figure 7-25. Isothermal and experimentally measured temperature-time histories at the center of the block, 4 in. below the exposed top surface of Mixture 3.

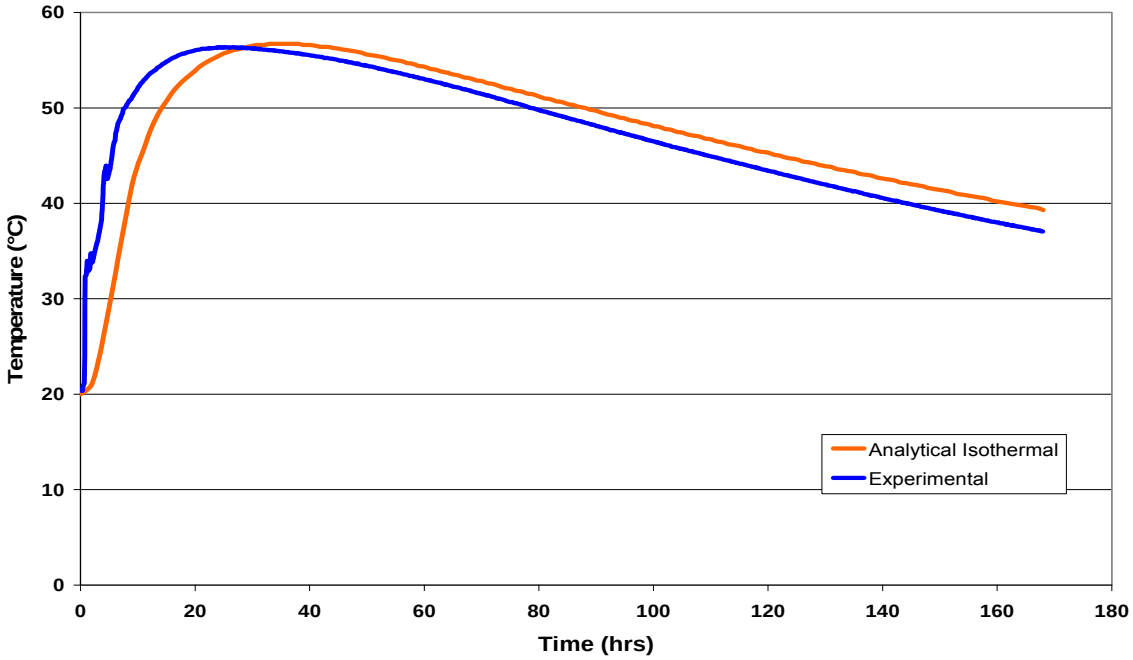

Figure 7-26. Isothermal and experimentally measured temperature-time histories at the center of the block, 21 in. below the exposed top surface of Mixture 3.

The trend of the temperature increases obtained from the model of the block with Mixture 4 differed from what was obtained in the experimental block, as shown in Figures 7-27 through Figure 7-29. The reason for this difference is unknown, but the fact that the peak temperatures obtained at 2 in., 4 in., and 21 in. were all within 2.2° C (4° F) of the peak temperatures measured in the experimental block, and the decreasing trend was also similar, provided enough comfort that the temperature gradient within the block was properly modeled.

7.4 Summary of Findings

The semi-adiabatic calorimeter was designed to obtain the temperature rise of the concrete in the field, therefore, was never intended to serve as a high precision instrument. The temperature results for each of the mixtures modeled were less than the temperatures measured experimentally. This suggests an underestimation of the adiabatic temperature rise of the

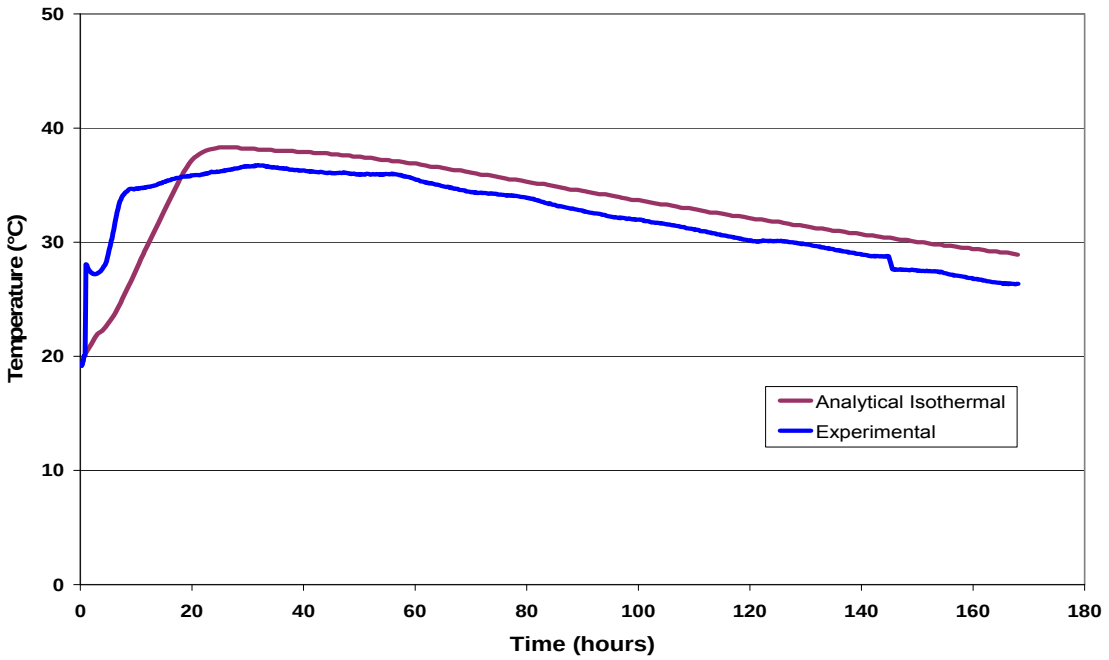

Figure 7-27. Isothermal and experimentally measured temperature-time histories at the center of the block, 2 in. below the exposed top surface of Mixture 4.

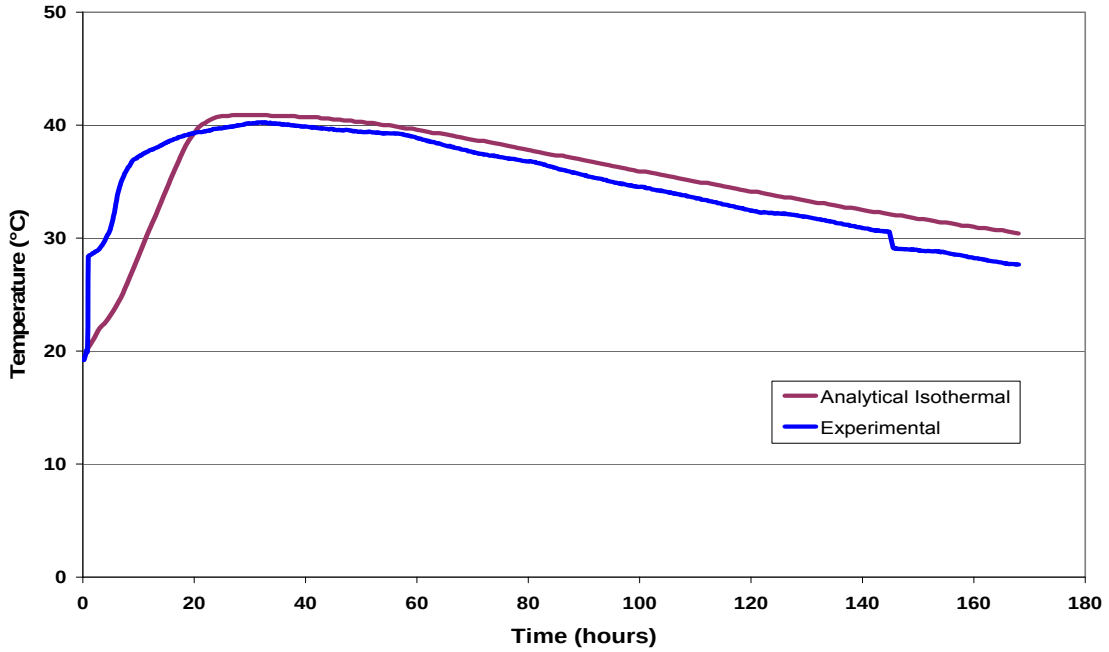

Figure 7-28. Isothermal and experimentally measured temperature-time histories at the center of the block, 4" below the exposed top surface of Mixture 4.

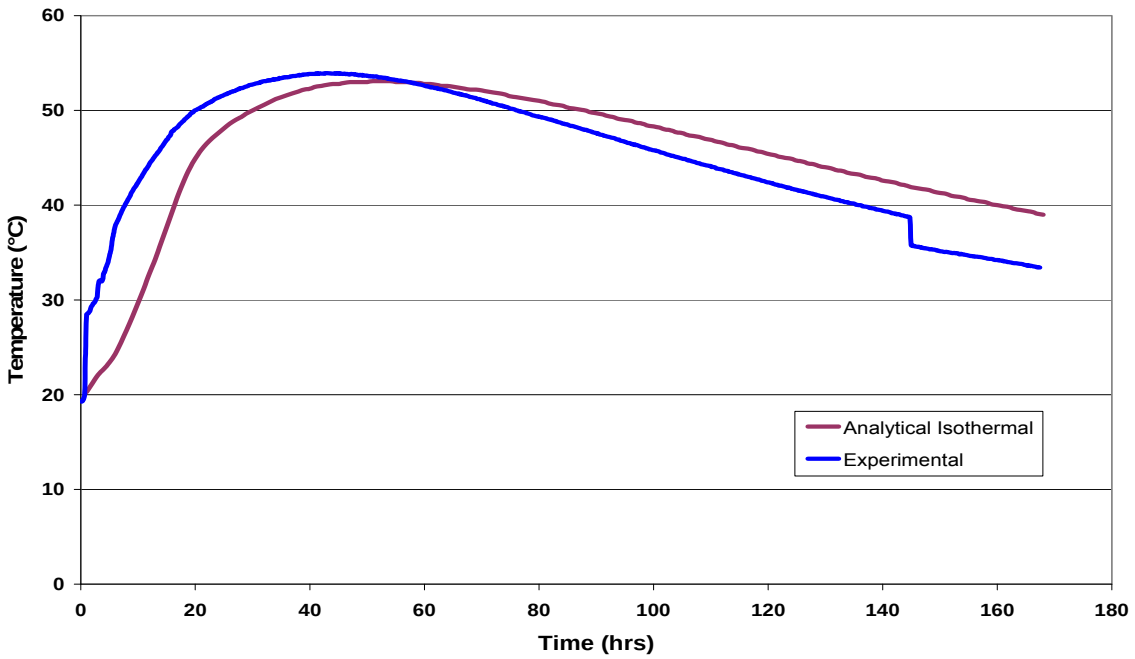

Figure 7-29. Isothermal and experimentally measured temperature-time histories at the center of the block, 21 in. below the exposed top surface of Mixture 4.

concrete mixtures and, by extension, confirms that not all the energy evolved from the concrete was measured.

The adiabatic temperature input from the isothermal calorimetry tests produced temperature profiles that were very similar to the temperatures measured experimentally. In some cases, the temperatures in the model were higher than what was obtained in the experimental block. Accordingly, the temperatures obtained from isothermal calorimetry can be considered conservative, and thus, the preferred input for modeling concrete.

CHAPTER 8
STRUCTURAL ANALYSIS RESULTS

8.1 Stress Results

In this chapter, the stresses and strains induced by the differences in temperature within the hydrating concrete using the isothermal calorimetry data are presented and discussed. As stated earlier, these temperature gradients are produced when the heat being generated in the concrete is dissipated to the surrounding environment causing the temperature at regions close to the surface of the concrete to be lower than the temperature at the interior of the concrete. At the same time, the heat generated is a function of the temperature and time history of the concrete, therefore, individual locations in the concrete will experience different levels of heat. Figure 8-1 shows the location of the elements that will be analyzed for their stress and strain states during the hydration process. These locations were chosen because the largest tensile and compressive actions will be experienced at the top and central region of the concrete, respectively.

Figure 8-2 presents the calculated stress in the X-X plane, occurring in the block with Mixture 1, with respect to time of Element 4069 (node 638) and Element 5069 (node 508), which are located at the center and top center of the finite element model, respectively. The plot shows the model accurately predicts that Element 5069 undergoes tensile (positive) stresses as the concrete hydrates and expands, while Element 4069 experiences compressive stresses. This is consistent with the theory that a faster hydrating central region of a massive concrete structure will be in compression as it tries to expand, but is restricted by the less mature concrete around it. Figure 8-3 presents the calculated stress in the X-X plane with respect to time of Element 4259 (node 1208) and Element 5159(node 618), which are located at the center edge and top edge of the finite element model, respectively. Element 5159 undergoes tensile (positive) stresses as the concrete hydrates and expands. Element 4259 also acts in tension as it is being pushed against

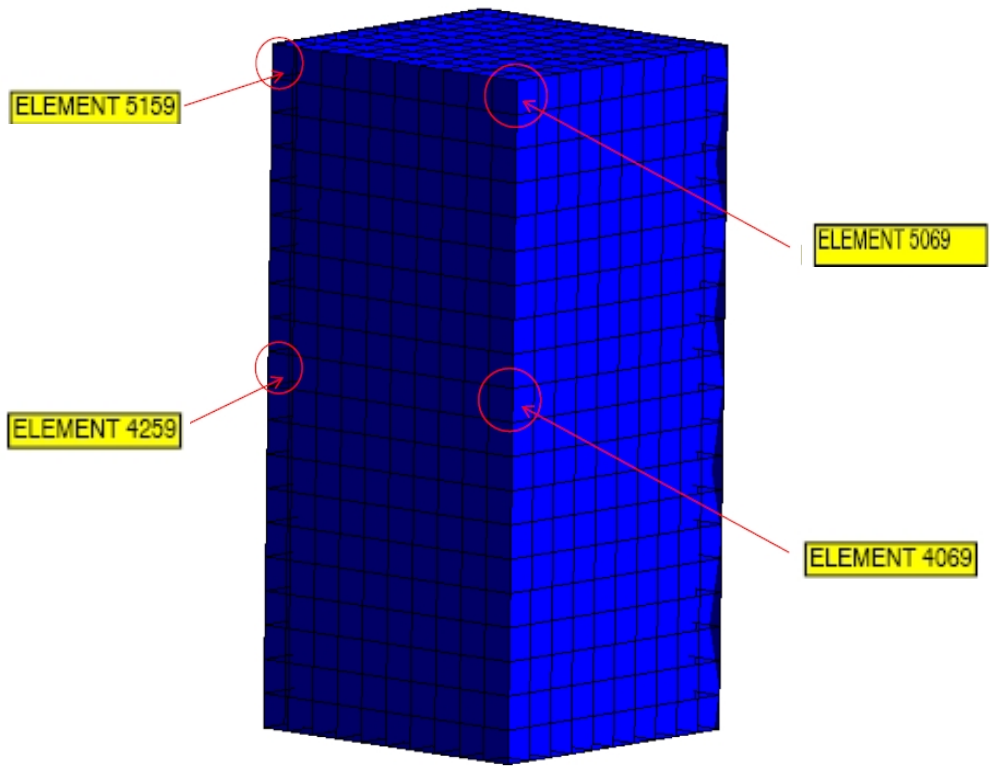

Figure 8-1. Location of elements analyzed for stress.

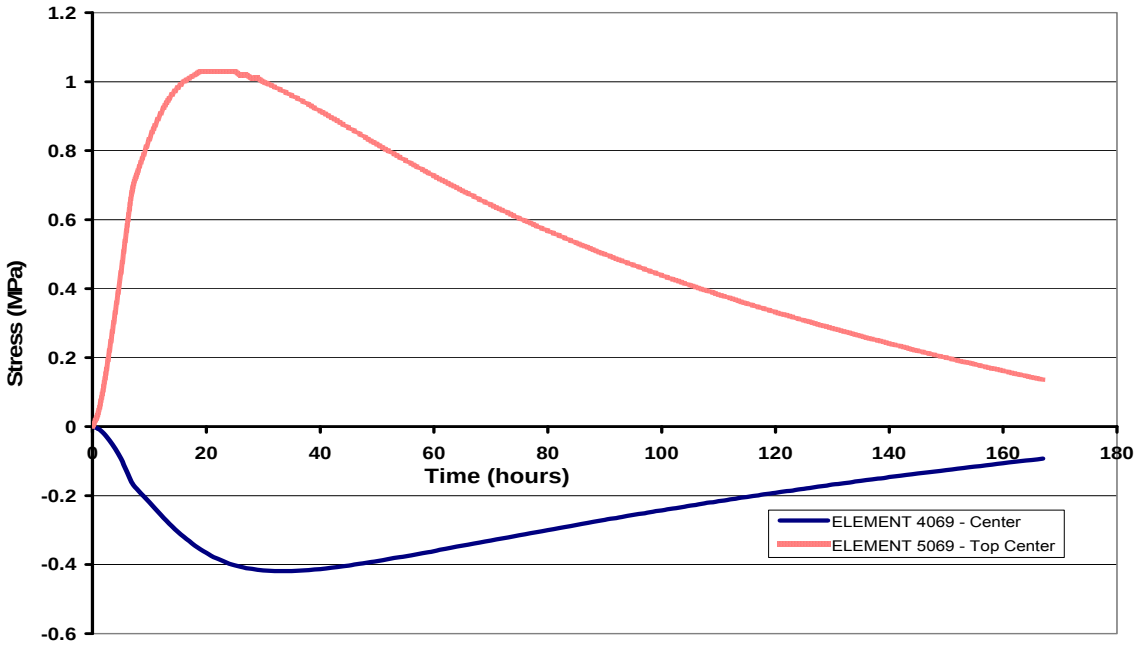

Figure 8-2. Stress state at the top center and center of the finite element concrete block with Mixture 1.

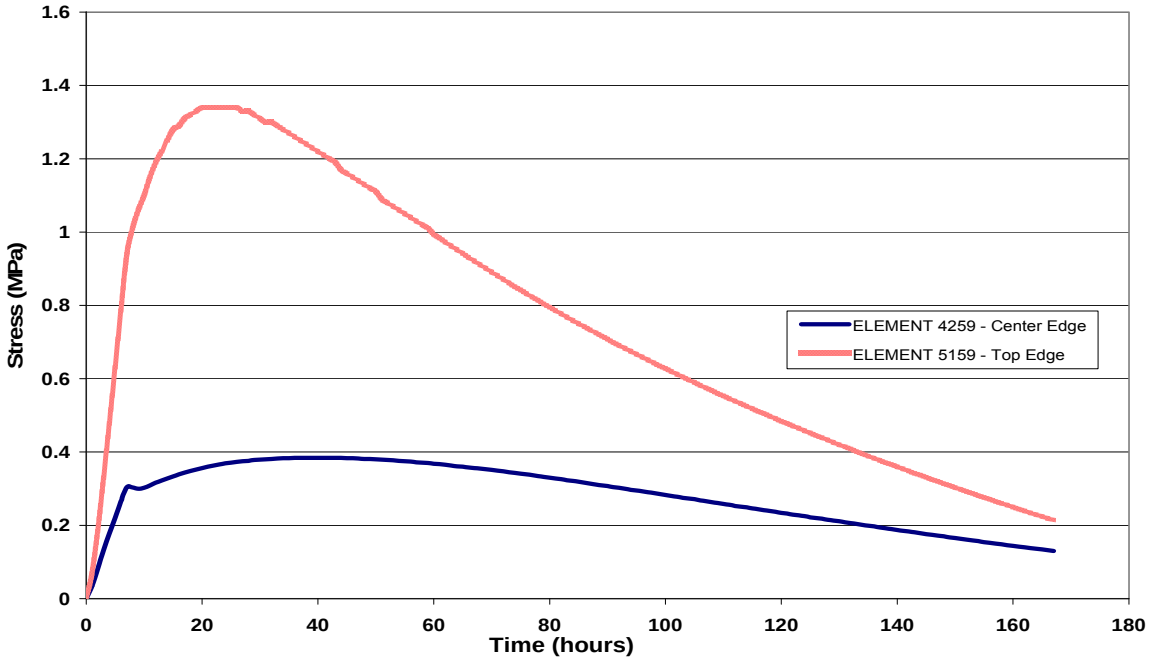

Figure 8-3. Stress state at the top edge and center edge of the finite element concrete block with Mixture 1.

by the expanding inner concrete. As expected, the maximum tensile stress of 1.34 MPa (194 psi) occurs at the top edge of the block in Element 5159.

The effect on the induced stresses in the concrete of Mixture 2 which contains slag is shown in Figures 8-4 and 8-5. The peak tensile stresses in Element 5069 (0.97 MPa or 141 psi) and Element 5159 (1.18 MPa) at the top of the block, were slightly less than the tensile stresses experienced in Mixture 1 containing 100% Portland cement, but occurred approximately 10 hours later. The similarities in peak tensile stress values is a result of the closeness of the peak temperatures in each mixture, while the time difference can be attributed to the slow rate of hydration, and hence, slow rate of temperature increase in the concrete. Interestingly, the stresses across the top of the block transition to compressive stresses 150 hours after placement. The stress at the center edge of the block (Element 4259) acts in tension, as was the case in Mixture 1. The stress in Element 4069 begins in compression, but becomes tensile after 164 hours of hydration.

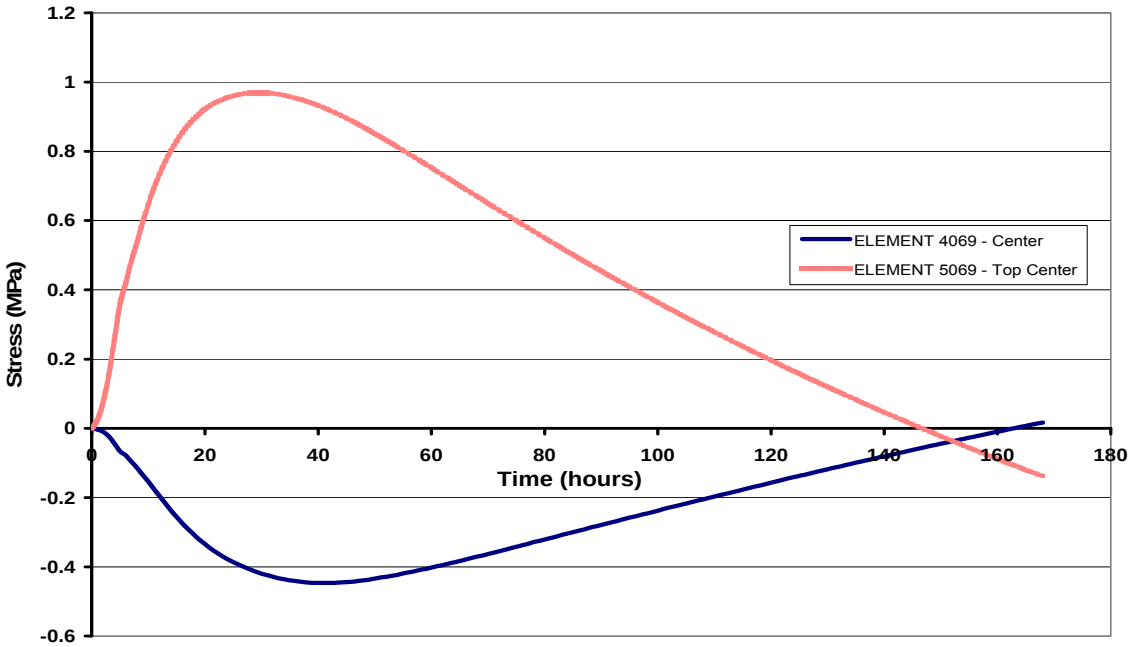

Figure 8-4. Stress state at the top center and center of the finite element concrete block with Mixture 2.

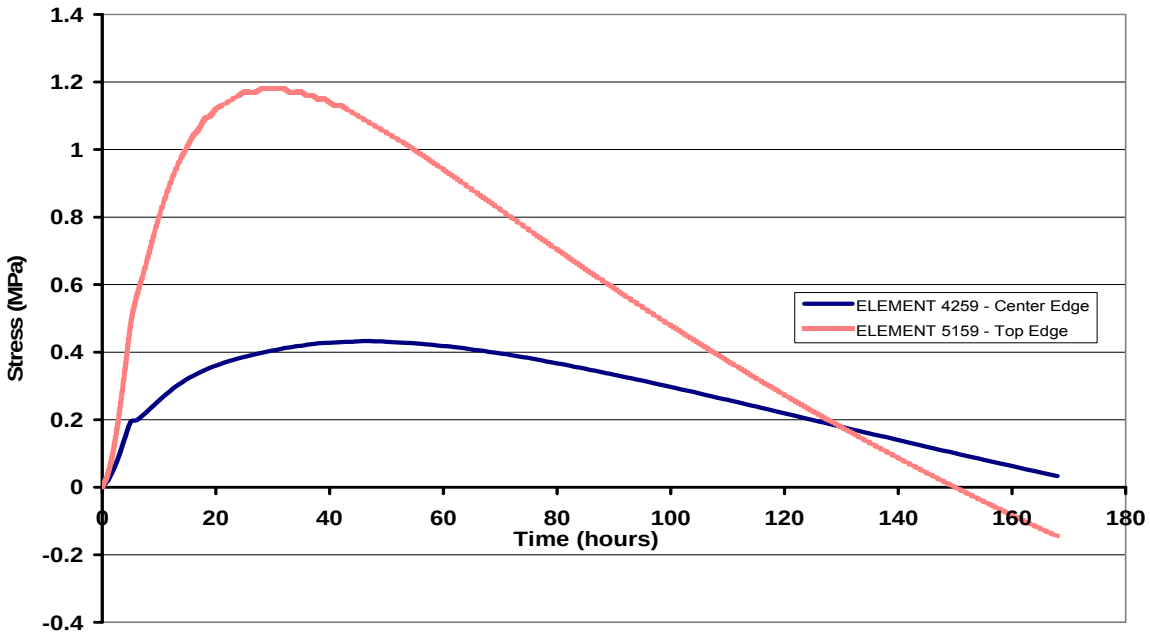

Figure 8-5. Stress state at the top edge and center edge of the finite element concrete block with Mixture 2.

The stresses produced in Mixture 3 were similar in trend to those obtained in Mixture 1. This is to be expected given that the rate of temperature rise in Mixture 3 was steep, as was the case of the temperature rise in Mixture 1. Figure 8-6 shows that the highest tensile stress experienced at the top center of the block (Element 5069) was 0.878 MPa (127 psi) occurring 26 hours after concrete placement, while the maximum compressive stress of 0.358 MPa (52 psi), at the center of the block (Element 4069), occurred 40 hours after placement. The maximum tensile stress value of 1.10 MPa (160 psi) again occurred at the top edge of the block (Element 5159) as shown in Figure 8-7.

Figure 8-8 shows the stresses calculated in the top center and center of the block containing Mixture 4, while Figure 8-9 presents the stresses at the edge. The tensile stresses induced in this block were significantly less than the stresses in Mixture 1and Mixture 3, but slightly larger than the stresses in Mixture 2. The rate of temperature rise of Mixture 4 like Mixture 2, both of

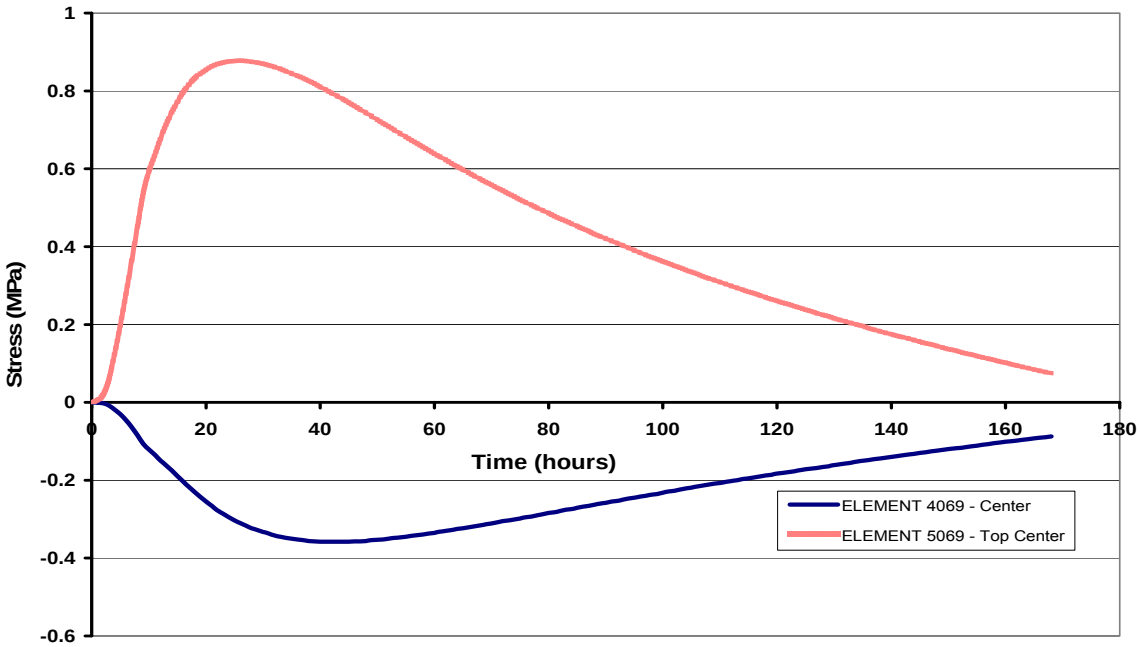

Figure 8-6. Stress state at the top center and center of the finite element concrete block with Mixture 3.

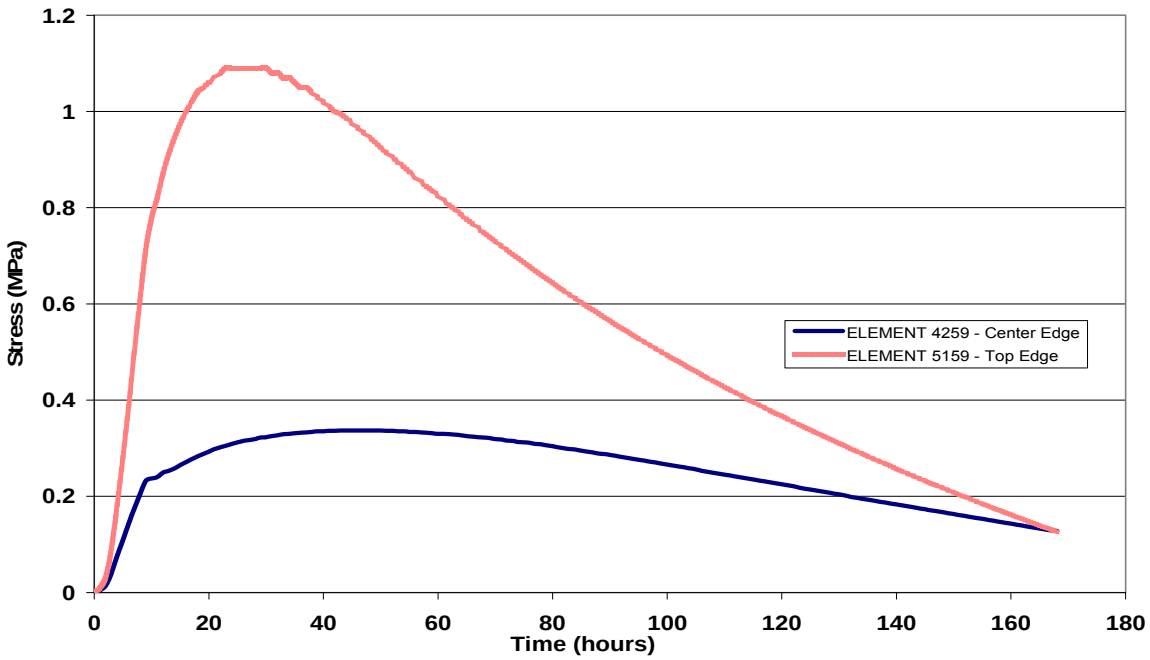

Figure 8-7. Stress state at the top edge and center edge of the finite element concrete block with Mixture 3.

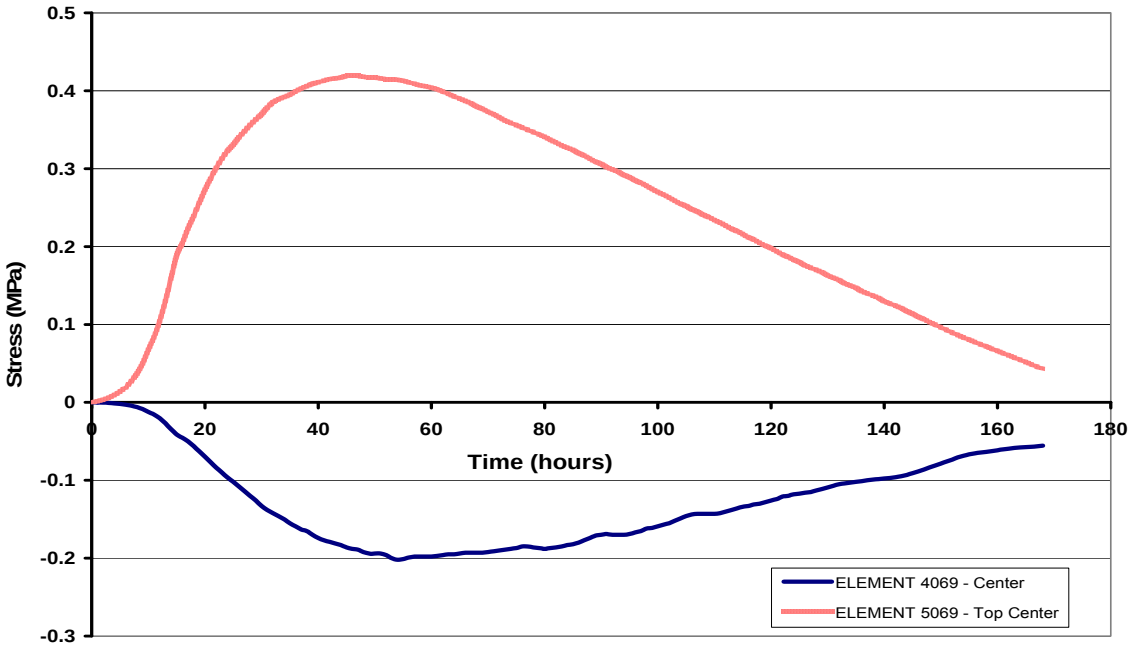

Figure 8-8. Stress state at the top center and center of the finite element concrete block with Mixture 4.

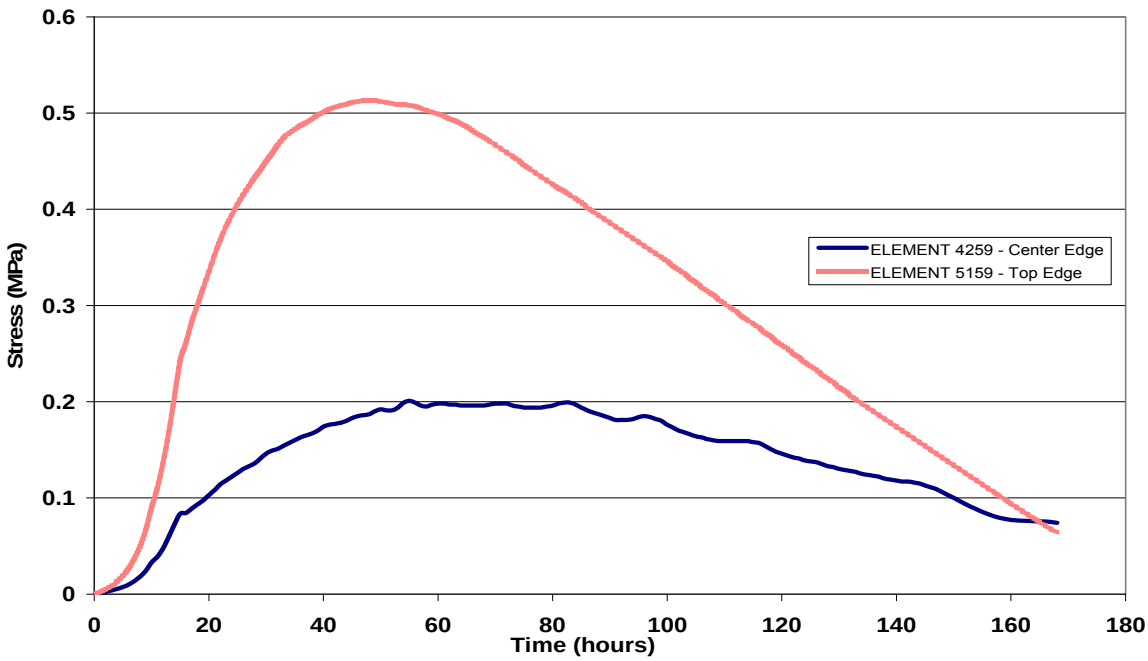

Figure 8-9. Stress state at the top edge and center edge of the finite element concrete block with Mixture 4.

which were presented in Chapter 7, was slow. Therefore, this reduction in tensile stresses can likely be attributed to the presence of the ground granulated blast-furnace slag.

8.2 Cracking Potential

Cracking in concrete will occur when the tensile stresses induced by the temperature gradients exceed the low tensile strength that exists at early ages. The probability of cracking is measured by the function presented in Equation 8-1 called the cracking index.

$$I_{cr}(t) = \frac{f_t(t)}{\sigma_I(t)} \tag{8-1}$$

where I_{cr} = the crack index;
f_t = the tensile strength; and
σ_I = the maximum principal stress.

The crack index (I_{cr}) is given a value of 100 if $\sigma_I \leq 0.01 f_t$. If I_{cr} falls below 1.0, this is an indication that cracking has been initiated.

A plot of the progression of the crack index along the center line of the block in Mixture 1 is presented in Figure 8-10. It shows that almost immediately after the concrete hardens, the crack index for Element 5069 is less than 1.0, indicating that the tensile stress at the top surface edge exceeded the tensile strength of the concrete, and hence, cracking has occurred. Element 4069, which is at the center of the block, is always in a compressive state, therefore, has a constant crack index of 100. Figure 8-11 shows the crack indices for the center edge (Element 4259) and top edge (Element 5159), respectively. Element 4259 remains only just above 1.0, while Element 5159 shows a high probability that cracking occurs during the first 25 hours. This was confirmed by a close examination of the experimental block that contained mixture 1, shown in Figure 8-12, where cracking can be observed at all the top surface edges.

In Mixture 2, cracking occurs at the top center of the block approximately 10 hours after pouring, as shown in Figure 8-13. The same figure also shows that while the center of block goes into tension after 80 hours, the concrete is in a mature state and the tensile strength is well developed. Figure 8-14 shows the crack indices at the edge of the block. As was expected,

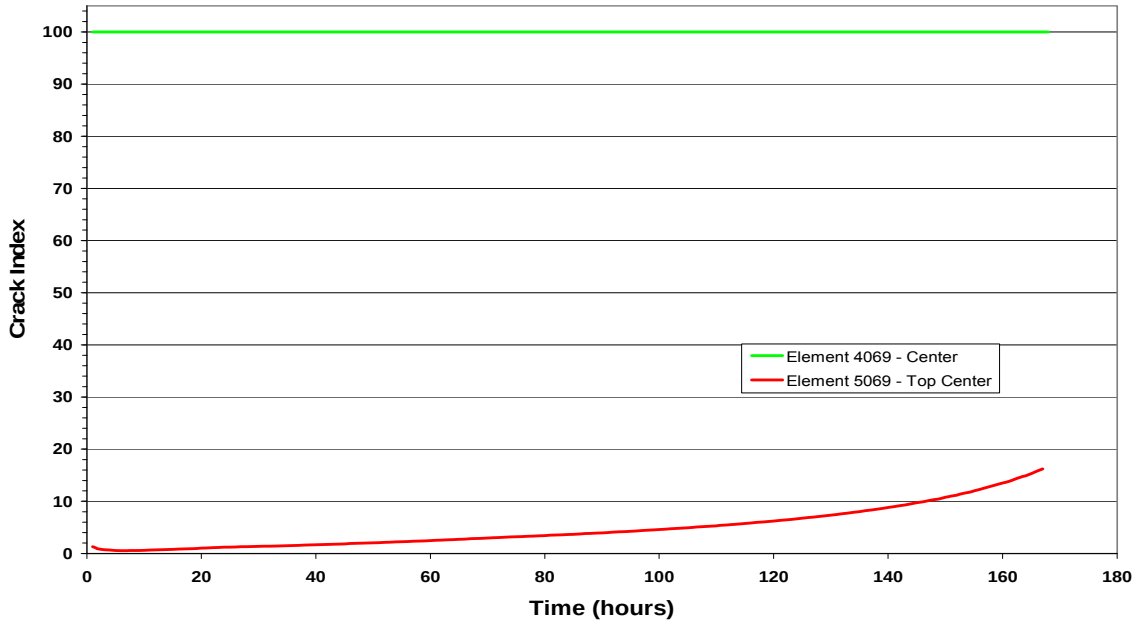

Figure 8-10. Crack index for elements along the center line of block with Mixture 1.

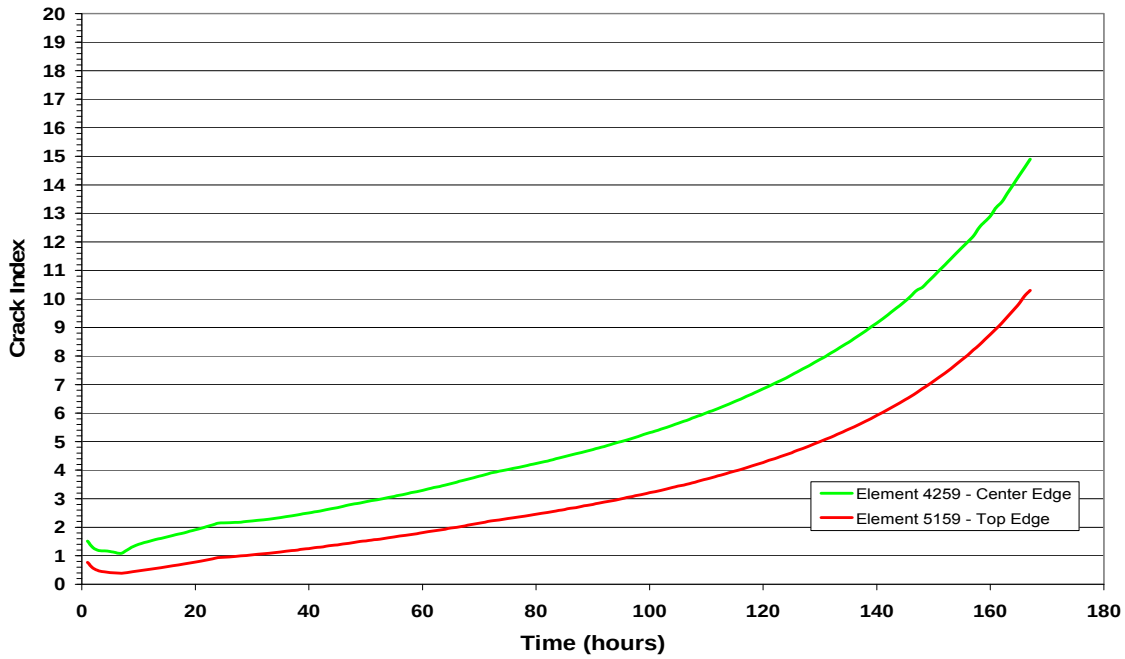

Figure 8-11. Crack index for elements along the edge of block with Mixture 1.

Figure 8-12. Top surface of experimental block containing Mixture 1 showing numerous cracks along the edges.

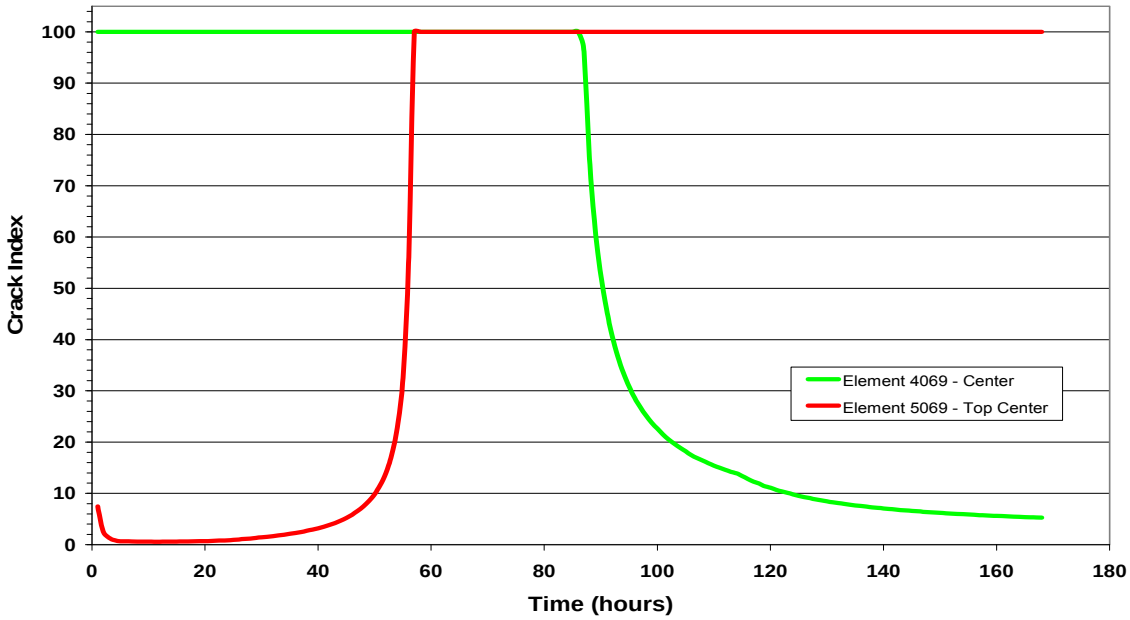

Figure 8-13. Crack index for elements along the center line of block with Mixture 2.

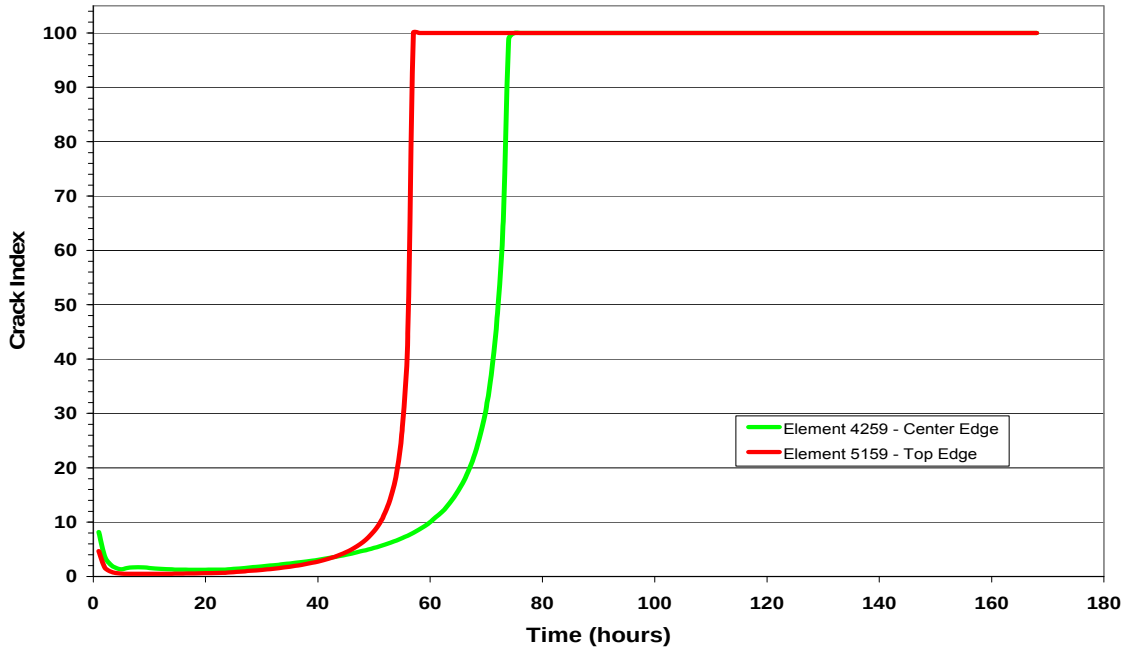

Figure 8-14. Crack index for elements along the edge of block with Mixture 2.

cracking occurs at the top edge of the block, however, the center edge of the block just barely stays above the crack threshold.

Mixtures 3 and 4 act in a similar manner to Mixture 1, where their centers are constantly in compression, and hence, have negligible risks of cracking. In Mixture 3, the crack indices in Element 5069 and Element 5159 suggest that cracking will occur, shown in Figures 8-15 and 8-16, respectively, while Figures 8-17 and 8-18 show that, for Mixture 4, the tensile stresses that develop in these elements will not exceed their tensile strength, and hence, will not crack.

It appears that the ratio of substitution of cementitious materials used in the concrete of Mixture 4 is effective in mitigating the cracking risk in massive concrete elements.

8.3 Temperature Difference and Cracking

As previously stated, the requirements for the control of heat generation and, in particular the maximum allowable temperature difference in mass concrete, vary on a state-by-state basis. Currently, there is no agreement on what the maximum allowable temperature differential should

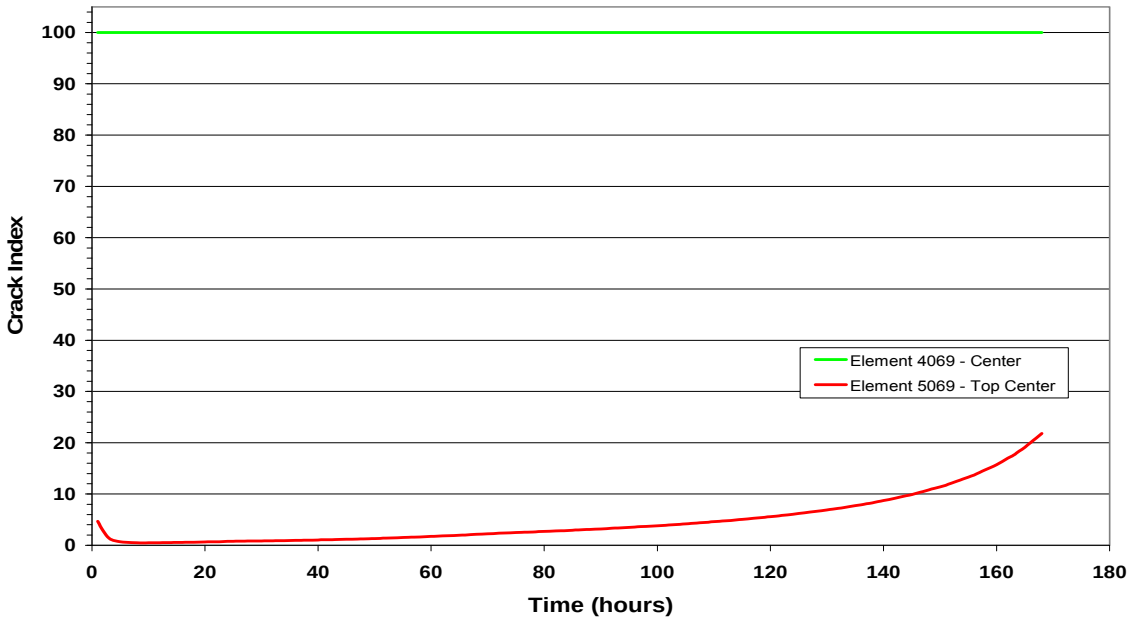

Figure 8-15. Crack index for elements along the center line of block with Mixture 3.

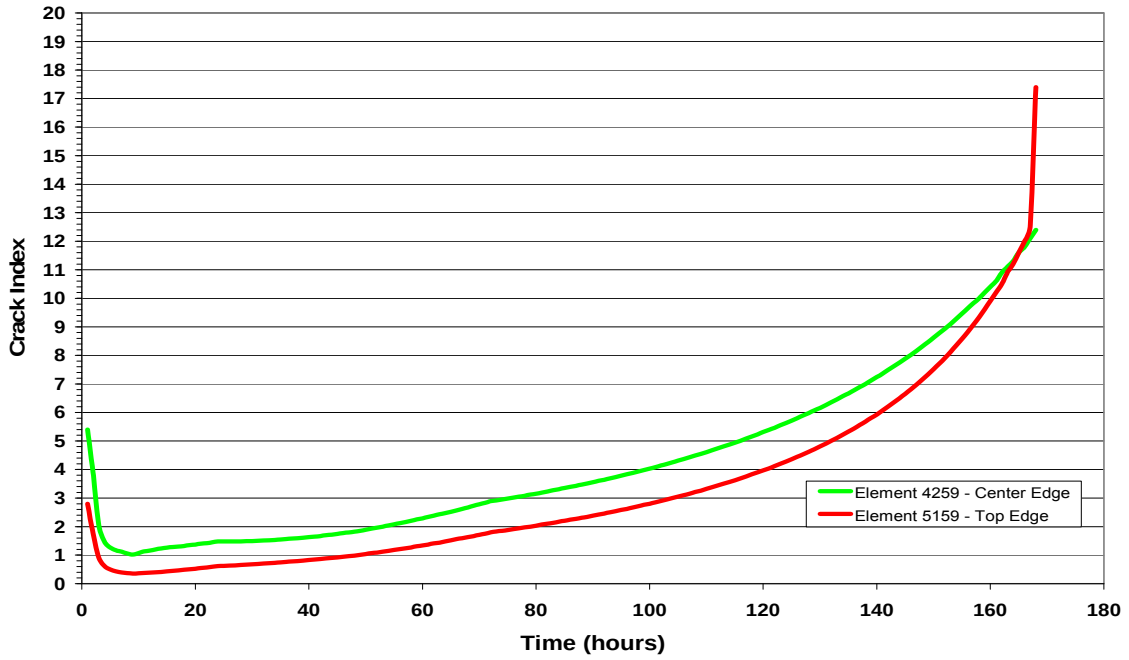

Figure 8-16. Crack index for elements along the edge of block with Mixture 3.

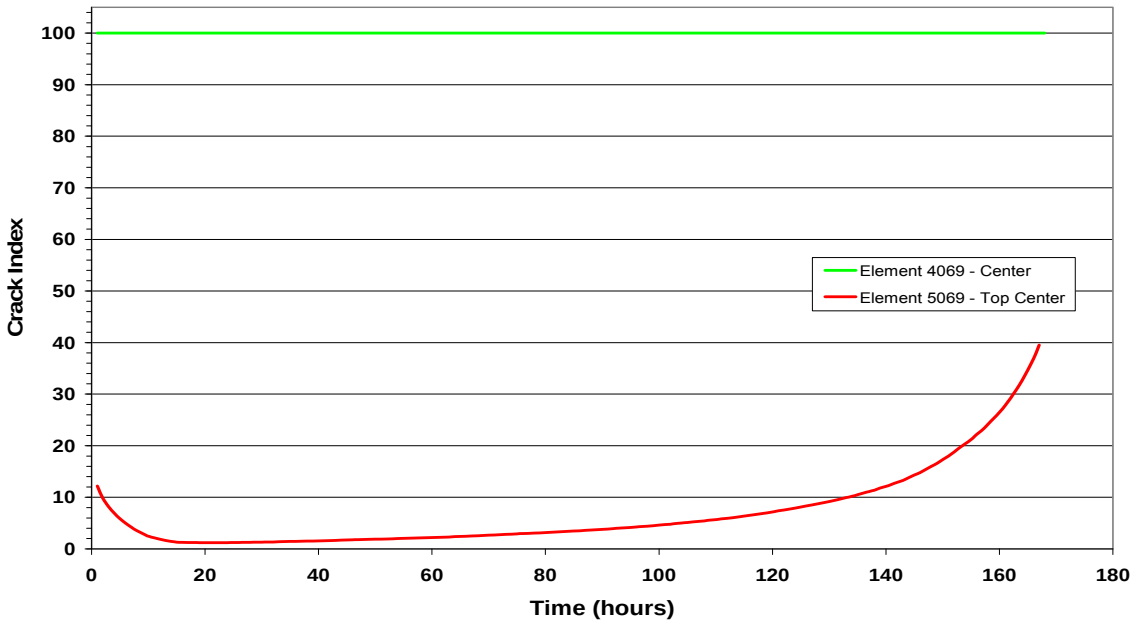

Figure 8-17. Crack index for elements along the center line of block with Mixture 4.

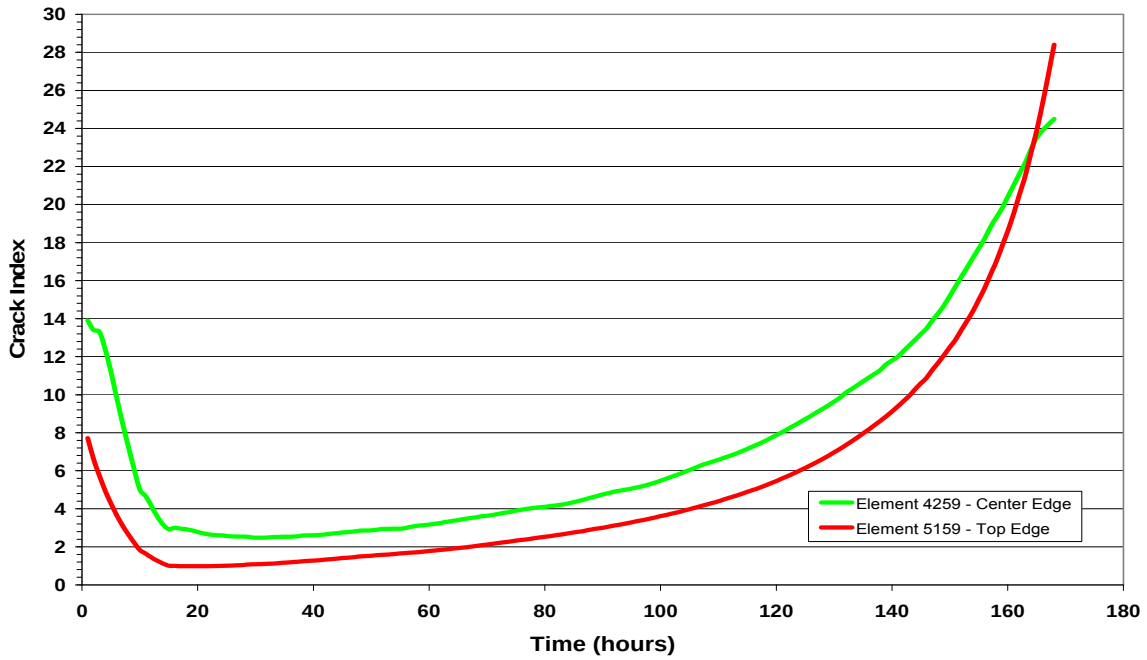

Figure 8-18. Crack index for elements along the edge of block with Mixture 4.

be between the center of a mass concrete element and its surface so as to reduce the occurrence of thermal cracking. The critical temperature differences for the mixtures used in this project are determined from the results of the finite element analyses on each block.

Figure 8-19 shows the plot of the temperature difference between the center and surface of the block with Mixture 1. The calculated tensile stresses at the surface exceeded the early age tensile strength value of 1.25 MPa (181 psi) at a temperature differential of 17.3° C (31.1° F).

Cracking in Mixture 2, which contained ground granulated blast-furnace slag, occurred when the temperature differential reached about 3.2° C (5.8° F), as shown in Figure 8-20. This is significantly less than the differential in Mixture 1, which shows that although the addition of slag to Portland cement slowed the rate of temperature rise, it also caused the concrete to have a lower early age tensile strength of 0.255 MPa. This was to the detriment of the integrity of the structure.

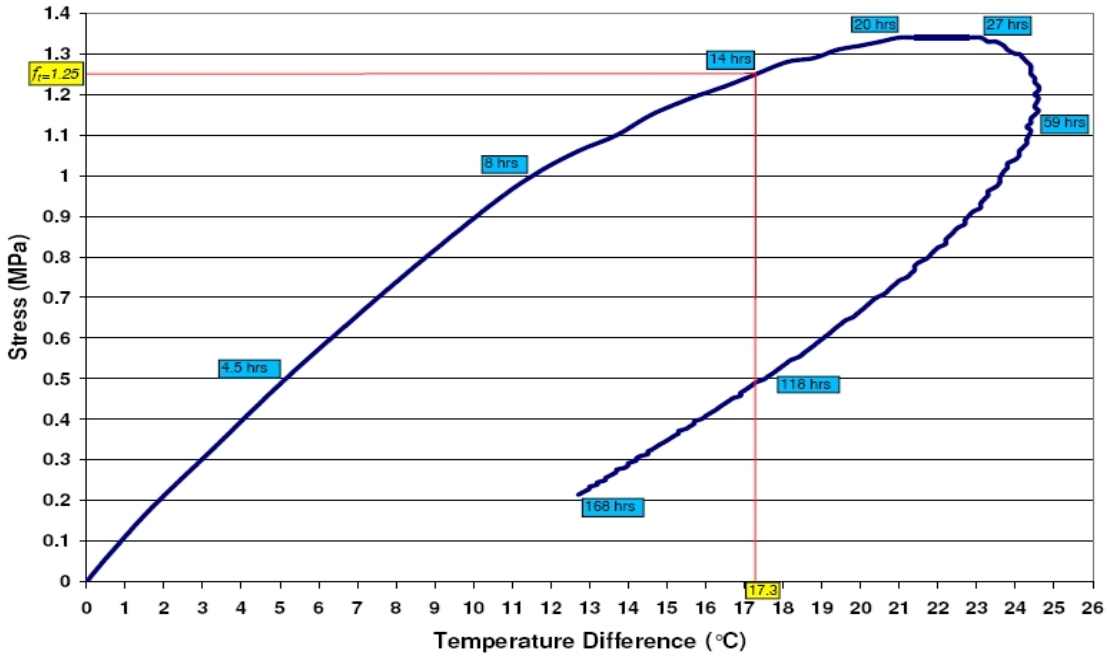

Figure 8-19. Induced stress with respect to temperature differential for Mixture 1.

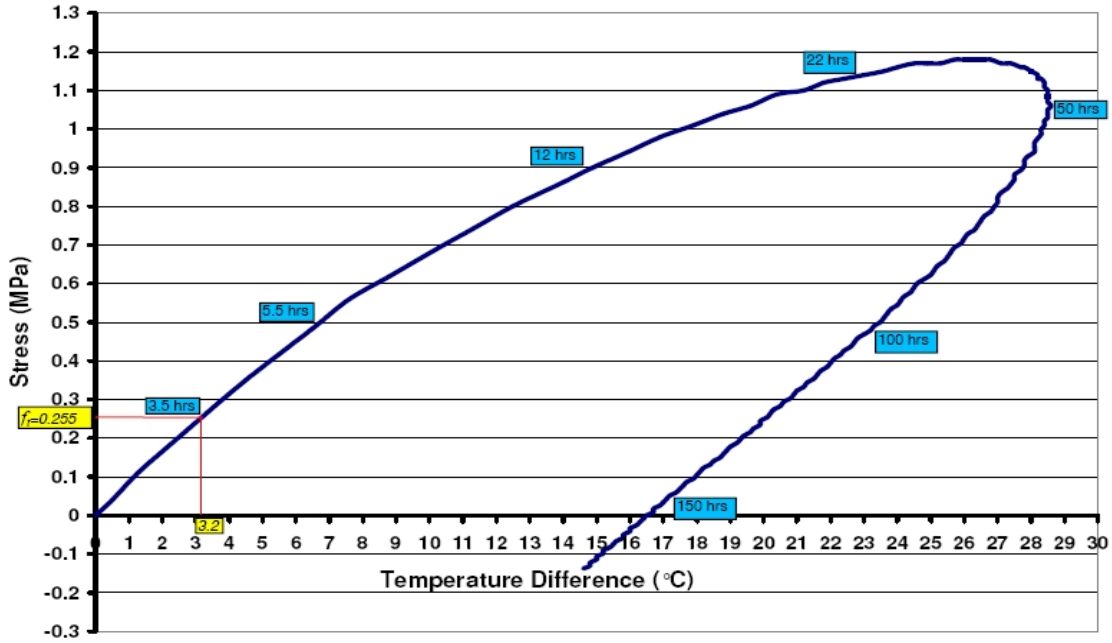

Figure 8-20. Induced stress with respect to temperature differential for Mixture 2.

The temperature differential of 8.4° C (15.1° F) at which cracking initiated in Mixture 3, shown in Figure 8-21, was larger than the differential in Mixture 2. In this case, although the fly ash lowered the peak temperature of the concrete, as shown in Figures 7-12 through 7-14, it did not have any effect on rate of initial temperature rise, and therefore, a low value of the tensile strength caused the concrete to crack at a lower temperature differential than the block with Mixture 1.

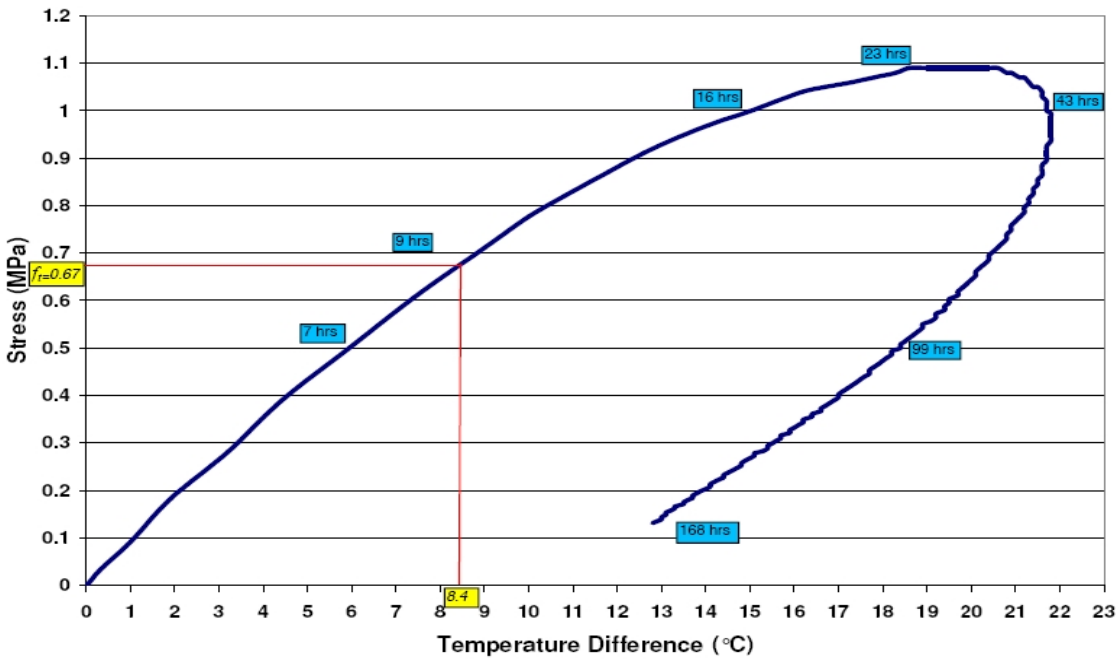

Figure 8-21. Induced stress with Respect to temperature differential for Mixture 3.

Although the crack index for Mixture 4, presented in Figure 8-17, shows that thermal cracking does not occur, it was only just avoided. It was, therefore, decided to still investigate the relationship between the temperature difference and induced stress at the surface of the block. Figure 8-22 shows the plot of this relationship, and it can be seen that the induced stress reaches the 24-hour (Day 1) tensile strength of 0.393 MPa, when the temperature differential is 20.6° C (37.1° F), 26 hours after being poured.

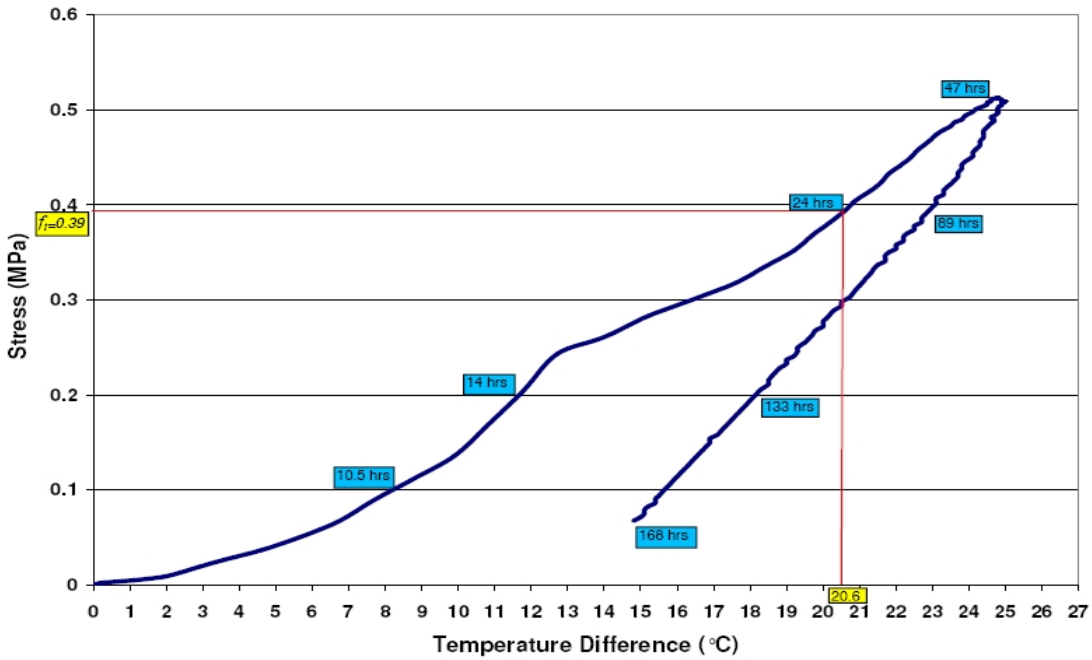

Figure 8-22. Induced stress with respect to temperature differential for Mixture 4.

8.4 Summary of Findings

The investigation of the structural response of the concrete used in each mixture to the internal heat generation and resulting temperature distribution found that:

- The concrete mixture containing 100% Portland cement had the highest induced stress, but also cracked at the highest temperature difference.
- Although the concrete containing ground granulated blast furnace slag had a slower rate of temperature increase, it cracked at a very low temperature differential. This was due to the lower tensile strength typical of slag concrete.
- The concrete containing fly ash cracked at a low temperature differential of 8.4° C (15.1° F). It was due to the low tensile strength of the concrete at early age, which was lower than the induced stresses in the concrete.
- The mixture proportion of 50% Portland cement, 30% slag, and 20% fly ash effectively reduced the probability of thermal cracking due to hydration reaction. Nevertheless, the temperature differential at which cracking could occur is derived as 20.6° C (37.1° F).

CHAPTER 9
PARAMETRIC STUDY

9.1 Introduction

This chapter discusses the results of a parametric study conducted with the aid of the DIANA finite element program. The parameters investigated are effects of the heat generation rate, size of the structure, and the amount of insulation on the peak temperature, temperature distribution, and induced stresses in mass concrete structures.

9.2 Effect of Specimen Size

The standard specimen size used in this study was a block size of 1.07 m × 1.07 m × 1.07 m. To study the effect of size on the behavior of concrete, three additional block sizes were modeled. The sizes chosen were a half-sized block (0.5 m × 0.5 m × 0.5 m), a block twice the size (2 m × 2 m × 2 m), and a block four times the size (4 m × 4 m × 4 m). A comparison of the temperature profiles at the center of blocks containing concrete using mix 1 is presented in Figure 9-1. Figure 9-2 shows the progression of the peak temperatures calculated in the block, as the size is increased. As expected, the peak temperature increased as the size of the block increased. A closer analysis of the effect of block size on the maximum temperature difference is presented in Figure 9-3, where it is shown that the maximum temperature differential between the center and top surface edge increases from 12.8° C (55.0° F) in the 0.5-m block to 56.5° C (101.7° F) in the 4-m block. Figures 9-4 and 9-5 are plots of the induced stress at the center of the top surface and the top surface edge, respectively. In the 1-m × 1-m × 1-m and the 2-m × 2-m × 2-m blocks, the induced stress increases as we move from the center towards the edge of the blocks. However, in the 4-m × 4-m × 4-m block, the stresses are the same at the top surface center and top surface edge suggesting that the stress is constant across the entire surface. The

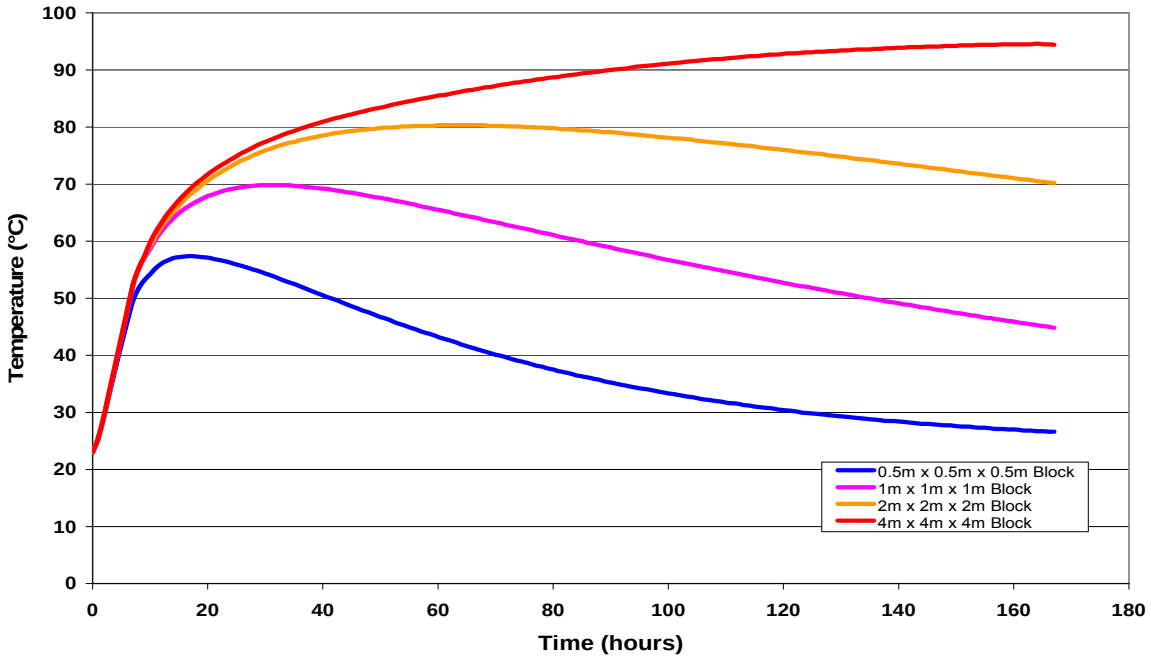

Figure 9-1. Comparison of temperature profiles calculated at the center of each block.

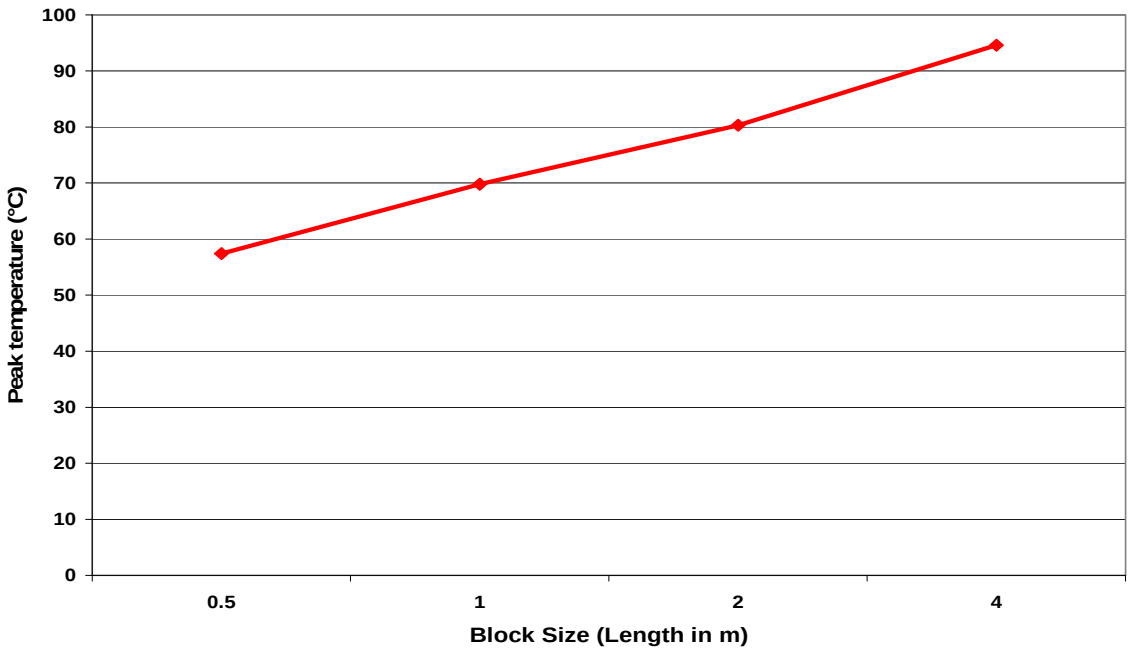

Figure 9-2. Calculated peak temperature values with respect to block size.

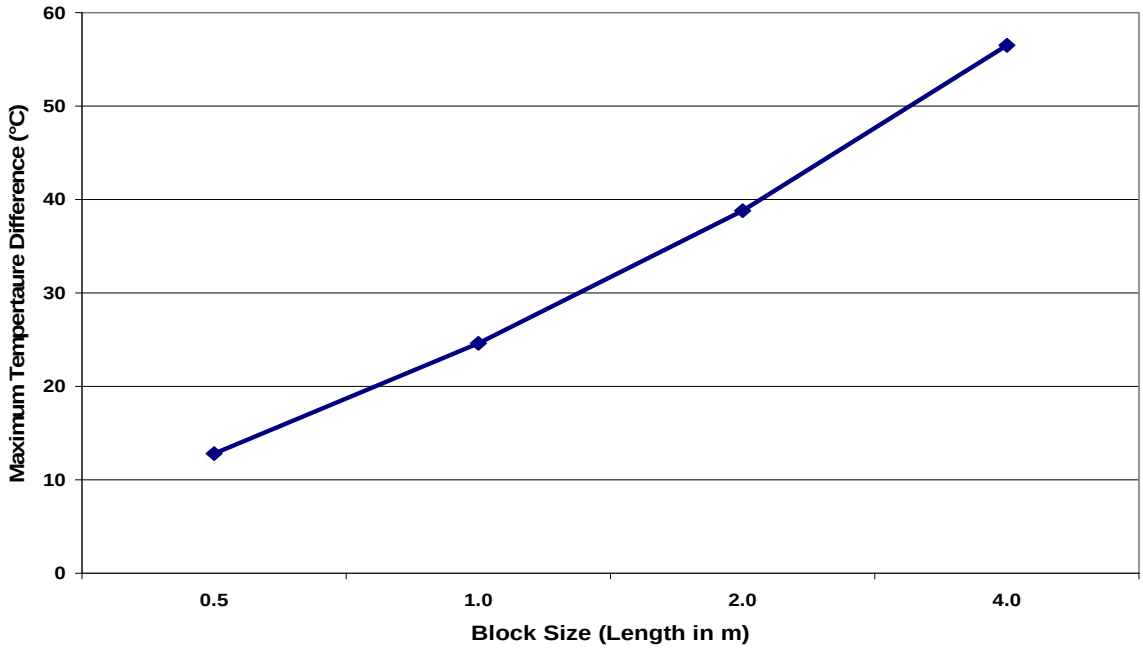

Figure 9-3. Effect of concrete block size on the maximum internal temperature difference.

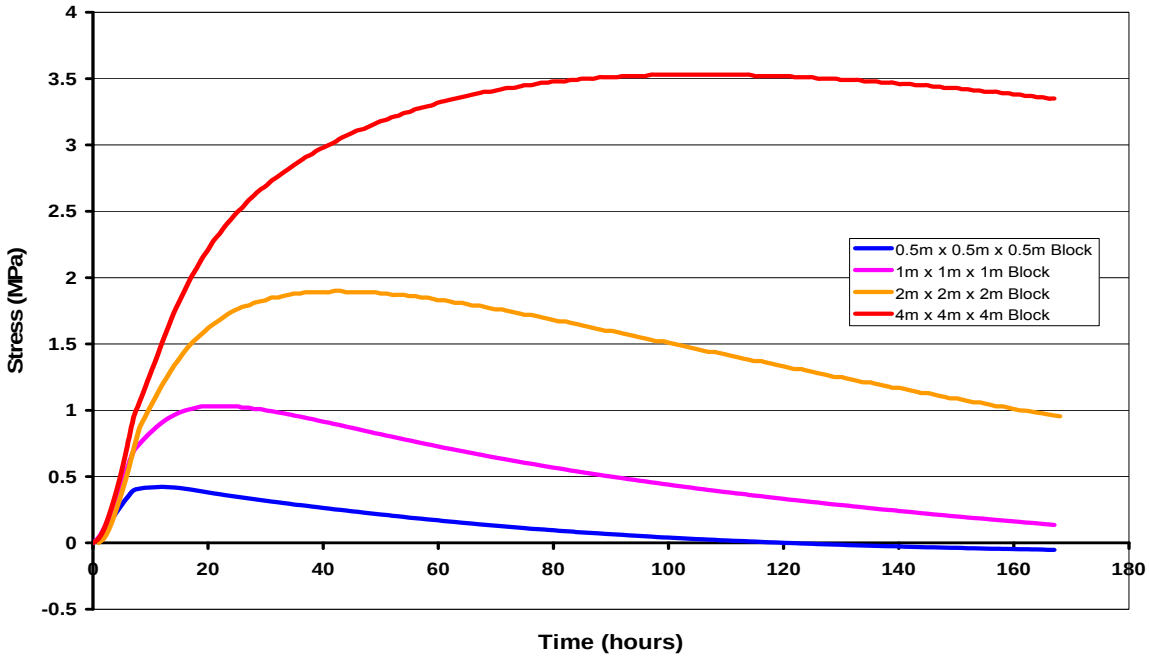

Figure 9-4. Comparison of stresses at the center of the top surface of each block.

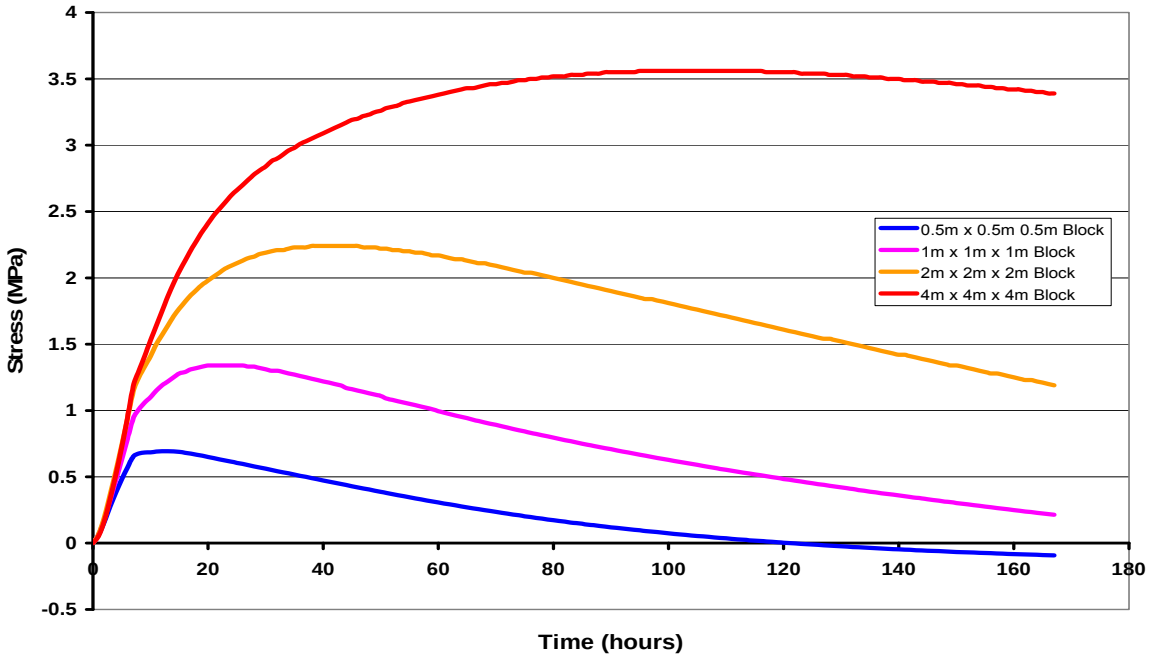

Figure 9-5. Comparison of stresses at the top surface edge of each block.

relationship between the maximum induced stress and the increasing maximum temperature differential caused by increasing block size is presented in Figure 9-6, which shows that for a given concrete mixture, the maximum induced stress will increase with increasing maximum temperature differential. Figure 9-7 presents the maximum stress induced in each of the four types of concrete mixtures that were discussed in the previous chapters with respect to the maximum temperature difference for each size block. The maximum temperature difference and resulting stress in concrete elements larger than 1.07 m × 1.07 m × 1.07 m is highly dependent on the type of concrete used.

Figure 9-8 shows the maximum induced stress with respect to maximum temperature gradient in each of the four types of concrete mixtures for each size block. The temperature gradients in the larger blocks tend to be lower for each type of concrete used in this study. A comparison of the results presented in Figure 9-7 with those presented in Figure 9-8 show that

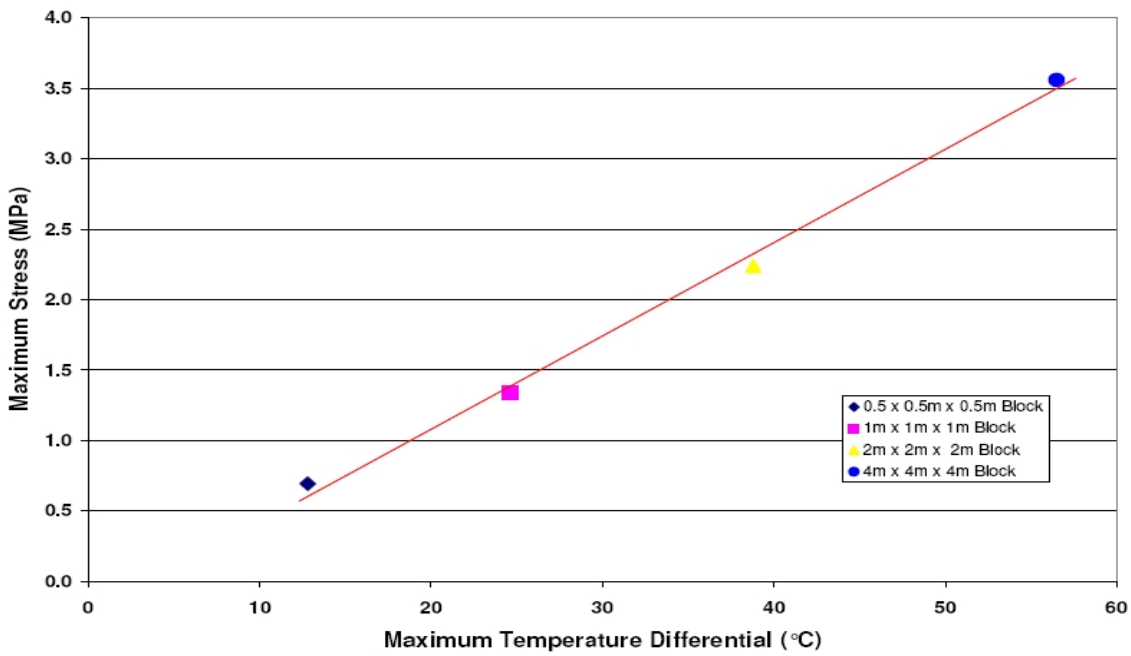

Figure 9-6. Maximum induced stress with respect to maximum temperature differential as a result of increasing block size.

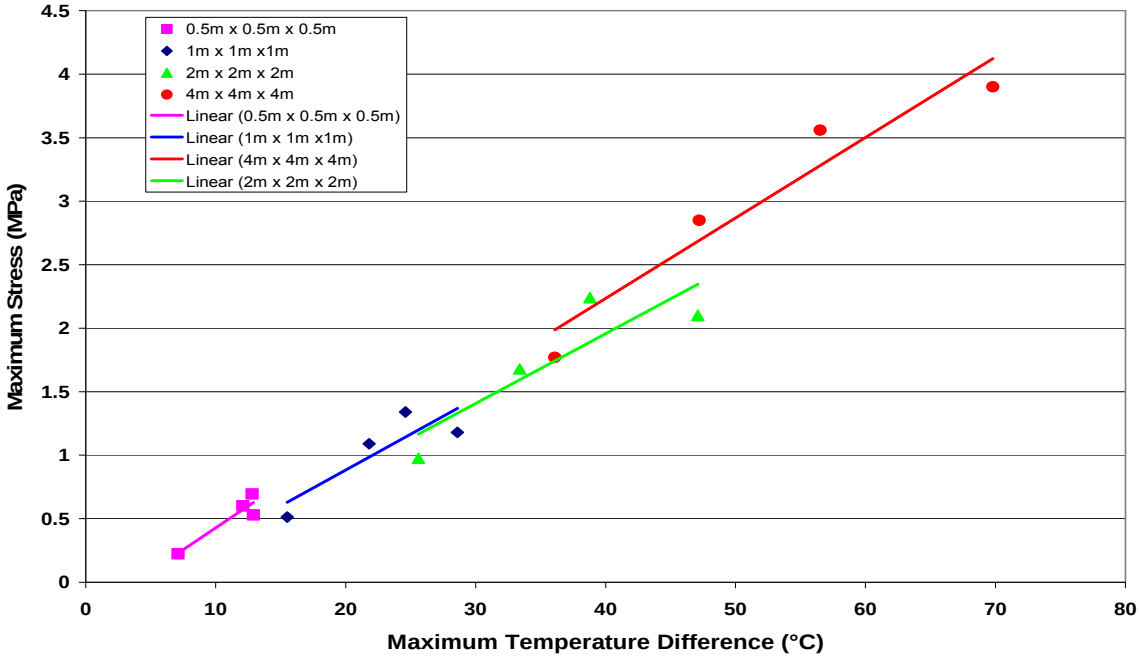

Figure 9-7. Plot of maximum stress versus maximum temperature difference with respect to block size and type of concrete used.

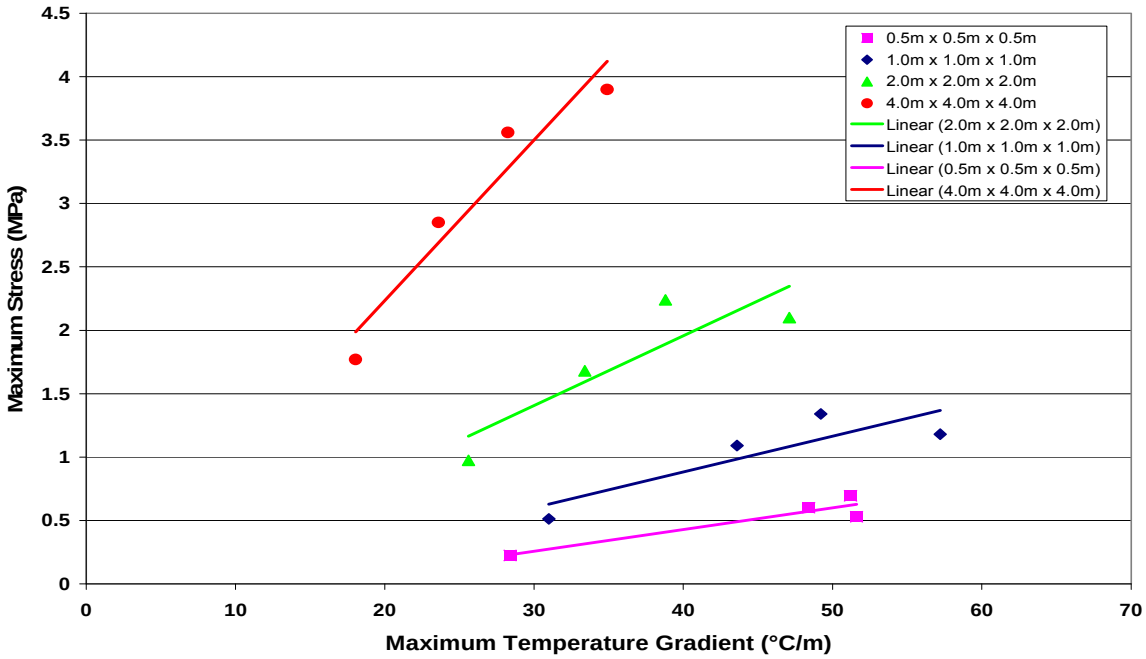

Figure 9-8. Plot of maximum stress versus maximum temperature gradient with respect to block size and type of concrete used.

while maximum stress appears to be a function of temperature difference regardless of block size, it is not a function of temperature gradient alone. It appears that temperature difference, rather than temperature gradient, is a better indicator of maximum stress in mass concrete.

9.3 Effect of Insulation Thickness

Two model blocks, one insulated 1.5-in. thick layer of polystyrene foam, and the other with a 6-in. thick layer polystyrene foam, were created, analyzed, and their results compared with the model analyzed in the previous chapters, to quantify the effect that the amount of insulation would have on the temperature distribution in a hydrating concrete element containing 100% Portland cement. Figures 9-9 and 9-10 present the temperature profiles with respect to time of the concrete block insulated with 1.5-in. thick and 6-in. thick layers of polystyrene foam, respectively. The block with the 1.5-in. thick layer of insulation had a maximum temperature

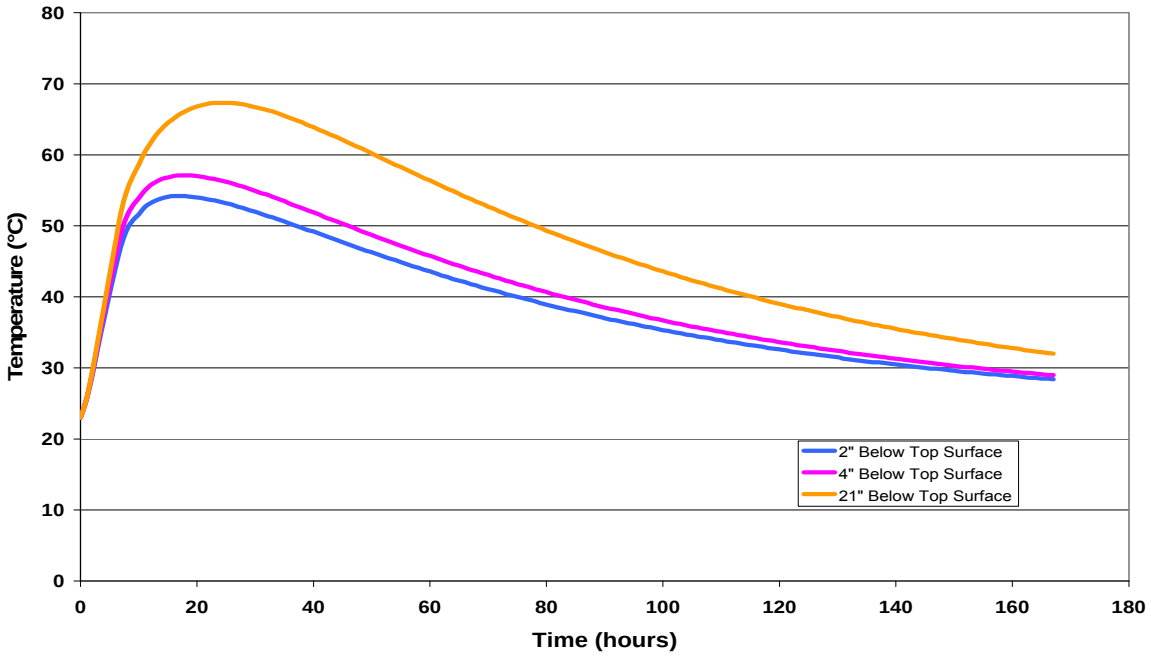

Figure 9-9. Temperature profiles with respect to time 2 in., 4 in., and 21 in. below the top surface of the block insulated with a 1.5-in. thick layer of polystyrene foam.

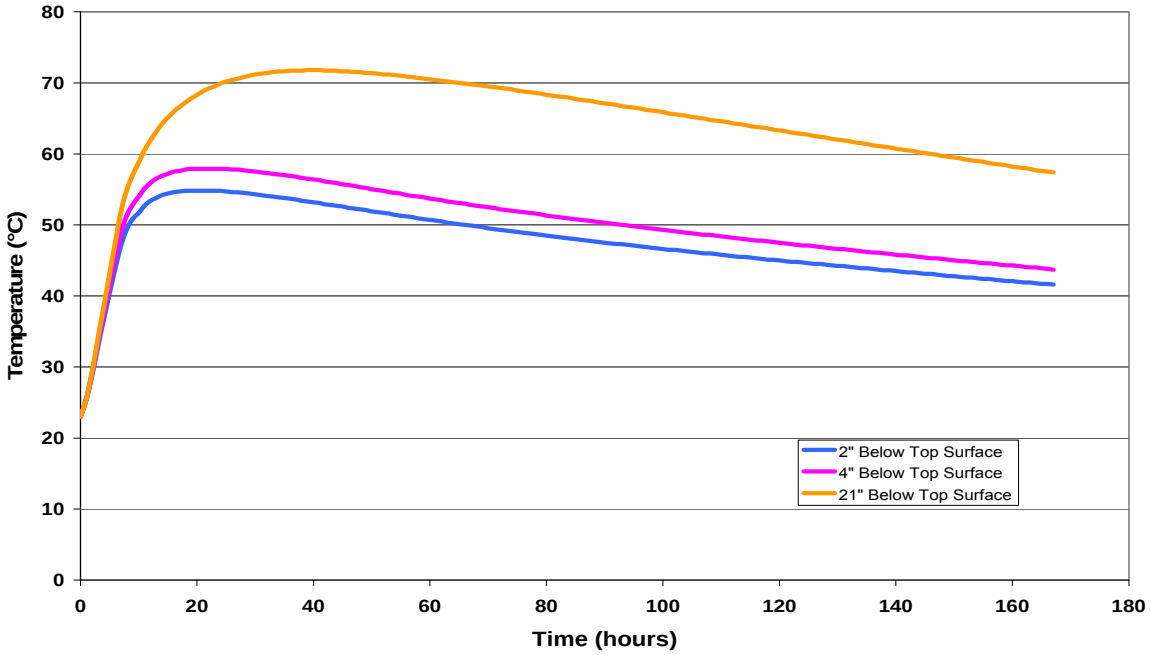

Figure 9-10. Temperature profiles with respect to time 2 in., 4 in., and 21 in. below the top surface of the block insulated with a 6.0-in. thick layer of polystyrene foam.

difference between the center of the block and a point 2 in. below the exposed top surface of 14.9° C (26.8° F), occurring 32 hours after casting and was maintained for 7 hours before steadily decreasing to 3.6 °C (6.5° F). The maximum temperature difference between the center and a point 2 in. below the exposed top surface calculated in the block with the 6-in. layer of insulation was 20° C (36° F). This maximum difference was attained after 70 hours of hydration, slowly decreasing to 15.8° C (28.4° F) at the end of the analysis at 167 hours.

Figure 9-11 shows the comparison of the temperatures with respect to time 2 in. below the exposed top surface of the concrete blocks with varying insulation thickness. The peak temperature at this location was found to be the same and occurred at the same time in all three blocks. However, the rate of temperature decrease was slowest in the model with the 6-in. insulation, and fastest in the model with the 1.5-in. insulation. The temperatures 4 in. below the top surface presented in Figure 9-12 were similar to those observed at 2 in. in terms of the three blocks attaining the same peak temperature at approximately the same time but having different rates of decline.

The comparison of the temperatures 21 in. below the top surface are shown in Figure 9-13. At this depth, the peak temperature and the time it is attained increase in accordance with the thickness of the polystyrene foam.

Although the top surface of the blocks modeled in this project were exposed to ambient conditions, the effectiveness of the insulation in reducing temperature differences within the concrete varied with respect to its thickness. This was determined by evaluating the temperature difference between the center of the block and a point at the same depth, but on the side of the block. Figure 9-14 shows the temperature in the concrete block modeled with the 1.5-in. thick polystyrene insulation, where a maximum temperature difference of 8.3° C (14.9° F) between the

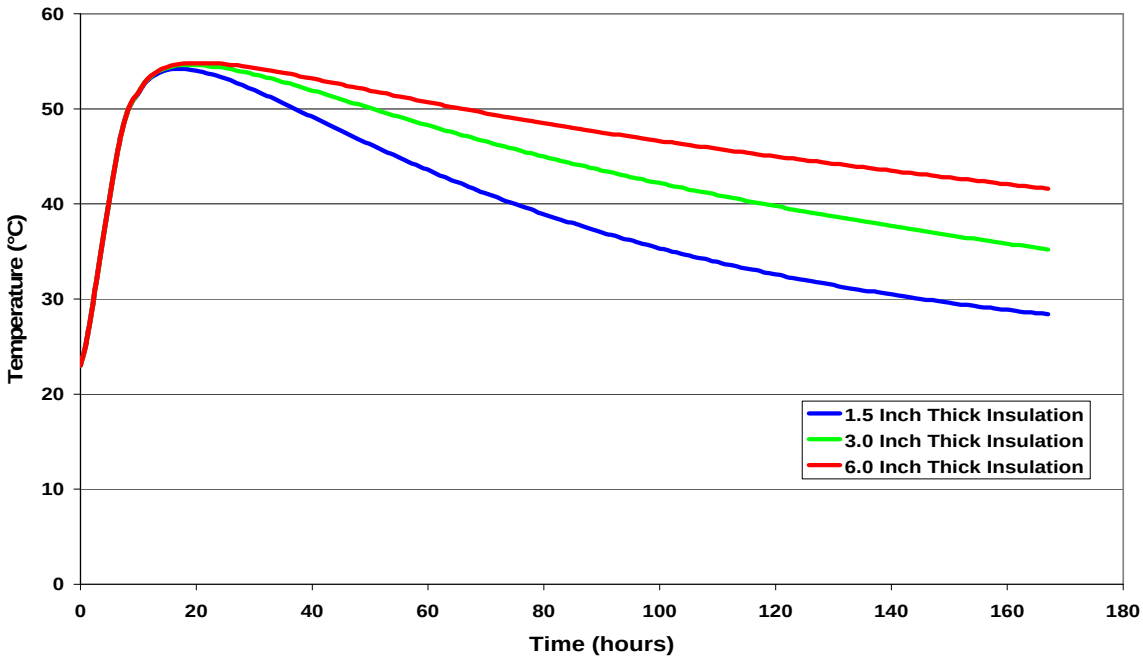

Figure 9-11. Comparison of temperature profiles with respect to time 2 in. below the top surface of the blocks with varying thicknesses of polystyrene foam insulation.

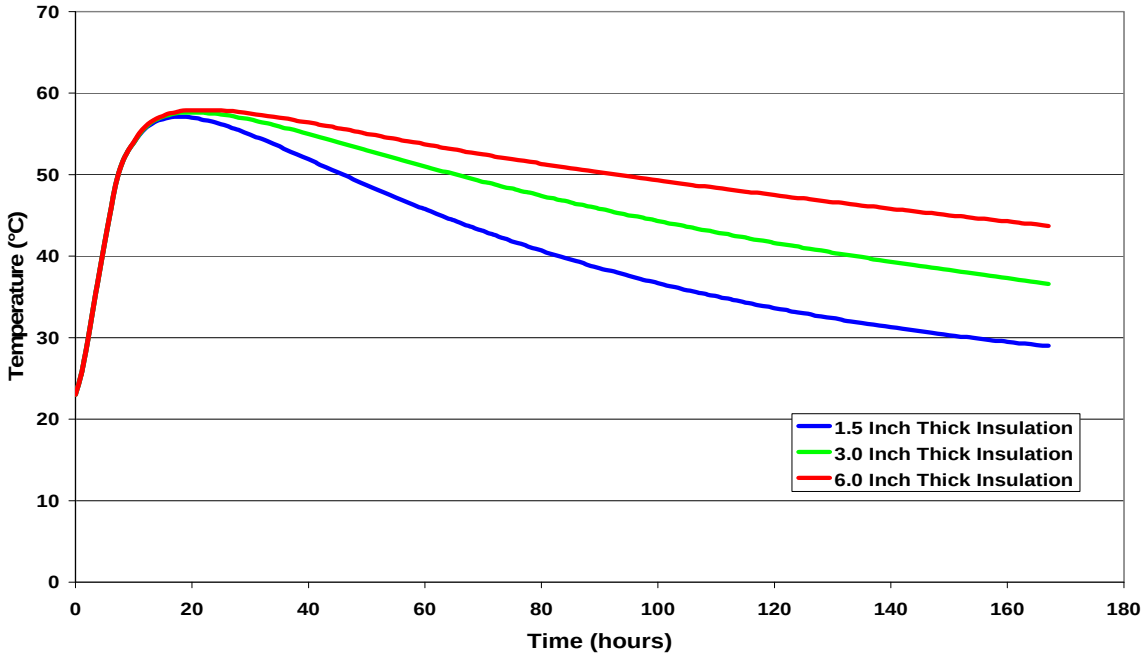

Figure 9-12. Comparison of temperature profiles with respect to time 4 in. below the top surface of the blocks with varying thicknesses of polystyrene foam insulation.

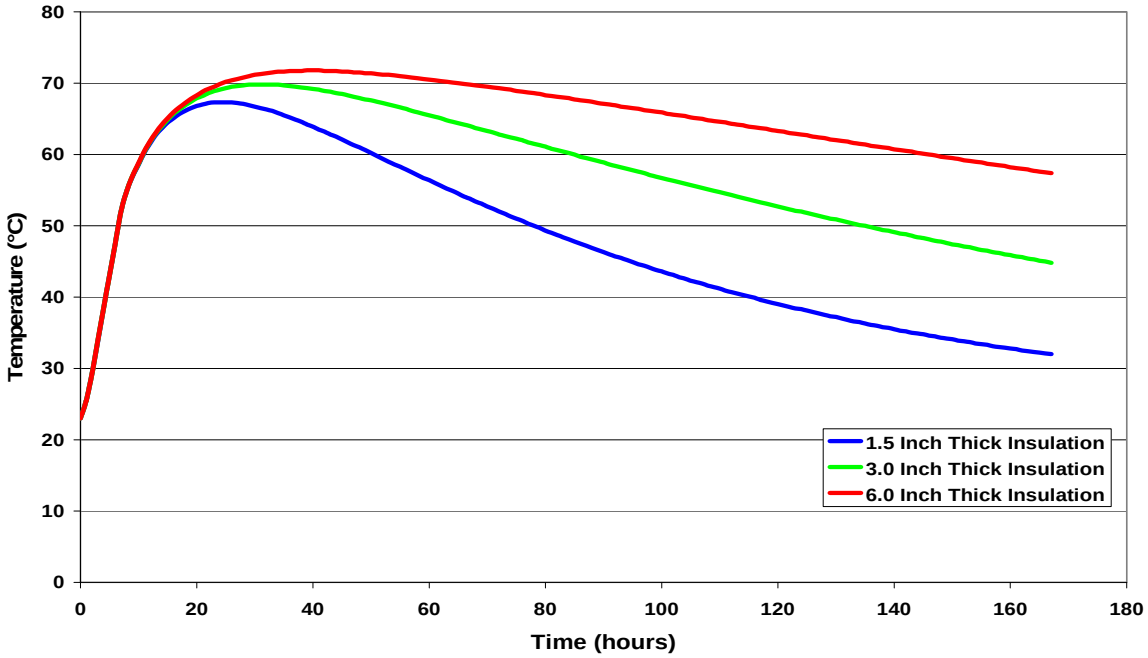

Figure 9-13. Comparison of temperature profiles with respect to time 21 in. below the top surface of the blocks with varying thicknesses of polystyrene foam insulation.

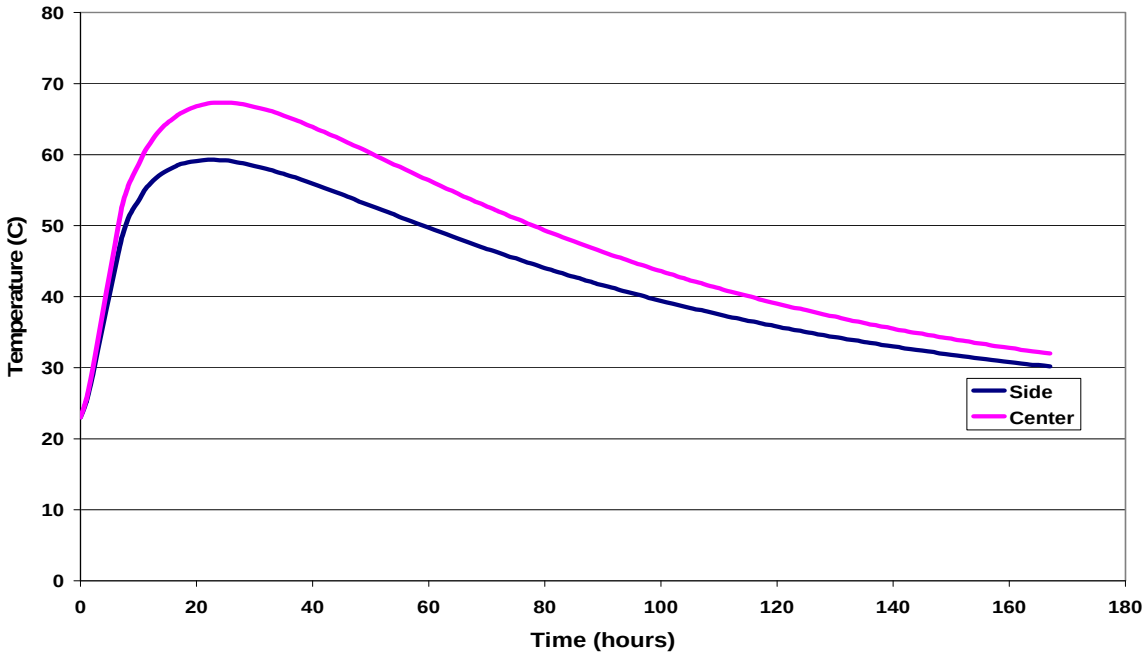

Figure 9-14. Temperatures calculated at the side and center of a concrete block with 1.5-in. thick insulation.

center and the side is observed. The temperatures in the block with the 3-in. thick polystyrene insulation are presented in Figure 9-15. Here, the maximum temperature difference between the two points decreases to 3.4° C (6.1° F). Figure 9-16, shows that for the block insulated with a 6-in. thick layer of polystyrene, the temperature difference was only 1.9° C (3.4° F).

Having assessed the effects of the insulation thickness on the temperature distribution in the uncovered block, an investigation on the effect of the insulation thickness on the maximum temperature differential and maximum induced stress in a concrete block insulated on all faces was conducted. Figures 9-17 and 9-18 show comparisons of the experimentally measured and numerically calculated temperature profiles at 2 in. and 4 in. below the top surface of the fully insulated concrete block with Mixture 1 for validation purposes.

Figure 9-18 presents the variation in maximum temperature differential within the concrete with respect to insulation thickness. Figure 9-19 also shows how the block size determines the effect increasing the insulation thickness will have on the maximum temperature differential within the concrete. As shown in Figure 9-19, increasing the insulation thickness from 1.5 in. up to 9 in. will reduce the temperature difference between the center and top surface of the block. In the 0.5-m block, the maximum temperature difference moved from 5.6° C (10.1° F) with 1.5 in. of insulation, to 4.2° C (7.6° F) with 3 in. of insulation, to 3.2° C (5.8° F) with 6 in. of insulation, to 2.8° C (5.0° F) with 9 in. of insulation. The 1.07-m block had values of 12.4° C, 8.9° C, 6.5° C, and 5.4° C (22.3° F, 16.0° F, 11.7° F, and 9.7° F) with insulation thicknesses of 1.5 in., 3 in., 6 in., and 9 in., respectively. The 2-m block had a temperature difference of 22.8° C (41.0° F) at 1.5 in., 16.7° C (30.1° F) at 3 in., 11.6° C (20.9° F) at 6 in., and 9.3° C (16.7° F) at 9 in. Finally, the 4-m block saw the largest reduction in the magnitude of the maximum temperature difference with increasing insulation thickness. The maximum

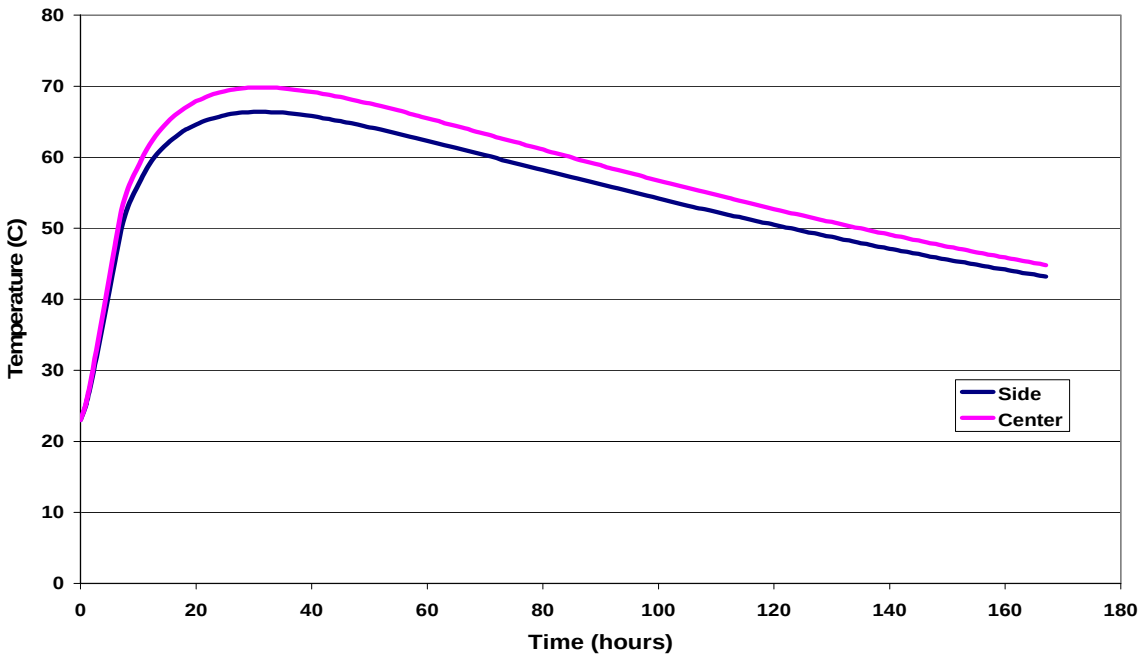

Figure 9-15. Temperatures calculated at the side and center of a concrete block with 3.0-in. thick insulation.

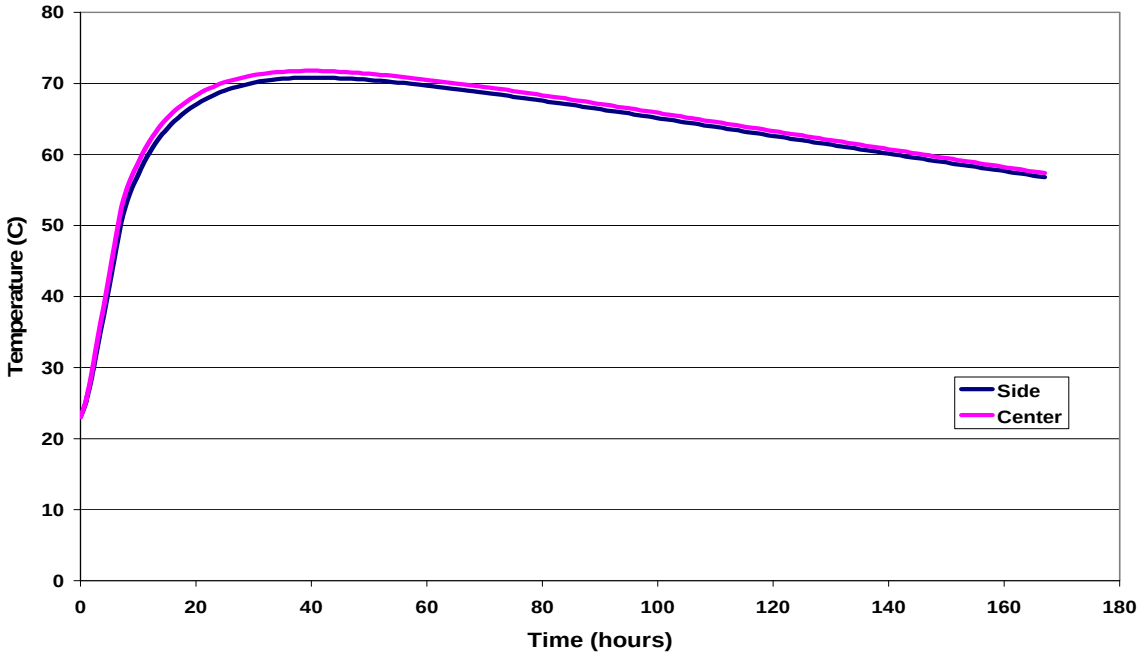

Figure 9-16. Temperatures calculated at the side and center of a concrete block with 6.0-in. thick insulation.

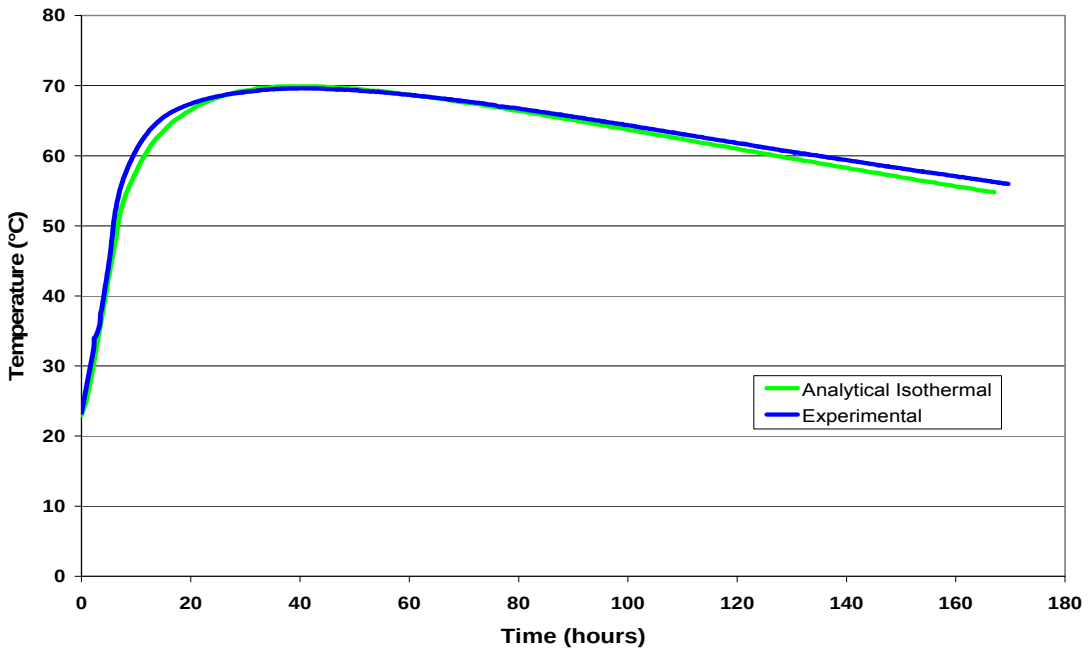

Figure 9-17. Comparison of experimentally measured and calculated temperature profiles 2 in. below the top surface at the centerline of concrete block with 3.0-in. thick insulation.

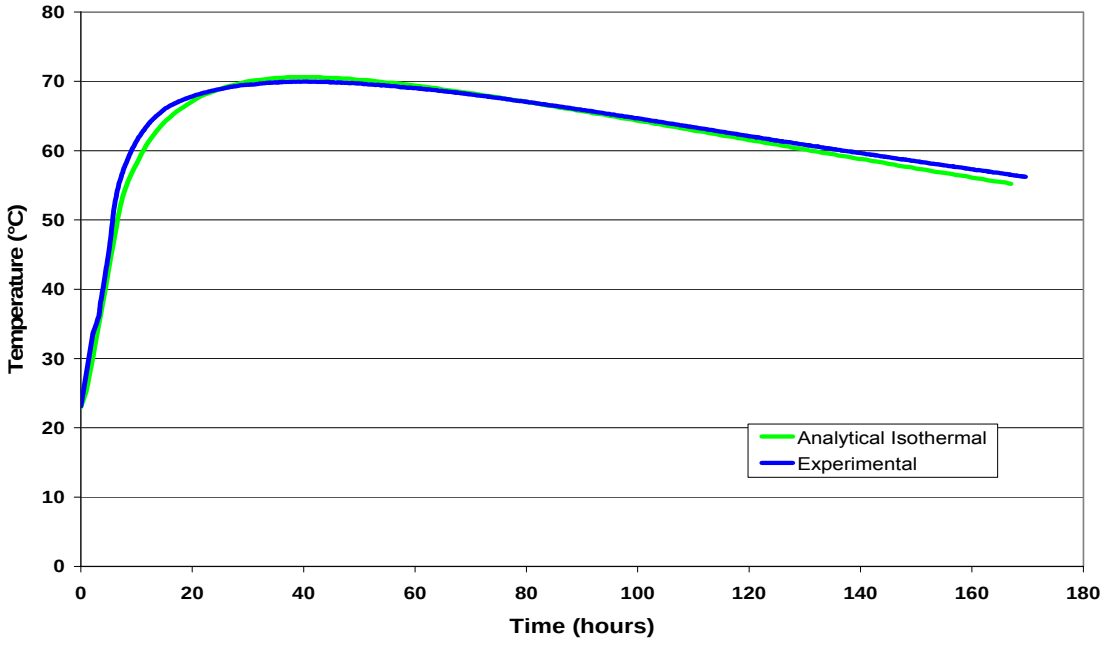

Figure 9-18. Comparison of experimentally measured and calculated temperature profiles 4 in. below the top surface at the centerline of concrete block with 3.0-in. thick insulation.

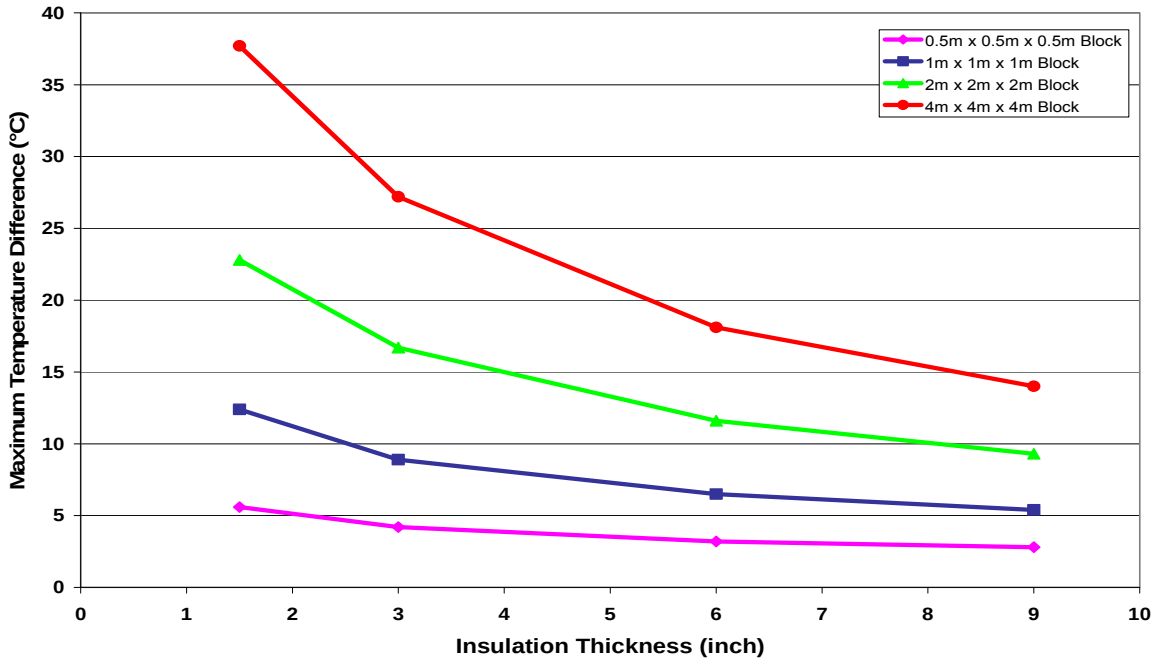

Figure 9-19. Variation in maximum temperature differential within the concrete with respect to insulation thickness for each block size.

temperature difference in the block with 1.5 in. of insulation was calculated at 37.7° C (67.9° F), with 3 in. of insulation, 27.2° C (49.0° F), 6 in. of insulation, 18.1° C (32.6° F), and finally, with 9 in. of insulation, 14° C (25.2° F).

Figures 9-20 and 9-21 show the effect of increasing the insulation thickness had the maximum induced stress in the concrete with respect to temperature difference. Figure 9-20 shows that the reduced magnitude of temperature difference caused by an increase in insulation thickness will result in lower induced stress within the concrete block. Figure 9-21 shows that by increasing the insulation thickness, significant reductions in stresses can be achieved in large concrete elements.

9.4 Time of Formwork Removal Effect

The effect model was modified so that the effect that the time of removal of the formwork had on the induced concrete stresses could be assessed. Knowledge of the optimal time to

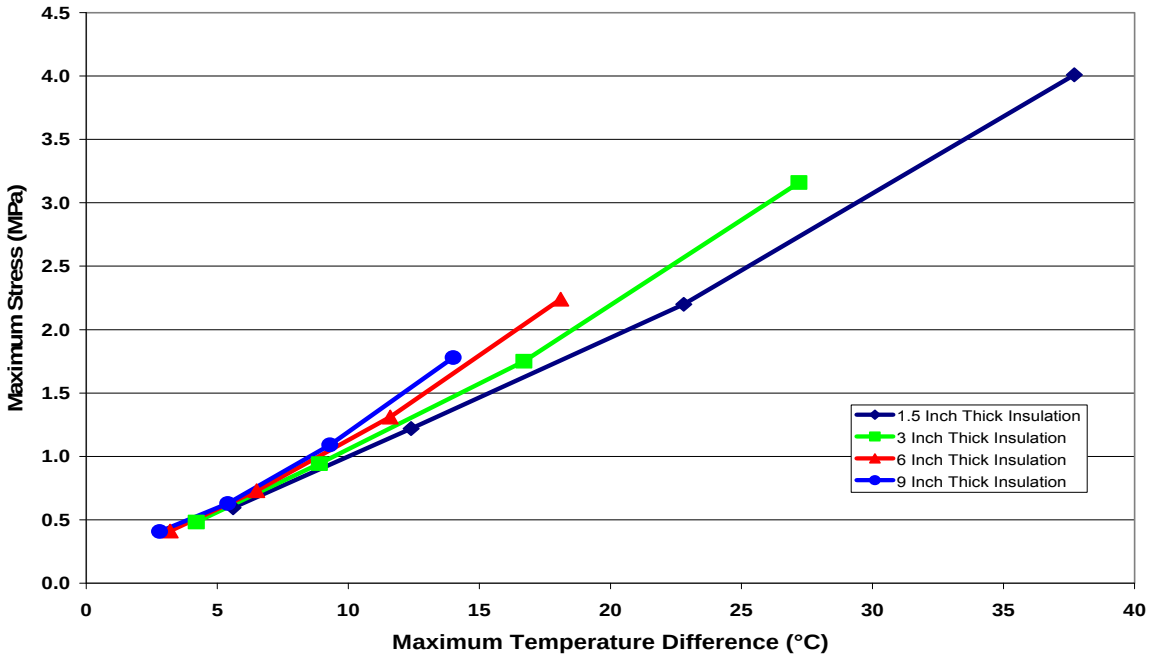

Figure 9-20. Effect of reduction of temperature differential caused by increasing insulation thickness on the maximum induced stress.

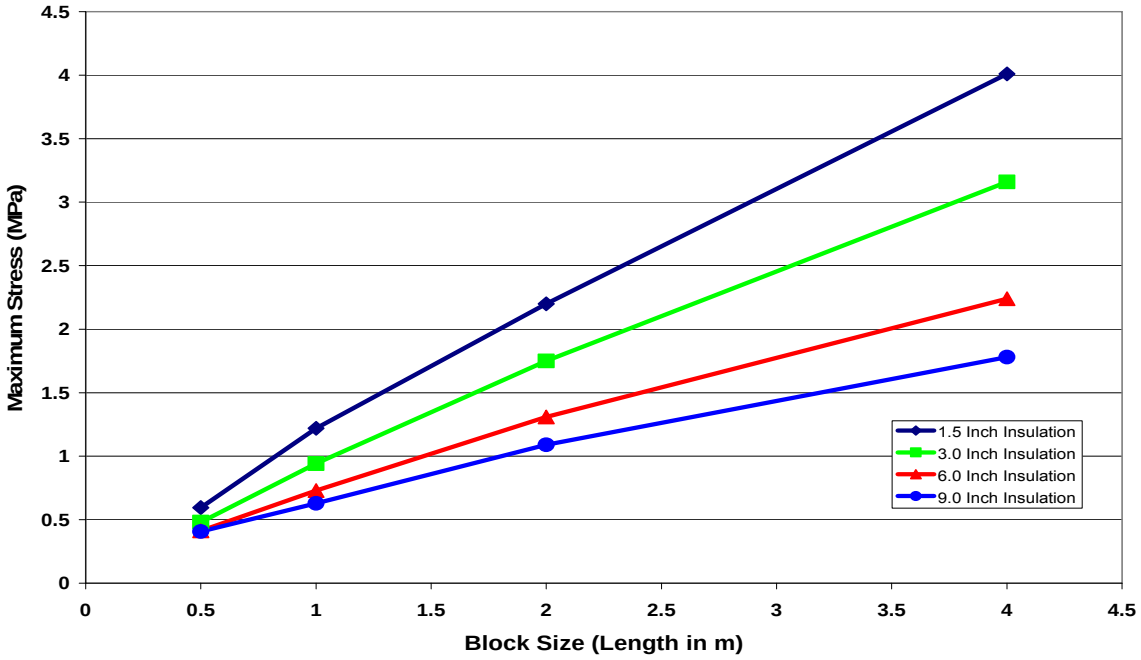

Figure 9-21. Effect of insulation thickness on the maximum induced stress in each block size.

remove the formwork and insulation around mass concrete is important in that the scheduling of the construction time sequence is an essential aspect of project management. The times chosen for analysis were 12 hours, 1 day, 2 days, 3 days, 4 days and 6 days after pouring of the concrete.

Figures 9-22 through 9-27 show the induced stress with respect to time in a 1.07-m × 1.07-m × 1.07-m concrete block concrete when the formwork and insulation is removed at times of 12 hours, 1 day, 2 days, 3 days, 4 days and 6 days.

A sharp sudden increase in tensile stress occurred along the surface immediately after formwork removal. The peak stress calculated for the removal times at 12 hours, 1 day, 2 days, and 3 days, were 0.964 MPa, 1.08 MPa, 1.31 MPa, 1.30 MPa, respectively. These were 77% 86.4%, 79%, and 67.4% of the attained concrete tensile strength, respectively. While not exceeding the tensile strength of the concrete, these stress levels are high enough to cause micro-cracking. These micro-cracks do not pose an immediate threat to the structural integrity of the concrete, however, they will provide an entry point for invasive deleterious substances that can compromise the long-term durability of the concrete. Figure 9-26 shows the state of stress in concrete when the formwork is removed after 4 days of hydration. The stress also undergoes a sharp increase in magnitude the instant the formwork is removed, but is only slightly above 50% of the tensile strength at 4 days, therefore the risk of micro-cracking is small. Figure 9-27 shows the stresses for the concrete that had the formwork and insulation removed after 6 days of hydration. Here, the peak stress of 1.08 MPa is 49% of the tensile strength of the concrete.

The results of the parametric study on the effect time of formwork and insulation removal suggests that the risk of micro-cracking is substantially reduced if the removal is done a minimum of 4 days after the concrete is poured.

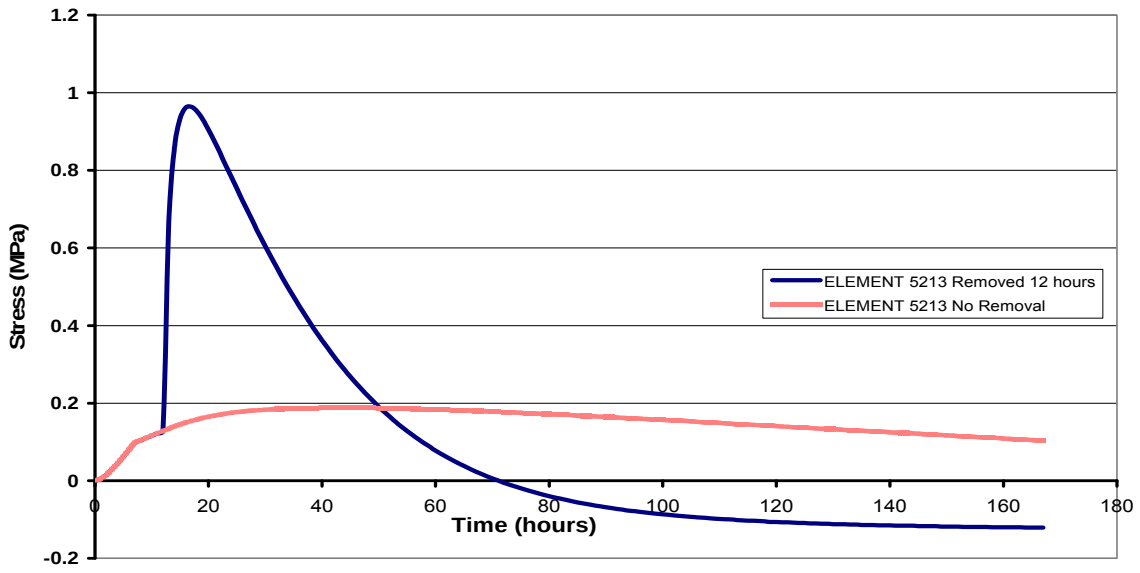

Figure 9-22. Plot of stress versus time at a point on the center of the surface of the concrete block when formwork is removed 12 hours after casting.

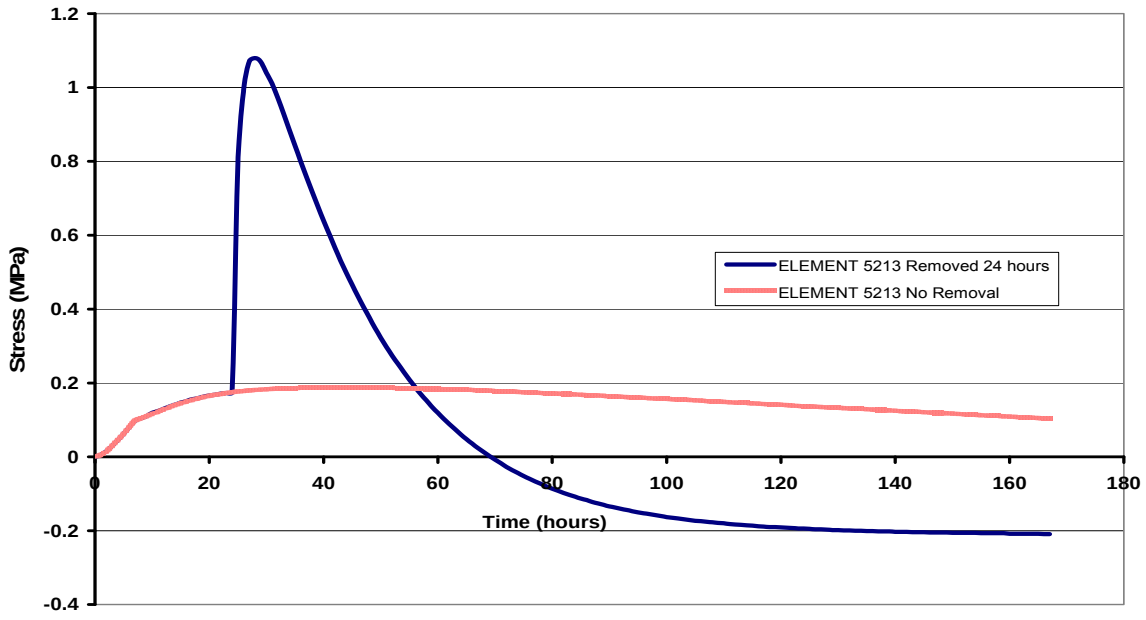

Figure 9-23. Plot of stress versus time at a point on the center of the surface of the concrete block when formwork is removed 1 day after casting.

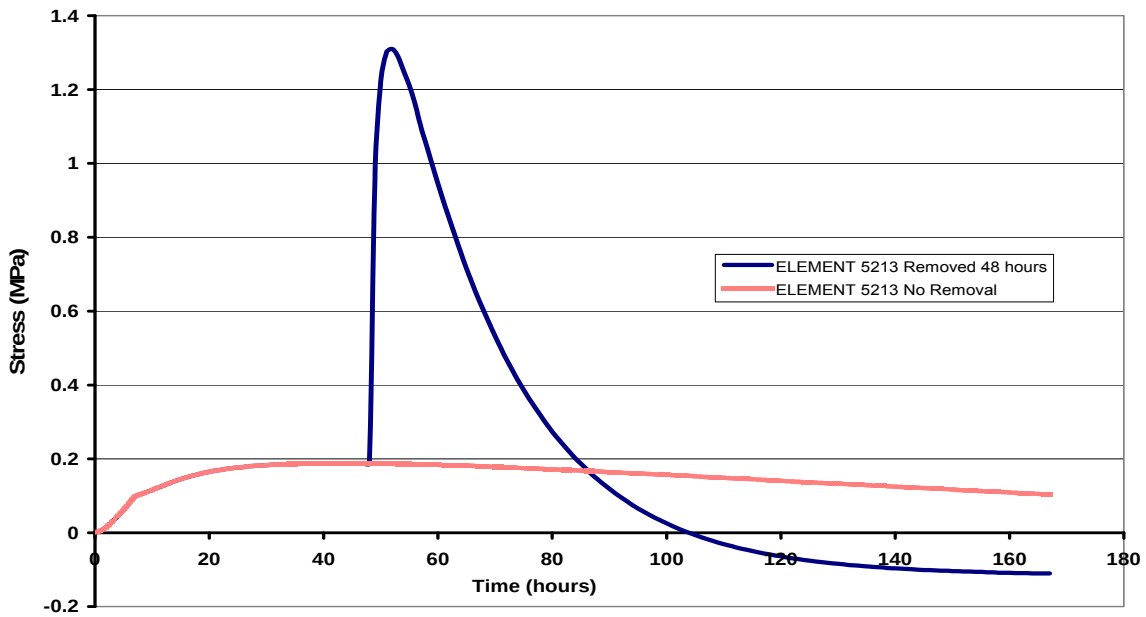

Figure 9-24. Plot of stress versus time at a point on the center of the surface of the concrete block when formwork is removed 2 days after casting.

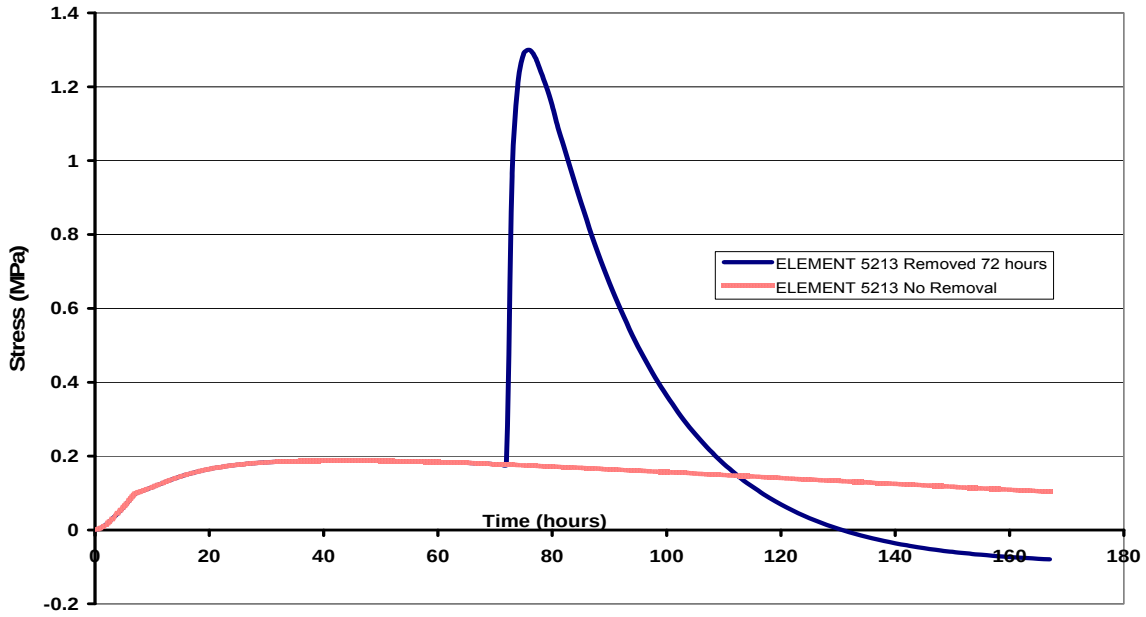

Figure 9-25. Plot of stress versus time at a point on the center of the surface of the concrete block when formwork is removed 3 days after casting.

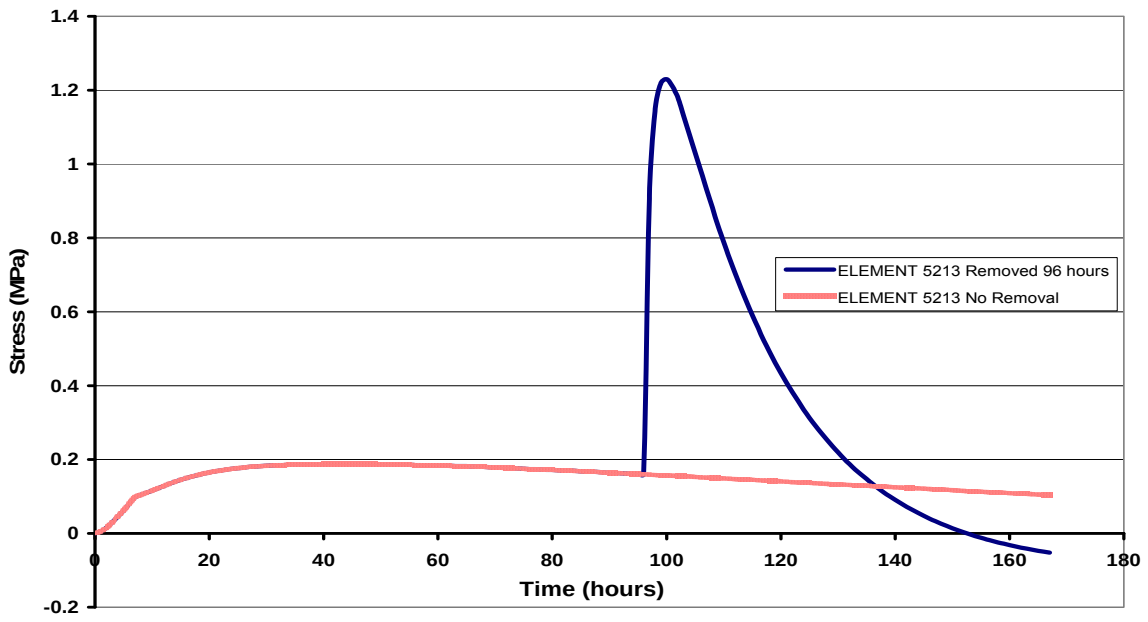

Figure 9-26. Plot of stress versus time at a point on the center of the surface of the concrete block when formwork is removed 4 days after casting.

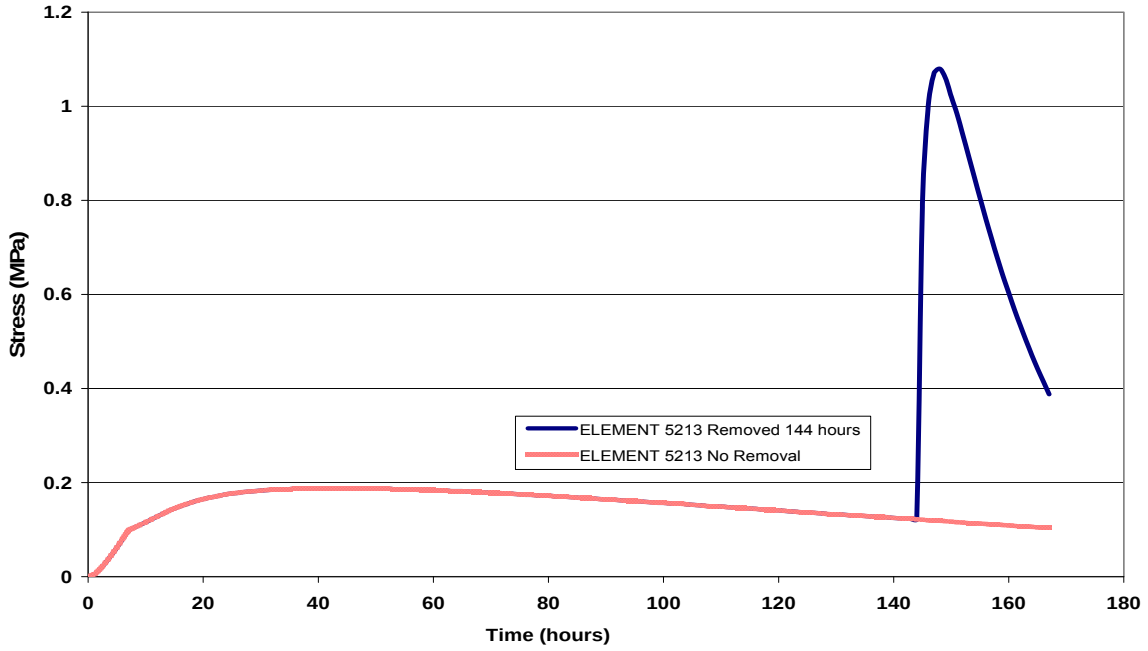

Figure 9-27. Plot of stress versus time at a point on the center of the surface of the concrete block when formwork is removed 6 days after casting.

9.5 Heat Generation Rate Effect

The effect the rate of internal heat generation has on the distribution of temperatures in a concrete element can be seen from the analysis of the block model with varying mixture designs described in Chapter 7. It was observed that concrete with 100% Portland cement generated heat at the fastest rate, followed by the concrete with 35% replacement of fly ash, then by the substitution of 50% ground granulated blast-furnace slag, and the slowest rate of heat generation occurred in the mixture with 50% Portland cement, 30% slag, and 20% fly ash (ternary blend). Figure 9-28 shows the temperature profile with respect to time at the center of the concrete blocks containing each mix. It is seen that the concrete containing the highest rate of heat generation (100% Portland cement) had the sharpest rise in temperature and the highest peak temperature. The ternary blend concrete with the slowest rate of heat generation had the lowest temperature rise slope and also the lowest peak temperature.

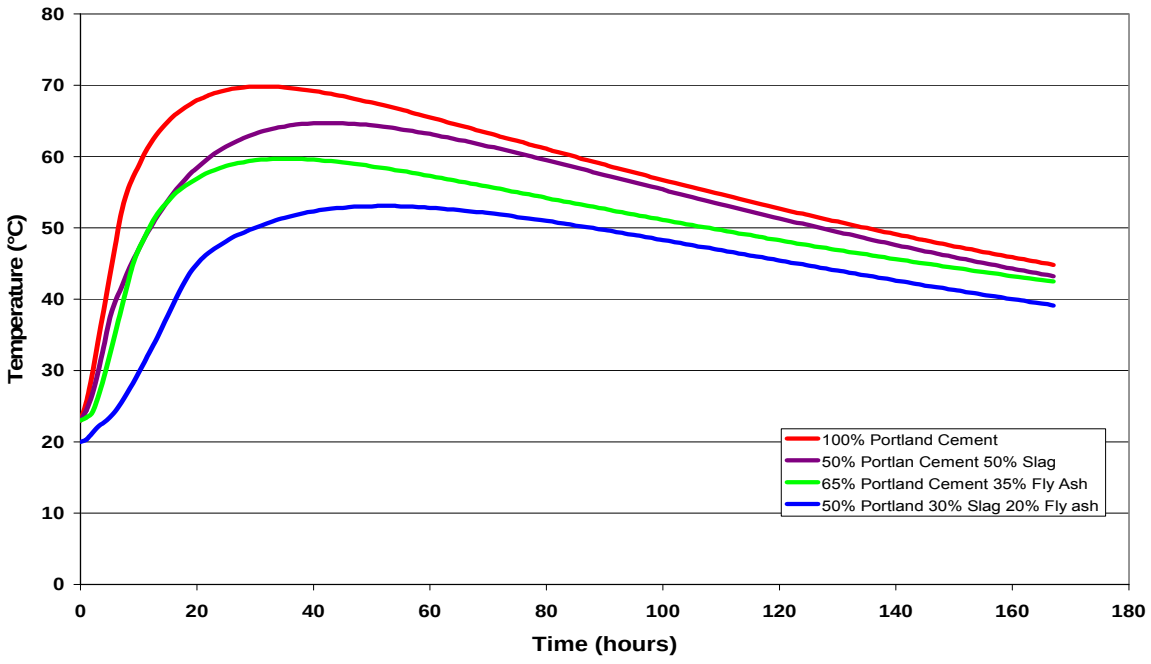

Figure 9-28. Temperature profiles with respect to time at the center of a concrete block with varying heat generation rates.

9.6 Summary of Findings

The parametric study of the factors affecting the behavior of concrete resulted in the following:

- The peak temperature, internal temperature gradients, and induced thermal stresses increase as the amount of concrete used in any one pour is increased.
- The thickness of the insulating layer around the block formwork has an indirect effect on the magnitude of the maximum temperature difference in the hydrating concrete. For a given resistance value (R-Value) of an insulating material, the temperature difference in concrete will decrease with increasing insulation thickness.
- Concrete with a fast rate of heat generation will have higher peak temperatures increasing the likelihood that thermal cracking will occur.
- The effectiveness of insulation thickness in the reduction of the maximum temperature differential in concrete is dependent on the size of the concrete block. An increase in insulation thickness from 1.5 in. to 9 in. reduced the maximum temperature differential by 50% in a 0.5-m × 0.5-m × 0.5-m block while the reduction in a 4-m × 4-m × 4-m block was 62.9%.
- Increasing the insulation thickness can achieve significant reductions in thermal stresses in large concrete elements.
- Although the tensile stresses that resulted from the removal of formwork and insulation at 12 hours, 1 day, 2 days, and 3 days after pouring of the concrete were less than the tensile strength of the concrete as measured in the laboratory, the stresses were large enough to initiate micro-cracking. These micro-cracks can serve as an entry point for deleterious materials that can undermine the durability of the concrete.

CHAPTER 10
RECOMMENDED TESTING REGIMEN FOR MASS CONCRETE

10.1 Recommended Testing Method for Measurement of Heat Generation

Three calorimetry methods were investigated for the measurement of heat generation in concrete materials: isothermal conduction calorimetry, semi-adiabatic calorimetry, and Sure-Cure/adiabatic calorimetry. Of the three methods investigated, the isothermal calorimetry method was determined to be the most appropriate method for the quantification of heat generation of cementitious materials at early ages. There are several reasons as to why the isothermal calorimetry method was favored over the other calorimetry techniques. Firstly, the isothermal calorimetry method provided the most accurate and repeatable results for the measurement of the heat generation of cementitious materials. Secondly, the results provided by the isothermal calorimetry are in units of power (mW/g) and energy (J/g). Although this research established some baseline values for the specific heat capacity of the ingredients used to make concrete, there are potential errors in those values which could provide erroneous results in the conversion from temperature rise as measured by semi-adiabatic and adiabatic calorimetry. Thirdly, the isothermal conduction calorimeter is commercially available and standardization of the test method for the determination of energy rise of cementitious materials is imminent. Finally, there have been some recent developments in modeling/prediction software programs which utilize the energy rise data for cementitious materials for input parameters. Therefore, the use of the isothermal conduction calorimeter is recommended for the measurement of heat/energy rise of concrete for the purposes of prediction of the behavior of mass concrete.

10.2 Recommended Testing Method for Measuring Maturity/Equivalent Age

The laboratory testing method for the establishment of maturity and equivalent age relationships based on the time-temperature history falls under ASTM 1074. The relative strength relationships developed by the maturity method (ASTM 1074-6.2) also known as the Nurse-Saul maturity method, did not yield accurate results. Therefore, it is recommended not to use the Nurse-Saul method for the prediction of strength properties of mass concrete.

The standardized equivalent age method developed relative strength relationships per ASTM 1074-6.3 (also known as the Arrhenius equation), which utilized a hyperbolic mathematical model for the evolution of compressive strength of mortar cubes. This research investigated a second equivalent age method (Schindler 2002) which utilized the compressive strength of mortar cubes as well, but used an exponential mathematical model rather than the model prescribed in ASTM 1074.6.3 (hyperbolic method) for the establishment of activation energy (E_a). A third method for the establishment of equivalent age and E_a was investigated utilizing isothermal calorimetry of cementitious material in lieu of compressive strength testing of mortar cubes. As previously stated, the isothermal calorimetry test is required for the determination of the measurement of heat generation characteristics of the cementitious materials. Accordingly, it is possible to use the data obtained from isothermal calorimetry testing (for heat generation) to determine the E_a of the cementitious material. Therefore, the compressive strength testing per ASTM 1074 would not be needed for the determination of E_a, if the isothermal calorimetry testing was used in its place.

Each of the three equivalent age techniques produced accurate results for the prediction of the relative strength of concrete which utilized Portland cement as the only cementitious material. However, initial testing indicated that the E_a results obtained by the isothermal testing

method were the most accurate for cementitious materials in which Portland cement was replaced with a large percentage of supplementary cementitious material (35-50%). However, the current models established for equivalent age relationships for concrete with large amounts of supplementary cementitious materials do not adequately predict the behavior of relative strength of concrete.

Therefore, the equivalent age relationships should be used to predict the strength behavior of concrete. Following the results obtained in this research, the E_a, as calculated via isothermal calorimetry testing and the standardized test method, may be used for the prediction of concrete with large replacement of SCM. However, the models do not adequately predict the behavior of relative strength of concrete with large replacements of SCM.

10.3 Recommended Testing Methods for Strength and Modulus of Elasticity

10.3.1 Compressive Strength

The most commonly measured property of hardened concrete is compressive strength. The FDOT specification requires a standardized minimum compressive strength, at an age of 28 days of all structural concrete used in the State of Florida. Thus, the compressive strength has become the fundamental strength test for concrete. Despite the fact that mass concrete will rarely experience failure in a compressive manner, it is recommended to perform compressive strength testing of concrete for acceptance and comparative purposes.

10.3.2 Compressive Modulus of Elasticity

The modulus of elasticity is the most important strength parameter for the prediction of the behavior of mass concrete. Near surface tensile strains (as predicted by CTE measurements), due to the expansion of the hotter inner core of mass concrete, can be used to calculate tensile

stress, if the modulus of elasticity is known. Therefore, the modulus of elasticity is an important parameter for the prediction of potential thermal/tensile cracking of mass concrete.

The compressive modulus of elasticity test is the only standardized test for measurement of the modulus of elasticity for concrete. The findings of this research indicate that the compressive modulus of elasticity is approximately the same as the tensile (flexural) modulus of elasticity when tested at loads of 33% of ultimate. Therefore, the modulus of elasticity measured compressively can be considered the same value for the tensile modulus of elasticity for prediction and modeling purposes of mass concrete. Therefore, it is not necessary to determine tensile/flexural modulus of elasticity via laboratory testing.

10.3.3 Tensile Strength

Tensile strength is particularly important for the prediction of mass concrete since the failure of mass concrete at early ages is typically tensile in nature. Near surface tensile stresses (as predicted by CTE) and modulus of elasticity measurements of mass concrete (as predicted by modeling software) can be compared with tensile strength obtained via laboratory testing. Accordingly, the prediction of cracking can be established with respect to the expansive nature (due to temperature rise or temperature differentials) within the mass concrete. When the predicted tensile stress exceeds the ultimate tensile stress of the concrete obtained by laboratory testing, cracking will occur.

10.4 Recommended Testing Method for Measurement of Coefficient of Thermal Expansion

The coefficient of thermal expansion of concrete is perhaps the most important parameter to accurately quantify with respect to mass concrete. Currently, the standardized method for the measurement of CTE (AASHTO TP-60-2007) has been withdrawn due to the potential concerns with the calibration factor (of stainless steel) used to calibrate the test (Crawford 2009).

Therefore, the results obtained under this research were calculated per the calibration testing performed at the FDOT SMO. Considering the recent developments and potential problems regarding the CTE test method, it is recommended to perform CTE testing in the laboratory for the prediction of mass concrete. Furthermore, it should be noted that early-age CTE is a necessary parameter to properly establish and consider its variability in the prediction of the behavior of mass concrete.

10.5 Recommended Physical Parameter for the Concrete Diffusivity

The thermal diffusivity testing reported in this research indicates that the thermal diffusivity values for concrete at early ages range from 0.513 ft^2/day to 0.748 ft^2/day, whereas the thermal diffusivity of concrete made with limestone aggregate as reported by ACI 207.2 is 1.22ft^2/day. The reason for the difference in the diffusivity values obtained in this research, and those obtained by ACI 207.2, is due to the coarse aggregate within the concrete. Therefore, the values for thermal diffusivity reported in this research should be used for the prediction of mass concrete which incorporate coarse aggregate from Florida. However, for concrete created with coarse aggregate from elsewhere, the values per ACI 207.2 should be considered for the prediction of the behavior of mass concrete.

10.6 Recommended Physical Parameter for the Specific Heat Capacity

The specific heat capacity testing reported in this research indicates that the specific heat capacity values for concrete at early ages range from 1.1 to 1.2 J/(g-°C), whereas the specific heat capacity of concrete made with limestone aggregate as reported by ACI 207.2 is 0.91 to 1.05 J/(g-°C). The reason for the difference in the diffusivity values obtained in this research, and those obtained by ACI 207.2, is due to the coarse aggregate within the concrete. Similar to

the results obtained for thermal diffusivity, the specific heat capacity values reported in this research should be used for the prediction of behavior of mass concrete which incorporates coarse aggregate from Florida. However, for concrete created with coarse aggregate from elsewhere, the values per ACI 207.2 should be considered for the prediction of the behavior of mass concrete.

10.7 Summary of Testing Program

The laboratory testing program for the prediction of the behavior of mass concrete should include the following tests:

1) Isothermal calorimetry for the measurement of heat generation rate;
2) Compressive strength per ASTM 1074 or isothermal calorimetry testing for the determination of activation energy;
3) Compressive strength of concrete cylinders;
4) Splitting tensile strength of concrete cylinders;
5) Compressive modulus of elasticity at 30% of ultimate strength (for the determination of tensile modulus of elasticity);
6) Coefficient of thermal expansion; and
7) Thermal diffusivity and specific heat capacity.

CHAPTER 11
CONCLUSIONS AND RECOMMENDATIONS

11.1 Findings

A finite element model was built to predict the early age behavior of hydrating concrete element. To validate the accuracy of the model and hence verify the results obtained from the model, four different concrete mixtures were used in experimental blocks with dimensions 3.5 ft. × 3.5 ft. × 3.5 ft. (1.07 m × 1.07 m × 1.07 m) and monitored for temperature distributions. The material and physical properties of the concretes used were obtained from laboratory testing and used in the finite element model. The two types of tests done on the concrete mixtures to determine the energy released during hydration were semi-adiabatic calorimetry and isothermal calorimetry. The calculated adiabatic energy rise obtained from each test was used in the model to determine which procedure would give the best results when compared with the temperatures measured in the experimental block.

Based on the results of the thermal analysis of the concrete block model, the following findings were made:

- The semi-adiabatic calorimetry test consistently gave lower heat of hydration and lower predicted temperature of concrete as compared with the isothermal calorimetry test.
- The input of adiabatic energy captured in the isothermal calorimetry test provided temperature distributions that were very similar to those measured in the experimental blocks. At some locations, the predicted temperatures were higher than the measured temperatures, and so the isothermal test can be said to provide conservative predictions of the temperature distribution.

The induced stresses caused by the varying temperatures within the concrete element of each mixture were analyzed using the results from the model that utilized the energy from

isothermal calorimetry test. The magnitude and type of stresses were of particular interest in determining the likelihood of thermal cracking. The results of this structural analysis for the concrete block study led to the following observations:

- The highest tensile stresses were located at the top edge of the surface exposed to ambient conditions.
- Concrete containing 100% Portland cement experienced tensile stresses high enough to cause cracking on all surfaces, even those insulated, when the temperature difference was 17.3° C (31.1° F).
- In the case where 50% of the Portland cement was replaced with ground granulated blast-furnace slag, the rate of hydration reaction and, hence rate of temperature increase, was significantly slower. The associated reduction in early age tensile strength resulted in the cracking risk not being reduced.
- In the case where 35% of the Portland cement was substituted with fly ash, there was little effect on the early age rate of hydration, and thus, the time in which the maximum temperature was achieved was not affected significantly. However, the maximum temperature achieved was itself significantly less. Again, the early age tensile strength was less than the 100% Portland cement case, resulting in similar cracking on all surfaces as before, even though the tensile stresses experienced were less.
- Concrete that had a blend of 50% Portland cement, 30% slag, and 20% fly ash performed the best in terms of reducing the induced thermal stresses relative to the tensile strength, and hence, the cracking potential.
- The temperature differential that induced cracking in the concretes used in this project varied from mixture to mixture. This was due to the corresponding changes in the tensile strength.

The parametric study on factors affecting the temperature distribution in concrete produced very interesting results as follows:

- The thermal stresses in large mass concrete elements were effectively reduced with the use of thick layers of insulating polystyrene foam. This method is advantageous

because the polystyrene foam, if removed carefully, can be reused often making it relatively inexpensive when compared to other single use methods such as cooling pipes and liquid nitrogen.

- Although the tensile stresses that resulted from the removal of formwork and insulation 12 hours, 1 day, 2 days, and 3 days after the pouring of the concrete were less than the tensile strength of the concrete as measured in the laboratory, the stresses could be large enough to initiate micro-cracking. These micro-cracks can serve as an entry point for deleterious materials that can undermine the durability of the concrete. For insulation removed after 4 days, the tensile stresses were significantly less than the tensile strength, reducing the risk of micro-cracking.

11.2 Conclusions

Based on the results obtained in this study, the following conclusions are made:

- The heat of hydration energy data obtained from the isothermal calorimetry test should be used for the input for the heat generation function in the finite element modeling of concrete hydration.
- Reliance on a limiting maximum temperature differential to control cracking in massive concrete applications should be supplemented with a requirement for the presentation of a finite element analysis showing the calculated stress response to the predicted temperature distribution within the concrete, to ensure that the induced tensile stresses will not exceed the tensile strength of the concrete.
- Adequate insulation should be used in conjunction with the usual formwork material to reduce the temperature differentials during the early age hydration of massive concrete. However, caution should be taken, as the occurrence of delayed ettringite formation (DEF) and drying shrinkage due to high concrete temperatures was not studied.
- A safety factor should be applied to the tensile strength values for concrete obtained from the splitting tension and third-point flexural strength tests to guard against the initiation of micro-cracks which, although by themselves will not cause structural failure, can act as an entry point for deleterious materials which can undermine the durability of the concrete.

- The current restrictions on maximum temperature imposed by state regulating bodies should take into consideration the type of cementitious materials that will be used in the concrete mix.

11.3 Recommendations for Future Research

It is recommended that additional blends of cementitious materials and additional larger blocks of mass concrete be tested in order to assess the universal applicability of the hypotheses deduced and concluded from this study.

LIST OF REFERENCES

ACI Committee 207. (2005). *207.1R-05: Guide to Mass Concrete*, Farmington Hill, MI.

ACI Committee 207. (2005). *207.2R-07: Report on Thermal and Volume Change Effects on Cracking of Mass Concrete*, Farmington Hills, MI.

Ayotte, E., Massicotte, B., Houde, J., and Gocevski, V. (1997). "Modeling of Thermal Stresses at Early Ages in a Concrete Monolith." *ACI Materials Journal*, Vol. 94, No. 6, p. 577-587.

Bamforth, P.B. (1984). "Mass Concrete." *Concrete Society Digest*. Concrete and Cement Association.

Bhatty, J.I., and Taylor, P.T. (2006). *Sulfate Resistance of Concrete Using Blended Cements or Supplementary Cementitious Materials*. Portland Cement Association, Skokie, IL.

Boyd, A.J., and Mindess, S. (2002). *An Indirect Tension Test for Concrete, Fifth International Symposium on Cement & Concrete*. Tongji University Press, Shanghai, China, Vol. I, pp. 590-594.

Boyd, A.J., and Mindess, S. (2004). "The Use of Tension Testing to Investigate the Effect of W/C Ratio and Cement Type on the Resistance of Concrete to Sulfate Attack." *Cement and Concrete Research*. Elsevier, Vol. 34, No. 3, pp. 373-377.

Bremner, T.W., Boyd, A.J., Holm, T.A., and Boyd, S.R. (1998). "Indirect Tensile Testing to Evaluate the Effect of Alkali-Aggregate Reaction in Concrete." *Proceedings*, Structural Engineering World Wide. ASCE, San Francisco, CA, CD-ROM Paper T192-2, 12 pp.

Chini , A.R., Muszynski, L.C., Acquaye, L., and Tarkhan, S. (2003). *Determination of the Maximum Placement and Curing Temperatures in Mass Concrete to Avoid Durability Problems and DEF*. FDOT Contract BC-354-29. Florida Department of Transportation, Tallahassee, February.

Crawford, G. (2009). "Concrete Coefficient of Thermal Expansion." Presentation to AASHTO Joint Technical Committee on Pavements. Jackson Hole, WY, May 27-28.

De Schutter, G., and Taerwe, L. (1995). "General Hydration Model for Portland Cement and Blast Furnace Slag Cement." *Cement and Concrete Research*, Vol. 25, No. 3, pp. 593-604.

De Schutter, G., and Taerwe, L. (1995). "Specific Heat and Thermal Diffusivity of Hardening Concrete." *Mag. Concr. Res*., Vol. 47, No. 172, pp. 203-208.

Divet, L., and Pavione, A. (2002). "Delayed Ettringite Formation in Massive Concrete Structure:, an Account of Some Studies of Degraded Bridges." *Proceedings*, International RILEM TC 186-ISA Workshop, RILEM. Villars, Switzerland, pp. 98-126.

Drimalas T. (2004). "Laboratory Testing and Investigations of Delayed Ettringite Formation." Masters Thesis. University of Texas, Austin, TX.

Florida Department of Transportation. (2007). *Standard Specifications for Road and Bridge Construction*. Florida Department of Transportation (FDOT), Tallahassee.

Florida Department of Transportation. (2009). *FDOT Structures Manual*. Florida Department of Transportation (FDOT), Tallahassee.

Gajda, J. (2007). *Mass Concrete for Buildings and Bridges*. Portland Cement Association, Skokie, IL.

Ghorab, H.Y. (2002). "On the Chemistry of Delayed Ettringite Formation." *Proceedings*, International RILEM TC 186-ISA Workshop, RILEM. Villars, Switzerland, pp. 65-81.

Higginson, E.C. (1970). "The Effect of Cement Fineness on Concrete. *Fineness of Cement. STP 473*. American Society for Testing and Materials (ASTM), Philadelphia, PA, pp. 71-81.

Kelham, S. (2002). "Effects of Cement Parameters on Expansion Associates with DEF." *Proceedings*, International RILEM TC 186-ISA Workshop, RILEM. Villars, Switzerland, pp. 98-126.

Lane, D.S., and Ozyildrirm, H.C. (1999). "Evaluation of the Potential for Internal Sulfate Attack Through Adaptation of ASTM C 342 and the Duggan Test Cement." *Concrete & Aggregates*, ASTM, Vol. 21, No. 1, pp. 43-58.

Larsen, T.J. (1991). *The Effects of Variation in Tricalcium silicate of Portland Cement on Concrete Properties*. August 1989, Revised Feb 1991, Florida Department of Transportation, Tallahassee.

Lawrence, C.D. (1998). *Physiochemical and Mechanical Properties of Portland Cements, Lea's Chemistry of Portland Cement*. 4th Edition. Arnold Publisher, Edited by P.C. Hewlett, pp. 343-349.

Lindstrom, L., and Westerberg, B. (2003). "Fine Ground Cement in Concrete - Properties and Prospects." *ACI Materials Journal*, Vol. 100, No. 5, pp. 398-406.

Machida, N., and Uehara, K. (1987). "Nonlinear Thermal Stress Analysis of a Massive Concrete Structure." *Comput. Struct*., Vol. 26, pp. 287-296.

Malhotra, V.M., and Mehta, P.K. (1996). *Pozzolanic and Cementitious Materials*. Gordon and Breach Publishers, Canada.

Mehta, P.K., and Monteiro, P. J. M. (2006). *Concrete – Microstructure, Properties and Materials*. 3rd Edition. McGraw-Hill.

Miller, F. M., and Conway, T. (2003). "Use of Ground Blast Furnace Slag for the Reduction of Expansion Due to Delayed Ettringite Formation." *Cement, Concrete & Aggregates*, ASTM, Vol. 25, No. 1, pp. 43-58.

Neville, A. (1995). *Properties of Concrete*. 4th Edition. Essex, England Pearson Education Limited.

Poole, T. (2004). *Predicting Heat of Hydration in Hydraulic Cement*. U.S. Army Research and Development Center, Vicksburg, MS, April.

Price, W.H. (1974). "Practical Qualities of Cement." *Journal of the American Concrete Institute*, Vol. 71, No. 9, September, pp. 436-444.

Radovanic, S. (1998). *Thermal and Structural Finite Element Analysis of Early Age Mass Concrete Structures*. University of Manitoba, Winnipeg, Manitoba, Canada.

Ramlochan, T., Zacarias, P., Thomas, M..D.A., and Hooton, R.D. (2003). "The Effect of Pozzolans and Slag on the Expansion of Mortars Cured at Elevated Temperature, Part I: Expansive Behaviour." *Cement and Concrete Research*, Elsevier, Vol. 33, pp. 807-814.

RILEM 119-TCE 1. (1997). "Adiabatic and Semi-Adiabatic Calorimetry to Determine the Temperature Increase in Concrete Due to Hydration Heat of Cement." *Materials and Structures*, Vol. 30, pp. 451-457.

Schindler, A.K. (2002). "Concrete Hydration, Temperature Development, and Setting at Early Ages." Ph.D. Dissertation. University of Texas at Austin, Austin, TX.

Schlorholtz, S., and .Bergeson, K.L. (1993). "Evaluation of Chemical Durability of Iowa Flyash Concrete." Iowa Department of Transportation, Ames, IA, March.

Skalny, J., Marchand, J., and Older, I. (2002). Sulfate Attack on Concrete. Spon Press, London.

Tanabe, T., Kawasumi, M., and Yamashita, Y. (1986) "Thermal Stress Analysis of Massive Concrete", Seminar Proceedings For Finite Element Analysis of Reinforced Concrete Structures, Tokyo, Japan, May 21-24, 1985, ASCE, New York, N.Y.

Taylor, H.F.W. (1997). *Cement Chemistry*. Heron Quay, London: Thomas Telford Publishing.

Thomas, M., Folliard, K., Drimala, T., and Ramlochan, T. (2008). "Diagnosing Delayed Ettringite Formation in Concrete Structures." *Cement and Concrete Research*, Vol. 38, pp. 841-847.

U.S. Army Corps of Engineers. (1997). "Appendix A: Techniques for Performing Concrete Thermal Studies." *Manual ETL 1110-2-542*, Washington, D.C.

Woods, H., Steinour, H.H., and Starke, H.R. (1933). "Heat Evolved by Cement in Relation to Strength." *Engineering News Record*, Vol. 110, April 6, pp. 431.

APPENDIX A
GRAPHICAL USER INTERFACE INPUT COMMANDS

Define Geometry Points for Base of Model

```
GEOMETRY POINT COORDINATE  0 0 0
GEOMETRY POINT COORDINATE  0.5334 0 0
GEOMETRY POINT COORDINATE  0.552445 0 0
GEOMETRY POINT COORDINATE  0.62865 0 0
GEOMETRY POINT COORDINATE  0 0.5334 0
GEOMETRY POINT COORDINATE  0.5334 0.5334 0
GEOMETRY POINT COORDINATE  0.552445 0.5334 0
GEOMETRY POINT COORDINATE  0.62865 0.5334 0
GEOMETRY POINT COORDINATE  0 0.55245 0
GEOMETRY POINT COORDINATE  0.5334 0.55245 0
GEOMETRY POINT COORDINATE  0.552445 0.55245 0
GEOMETRY POINT COORDINATE  0.62865 0.55245 0
GEOMETRY POINT COORDINATE  0 0.62865 0
GEOMETRY POINT COORDINATE  0.5334 0.62865 0
GEOMETRY POINT COORDINATE  0.552445 0.62865 0
GEOMETRY POINT COORDINATE  0.62865 0.62865 0
```

Connectivity

```
GEOMETRY SURFACE 4POINTS P1 P2 P6 P5
GEOMETRY SURFACE 4POINTS P2 P3 P7 P6
GEOMETRY SURFACE 4POINTS P3 P4 P8 P7
GEOMETRY SURFACE 4POINTS P5 P6 P10 P9
GEOMETRY SURFACE 4POINTS P6 P7 P11 P10
GEOMETRY SURFACE 4POINTS P7 P8 P12 P11
GEOMETRY SURFACE 4POINTS P9 P10 P14 P13
GEOMETRY SURFACE 4POINTS P10 P11 P15 P14
GEOMETRY SURFACE 4POINTS P11 P12 P16 P15
```

Merge Geometries

```
CONSTRUCT SET BOTFOAM APPEND ALL
VIEW GEOMETRY ALL BLUE
LABEL GEOMETRY LINES ALL RED
LABEL GEOMETRY SURFACE ALL BLUE
```

Group Lines with Equal Divisions into Sets

```
CONSTRUCT SET SELIN1 APPEND LINES L1 L2 L3 L4 L6 L9 L12 L19
CONSTRUCT SET SELIN2 APPEND LINES L5 L7 L8 L10 L11 L13 L14 L15 L16 L17
CONSTRUCT SET SELIN2 APPEND LINES L18 L20 L21 L22 L23 L24
```

Divide Lines

```
MESHING DIVISION LINE SELIN1 10
MESHING DIVISION LINE SELIN2 1
```

Create Volumes for 3D Model

```
GEOMETRY SWEEP BOTFOAM BOTPLY 1 TRANSLATE 0 0 0.762
GEOMETRY SWEEP BOTPLY BOTBLOCK 1 TRANSLATE 0 0 0.0381
GEOMETRY SWEEP BOTBLOC TOPBLOC 20 TRANSLATE 0 0 1.0668


CONSTRUCT SET MODEL APPEND ALL

LABEL GEOMETRY BODIES ALL BLUE
```

Group Geometries into Materials

```
CONSTRUCT SET CONCRETE APPEND BODIES B19
CONSTRUCT SET OPEN POLSTYRENE
CONSTRUCT SET APPEND BODIES B1 B2 B3 B4 B5 B6 B7 B8 B9 B12
CONSTRUCT SET APPEND BODIES B15 B16 B17 B18 B21 B24 B25 B26 B27
CONSTRUCT SET CLOSE
CONSTRUCT SET PLYWOOD APPEND BODIES B10 B11 B13 B14 B20 B22 B23
```

Generate Mesh for Entire Model

```
MESHING TYPES MODEL HE8 HX8HT
MESHING GENERATE
```

Turn of DIANA's Element Space Conflict Check

```
CONSTRUCT SPACE TOLERANCE OFF
GEOMETRY COPY CONCRETE CONC TRANSLATE 0 0 0
```

Specifiy Element Type For Concrete used in Flow-Stress Analysis

```
CONSTRUCT SET SELIN3 APPEND LINES L145 L146 L147 L148 L149 L150 L151
                                                    L152
CONSTRUCT SET SELIN4 APPEND LINES L153 L154 L155 L156
MESHING DIVISION LINE SELIN3 20
MESHING DIVISION LINE SELIN4 40
MESHING TYPES CONC HE20 CHX60
MESHING GENERATE
MESHING MERGE ALL 0.001          Merges all nodes within a distance of 0.001
```

Identify Surfaces that Experience Boundary Convection

CONSTRUCT SET OPEN BOUNDA
CONSTRUCT SET APPEND SURFACES S1 S2 S3 S4 S5 S6 S7 S8 S9 S27
CONSTRUCT SET APPEND SURFACES S34 S37 S40 S41 S42 S60 S67 S70 S73 S74
CONSTRUCT SET APPEND SURFACES S75 S77 S78 S79 S81 S82 S83 S84 S93 S100
CONSTRUCT SET APPEND SURFACES S103 S106 S107 S108 S110
CONSTRUCT SET CLOSE

CONSTRUCT SPACE TOLERANCE OFF
GEOMETRY COPY BOUNDA OUTER TRANSLATE 0 0 0
MESHING TYPES OUTER QU4 BQ4HT
MESHING GENERATE
MESHING MERGE ALL 0.001

Define Material Properties
Properties are Defined Using the Property Manager Dialog Box
View Property Manager
Materials Material Name: CONC
External External Data from File: concrete.dat

Material Name: MAPLY (Plywood)
Conductivity=540 J/m-hr-°C, Heat Capacity=8.54E5 J/m^3-°C
Material Name: MAINSUL (Polystyrene Insulation)
Conductivity=126 J/m-hr-°C, Heat Capacity=2.84E4 J/m^3-°C

Material Name: MAOUT (Boundary Elements)
Convection Coefficient=2.016E4 J/m^3-hr-°C

Assign Properties to Geometries and Elements

PROPERTY ATTACH CONC MACONC
PROPERTY ATTACH PLY MAPLY
PROPERTY ATTACH POLYSTRENE MAINSUL
PROPERTY ATTACH OUTER MAOUT

Boundary Conditions

PROPERTY LOADS EXTTEMP 1 OUTER 23
PROPERTY LOADS GRAVITY 2 CONC -0.981E-5 3 *Weight acting downwards*

Assign Variations of Loads and Boundary Conditions to Time

CONSTRUCT TCURVE TCDUM LIST 0 1. 168.1.
PROPERTY ATTACH LOADCASE 1 TCDUM
PROPERTY ATTACH LOADCASE 2 TCDUM

Boundary Constraints ie. Support Conditions and Symmetry Conditions

PROPERTY BOUNDARY CONSTRAINT S109 Z
PROPERTY BOUNDARY CONSTRAINT S111 Y
PROPERTY BOUNDARY CONSTRAINT S114 X

Set Initial Temperatures

PROPERTY INITIAL INITEMP ALL 23

UTILITY WRITE DIANA QUARTERBLOCKMODEL

APPENDIX B
BATCH FILE INPUT COMMANDS

```
FEMGEN MODEL      : QUARTERBLOCK1
ANALYSIS TYPE     : Heatflow-Stress Staggered 3D
'UNITS'
LENGTH   M
TIME     HOUR
TEMPER   CELSIU
FORCE    N
'COORDINATES'
   1     0.000000E+00    0.000000E+00    0.000000E+00
   2     5.334000E-02    0.000000E+00    0.000000E+00
   3     1.066800E-01    0.000000E+00    0.000000E+00
   4     1.600200E-01    0.000000E+00    0.000000E+00
   5     2.133600E-01    0.000000E+00    0.000000E+00
   6     2.667000E-01    0.000000E+00    0.000000E+00
   7     3.200400E-01    0.000000E+00    0.000000E+00
   8     3.733800E-01    0.000000E+00    0.000000E+00
   9     4.267200E-01    0.000000E+00    0.000000E+00
  10     4.800600E-01    0.000000E+00    0.000000E+00
```

Lines Skipped

```
12460     1.600200E-01    4.800600E-01    1.154430E+00
12461     2.133600E-01    4.800601E-01    1.154430E+00
12462     2.667000E-01    4.800601E-01    1.154430E+00
12463     3.200400E-01    4.800601E-01    1.154430E+00
12464     3.733800E-01    4.800601E-01    1.154430E+00
12465     4.267200E-01    4.800601E-01    1.154430E+00
12466     4.800600E-01    4.800601E-01    1.154430E+00
'ELEMENTS'
CONNECTIVITY
   1 HX8HT  1 2 13 12 122 123 134 133
   2 HX8HT  2 3 14 13 123 124 135 134
   3 HX8HT  3 4 15 14 124 125 136 135
   4 HX8HT  4 5 16 15 125 126 137 136
   5 HX8HT  5 6 17 16 126 127 138 137
   6 HX8HT  6 7 18 17 127 128 139 138
   7 HX8HT  7 8 19 18 128 129 140 139
   8 HX8HT  8 9 20 19 129 130 141 140
   9 HX8HT  9 10 21 20 130 131 142 141
  10 HX8HT  10 11 22 21 131 132 143 142
```

Lines Skipped

```
 3168 HX8HT  3589 3609 3869 3849 3588 3608 3868 3848
 3169 CHX60  339 3888 340 3899 351 3909 350 3898 4347 4386 5888 5868
          647 4366 666 6050 5969 6059 1388 5887
```

```
3170 CHX60  340 3889 341 3900 352 3910 351 3899 4386 4425 5889 5888
        666 4405 685 6051 5970 6060 5969 6050
3171 CHX60  341 3890 342 3901 353 3911 352 3900 4425 4464 5890 5889
        685 4444 704 6052 5971 6061 5970 6051
3172 CHX60  342 3891 343 3902 354 3912 353 3901 4464 4503 5891 5890
        704 4483 723 6053 5972 6062 5971 6052
3173 CHX60  343 3892 344 3903 355 3913 354 3902 4503 4542 5892 5891
        723 4522 742 6054 5973 6063 5972 6053
3174 CHX60  344 3893 345 3904 356 3914 355 3903 4542 4581 5893 5892
        742 4561 761 6055 5974 6064 5973 6054
3175 CHX60  345 3894 346 3905 357 3915 356 3904 4581 4620 5894 5893
        761 4600 780 6056 5975 6065 5974 6055
3176 CHX60  346 3895 347 3906 358 3916 357 3905 4620 4659 5895 5894
        780 4639 799 6057 5976 6066 5975 6056
3177 CHX60  347 3896 348 3907 359 3917 358 3906 4659 4698 5896 5895
        799 4678 818 6058 5977 6067 5976 6057
3178 CHX60  348 3897 349 3908 360 3918 359 3907 4698 4737 4776 5896
        818 4717 837 4756 856 6068 5977 6058
```

Lines Skipped

```
5168 CHX60  12205 12376 990 5089 1009 5128 1028 12385 12466 5069 5108
        5147 616 4306 617 4317 628 4327 627 4316
5169 BQ4HT  1 2 13 12
5170 BQ4HT  2 3 14 13
5171 BQ4HT  3 4 15 14
5172 BQ4HT  4 5 16 15
5173 BQ4HT  5 6 17 16
5174 BQ4HT  6 7 18 17
5175 BQ4HT  7 8 19 18
5176 BQ4HT  8 9 20 19
5177 BQ4HT  9 10 21 20
5178 BQ4HT  10 11 22 21
5179 BQ4HT  12 13 24 23
```

Lines Skipped

```
5982 BQ4HT  626 627 3377 3376
5983 BQ4HT  627 628 3378 3377
```

:Nodes Grouped to Materials

```
MATERIALS
/ 145-254 265-275 2289-2488 2689-2908 /  1
/ 5169-5983 /  2
/ 3169-5168 /  3
/ 1-144 255-264 276-288 2489-2688 2909-3168 /  4
```

```
'MATERIALS'

:Plywood Properties
  1 CONDUC    5.400000E+02
    CAPACI    8.543999E+05

:Boundary Properties
  2 CONVEC    2.016000E+04

:Concrete Properties
  3 CONDUC    7.920E+03
    CAPACI    2.675596E+06
    ADIAB     0.0      23
          1.0      23.73796428
          2.0      25.42189049
          3.0      28.73104768
          4.0      33.31326448
          5.0      38.24138423
          6.0      42.95409819
          7.0      47.74431264
          8.0      52.63938071
          9.0      56.42322844
          10.0     59.06166443
          11.0     61.06186104
          12.0     62.68025374
          13.0     64.07070381
          14.0     65.2901969
          15.0     66.38432155
          16.0     67.38157057
          17.0     68.30473824
          18.0     69.14242742
          19.0     69.94022664
          20.0     70.68673876
          21.0     71.37626523
          22.0     72.03160031
          23.0     72.65274398
          24.0     73.23969627
          25.0     73.78675859
          26.0     74.30532808
          27.0     74.79540474
          28.0     75.26838571
          29.0     75.71287385
          30.0     76.13456772
          31.0     76.5391659
          32.0     76.91527124
          33.0     77.28567802
```

34.0	77.63329054
35.0	77.96950592
36.0	78.29432418
37.0	78.60204673
38.0	78.90407072
39.0	79.18899902
40.0	79.46822874
41.0	79.73606134
42.0	80.00389393
43.0	80.2603294
44.0	80.50536773
45.0	80.75040606
46.0	80.98404726
47.0	81.22338703
48.0	81.43993253
49.0	81.6621766
50.0	81.87302353
51.0	82.08956904
52.0	82.29471741
53.0	82.49986578
54.0	82.70501415
55.0	82.90446395
56.0	83.09251663
57.0	83.28626786
58.0	83.4800191
59.0	83.66237321
60.0	83.84472732
61.0	84.02708142
62.0	84.20373697
63.0	84.37469394
64.0	84.55704805
65.0	84.72230646
66.0	84.89326343
67.0	85.05852184
68.0	85.22947882
69.0	85.3833401
70.0	85.54859851
71.0	85.70815835
72.0	85.86201963
73.0	86.01588091
74.0	86.16974219
75.0	86.32930203
76.0	86.47746474
77.0	86.61992889
78.0	86.77379017
79.0	86.91625431

80.0	87.05871846
81.0	87.20688117
82.0	87.34364675
83.0	87.48041233
84.0	87.62287648
85.0	87.75964206
86.0	87.88501051
87.0	88.02177609
88.0	88.15854167
89.0	88.28960868
90.0	88.41497713
91.0	88.54604415
92.0	88.67711116
93.0	88.80817817
94.0	88.92784806
95.0	89.05321651
96.0	89.17288639
97.0	89.29825484
98.0	89.41792472
99.0	89.5375946
100.0	89.65156592
101.0	89.7712358
102.0	89.89090569
103.0	90.004877
104.0	90.11314976
105.0	90.22712107
106.0	90.34109239
107.0	90.44936514
108.0	90.55193933
109.0	90.66591064
110.0	90.77418339
111.0	90.87675758
112.0	90.9907289
113.0	91.08760452
114.0	91.1901787
115.0	91.29845145
116.0	91.39532707
117.0	91.49220269
118.0	91.60047544
119.0	91.6916525
120.0	91.79422668
121.0	91.87970517
122.0	91.98227935
123.0	92.07915497
124.0	92.17033203
125.0	92.26150908

126.0	92.35268613
127.0	92.44956175
128.0	92.53504024
129.0	92.63191586
130.0	92.71739435
131.0	92.8085714
132.0	92.89404989
133.0	92.97952838
134.0	93.06500687
135.0	93.15048535
136.0	93.24166241
137.0	93.3271409
138.0	93.40122225
139.0	93.49239931
140.0	93.57217923
141.0	93.65765772
142.0	93.7431362
143.0	93.82291612
144.0	93.90839461
145.0	93.98247597
146.0	94.06225589
147.0	94.14203581
148.0	94.23321287
149.0	94.30159566
150.0	94.38707414
151.0	94.45545693
152.0	94.53523686
153.0	94.61501678
154.0	94.68909813
155.0	94.76317949
156.0	94.84295941
157.0	94.92273933
158.0	94.99682069
159.0	95.07090205
160.0	95.1449834
161.0	95.21906476
162.0	95.28744755
163.0	95.3615289
164.0	95.4299117
165.0	95.50399305
166.0	95.57237584
167.0	95.6464572

ARRHEN 4117.75
EQUAGE ARRTYP
TEMREF 23.0
YOUNG 2.523500E+04

```
    POISON    2.000000E-01
    DENSIT    2.2480000E+03
    THERMX    9.160000E-06
    FTTIME    0. 24.  48.  72.  167.
    FTVALU    0. 1.25 1.66 1.93 2.206
    MAXWEL    1
 ,1
    TIME      0. 24. 48. 72. 167.
    YOUNG     13445. 13445. 16892. 18064. 20202.

:Polystyrene Properties
  4 CONDUC    2.248500E+02
    CAPACI    2.082400E+04

:Geometry and Element Groupings
'GROUPS'
NODES
  1 BOTFOAM / 1-121 243-253 265-275 287-297 309 311 313-323 335
            337 /
  2 SELIN1 / 1-12 22 23 33 34 44 45 55 56 66 67 77 78 88 89 99 100
           110-121 243-253 265-275 287-297 313-323 /
  3 SELIN2 / 11 111 121 243 253 265 275 287 297 309 311 313 323
           335 337 /
  4 BOTPLY / 122-242 254-264 276-286 298-308 310 312 324-334 336
           338 /
  5 BOTBLOC / 339-507 /
  6 TOPBLOC / 508-628 2928-2938 3148-3158 3368-3378 3588 3608 3628-3638
            3848 3868 /
ELEMEN
  7 MODEL / 1-3168 /
NODES
  8 MODEL_N / 1-3887 /
ELEMEN
  9 CONCRE / 289-2288 /
NODES
 10 CONCRE_N / 339-459 508-2927 /
ELEMEN
 11 POLYSTY / 1-144 255-264 276-288 2489-2688 2909-3168 /
NODES
 12 POLYSTY_N / 1-338 460-507 2928-3887 /
ELEMEN
 13 PLY / 145-254 265-275 2289-2488 2689-2908 /
NODES
 14 PLY_N / 122-242 254-264 298-308 310 339-470 482-493 518 529
          540 551 562 573 584 595 606 617-628 819-1217 2928-3147
          3368-3607 /
```

```
ELEMEN
  15 CONC / 3169-5168 /
NODES
  16 CONC_N / 339-459 508-1388 3888-12466 /
  17 SELIN3 / 339-350 360 361 371 372 382 383 393 394 404 405 415 416
            426 427 437 438 448-459 508-519 529 530 540 541 551 552
            562 563 573 574 584 585 595 596 606 607 617-628 3888-3898
            3908 3919 3929 3940 3950 3961 3971 3982 3992 4003
            4013 4024 4034 4045 4055 4066 4076 4087 4097-4118
            4128 4139 4149 4160 4170 4181 4191 4202 4212 4223
            4233 4244 4254 4265 4275 4286 4296 4307 4317-4327 /
  18 SELIN4 / 339 349 449 459 508 518 618 628-647 819-837 1009-1027
            1199-1217 4328-4347 4718-4737 5108-5127 5498-5517 /
  19 BOUNDA / 1-121 243-253 265-297 309 311-338 471-481 494-628
            2928-2938 3148-3378 3588 3608-3887 4108-4327 /
ELEMEN
  20 OUTER / 5169-6283 /
NODES
  21 OUTER_N / 1-121 243-253 265-297 309 311-338 471-481 494-628
             2928-2938 3148-3378 3588 3608-3887 4108-4327 /
'SUPPORTS'                                        (Boundary Constraints)
 / 339 350 361 372 383 394 405 416 427 438 449 508 519 530 541 552
   563 574 585 596 607 618 629-647 1199-1388 3898 3919 3940 3961
   3982 4003 4024 4045 4066 4087 4118 4139 4160 4181 4202 4223 4244
   4265 4286 4307 4328-4347 5498-5887 /   TR     1
 / 339-349 508-518 629-837 3888-3897 4108-4117 4328-4737 /   TR     2
 / 339-459 3888-4107 /   TR     3

:Ambient Temperature
'BOUNDA'
CASE 1
ELEMEN
5169  EXTEMP    0.230000E+02
5170  EXTEMP    0.230000E+02
                                                        Lines Skipped

5982  EXTEMP    0.230000E+02
5983  EXTEMP    0.230000E+02

:Ambient Temperature Variation with Time
'TIMEBO'
BOUNDA 1
TIMES  0.000000E+00   0.167000E+03   /
FACTOR 0.100000E+01   0.100000E+01   /
```

```
:Selfweight/Gravity Load
'LOADS'
CASE 2
WEIGHT
 3    -0.981000E-05

:Variation of Load  with Time
'TIMELO'
LOAD   2
TIMES  0.000000E+00   0.167000E+03   /
FACTOR 0.100000E+01   0.100000E+01   /

:Initial Temperatures
'INIVAR'
TEMPER 1
   1     0.230000E+02
   2     0.230000E+02
                                                                    Lines Skipped
12466     0.230000E+02
'DIRECTIONS'
   1   1.000000E+00   0.000000E+00   0.000000E+00
   2   0.000000E+00   1.000000E+00   0.000000E+00
   3   0.000000E+00   0.000000E+00   1.000000E+00
'END'
```

APPENDIX C
STAGGERED ANALYSIS COMMANDS

In this appendix, the analysis commands for the standard staggered analysis are presented. The standard staggered analysis is one in which the thermal flow analysis is coupled with the structural analysis. The temperatures calculated in the thermal analysis are automatically converted to input for the structural analysis.

```
*FILOS
INITIA                                          Initiate Analysis
*INPUT
*HEATTR                                         Analysis Type Thermal
BEGIN INITIA
 BEGIN NONLIN
  EQUAGE                                        Calculate Equivalent Age
  HYDRAT DGRINI=0.01
 END NONLIN
 TEMPER INPUT FIELD=1
END INITIA
BEGIN EXECUT
 BEGIN NONLIN
  HYDRAT ITERAT
  BEGIN ITERAT
   CONVER TEMPER TOLCON=0.01
   MAXITE=30                                    Maximum No. of Iterations
  END ITERAT
 END NONLIN
 SIZES 1.0(167)                                 Magnitude & No. Time Steps
END EXECUT
BEGIN OUTPUT FEMVIE FILE="FLOW"            File to print to output
 EQUAGE TOTAL INTPNT
 TEMPER
 REACTI TOTAL INTPNT
END OUTPUT
*NONLIN
BEGIN TYPE
 BEGIN PHYSIC                                   Analysis Type Structural
  TEMPER                                        Read Temperatures as Input
  VISCOE                                        Viscoelastic Behaviour
 END PHYSIC
END TYPE
```

```
BEGIN EXECUTE
 TIME STEPS EXPLIC SIZES 1.0(167)
 BEGIN ITERAT
  BEGIN CONVER
   SIMULT
   FORCE TOLCON=1.0E-2
   DISPLA TOLCON=1.0E-2
  END CONVER
 END ITERAT
END EXECUT
BEGIN OUTPUT FEMVIE FILE="STRUC"
 DISPLA
 STATUS
 STATUS CRACK
 STRAIN TEMPER
 STRAIN
 STRAIN CRACK GREEN
 STRESS
 STRESS TOTAL CAUCHY PRINCI
 STRESS TOTAL CAUCHY CRKIND
 TEMPER
END OUTPUT
*END
```

APPENDIX D
PHASED ANALYSIS COMMANDS

In this appendix, the analysis commands for the phased analysis in which the formwork is removed sometime during the hydration process is presented. The example presented here is for the removal of the formwork 96 hours (4 days) after the hydration reaction commences.

```
*FILOS
INITIA
*INPUT
*PHASE                                                    Start Phase 1
ACTIVE ELEMEN CONC PLY POLYSTY OUTER                      Elements active in Phase 1
*HEATTR
BEGIN INITIA
 BEGIN NONLIN
  EQUAGE
  HYDRAT DGRINI=0.01
 END NONLIN
 TEMPER INPUT
END INITIA
EXECUT SIZES 1.0(96)
BEGIN OUTPUT FEMVIE FILE="FLOW_1m4Days"
 EQUAGE
 TEMPER
 REACTI
END OUTPUT
*NONLIN
BEGIN TYPE
 BEGIN PHYSIC
  TEMPER
  VISCOE
 END PHYSIC
END TYPE
BEGIN EXECUTE
 TIME STEPS EXPLIC SIZES 1.0(96)
 BEGIN ITERAT
  BEGIN CONVER
   SIMULT
   FORCE TOLCON=1.0E-2
   DISPLA TOLCON=1.0E-2
  END CONVER
 END ITERAT
```

```
END EXECUT
BEGIN OUTPUT FEMVIE FILE="STRUC_1m4Days"
 DISPLA
 STRAIN TEMPER
 STRAIN
 STRESS
 STRESS TOTAL CAUCHY PRINCI
 STRESS TOTAL CAUCHY CRKIND
 TEMPER
END OUTPUT
*END


*PHASE                                                    Start Phase 2
BEGIN ACTIVE
 ELEMEN CONC OUTER2                                       Elements active in Phase 2
END ACTIVE
*HEATTR                                                   Analysis Type Thermal
BEGIN INITIA
 BEGIN NONLIN
  EQUAGE
  HYDRAT DGRINI=0.01
 END NONLIN
 TIME=96.                                                 Phase 2 Start time
 TEMPER INPUT
END INITIA
EXECUT SIZES 1.0(71)
BEGIN OUTPUT FEMVIE FILE="FLOW_1m4Days2"
 EQUAGE TOTAL INTPNT
 TEMPER
 REACTI TOTAL INTPNT
END OUTPUT
*NONLIN
BEGIN TYPE
 BEGIN PHYSIC                                             Analysis Type Structural
  TEMPER
  VISCOE
 END PHYSIC
END TYPE
BEGIN EXECUTE
 BEGIN START
  TIME=96.0                                               Phase 2 Start time
  INITIA STRESS PHASE
  LOAD LOADNR=3                                           Activate Load No. 3
  STEPS
 END START
```

```
 BEGIN ITERAT
  BEGIN CONVER
   SIMULT
   FORCE TOLCON=1.0E-2
   DISPLA TOLCON=1.0E-2
  END CONVER
 END ITERAT
END EXECUT
BEGIN EXECUTE
 TIME STEPS EXPLIC SIZES 1.0(71)
 BEGIN ITERAT
  BEGIN CONVER
   SIMULT
   FORCE TOLCON=1.0E-2
   DISPLA TOLCON=1.0E-2
  END CONVER
 END ITERAT
END EXECUTE
BEGIN OUTPUT FEMVIE FILE="STRUC_1m4Days2"
 DISPLA
 STRAIN TEMPER
 STRAIN
 STRESS
 STRESS TOTAL CAUCHY PRINCI
 STRESS TOTAL CAUCHY CRKIND
 TEMPER
END OUTPUT
*END
```

APPENDIX E
METHOD OF TESTING FOR MEASURING THE HEAT OF HYDRATION OF HYDRAULIC CEMENT USING ISOTHERMAL CONDUCTIVE CALORIMETRY

This test method was used to determine the rate of heat of hydration from hardened cementitious materials by isothermal conduction calorimetry. This procedure was written in an effort to conform to the procedure currently being developed by ASTM committee C01 for measurement of heat evolution of cementitious materials at early ages using the internal mixing method.

Terminology

- Isothermal conduction calorimeter – A colorimeter that measures heat flow form a sample maintained at a constant temperature by intimate thermal contact with a constant-temperature heat sink.
- Thermal power – Heat production rate measured in watts (W) or joules per second (J/s), and is the property measured by the calorimeter.
- Heat – Heat is the time integral of thermal power measured in Joules (J).
- Baseline – The signal from the calorimeter when a sample of approximately the same mass and thermal properties as a cement sample, but which is not undergoing any exothermic or endothermic reactions.
- Reference cell – A heat-flow cell that is dedicated to outputting power from a sample that is generating no heat. The purpose of the reference cell is to correct for certain errors caused by drift and other systematic errors that can occur in heat-flow measuring equipment.

Summary of Test Method

An isothermal heat conduction calorimeter consists of a constant-temperature heat sink to which two heat-flow sensor and sample holders are attached with good thermal conductivity. One heat-flow sensor and sample holder contains the sample of interest. The other heat-flow sensor is a reference cell containing a blank sample (in this case glass beads) that evolves no heat. The heat of hydration released by the reacting cementitious sample is passed across the sensor and into the heat sink. The output from the calorimeter is the difference in heat flow (thermal power), the sample cell and the reference cell. The heat-flow sensor actually senses a small temperature gradient that develop from the sample side to the heat-sink side, however the heat is removed from the hydrating sample fast enough that, for practical purposes, the sample is at a constant temperature (isothermal).

The output from the heat-flow sensor is an mV signal that is proportional to the thermal power from the sample. This output must be calibrated to a known thermal power. In this method, this is accomplished by measurements on a sample that emits a constant and known power level. The integral of the thermal power over the time of the test is the heat of hydration.

Significance and Use
This method is suitable for determining the total heat of hydration of hydraulic cement at constant temperature at ages up to 7 days to confirm specification compliance. It gives test results equivalent to ASTM C 186 up to 7 days of age.

Apparatus

- Balance – accurate to 0.001 g.
- Volumetric dispenser – device for measuring volume or mass of water, accurate to 0.1 mL. This could be a syringe, pipette, weighting, etc.
- Sample holder – holds the cement paste and provides intimate contact with the colorimeter heat sensing device and prevents evaporation of Mixing water.
- Resistance heater – fabricated from material with similar heat capacity and shape as the test sample, but containing a resistor connected to a constant-voltage power supply such that a stable output of 0.01 ± 0.0002 watt can be generated.
- Blank specimen – fabricated from material with similar heat capacity and shape as the test sample.
- Multimeter – an instrument for measuring DC voltage and resistance to an accuracy of 1% over the range of measurements required for calibration and execution of the test (Note 2). This instrument is only required if the user is not following instrument specific calibration procedures.
- Power supply – A constant voltage DC power supply with a voltage output range of at least 0 to 10 volts and a power rating of at least 0.25 watts.
- Calorimeter – The schematic design of a calorimeter is given in Figure E-1. It consists of a sample holder for the test and a reference sample, each thermally connected to heat flow sensors, which are thermally connected to a constant-temperature heat sink. The minimum sensitivity for measuring heat output is 100 μW.

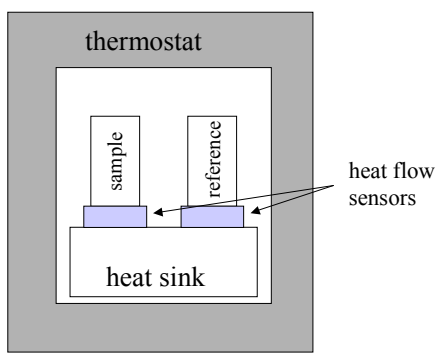

Figure E-1. A schematic drawing of a heat conduction calorimeter.

- The baseline (the power output when no heat is being generated by the sample, U_0 in the calibration sequence) shall exhibit a low random noise level and be stable against drift. The rate of change of the baseline measured during a time period of three days shall be less than or equal to 20 μW per gram of sample, per hour and a baseline random noise level of less than or equal to 10 μW per gram sample. In practice, the baseline is measure for three days and a straight line is fitted to the data using a linear

least squares procedure. The long term drift is then the slope in the line and the baseline noise level is the standard deviation around this regression line.

- Data acquisition equipment – The data acquisition equipment used for this experiment was capable of performing continuous logging of the calorimeter output measurement at a time interval of 60 seconds. It is useful, for purposes of reducing amount of data, to have the flexibility to adjust the reading interval up to 30 minutes when power output from the sample is low.

Instrument Calibration and Operating Parameters

The objective of electrical calibration is to calculate a calibration constant for each individual twin calorimetric channel. The calibration constant was entered into the PicoLog software as a factor to correct the amplifier output to read the experimental results directly in mW. Each channel has a permanent precision calibration heater on side A, the sample side. Side B, used for the inert reference, does not need to be calibrated. The heater has a resistance of 100 ± 0.1 Ω and a very low temperature coefficient. The eight calibration heaters are connected in series together with a reference calibration resistor, also 100 ± 0.1 Ω. To provide the calibration power, an internal power supply was turned on through a toggle switch, marked 'Calibration Power' on the front panel of TAM Air. The calibration power applied was in the range of 35 mW, independent on the measuring range. During the calibration, a digital voltmeter is connected to the two sockets marked 'Voltmeter'. This voltage measurement was used as part of the calculation of the calibration constant.

Calibration was performed with empty calorimetric channels. Once a stable baseline has been achieved, a known voltage is applied over the calibration heater by switching the toggle switch. A stable signal, as shown below, indicates that the power input was leaving the measuring area at the same rate as it was applied. This is called a 'steady state'. Steady state calibration is simple to evaluate and does not require any form of integration as shown in Figure E-2.

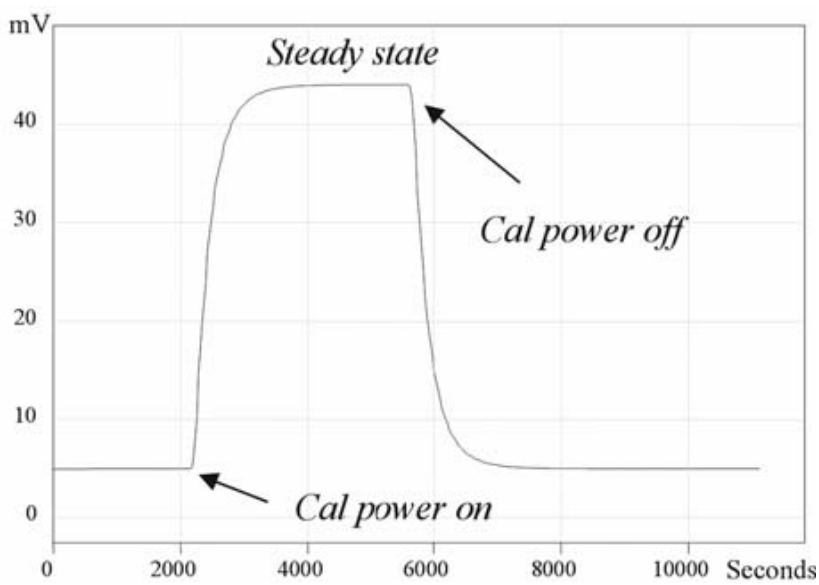

Figure E-2. Steady state calibration plot.

The calibration was performed regularly, prior to performing each isothermal temperature for example, once calibration was performed at 15 °C and 23 °C etc. Each channel was independently calibrated.

Testing Procedure

- The calorimeter equipment and data acquisition unit was turned on. It was determined that the calorimeter was at temperature equilibrium by verifying that the baseline (0.0V) was stable over a period of a few minutes. The temperature of the heat sink during the test was 15.0, 23.0 ± 1.0 °C.
- Cement Specimens
  - 4 grams of cementitious material was weighed the mass recorded to the nearest 0.001 grams, and was placed in the calorimeter cell. For each of the Mixes, 2.000 grams of was used to provide a consistent water-cement ratio of at least 0.50 for each paste. After the water and cement are weighted, the cell was placed in the calorimeter as shown in Figure E-3.
  - Allow any change in calorimeter output caused by this process to return to the baseline level. Typically, a 24-hour interval is necessary for a return to the baseline level.

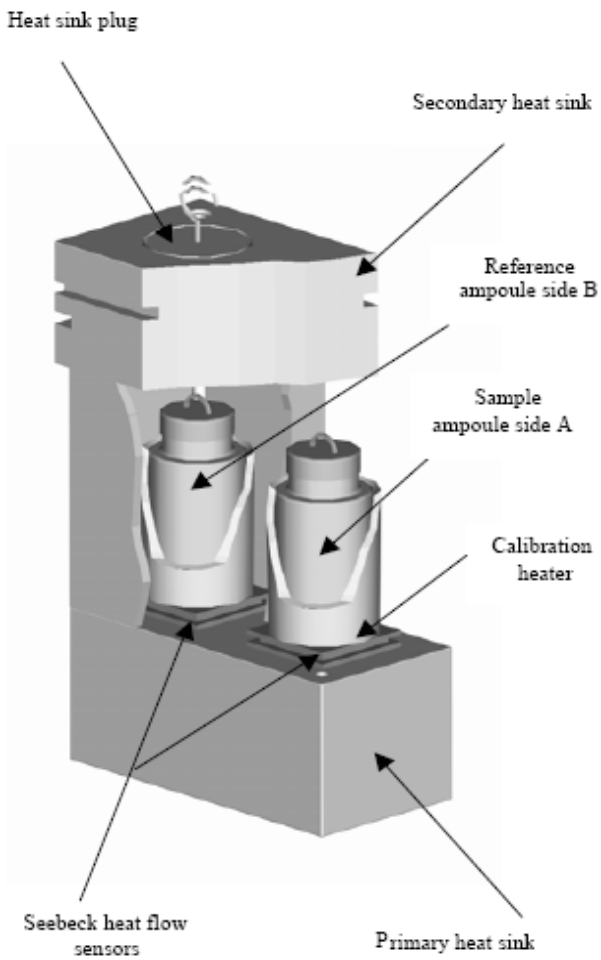

Figure E-3. Cutaway of one of the 8 calorimetric channels showing the twin configuration.

- Mortar Specimens
  - 4 grams of cementitious material was weighed the mass recorded to the nearest 0.001 grams, and was placed in the calorimeter cell. For each of the Mixes, 2.000 grams of was used to provide a consistent water-cement ratio of at least 0.50 for each paste.
  - 6 grams of silica sand was weighted to the nearest 0.001g and added to the calorimeter cell
  - After the water and cement are weighted, the cell was placed in the calorimeter same manner as the procedure used for the "cement specimens" noted above.
- After the baseline level was reached, the data collection was started and the water was injected into the cementitious materials to form a uniform paste. Cementitious paste specimens were mixed for 1 minute each. Mortar specimens were Mixed for 2 minutes each.
- Data was collected on an interval of 1 minute for the duration of the test (72-336 hours).

Calculation or Interpretation of Results

The purpose of the evaluation is to calculate the heat produced during the first 4-14 days of hydration. The evaluation method consists of the following steps:
Remove the baseline:

$$U(t) = U_{raw}(t) - U_{bl} \tag{E-1}$$

Here U_{raw} is the signal from the calorimeter and U_{bl} is the measured baseline of the calorimeter.

Apply the calibration coefficients (A and B) and divide by the mass of cement (m_c) in the sample to get the specific thermal power P:

$$P = \frac{A + B \times U(t)}{m_c} \tag{E-2}$$

where P (J/s/g) is the power output per gram of dry cement, A and B are the calibration coefficients determined during the calibration process, $U(t)$ is the voltage output at each data collection point, and m_c is the mass of dry cement used in the test.

The total heat of hydration of the sample is calculated by integrating the power/g versus time data over the time interval of the test (t_i to t_e):

$$Q = \int_{t=t_i}^{t_e} P\,dt \tag{E-3}$$

Where, Q (J/g_{cement}) is the heat produced from the sample, t_i is the time the sample was charged into the calorimeter, and t_e is the time of the end of the measurement as calculated from the time of Mixing cement and water.

Operationally, the integration is executed by averaging the power output from two consecutive readings and multiplying by the time interval of the reading, giving an output for each time

increment in units of J/g. The heat so calculated in each time increment is then summed over the duration of the test, as in the following equation.

$$Q = \sum_{i=t_i}^{t_e} \left(\frac{P(t_i) - P(t_{i+1})}{2} \right) \times (t_{i+1} - t_i) \qquad \text{(E-4)}$$

Where $P(t_i)$ is the power output at time t_i, and $P(t_{i+1})$ is the power output at the next time interval (t_{i+1}). In this method (internally Mixed procedure), t_i is taken as zero when water is added to the cement.